STUDIES ON SOME FAST ION CONDUCTORS

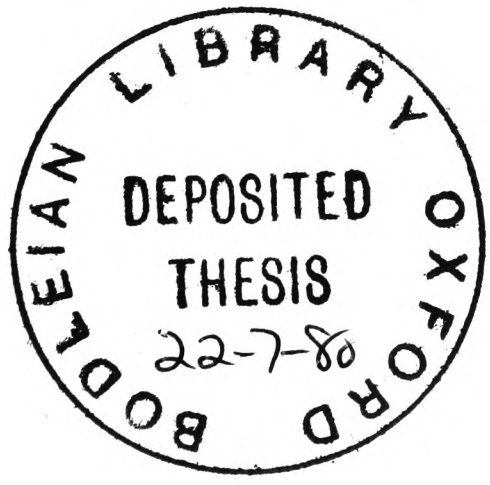
A thesis

submitted for the degree of Doctor of Philosophy

to the Board of the

Faculty of Physical Sciences

in the University of Oxford



J.M.Newsam

Lincoln College

Hilary 1980

ABSTRACT

Studies on some Fast Ion Conductors

A Thesis submitted for the degree of Doctor of Philosophy in the University of Oxford by J.M. Newsam, Lincoln College.
Hilary Term 1980

We report diffraction experiments on some representative Fast Ion Conductors.The structures of anhydrous stoichiometric deuterium ($DAl_{11}O_{17}$) and silver ($AgAl_{11}O_{17}$) beta aluminas have each been determined at four temperatures in the range 4.2K - 773K using powder neutron diffraction (PND) data.In $DAl_{11}O_{17}$,a strong D-O(5) hydroxyl linkage is maintained at all four temperatures.For $AgAl_{11}O_{17}$ at 4.2K,we have observed,for the first time in metal beta aluminas,a completely ordered cation distribution.The material, which was prepared by a new route,is accurately stoichiometric.At 298K,the silver atoms have become somewhat delocalised and by 773K they are organised in a highly diffuse manner.

Single crystal neutron diffraction was used to elucidate the proton distributions in ammonium beta alumina,$(NH_4)_{1.25}Al_{11}O_{17.125}$,and the two derivatives $(NH_4)_{0.78}H_{0.25}Al_{11}O_{17}$ and $'HAl_{11}O_{17}$.In the parent compound,the positions and orientations of the two independant (NH_4^+) species are such that all protons are involved in favourable hydrogen-bonding schemes.In formation of the first derivative,one of these sites becomes completely depopulated.Our results clarify the thermal behaviour of $(NH_4)_{1.25}Al_{11}O_{17.125}$ and we propose schemes by which stoichiometric beta aluminas are formed from this precursor and the related $(H_3O)_{1+x}Al_{11}O_{17+x/2}$.

The crystal structures of I-Ag_3PO_4 (25°C and 375°C), II-Ag_3PO_4 (650°C),II-Na_3PO_4(γ)(400°C) and the solid solutions $Na_{3(1-x)}Al_xPO_4$ are described.The high-temperature forms are considered in relation to the fluorite structure and mechanisms for the ionic conduction of these phases are proposed.

A single crystal X-ray diffraction study of β-Ag_2SO_4(25°C) reveals that it is isostructural with thenardite, V-Na_2SO_4.The high-temperature modifications α-Ag_2SO_4 (490°C) and α-K_2SO_4 (620°C) have been characterised using PND data.

A PND experiment on silver(I) fluoride confirms that it adopts the rocksalt structure and we find no firm evidence for a significant population of defects.

"To see a World in a Grain of Sand
And a Heaven in a Wild Flower
Hold Infinity in the palm of your hand
And Eternity in an hour "

William Blake (1805)

For my parents

ACKNOWLEDGEMENTS

It is often difficult to express a deep gratitude verbally and it therefore proves to be one of the pleasures of writing this thesis in my being able to record, in albeit ephemeral words, my appreciation for the help and guidance that I have received.Firstly , I am indebted to my supervisor, A.K.Cheetham, whose accurate scientific insight has often made plain what had previously appeared intractable and to B.C.Tofield for providing a ready and well-versed interest in problems, together with many technical facilities. Everyone in the Chemical Crystallography Lab. has been very helpful, but I must single out C.K.Prout for deputising as my supervisor, D.J.Watkin for being patient with my many queries, A.J.Skarnulis and my contempories P.D.Battle and A.R. Rae-Smith. In other departments I have had rewarding discussions with P.Bendall, S.J.Turner, W.A.England and L.Holden.

At A.E.R.E,Harwell I thank those of the University Support Group and the many others who have given invaluable assistance, including C.F.Sampson, R.Gillespie, G.Proudfoot and W.Futcher. Similarly, at the ILL, Grenoble, our experiments were made possible through the efforts of A.W.Hewat, C.Riekel, R.Chagnon, P.Berneron and A.Wright. I spent a very enjoyable summer at Los Alamos Scientific Laboratory for which I am grateful to all those in Group P-8, but, in particular, T.A.Kitchens and J.L.Yarnell.

Finally, I thank Judith Adams for typing this thesis and Keith Waters for undertaking most of the photography.

I acknowledge financial support by A.E.R.E, Harwell under the terms of a research contract (No. H4B 2952 EMR) and the provision of neutron scattering facilities by the Science Research Council.

CONTENTS

			Page
Chapter 1		AIMS OF RESEARCH	1
Chapter 2		INTRODUCTION TO EXPERIMENTAL METHODS	5
	2.1	Single crystal X-ray analysis	6
	2.2	Neutron diffraction	9
	2.3	The problems with powders	10
	2.4	Neutron diffraction instruments	15
		2.4(a). D12A and D12B Neutron Film Cameras	15
		2.4(b). The Mark VI and D9 single crystal diffractometers	16
		2.4(c). Powder neutron diffraction instruments	16
Chapter 3		AN INTRODUCTION TO BETA ALUMINAS	21
	3.1	The structures of sodium beta and beta" aluminas	22
	3.2	Exchange properties and conductivity	27
	3.3	Structural studies of other beta and beta" aluminas	31
	3.4	Studies by other techniques	35
	3.5	Hydrogen-containing beta aluminas	38
	3.6	Stoichiometric beta aluminas	43
	3.7	Analogous systems	43
Chapter 4		DEUTERIUM BETA ALUMINAS	48
	4.1	Introduction	49

	4.2	Sample preparation	49
		4.2(a). Deuterium beta alumina	49
		4.2(b). Deuterium beta" alumina	50
	4.3	Powder neutron diffraction experiments	53
	4.4	Results	55
		4.4(a). Deuterium beta alumina at 4.2K	55
		4.4(b). Deuterium beta alumina at 298K	59
		4.4(c). $DAl_{11}O_{17}$ at 573K and 720K	64
		4.4(d). Deuterium beta" alumina at 4.2K	69
	4.5	Conclusion	78
Chapter 5		SILVER BETA ALUMINAS	90
	5.1	Introduction	91
	5.2	Single crystal neutron diffraction study of $Ag_{1.25}Al_{11}O_{17.125}$	92
	5.3	Polycrystalline $AgAl_{11}O_{17}$ - Experimental details	98
	5.4	Polycrystalline $AgAl_{11}O_{17}$ at 4.2K - Results	100
	5.5	Polycrystalline $AgAl_{11}O_{17}$ at 25°C - Results	107
	5.6	Polycrystalline $AgAl_{11}O_{17}$ at 300°C and 500°C - Results	112
	5.7	Conclusion	117
Chapter 6		AMMONIUM BETA ALUMINA AND ITS DERIVATIVES	127
	6.1	Introduction	128
	6.2	Sample preparation	128
	6.3	Single crystal X-ray diffraction study of ammonium beta alumina	131

6.4 Single crystal neutron diffraction study of ammonium beta alumina 134

6.5 Single crystal neutron diffraction study of ammonium/hydrogen beta alumina 142

6.6 Single crystal neutron diffraction study of 'hydrogen beta alumina' 145

6.6(a). Photographic neutron diffraction experiment 145

6.6(b). Neutron diffraction experiment on the D9 diffractometer 149

6.7 Discussion and conclusion 152

Chapter 7 SODIUM AND SILVER ORTHOPHOSPHATES 174

7.1 Introduction 175

7.2 Single crystal X-ray diffraction study of I-Ag_3PO_4 177

7.3 Powder neutron diffraction investigation of I-Ag_3PO_4 at 375°C 179

7.4 Powder neutron diffraction experiment on I-Na_3PO_4 at 25°C 183

7.5 Powder neutron diffraction studies of II-Na_3PO_4 (400°C) and II-Ag_3PO_4(650°C) 185

7.6 Powder neutron diffraction measurements on the solid solutions $Na_{3(1-x)}Al_xPO_4$ 194

7.6(a) Experimental 194

7.6(b) Results for the composition $Na_{2.925}Al_{0.025}PO_4$ 198

7.6(c) Results for the composition $Na_{2.4}Al_{0.2}PO_4$ 202

7.6(d) Conclusion 205

7.7 Conclusion 208

Chapter 8		ANHYDROUS SULPHATE SYSTEMS	217
	8.1	Introduction	218
	8.2	Single crystal X-ray diffraction study of β-Ag_2SO_4	223
	8.3	Powder neutron diffraction investigation of α-Ag_2SO_4 at 490°C	226
	8.4	Powder neutron diffraction study of α-K_2SO_4 at 620°C	230
	8.5	Conclusion	232
Chapter 9		SILVER (I) FLUORIDE	240
	9.1	Introduction	241
	9.2	Experimental	243
	9.3	Results	244
	9.4	Conclusion	245
REFERENCES			247
APPENDICES			after page No. 264
	Appendix I		A2
	Appendix II		A19
	Appendix III		A38
	Appendix IV		A60
	Appendix V		A66

CHAPTER 1

AIMS OF RESEARCH

Solid materials in which there is appreciable ionic mobility have been known for many years, although interest in such systems has recently been enhanced by a realisation of their technological importance. In batteries, solid electrolytes present several advantages over traditional systems. They allow the use of liquid electrodes and, with purely ionic conductivity, there is no internal short-circuiting which limits the life of conventional wet-cells. High energy-densities can be achieved which will facilitate the use of electrochemical power for traction and with the possibility of elevated operating temperatures, conditions under which high efficiency can be obtained, the use of batteries in load-levelling schemes becomes feasible. Proton conductors are in demand as electrodes for fuel cells and, in a reverse sense, in the electrolysis of water. Zirconia-based oxide ion conductors are already employed in oxygen-sensing systems. Other ion-specific solid electrolytes could have similar functions.

These applications stem from an ionic mobility in the solid which approaches that of the fused state. This implies a diffusion coefficient of $\sim 10^{-5} cm^2 s^{-1}$ or a conductivity of $\sim 10^{-2} \Omega^{-1} cm^{-1}$ or higher. While mixed ionic/electronic conductors are of use as electrode systems, we are concerned here principally with systems which have, in addition, negligible electronic conductivity. Despite much recent work on other potential systems, the best solid electrolytes are those of the beta alumina family or compounds of Ag^+ such as $RbAg_4I_5$. The latter are, of course, of limited commercial use for economic reasons. In the work described here, we have studied the structures of some representative systems using diffraction techniques.

The first of the two chosen classes comprises beta

aluminas, in particular those which contain protons in the conducting planes and those which closely approach the stoichiometric composition. In the studies of ammonium beta alumina, $(NH_4)_{1.25}Al_{11}O_{17.125}$, and its derivatives, which are described in Chapter 6, single crystal neutron diffraction was used to investigate the potentially disordered distribution of protons in the presence of heavier elements. Such problems cannot be tackled adequately by X-ray diffraction. With other systems, it has not been possible to prepare suitable single crystals. In these cases, the profile refinement of powder neutron diffraction (PND) data provides the means by which accurate structural information may be obtained. In addition, this technique lends itself to the facile collection of data at temperatures other than ambient. Studies of anhydrous stoichiometric deuterium ($DAl_{11}O_{17}$) and silver ($AgAl_{11}O_{17}$) beta aluminas as a function of temperature are described in Chapters 4 and 5 respectively. These systems have also provided a suitable testing-ground in which the applicability of Fourier methods to PND data analysis may be evaluated.

The second class of materials which was selected for study comprises systems which contain anions of tetrahedral geometry, such as sodium orthophosphate and silver sulphate. These compounds exist in ordered low-temperature phases, but they transform as the temperature is raised to modifications in which the anions are subject to rotational disorder. Appreciable cation mobility has been observed in some of these high-temperature forms. In this case, single crystal X-ray analysis can be employed to examine the phase stable under ambient conditions. However, the volume changes associated with the order-disorder transition necessitate the use of powders for

the investigation of the high-temperature forms. The limited success of X-ray powder profile refinement and the relative scattering powers of the species involved implied that PND would again be the most successful technique. In Chapter 7 I describe structural studies of the Na_3PO_4 and Ag_3PO_4 systems. The high-temperature phases have ostensibly the same symmetry as the fluorite structure and these phases are therefore considered as cation-excess anti-fluorites. This possible relationship is further probed in an examination of the system $Na_{3(1-x)}Al_x\square_{2x}PO_4$ (where $\square$ represents a vacancy) in which the level of apparent cation-excess is reduced.

In Chapter 8 I present the results of work on some anhydrous sulphate systems including Ag_2SO_4 and K_2SO_4. Finally, in Chapter 9, I report the details of the structure of AgF at room temperature as determined from PND data.

CHAPTER 2

INTRODUCTION TO EXPERIMENTAL METHODS

I present here a brief introduction to the principles and practice of the techniques which were used in this work (sections 2.1-3). In section 2.4 I record the characteristics of the neutron diffraction instruments on which data were collected.

2.1 Single Crystal X-ray Analysis

The periodic repetition of a basis unit throughout a crystal structure allows diffraction to occur according to the Bragg condition:

$$n\lambda = 2d \sin\theta \qquad (1)$$

The distribution of reflections in reciprocal space defines the unit cell which gives rise to it. Further, the systematic absence of particular classes of reflections indicates which translational symmetry elements are present. It is the distribution of scattering matter in the unit cell which determines the intensity of a Bragg reflection, I_{hkl}, according to:

$$I_{hkl} = \frac{|F_{hkl}|^2 . Lp}{K} \qquad (2)$$

where L is the Lorentz factor

p is the polarisation correction

K is a scaling constant

and F_{hkl} is the general structure factor given by:

$$F_{hkl} = \sum_j f_j \exp\{2\pi i(hx_j + ky_j + lz_j)\} \qquad (3)$$

where the summation is over all atoms, j, within the unit cell. The effect of thermal vibration is included by multiplying the atomic scattering factor, in the isotropic approximation, by the expression:-

$$\exp\{-B_j(\sin^2\theta)/\lambda^2\} \qquad (4)$$

where B_j is related to the mean square amplitude of vibration $\bar{u}_j^2$ according to:

$$B_j = 8\pi^2\bar{u}_j^2 \qquad (5)$$

The effect of anisotropic vibration is included by use of the general temperature factor expression:

$$\exp\{-\tfrac{1}{4}(B_{11}h^2a^{*2} + B_{22}k^2b^{*2} + B_{33}l^2c^{*2} + 2B_{12}hka^*b^* + 2B_{13}hla^*c^* + 2B_{23}klb^*c^*)\} \qquad (6)$$

although the site symmetry of a particular atom may impose restrictions on the thermal-motion tensor coefficients[1].

In a single crystal experiment, the measured quantity is I_{hkl} (Equation 2), where the measured reflections, hkl, cover at least a unique volume of the limiting sphere. The observed data is corrected for Lorentz and polarisation factors (absorption and scaling terms may also be included) and the corrected data is merged to yield a unique set of structure factor moduli $|F_{hkl}|$. The electron density distribution is related to these moduli according to:

$$\rho(x,y,z) = \frac{1}{V}\sum_h\sum_k\sum_l |F_{hkl}|\exp\{-2\pi i(hx + ky + lz - \alpha'_{hkl})\} \qquad (7)$$

where $2\pi\alpha'_{hkl}$ is the phase angle and the summation is over <u>all</u> hkl. The observed data contains no prior information about α_{hkl}. To overcome this phase problem, a trial structure is determined from a Patterson synthesis[2], direct methods[3], or, less commonly, by indirect or other heavy-atom techniques. Using this trial model, structure factors are calculated according to Equation 3 and a measure of the representation of

the true structure by the trial model is gauged from the residuals:

$$R = \frac{\sum||F_{obs}| - |F_{calc}||}{\sum|F_{obs}|} \qquad R_w = \frac{\sum w||F_{obs}| - |F_{calc}||}{\sum|F_{obs}|} \tag{8}$$

If the phasing model is reasonable, a Fourier synthesis may be calculated (Equation 7) to complete the trial model. Alternatively, the quantities $(|F_{obs}| - |F_{calc}|)_{hkl}$ may be used as coefficients in a difference Fourier synthesis. This type of synthesis indicates errors or omissions in the trial model and, when such discrepancies are small, it is less susceptible to series-termination errors.

A satisfactory trial model may be optimised by least-squares techniques where the quantity minimised is:

$$D = \sum_{hkl} w_{hkl}(|F_{obs}| - |kF_{calc}|)^2 \tag{9}$$

The weight, w_{hkl}, is taken as unity in initial stages, but near the end of refinement other schemes may be employed. Weights derived from a truncated Chebyshev polynomial[4] are used in the work described here.

Constraints[5,6] may be applied to assist convergence or to hold ill-defined parameters close to chemically sensible values. In the final cycles of refinement, corrections for secondary extinction[7] and anomalous dispersion are made where appropriate. All of these calculations for the systems which are described subsequently were performed on the Oxford University 1906A computer using the CRYSTALS suite of programs[6]. Atomic scattering factors, f_j, were taken from Cromer and Mann[8], Spagna[9] (hydrogen only) and International Tables[1].

2.2 Neutron diffraction

This section contains a brief introduction to neutron diffraction. More detailed accounts of thermal neutron scattering are given by Bacon[10], Marshall and Lovesey[11] and Squires[12].

When a neutron impinges on a nucleus, it may be transmitted, scattered or absorbed. The scattering process may be elastic or it may involve transference of energy to or from the scattered neutron. Both processes may be coherent, that is arising in a regular fashion from the extended solid array, or they may be incoherent. Incoherent elastic scattering arises from non-periodic fluctuations in scattering power and may result from the presence of nuclear isotopes, nuclear spin, lattice defects or paramagnetic moments. These incoherent effects contribute to the general background in a diffraction experiment.

The Bragg condition (Equation 1) states that diffraction occurs only when the scattering vector given by the difference $\underline{\kappa} - \underline{\kappa}'$, where $\underline{\kappa}$, $\underline{\kappa}'$ are the wave vectors of the neutron before and after scattering, corresponds to a reciprocal lattice vector. The structure factor which describes the amplitude of the scattered wave can be written:

$$F^2_{hkl} = \left| \sum_j b_j \exp\{2\pi i(hx + ky + lz)\} \right|^2 \qquad (10)$$

which is directly analogous to the expression in X-ray diffraction, but b_j is now the scattering length of nucleus j. The effect of thermal motion on the effective magnitude of the structure factor is accounted for by Equations 4 and 6.

We note, firstly, that there is no tail-off in form-factor with $\sin\theta/\lambda$ as in the X-ray case. The nucleus is

effectively a point source compared with the wavelength of the incident beam. Therefore, elements of widely-differing atomic numbers, Z, may have similar scattering lengths. Secondly, due to the different contributions of potential and resonance scattering, the scattering lengths, b_j, of different isotopes of the same element or of atoms of similar Z may be markedly different. This is exemplified by the case of hydrogen with $b = -0.374$[13] whereas for deuterium, ^2H, $b = 0.667$[13]. Such factors can enable a distinction to be made between atoms which are effectively identical to X-rays. Thus the sites occupied by magnesium ($b = 0.52$, cf. Al, $b = 0.345$[14]) in Mg-stabilised sodium beta" alumina have been identified[15]. Further, the scattering lengths of some nuclides are close to zero, for example vanadium with $b = -0.05$. Such materials can then be used in experiments for the apparatus which controls the sample environment.

The course of data analysis in a single crystal experiment parallels that for X-ray data. However, because of the low flux of neutron beams, counting times are long and samples must be large. Extinction can then be an important factor although absorption is rarely significant. The size requirement severely limits the number of materials which can be investigated in single crystal form. For the single crystal studies which are described here, all calculations were performed using the CRYSTALS system[6] with scattering lengths taken from Bacon[13] or elsewhere as indicated.

2.3 The Problems with Powders

In a powder diffraction measurement, the observed data

is one-dimensional. For monochromatic radiation, it consists merely of a measured intensity at a given value of the Bragg angle, θ. In systems of high symmetry with small unit cells, it is possible that most reflections will be well-resolved in 2θ. If this is the case, an integrated intensity for each reflection, I_{hkl}, may be obtained by summing the observed counts minus an estimated background over the complete range of the peak. If hkl corresponds to a single set of equivalent reflections, a structure factor amplitude may then be calculated (cf. Equation 2):

$$|F_{hkl}|^2 = \frac{I_{hkl} \cdot (\sin^2\theta\cos\theta) . K}{p.m.A} \qquad (11)$$

where $(\sin^2\theta\cos\theta)$ is the Lorentz factor

p is the polarisation correction, applicable in the case of X-rays.

m is the multiplicity

A is an absorption correction, given by $\exp(-\mu t \sec\theta)$ for a cylindrical sample

and K is a scaling constant.

This structure factor may then be used in the least-squares and Fourier calculations which are described above.

Even in a well-resolved cubic pattern, however, the 511 and 333 reflections are exactly coincident. In systems of lower symmetry accidental overlap will occur so that integrated peak intensities will contain contributions from, perhaps, several non-equivalent reflections. Least-squares procedures can still be applied in this case, although the calculated structure factor is then the sum, $\sum_i F_{calc_i}$, over all the reflections which contribute to the observed peak intensity.

The quantity minimised is:

$$D = \sum w(|F_{obs}| - \sum_i |kF_{calc_i}|)^2 \qquad (12)$$

This type of calculation has been implemented in a computer program written by Wiseman[16].

In a typical diffraction pattern (see Figure 4.3), few peaks are sufficiently well-resolved for the integrated intensity approach to be viable. In addition, information about the relative intensities of overlapping peaks, which may be discernible in the profile, is lost when the integration is performed. To overcome this problem, Rietveld[17,18] recognised that structure refinement, using the entire observed pattern, was possible by minimising the quantity:

$$D = \sum_i w_i (y_{iobs} - y_{icalc})^2 \qquad (13)$$

where y_{iobs} is the intensity minus an estimated background at a single point, i, in the observed profile. The calculated intensity, y_{icalc}, is formed by summing the contributions from all reflections which overlap at the point i. For X-ray data, the shapes of reflections observed in a powder diffraction pattern are complex in form and are not readily described by an analytical expression[19,20,21]. However, for powder neutron diffraction (PND) data, collected on a conventional 2-circle diffractometer with monochromatic radiation, the peaks are accurately gaussian in shape[18].

We may therefore write the contribution, Y_i, of a Bragg reflection, hkl, centred at $2\theta_k$ to the measured intensity at point $2\theta_i$ as:

$$Y_i = \frac{t}{K} |F_{hkl}|^2 . m_{hkl} . L_k \cdot \frac{2(\ln 2)^{\frac{1}{2}}}{H_k \sqrt{\pi}} . \exp\{\{\frac{-4\ln 2}{H_k^2}\}\{2\theta_i - 2\theta_k\}^2\} \qquad (14)$$

where t is the step size which may be included in the scaling term K

m_{hkl} is the multiplicity

L_k is the Lorentz factor

H_k is the full width at half-height of the Bragg peak

and F_{hkl} is the structure factor calculated according to Equation 10.

For this special case of monochromatic PND data, the variation of half-width, H_k, with Bragg angle, θ_k, is adequately described by[22]:

$$H_k^2 = U \tan^2\theta_k + V \tan\theta_k + W \qquad (15)$$

The form of this curve is shown in Figure 2.1. The minimum of the curve, i.e. the value of 2θ at which optimum resolution is obtained corresponds to the take-off angle of the monochromator[23]. At low values of 2θ, where the radius of the Debye-Scherrer cones is small, the peak shapes do deviate from gaussian because of the finite height of the detector aperture. A correction, c_a, for this asymmetry may be made[18,24] according to:

$$c_a = \left(1 - \frac{P(2\theta_i - 2\theta_k)^2 . s}{\tan\theta_i}\right) \qquad (16)$$

where P is the asymmetry parameter

and s is unity but with sign $(2\theta_i - 2\theta_k)$.

However, this correction is unsatisfactory in practice and it is common to avoid the problem by omitting the low angle region from the calculations. If the crystallites comprising the powder sample have a pronounced habit, preferred orientation effects may occur and a correction, c_{PO}, can be made:

$$c_{PO} = \exp(-g\alpha^2) \qquad (17)$$

where α is the acute angle between the scattering vector and the preferred orientation (PO) axis, which is defined as the normal to the plane of plate-like crystals,
and g is the PO parameter.

Corrections for other effects should also be applied, if appreciable, to obtain reliable structural parameters[25]. These effects may include absorption (see Equation 11), thermal diffuse scattering and multiple Bragg reflection.

In the course of refinement, all atomic and instrumental parameters may be varied, together with the scale, K, cell constants, counter zero-point error and the correction factors described above. The residuals which describe the 'goodness of fit' are:

$$R_{Profile} = \frac{\sum |Y_i obs - (1/K) Y_i calc|}{\sum |Y_i obs|} \qquad (18)$$

$$R_{\substack{weighted \\ profile}} = \left(\frac{\sum w_i (Y_i obs - (1/K) Y_i calc)^2}{\sum w_i (Y_i obs)^2} \right)^{\frac{1}{2}} \qquad (19)$$

In addition, the observed profile may be deconvoluted into individual peak intensities allowing the calculation of:

$$R_{Intensity} = \frac{\sum |I_{obs} - (1/K) I_{calc}|}{\sum I_{obs}} \qquad (20)$$

A value of R_{WP} expected on purely statistical grounds is given by:

$$R_E = \left(\frac{N}{\sum w_i (y_i obs)^2} \right)^{\frac{1}{2}} \qquad (21)$$

where N is the number of data points minus the number of variable parameters.

The deconvoluted peak intensities may also be converted to structure factor moduli according to Equation 11. These can

be used as coefficients in Fourier symtheses, although such calculations are, of course, strcngly biased towards the calculated model.

All of these calculations, for the structures described in later chapters, were performed using a modified version of the Rietveld program[26,27] on the Oxford University 1906A computer and a similar interactive program suite[28] on the DEC-10 system at UMIST. Fourier sections were contoured by the Calcomp GPCP package[29]. The current state of the applications of profile analysis to PND data has recently been reviewed[30].

2.4 Neutron Diffraction Instruments

a) D12A and D12B Neutron Film Cameras

The D12 instruments in the neutron-guide hall at the ILL, Grenoble comprise a Laue and two Weissenberg cameras[31]. The first of these is of standard design, operating under ambient conditions. The second, which has normal-beam geometry, is vertical and it has an associated He-cryostat allowing sample temperatures down to ∿10K to be reached. The wavelength range, from a bent Cu crystal, is 1 - 4Å, a value of 1.5Å typically being chosen. The peak flux at the specimen is 2×10^{7} n $cm^{-2}s^{-1}$. In the neutron cameras, the photographic film is in close contact with a layer of scintillator based on ZnS and $Li^{6}F$ which converts the incident neutrons into an optical signal. The resulting exposures are indexed in the standard way and peak intensities may be measured using a photo-densitometer. This facility is then useful in exploratory investigations of phase transitions and for studying magnetic ordering or superlattice effects which arise from the long-range

order of elements of low atomic number, in particular hydrogen.

b) The Mark VI and D9 single crystal diffractometers

The characteristics of these two 4-circle diffractometers are summarised in Table 2.1. Both are conventional Eulerian geometry machines (the Enraf-Nonius CAD-4F diffractometer used for the single crystal X-ray work has kappa geometry in which the χ-axis is replaced by the κ-axis orientated at 40° below the horizontal plane[32]). D9, being on the hot-source, operates at short wavelengths. This enables large numbers of reflections to be collected, even for high symmetry systems, although, because of the small take-off angle, the resolution at higher values of θ is poor. The controlling computer program is written in Fortran and it allows great flexibility both in preliminary setting-up and in data collection itself. Recent mechanical improvements have further enhanced its performance. The operating system for the Mark VI Channel I diffractometer is slightly more restricted, although, in favourable circumstances, accurate data sets are readily obtained. The experimental time required for a typical run on one of the beta alumina systems, which are discussed shortly, is about 30 days for either machine.

c) Powder neutron diffraction instruments

The characteristics of six powder diffractometers are summarised in Table 2.2. Of these, CURRAN and D1B have not been used in the work reported here. The key figures are the flux at sample and the resolution which is described by the parameters U, V and W (Equation 15). However, the listed parameters were derived from profile refinements and the observed

peak widths may be sensitive to the microscopic nature of the sample. The variation of peak half-width as a function of Bragg angle, determined in such refinements, is plotted in Figure 2.1 for PANDA, D1A and D2. The larger take-off angles are responsible for the better resolutions of PANDA and D1A, although partly at the expense of incident neutron flux. The performance of D1A is further enhanced by the excellent signal-to-noise ratio achieved by the use of 10 counters and by its large separation from the reactor face which results in a very low, even background.

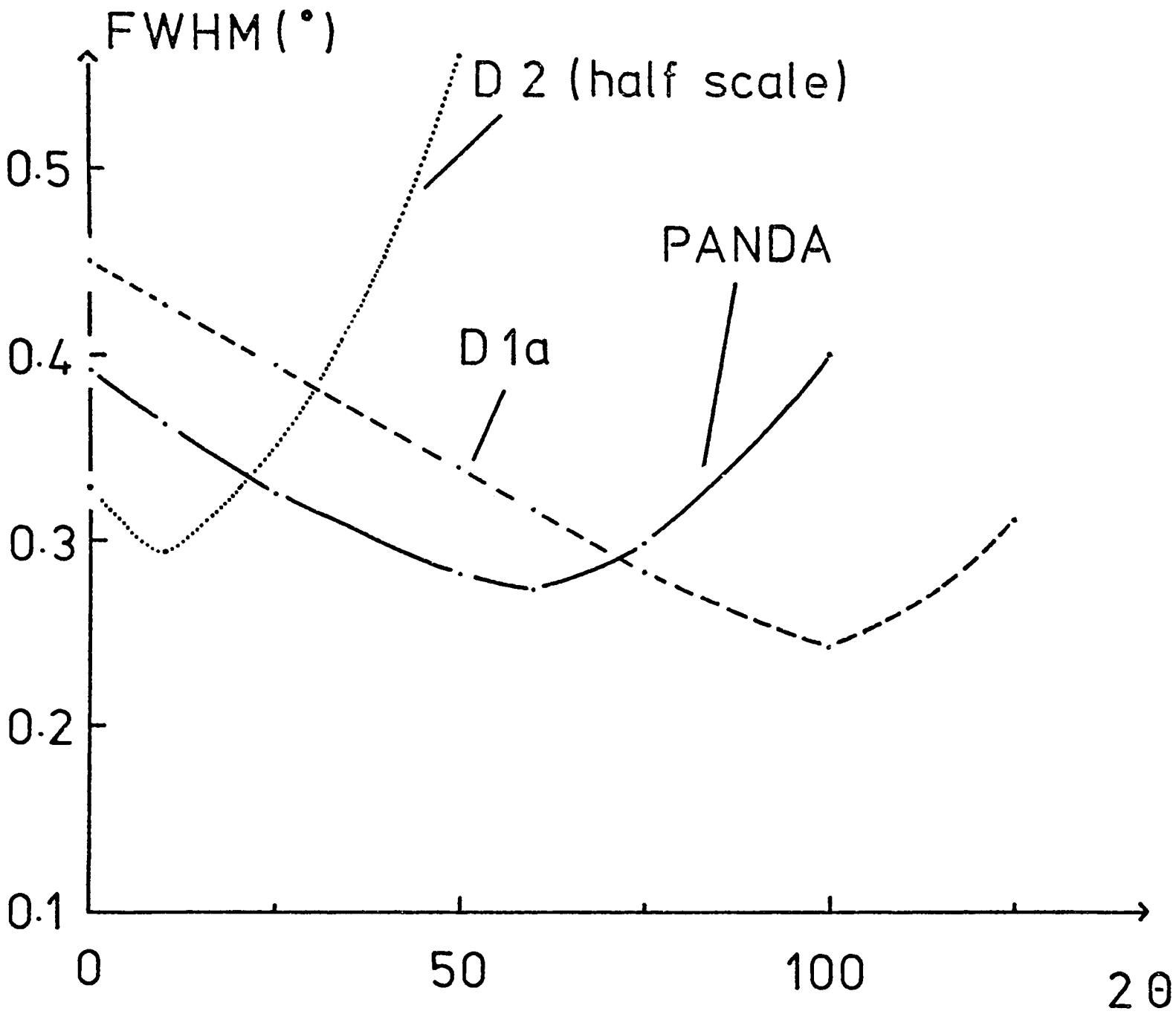


Figure 2.1. The variation with Bragg angle, θ, of the full width at half-height (FWHM) of Bragg reflections for three powder diffractometers. These resolution curves were determined in profile refinements of data collected from actual samples.

TABLE 2.1

SINGLE CRYSTAL NEUTRON INSTRUMENTS

Instrument	Mark VI Channel I[33]	D9[31]
Location	DIDO, A.E.R.E	ILL, Grenoble
Beam Hole	4H1	H3 (hot source)
Flux at Sample, n $cm^{-2}s^{-1}$	4×10^5	3×10^6
Wavelength range Å	-	0.4 - 0.8
Operating wavelength Å	1.1803	∿0.5
Monochromator	Cu[331]	Cu[200]
Take-off angle	∿90°	∿27°
Control Computer	PDP-8	T200 Téléme-canique
Time per reflection	∿30 mins	∿10 mins

TABLE 2.2 POWDER NEUTRON DIFFRACTION INSTRUMENTS

	PANDA[33]	CURRAN[33]	D2[31]	D1A[31,34]	D1B[31]	(TAS)[a]
Location	A.E.R.E	A.E.R.E	ILL	ILL	ILL	LASL
Beam tube	Pluto 7H4R	Dido 4H2	H11	H22	H22	-
Max. Flux n $cm^{-2}s^{-1}$	3.5×10^{5}	2×10^{6}	5×10^{7}	5×10^{6}	1×10^{6}	ca 10^{5}
Detectors No.	9	3	4	10	multi	1
Type	BF_3	BF_3	He^3	He^3	BF_3	BF_3
Monochromator	Ge	squashed Ge	Ge	Sq. Ge	graphite	Cu
Typical take-off angle	70°	47°	20°	122°	42°	60°
λ range Å	0.9-4.0	0.9-2.6	0.8-2.2	1.0-5.7	-	-
Typical λ Å	1.5	1.38	1.22	1.9	2.4	1.3
Typical counting time per profile	72hrs	24hrs	10hrs	24hrs	2hrs	50hrs
U[b]	6000	50000[c]	74000	900	-	2500
V	-5000	-32000	-17000	-2200	-	-800
W	2000	7000	4400	2000	-	2700

a modified triple-axis spectrometer at Los Alamos Scientific Laboratory, New Mexico

b U, V and W define the full peak width at half height, HW, according to $HW^2 = U\tan^2\theta + V\tan\theta + W$. The quoted values are derived from profile refinements based on actual samples and are given in hundredths of degrees

c P.D. Battle, personal communication

CHAPTER 3

AN INTRODUCTION TO BETA ALUMINAS

This chapter contains an introduction to the structural properties of beta alumina materials. We commence, in section 3.1, by describing the structures of sodium beta and beta" aluminas. Exchange properties and conductivity measurements are then outlined in section 3.2 with section 3.3 containing a summary of the crystallographic studies on the derivatives prepared by such exchange. Some aspects of other investigative techniques are presented in section 3.4. We discuss in sections 3.5 and 3.6 the work, much of it recent, which has been reported on hydrogen-containing and stoichiometric beta aluminas and, finally, in section 3.7 we mention the analogous alkali gallate and ferrite systems.

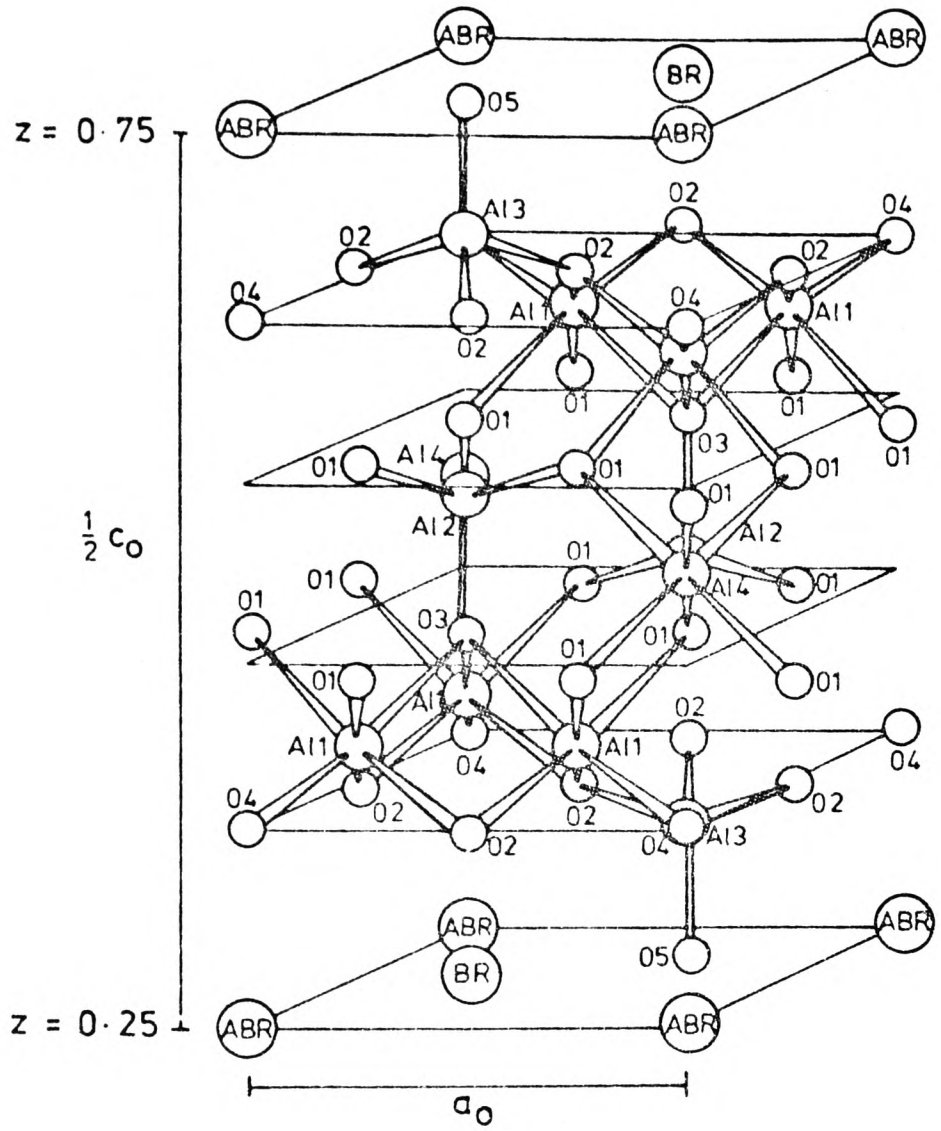
3.1 The structures of sodium beta and beta" aluminas

The name beta alumina derives from the original report by Rankin and Merwin in 1916[35] who believed the material to be an allotrope of Al_2O_3. Its crystal structure was first studied by Hendricks and Pauling[36] and subsequently by Bragg *et al.*[37]. With limited data, the latter determined the space group to be $P6_3/mmc$ (No. 194[1]) and they recognised both the presence of sodium, which had been suggested by Ridgway[38], and the similarity of its framework to that of spinel, $MgAl_2O_4$. Beevers and Ross[39] re-examined the material in 1937. They believed that the entire sodium content, as determined by improved chemical analyses[40] and density measurements[41], was located on the sites now named after these workers. Felsche[42], however, found these sites to be largely atom-deficient with mirror-plane oxygen vacancies being responsible for charge compensation.

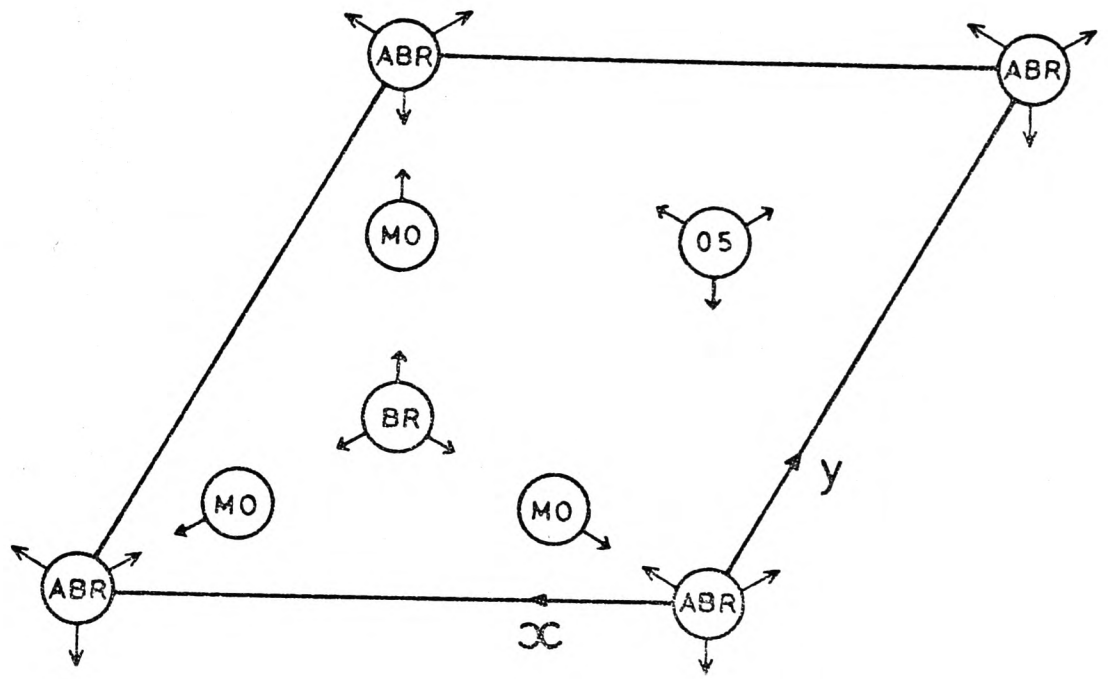
Peters et al.[43] then examined a more typical crystal with 4.93 wt% Na (this corresponds, in the light of subsequent knowledge, to the formula $Na_{1.29}Al_{11}O_{17.145}$*). Their analysis confirmed the space group $P6_3/mmc$, with a = 5.594Å, c = 22.53Å. They accounted for the full complement of sodium, with 75% close to the Beevers-Ross (BR) sites (2d) and the remainder close to positions half-way between the oxygens in the mirror-planes, the mid-Oxygen (mO) sites. This distribution has later been confirmed in a single crystal neutron study by Reidinger[44].

The general features of the structure are displayed in Figure 3.1. Perpendicular to the c-axis there are four layers of cubic close-packed (CCP) oxide ions. The aluminium ions occupy the octahedral and tetrahedral holes within the CCP layers in a fashion similar to that in spinel (and γ-Al_2O_3). These sections are therefore called 'spinel blocks'. The close-packed layers are separated by a plane with a much reduced atomic density which contains the sodium ions and an additional O^{2-}. This oxygen, O(5), which links the two adjacent spinel blocks in a Al(3)-O(5)-Al(3) bridge is commonly called the 'spacer oxygen'. The maximum constriction in this plane, which has crystallographic mirror symmetry, lies between the two O(4) ions, which are separated by 4.84Å. This rather large gap gives rise to a relatively even potential within the plane. The sodium ions can thus occupy several sites, their distribution being governed more by inter-planar than perpendicular inter-

* *In the absence of defects, the spinel block contains one $Al_{11}O_{16}^{+}$ unit. With inclusion of the spacer-oxygen (see text) and the counterion, the 'ideal' formula becomes $NaAl_{11}O_{17}$. It is to this unit, which describes one spinel block and one mirror plane, that we shall refer.*



(a)



(b)

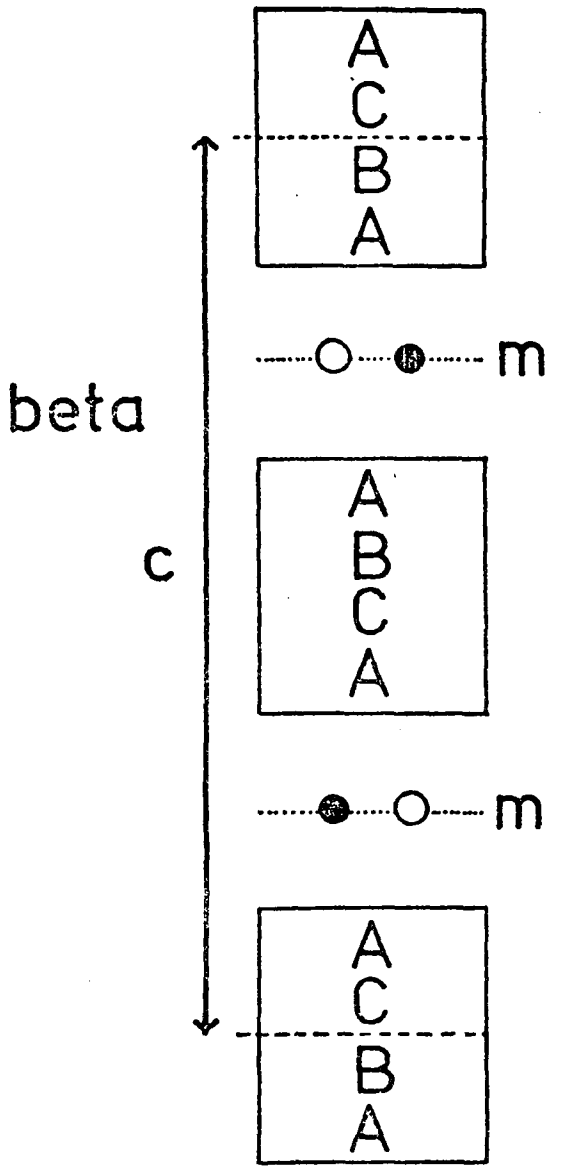
Figure 3.1 (a) The Beta Alumina Structure

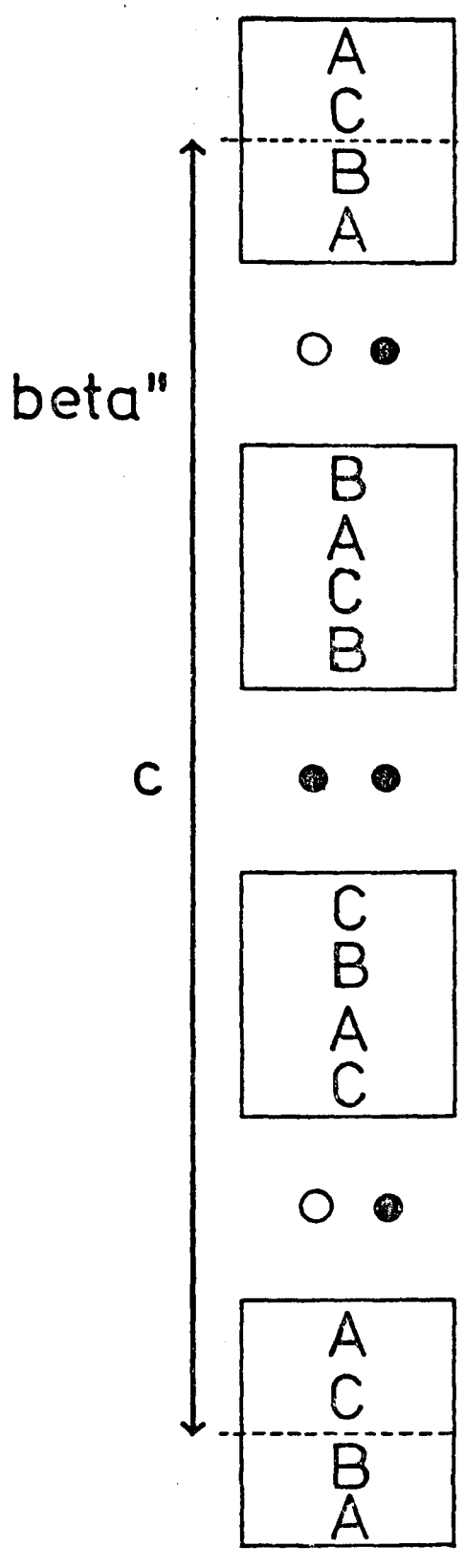
(b) A Projection of the Mirror Plane Showing the Beevers-Ross (BR), Anti-Beevers-Ross (ABR), Mid-Oxygen (MO) and O(5) Positions, and the Directions of Small Displacements Often Found.

actions.

The phase diagrams of the Na_2O-Al_2O_3 and Na_2O-MgO-Al_2O_3 systems were determined by Weber and Venero[45] and discussed by Kummer[46]. They demonstrate the existence of other beta alumina-type phases with differing Na_2O:Al_2O_3 ratios. Yamaguchi[47,48] had found three distinct phases which he termed β, β' and β" respectively although the second probably corresponds to the beta structure with a high sodium content. The 'ideal' formula of beta" alumina is $Na_2O.5Al_2O_3$ although it is normally sodium-deficient and small amounts of Li_2O or MgO are added for stabilisation[45]. Yamaguchi[48] had correctly predicted the structure of the beta" variant from powder data and his analysis was confirmed by the work of Bettman and Peters[49] on $Na_2MgAl_{10}O_{17}$.

The material has a rhombomedral cell, $R\bar{3}m$, with a = 5.614Å and c = 33.85Å. The structure again consists of spinel blocks, each of which contains four CCP oxide ion layers. However, these blocks are now related by a 3-fold screw axis and there are thus three such blocks in the unit cell. It can therefore be termed 3B4-β", with beta alumina being labelled 2B4-β[50]. The beta" arrangement is such that the CCP array is maintained throughout the structure, except in the loosely-packed planes (which do not now have mirror symmetry) where three-quarters of the oxide ions are missing. The beta material can then be visualised as derived from this model by a twinning operation in which every second spinel block is rotated by π radians[51]. This packing arrangement is depicted in Figure 3.2. We now find that the 'BR' and 'aBR' sites are equivalent, related by a centre of symmetry, although the oxygen distribution around these sites differs from that in the beta material





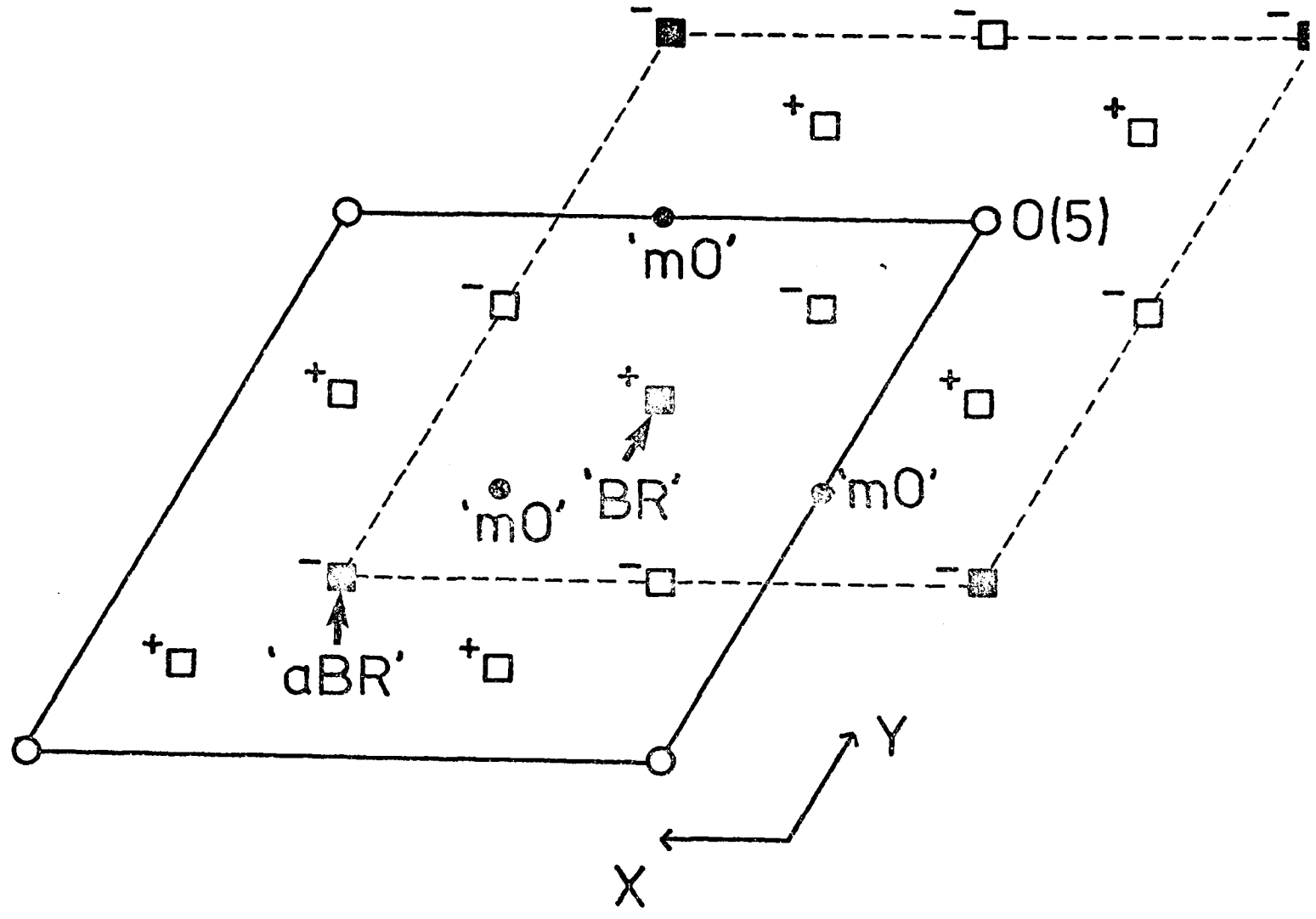


Figure 3.2 a) (Left) The packing arrangements of the CCP oxide ion layers in beta and beta" aluminas.

b) (Above) The locations of sites within the z = 1/2 conduction planes in beta" alumina. The projections of the O(4) (■) and O(2) (□) atoms above (+) and below (-) the plane are indicated. The solid and dashed lines indicate respectively the beta" unit cell and that corresponding to the conduction plane in the beta material.

(compare Figures 4.1 and 3.2(b)).

Bettman and Peters[49] found the sodium ions to occupy the 6c sites, 2/3 1/3 z with z ∿ 0.5. Later work, however, suggests that the sodiums are disordered about this site, with appreciable occupation of the more general 18h positions[15,52]. The single crystal neutron diffraction studies of Roth et al.[15,53] show that the stabilising Mg^{2+} ions are located mainly on the tetrahedrally coordinated Al(2) sites.

In addition to the β(β') and β" materials, the variants β''' and β'''' have been reported. These contain six CCP oxide ion layers between the loosely packed planes[54] and can be termed 2B6-β''' and 3B6-β'''' respectively (after Greis[50]). The synthesis of beta alumina has been studied by Ray and Subbarao[55]. Large single crystals may be made by the Czochralski process[56,57] and, recently, Bates et al.[58] have also been successful in preparing large crystals of the beta" material.

3.2 Exchange properties and conductivity

The interest in this class of materials was, to a large extent, stimulated by Yao and Kummer's[59] discovery of the high sodium ion conductivity in beta alumina which prompted its use as a solid electrolyte in the high energy-density Na-S battery[60]. In addition, this ionic mobility allows the exchange of Na^+ by other ions, a property which had been recognised in 1939[61]. Yao and Kummer[59] investigated the equilibria with the molten salts of Ag^+, K^+, Rb^+, Li^+, NH_4^+, Cs^+ (partial exchange), Tl^+ and In^+ (In metal via Ag^+) and they reported self-diffusion and interdiffusion coefficients. The extent of exchange with divalent ions was found to be small,

and was generally accompanied by crystal fracture. Exchanges with other monovalent cations have also been reported. These include NO^{+}(62), Ga^{+}(63), Cu^{+}(64,65), H^{+}(46) and H_3O^{+}(66). Nishikawa *et al.*(67) investigated exchange in aqueous solution.

The length of the a-axis in these monovalently substituted materials varies little, but the c-axis spacings broadly reflect the size of the ions which occupy the mirror plane (we shall see subsequently that these c-parameters are not genuinely correlated with the respective ionic radii, being sensitive to the nature of the occupied mirror plane sites and the level of non-stoichiometry). Typical lattice constants are given in Table 3.1. The variations in the length of the c-axis can be used to follow the effects of exchange in single crystals(68).

TABLE 3.1 LATTICE PARAMETERS OF EXCHANGED BETA ALUMINAS

Ion	a (Å)	c (Å)	Ref.
Na^{+}	5.594	22.53	43
Li^{+}	5.596	22.570	59
K^{+}	5.591	22.711	69
Rb^{+}	5.600	22.87	70
Ag^{+}	5.595	22.488	71
Tl^{+}	5.598	22.93	72
Ga^{+}	5.600	22.718	63
NO^{+}	5.597	22.711	62
H^{+}	5.602	22.677	46
D^{+}	5.606	22.619	73[a,b]
NH_4^{+}	5.596	22.888	59
H_3O^{+}	5.600	22.702	74
"	5.614	22.62	75[b]
"	5.605	22.81	76

[a] at 4.2K [b] 'stoichiometric'

The ionic conductivity, σ, is also very sensitive to the nature

of the conducting species. The reported values of σ for sodium beta alumina vary somewhat (see Kennedy[77]), reflecting the experimental difficulties, but a value of $\sigma = 0.033\Omega^{-1}cm^{-1}$ at 25°C[59,78], with an activation energy $E_a = 0.13eV$[79] is typical. The conductivity of sodium beta" alumina is slightly higher, with $\sigma = 0.06\Omega^{-1}cm^{-1}$ at 25°C[46], which is probably a result of the greater sodium content, the presence of two equivalent cation sites and the absence of interstitial oxygen within the conducting planes. The conductivity of other beta aluminas is lower, typically by two orders of magnitude. Measurements have been reported for the derivatives containing Ag^+[80], K^+[81,82], Tl^+[81], Li^+[81,82], H_3O^+[83], NH_4^+[84,85], Cu^+[65] and Na^+-Li^+[86,88]. For the last material the enhanced conductivity with respect to lithium beta alumina and the markedly differing mobilities of the two conducting ions were suggestive of a 'co-ionic' effect[86,88]. However, a more recent measurement of the Li^+ material[89] and data from other techniques[90] have shown that the effect is probably not of such major significance.

The conductivity is lowered by water absorption, particularly for beta" materials. However, their higher intrinsic conductivity has prompted much recent work including measurements on Li^+[89], Ag^+[91], K^+[91] and H_3O^+[92] derivatives. While the conductivity of the K^+, Na^+ and Li^+ materials is greater than that of their beta counterparts, the trend is reversed in the case of silver which probably reflects the favourable coordination of the Ag^+ ions[52,93].

All of the above values were derived from measurements on single crystals. Practical applications will, however, probably require the use of sintered polycrystalline samples

in which the conductivity will be lowered by grain boundary and tortuosity effects although the performance of such ceramics can be optimised by the careful control of sintering conditions[94] and by hot-pressing[95].

The conductivity of sodium beta alumina is also modified by spinel-block substitutions. Thus replacement of Al^{3+} by Mg^{2+} allows the incorporation of larger amounts of sodium with a reduction in the number of interstitial oxygens in the mirror planes. The effect of differing levels of MgO dopant on the sodium content and conductivity was studied by Kennedy and Sammells[96]. Similar measurements on materials with other divalent metal ions as dopants were made by Wynn Jones and Miles[97] and Itmai and Harata[98] and a summary of such systems was presented by Boilot *et al.*[99]. Substitution by paramagnetic ions enables physical methods other than diffraction[15] to be used to probe the location of the dopant in the host structure. Akridge *et al.* investigated doping with Cr^{3+} and Cr^{4+}[100], Fe^{2+} and Fe^{3+} [101], Mn^{2+}[102], Co^{2+}[102], Ni^{2+} and Ni^{3+}[102] using spectroscopic techniques. The site adopted by Mn^{2+} is dictated by the way in which doping is achieved. Thus if Mn^{2+} is present during crystal formation it is distributed mainly over the Al(2) and Al(3) tetrahedral sites[103], but if the Mn^{2+} is included by a diffusion process, it substitutes solely at the Al(3) position[104,105]. These conclusions were derived from EPR measurements (luminescence studies had been reported earlier[106,107]), a technique which was also used in the investigation of Gd^{3+}-doped beta alumina[108] and, more recently, EPR experiments have been reported for materials which contain the paramagnetic species Cu^{2+}[109] and Ag^{2+}[110] in the mirror planes. Mössbauer[111] and diffusion studies[112,113]

show that Eu^{2+} may reside both in the spinel blocks and in the mirror planes. Similarly, there is evidence from nuclear magnetic resonance (NMR)[114] and Raman[115] measurements that the monovalent ion, Li^{+}, can also adopt sites within the spinel blocks. Na^{+} may act likewise in the related sodium gallate[116]. A third possibility which is open to divalent ions in polycrystalline samples, is that they may congregate at grain boundaries or crystal imperfections. De Jonghe[117] has suggested that this occurs when CaO is the dopant and such an aggregation of Ca^{2+} at grain boundaries has been recorded by Auger spectroscopy[118].

3.3 Structural studies of other beta and beta" aluminas

Crystallographic studies of several beta aluminas have been reported. These include those of Ag^{+}[71], K^{+}[69,119], Co^{2+}-doped K^{+}[69], Tl^{+}[72,119], Rb^{+}[70], NH_4^{+}[75], H_3O^{+}[74,75] and Na^{+}-Li^{+}[120]. In all cases, the coordinates of the atoms comprising the spinel blocks vary little, but the distribution within the mirror planes is sensitive to the identity of the occupying ions. Unique amongst these structures is that of the Na^{+}-Li^{+} material, in which the lithium ions are displaced off the mirror plane, an arrangement which had been suggested by the spectroscopic evidence (section 3.4). For all other species, there is considerable occupancy at, or close to, the BR site with the remaining cations situated near either the aBR (Ag^{+} and Tl^{+}) or mO positions. The anomalous behaviour of Ag^{+} and Tl^{+} has been interpreted in terms of covalent interactions with the neighbouring O(4) atoms[71,72]. The silver material is of particular interest here. Roth[71] first

derived the silver distribution given in Table 3.2, an arrangement which has been verified at 4.2K and 298K from PND data [121,122]. Reidinger[44], however, re-examined Roth's data and found preference for a slightly altered distribution. The work of Colomban[52] also supports Reidinger's analysis (Table 3.2) although it is possible that all of these results represent nearly equivalent ways of describing a distribution of silver which is disordered along the direction connecting BR and aBR sites.

Reidinger[44] studied the structure of sodium beta alumina as a function of temperature. The relative populations of the BR, aBR and mO sites varied somewhat, but there was no evidence for long-range order at 80K. In the silver material, PND analysis[121,122] shows that the average distribution of silver persists at 4.2K. Le Cars *et al.*[123], Boilot *et al.*[124] and McWhan *et al.*[112,113] studied the X-ray diffuse scattering from this material and they observed the formation of micro-domains, of ∿45Å diameter, corresponding to a two-dimensional superstructure ($a\sqrt{3} \times a\sqrt{3}$) at temperatures below ∿80K (Roth[71] had suggested earlier a domain model for the non-stoichiometry). The extent of this short-range order was seen to decrease as the temperature was raised, until, at 750K, the conducting ions were organised in a two-dimensional quasi-liquid state[123]. For other beta aluminas, Boilot *et al.*[125,126] also observed short-range order effects at low temperatures, with a superstructure for Na^+ and K^+ based on $2a\sqrt{3} \times 2a\sqrt{3}$[125]. For Tl^+ the supercell was of dimensions analogous to that of the Ag^+ material[126].

One of the key questions raised in crystallographic studies has been the mechanism by which charge compensation occurs.

TABLE 3.2

THE CATION DISTRIBUTION IN THE MIRROR PLANES OF SILVER BETA ALUMINA, $Ag_{1+x}Al_{11}O_{17+\frac{1}{2}x}$

	Ag(1)		Ag(2)		Ag(3)	
	Occn.[a]	x[b]	Occn.	x	Occn.	x
Roth[71] x = 0.275	0.67	0.710	0.17	0.807	0.43	0.975
Reidinger[44] x = 0.275	0.31	0.703	0.56	0.76	0.39	0.970
Colomban[52]						
x = 0.25	0.39	0.701	0.42	0.773	0.44	0.976
x = 0.25 (Mg-doped)	0.47	0.698	0.29	0.762	0.46	0.981
x = 0.0	0.37	0.711	0.41	0.772	0.17	0.971

[a] occupancy per mirror plane

[b] all silver sites are of the 6h type, $x\bar{x}\frac{1}{4}$

The first suggestion was that aluminium vacancies were responsible[69]. In Roth's study of silver beta alumina[71], however, he proposed that interstitial oxygen was present which compensated for the excess cations. This hypothesis was substantiated by the direct observation of interstitial aluminium adjacent to the mirror plane[53] which could coordinate to additional oxygen on the mO sites. These Al_i interstitials derive from the Al(1) sites and so the observations of Peters et al.[43] also provide corroborative evidence. The Al_i sites have since been included in many analyses[44,52,119] although, as yet, no direct observation of the interstitial oxygen has been reported. This is because there is usually also considerable cation density at this site[15]. We shall see shortly, that the behaviour of hydrogen-containing beta aluminas provides further evidence in favour of this mechanism. Charge compensation may also be achieved by the replacement of Al^{3+} by divalent ions such as Mg^{2+} and Colomban et al.[52, 127] have used such doping to prepare cation-rich beta aluminas.

Crystallographic studies of beta" materials were initially hampered by preparative problems although work on Ag^{+}[52,93], Na^{+}[15,49,52] and K^{+}[93] beta" aluminas has now been reported. The behaviour of the silver compound is again anomalous in that there is appreciable occupation of the tetrahedrally-coordinated 6c site and this favourable situation presumably accounts for the lowered conductivity in this system. In the other beta" materials, the cations are disordered around this 3-fold (6c) position.

Electron microscopy can also provide useful structural

information. Roth[128] reported the production of silver dendrites in a sample of silver beta alumina under the electron beam. Bevan et al.[129] observed the disordered intergrowth of beta and beta" phases and the occurrence of mixed periods in these structure types was proposed as an explanation for the observed range of stoichiometries[130]. Bovin[51] noted the formation of close-packed slabs across the conduction planes in beta" alumina. Greis and Bevan[50] reported the occurrence of a 3a x 3a x c superstructure in a sample of sodium beta alumina. De Jonghe[131,133], Stevens[134] and Stevens and Miles[135] observed a variety of planar faults and dislocations. De Jonghe[117,133] has also examined grain boundaries in polycrystalline ceramics.

3.4 Studies by other techniques

Kummer[46] first used infra-red (IR) spectroscopy to monitor the effects of water absorption and the exchange of Ag^+ by $H^+(D^+)$ in beta alumina. Subsequently, it was realised that absorptions in microwave, far IR and Raman spectra could yield direct information about the motion of the conducting ions. IR[136,144], Raman[87,145-147] and microwave[142,148,149] measurements on beta aluminas have since been described. The main points of interest which were determined by these studies may be summarized:-

(1) Far IR[138], Raman[145] and microwave responses all favour a diffusive hopping process as the mechanism by which conduction occurs. The agreement between observed vibrational frequencies and those predicted by Wang et al.[150] using the interstitialcy mechanism[80] is good.

(2) Both Raman and IR spectra are modified as the temperature is lowered below ambient. The Raman absorption at 25cm^{-1} in silver beta alumina is, for example, split into two or more components below ~80K[145].

(3) The motion of the mobile ions is strictly perpendicular to the crystallographic c-axis, with little correlation with spinel block modes. The coupling between separate spinel blocks is weak so that vibrations within a given block are effectively independent of those in others[143,144].

(4) The behaviour of lithium beta alumina is anomalous[146] in that the Li^+ ions have some vibrational components parallel to the c-axis[149]. This probably reflects an off-plane location for Li^+[120].

(5) The observed spectra and microwave conductivity vary considerably depending on preparative conditions and, further, there is probably a distribution of barrier heights which are dictated by local conditions within the mirror planes. This gives rise to a series of closely-spaced vibrational modes in the far IR and Raman regions. (Of particular interest in this context would be the preparation of 'stoichiometric' materials in which the extent of such local perturbations may be minimised.)

IR and Raman investigations of beta" aluminas have been reported recently[58] and the optical studies on beta materials have been complemented by inelastic neutron scattering[151,152], heat capacity[153,154] and dielectric susceptibility[155,156] measurements.

Another technique which is capable of monitoring the motion of the conducting ions is nuclear magnetic resonance (NMR) probing, predominantly, the ^{23}Na (I = 3/2) nucleus. Measurements have been reported by Kline et al.[157], Jérome and Boilot[158],

Chung et al.[159,160], Bailey et al.[161], Walstedt et al.[162, 90], Roth et al.[163] and Dubin et al.[164]. In some respects, the information derived from these experiments is similar in nature to that obtained from optical studies. For single crystals, the linewidth of the ^{23}Na resonance can be measured as a function of the angle between the applied field and a chosen crystallographic axis[160,161]. Such measurements indicate that the sodium ions occupy several sites at low temperature[161]. The linewidth may be measured as a function of temperature[160,161] and above ∿170K considerable narrowing is observed as a result of the $^{23}Na^{+}$ ionic motion, from which an activation energy for diffusion can be calculated. The value, $E_a \sim 0.16eV$, of Chung et al.[160] is in good agreement with that obtained from diffusion (0.17eV[59]) and conductivity measurements (0.13eV[79]) but values quoted by other authors are lower than the diffusion values[161], a disparity which has yet to be resolved[90]. No ^{27}Al narrowing was observed as would be anticipated[157,165].

Spin-lattice relaxation times[158,162] also reflect Na^{+} ion mobility. Two such values for T_1 were noted at low temperature[158] indicating that two different types of motion were occurring. Further information is given by variations in the asymmetry parameter[160] and nuclear quadrupole coupling constant [53]. The effect of water[157,166] or additives[163,53] on the ionic mobility has been probed and, more recently, in a study of alkali-rich material[164], the existence of sodium with an anomalously low mobility has been reported. This phenomenon had been noted in exchange experiments[167], although the NMR study [164] presents evidence for the occurrence of these anomalous Na^{+} ions within the mirror planes. Measurements using the $^{7}Li^{+}$

ion have also suggested unusual behaviour for this species in Na-Li beta alumina[115]. ^{1}H NMR studies will be mentioned shortly.

The behaviour of the conducting ions in beta aluminas has been considered theoretically by several authors. Whittingham and Huggins[80] suggested, from calculation of Haven ratios [80,168], that an interstialcy mechanism was operating. Rice and Roth[169] considered the mobile species in terms of localised and free-ion states. Van Gool and Bottleberghs[170] discussed a domain model, while Huberman and Sen[171] viewed the conducting species as quasi-liquids. Sato and Kikuchi[172] considered diffusion characterised by a path probability in an interacting system. The analysis by Wang et al.[150] of the interstialcy mechanism has given good agreement with experiment, although their approach was undoubtedly simplistic in ignoring the implications of defects such as interstitial oxygen. Computer simulations have been reported by Murch and Thorn[173], Wolf[174] and De Leeuw and Perram[175].

3.5 Hydrogen-containing beta aluminas

Proton conduction in organic and inorganic solids has recently been reviewed[176]. Suitable conductors would find an immediate application in fuel cells, but typical materials, such as KH_2PO_4[177] and $Li_2SO_4.H_2O$[178], have conductivities less than $\sim 10^{-7} \Omega^{-1} cm^{-1}$ at 25°C. Improved performances have been reported for perchloric acid monohydrate, $HClO_4.H_2O$[179], and the uranyl phosphate $HUO_2PO_4.4H_2O$[180], but all of these systems have limited thermal stability. The preparation of beta

aluminas which contain protons in the conducting planes could potentially provide systems with reasonable conductivity and with good thermal stability. Some early experiments had suggested that high proton mobilities might indeed be attained [181,92], although more recent measurements have moderated the early enthusiasm.

The effect of absorbed water on the conductivity of beta aluminas has been studied by several authors (see ref. 182 and refs. cited) although it is now generally accepted as being detrimental[182]. Apart from this unwanted ingression, protons can be introduced quantitatively into the conducting planes by three methods.

Direct action of H_2 or D_2 gas on silver beta alumina at 300°C[46] yields the anhydrous hydrogen (deuterium) beta alumina. IR spectroscopy shows that this hydrogen is tightly bound[46] and structural studies indicate that, at least at 4.2K, it is bonded to the spacer oxygen in a hydroxyl linkage [73,181]. This preparative route appears to be the only reliable way of obtaining the anhydrous material whose structure is discussed as a function of temperature, in Chapter 4. On exposure to air, moisture uptake is observed and complete hydration may apparently be achieved by boiling in nitric acid[83].

The action of hot concentrated sulphuric acid on sodium beta alumina[66,67] effects exchange by H_3O^+, although this is generally accompanied by decomposition with the formation of aluminium sulphate. Saalfeld *et al.*[66] and Nishikawa *et al.*[67] followed the heat-induced changes in the hydronium beta alumina thus produced. Kato and Saalfeld[74] determined the structure of a material of nominal composition '$1.79H_2O.11Al_2O_3$' and they found that the oxygen of the H_3O^+ ion was

located on the BR site (a similar arrangement was also deduced in the analysis by Colomban et al. of stoichiometric hydronium beta alumina, $(H_3O)Al_{11}O_{17}$[75]). This preparative route and the dehydration of hydronium beta alumina have been re-investigated by Breiter et al.[184], Roth et al.[185] and Colomban et al.[186], the last using IR and Raman measurements. The conclusions which may be drawn from these studies are summarised:-

(1) approx. 3 moles 'H_2O' are incorporated per mole Na_2O, yielding a formula of $(H_3O)_{1+x}Al_{11}O_{17+\frac{1}{2}x}$ for hydronium beta alumina. Further moisture may be adsorbed on crystallite surfaces or crystal imperfections[182,184] although this adsorbed water is lost at 100-200°C[184]. Spectroscopic measurements[186] have revealed the existence of species such as $H_5O_2^+$. and $H_7O_3^+$ in the fully hydrated material.

(2) Weight loss corresponding to 1[184] - 1.8[66] moles H_2O occurs reversibly at ∿220°C[185]. Roth et al.[185] have termed this intermediate phase H^+-H_3O^+ beta alumina. IR and Raman studies[186] show that the H_3O^+ species in this material are isolated and that they occupy the BR site.

(3) Further weight loss occurs irreversibly at ∿800°C[67] giving a disordered intermediate phase which transforms at ∿1100°C to α-Al_2O_3[67] (the decomposition of the parent sodium compound occurs above 1400°C).

The conductivity of hydronium beta alumina, $(H_3O)_{1.3}Al_{11}O_{17.15}$ was found to be $10^{-11}\Omega^{-1}cm^{-1}$ at 20°C[83] whereas that of 'H^+-H_3O^+' is lower with $\sigma = 10^{-6}\Omega^{-1}cm^{-1}$ at 300°C[83]. The hydronium material has also been examined using ^{1}H-NMR[76,187]. Slade et al.[76] observed motional narrowing due to translation above 260K although the mechanism for relaxation below this temperature was not ascertained.

The third way in which protons may be introduced into the mirror planes is in the exchange of Na^+ by NH_4^+ in molten ammonium nitrate[46,59]. (Exchange of Ag^+ by NH_4^+ has also been described[68].) Colomban et al.[75] determined the structure of this material. One NH_4^+ group is close to the BR position while a second, of lower occupancy, is situated between mO and aBR sites. IR and Raman data were used to suggest possible locations for the hydrogens although the c-axis constant of 22.808Å was shorter than that given by Kummer[46] (22.888Å) implying that the NH_4^+ for Na^+ exchange may have been incomplete.

The thermal stability has been investigated by Colomban et al.[75], Hooper[84] and Farrington[89]. Substantial weight loss is observed at ∿460°C[84]. Farrington[89] suggests that this corresponds to complete loss of NH_3 to give stoichiometric hydrogen beta alumina which may pick up moisture, reversibly, at 180-225°C to form stoichiometric hydronium beta alumina. This scheme is in accord with the observations of Colomban et al.[75] who studied the hydronium material produced in this way. Conductivity measurements are reported by Colomban et al.[75], Hooper[84,68] and Farrington and Briant[75]. The activation energy in the range 25-250°C is 0.47eV[84,75], with $\sigma_{200°C} = 8 \times 10^{-4} \Omega^{-1} cm^{-1}$[68], although after the partial decomposition at ∿500°C, the conductivity is much lower with $\sigma_{500°C} = 3 \times 10^{-6} \Omega^{-1} cm^{-1}$.

Pulsed ^{1}H-NMR studies have been reported by Slade et al.[188] who observed motional broadening and determined a residence time between jumps of 4×10^{-9} sec. Gourier and Sapoval[189] measured ^{1}H-NMR spectra in the range 77-360K and

at 4.2K. Between 77K and 240K there was a single line corresponding to rapid 90° reorientation about a C_2 axis perpendicular to c and above 240K considerable motional broadening due to jump diffusion was apparent. The motion of the ammonium ion has also been examined, using inelastic neutron spectroscopy, by Axe et al.[190] who found that below 570K jump reorientation was rapid compared to translation diffusion, with a jump frequency of $10^{12} sec^{-1}$ at 298K. However, the models which they considered were derived from studies on the ammonium halides and recent work[191] suggests that the motional behaviour may be more complex. Raman measurements were reported by Bates et al.[192]. At 11K they observed bands at 165 and 145cm^{-1} which they assigned to translational modes.

In keeping with other aspects of the properties of beta aluminas, studies of hydrogen-containing beta" materials are relatively few in number. Farrington et al.[92] have shown that hydronium beta" alumina may be prepared by exchange in conc. H_2SO_4 and they reported a high conductivity of $5 \times 10^{-3} \Omega^{-1} cm^{-1}$ at 25°C for this system, although later work on single crystals[89] suggests that the true value is closer to $\sim 5 \times 10^{-5} \Omega^{-1} cm^{-1}$. This latter figure agrees with that derived from inelastic neutron scattering experiments[193]. The material loses water, reversibly, at 250-300°C. Further dehydration, accompanied by decomposition to α-Al_2O_3, then follows at 700°C. Exchange of Na^+ in ammonium nitrate apparently does not give complete exchange by NH_4^+, but rather some (H_3O^+) or $H^+(H_2O)_x$ is also incorporated[85]. Ammonia and water are lost at 230-350°C. Further weight loss occurs at 450-500°C followed by final degradation to α-Al_2O_3 above 750°C. The conductivity of the NH_4^+/

$H(H_2O)_x^+$ beta" material is $\sim 10^{-4}\Omega^{-1}cm^{-1}$ at 25°C[85].

3.6 Stoichiometric beta aluminas

The stoichiometric composition $MAl_{11}O_{17}$ does not exist as a stable entity in the equilibrium phase diagram[45]. In view of the locally inadequate distribution of charge about the mirror planes, it has been proposed[194] that such a species would not exist, a view supported by the work of Sato and Hirotsu[130]. The preparation and structure analysis of anhydrous deuterium beta alumina[73,181] suggested, however, that the stoichiometric composition might be approached in undoped materials. Colomban et al.[75] produced stoichiometric hydronium beta alumina by the thermal decomposition of the ammonium compound and back-exchange in molten silver nitrate could then be used to prepare stoichiometric silver beta alumina[52,195,196]. This material displays superlattice ordering at temperatures below ~250K and a model for this superstructure was proposed[196] based on a comparison with that suggested by the X-ray diffuse scattering studies for the non-stoichiometric silver compound[124]. Structural details have recently been reported[230]. At about room temperature, this superlattice disappears[196], suggesting that an order-disorder transition might occur in this system. Both of these preparative routes involve the introduction of protons into the mirror planes and the behaviour of hydrogen-containing beta aluminas will be referred to throughout the first half of this thesis.

3.7 Analogous systems

So far, we have considered only those materials which

contain predominantly Al^{3+} as the cation in the spinel blocks. Analogous systems are well known in which Al^{3+} is replaced by Ga^{3+}, the alkali gallates*, or Fe^{3+}, the ferrites. The magnetoplumbites, $M_A^{2+}O.6M_{B2}^{3+}O_3$, have an increased particle density in the connecting layers and they are, as a result, poor ionic conductors.

The formation of potassium beta gallate was first reported by Foster and Stumpf[197] and the preparation of both beta and beta" analogues has since been studied in more detail[198-201]. The c-axis constants are substantially reduced with respect to the beta aluminas (for example 22.13Å[200] *cf.* 22.53Å for the sodium beta materials). Brinkhoff[202] measured the conductivity of both sodium and potassium beta materials, $M(Al/Ga)_{11}O_{17}$, as a function of gallium content. He noted a practically complete range of solid solubility and found that while the conductivity of the sodium material was little affected by the extent of gallium substitution, that of the potassium compound decreased as the Ga/Al ratio increased. More recent measurements by Foster[116] suggest that up to 10% of the sodium in beta gallate may substitute for Ga in the spinel blocks.

IR[203] and Raman[204] measurements on both sodium beta and beta" materials have been reported. The spectra are directly comparable with those of the alumina systems when allowance is made for the difference in atomic mass. Low frequency Raman bands corresponding to translational modes are observed at $57cm^{-1}$ and $69cm^{-1}$ in the beta and beta" materials respectively. Moisture absorption by beta" gallate has been studied by Foster and Arbach[205] and EPR measurements on systems containing the

* *The problems of nomenclature are compounded in this case by the occurrence of a genuine allotrope of the oxide which has been named* β-Ga_2O_3.

divalent ions Cu^{2+}, Mn^{2+} and Eu^{2+} were reported by Title and Chandrasekhar[206].

In the system M_AO-Fe_2O_3-M_BO, a wealth of materials is formed[207]. These have similar structures, closely related to those of the beta aluminas, but with varying spacings between the connecting layers. The intergrowth of different periodicities in these compounds prompted Sato and Hirotsu[130] to suggest that the same situation may arise in the beta aluminas although such a wide variety of structures has not yet been found. For ionic conductivity we are most interested in the materials $M_2O{:}nFe_2O_3$, around the compositions $MFe_{11}O_{17}$ and MFe_5O_8, which are the analogues of the 2B4-β and 3B4-β" aluminas respectively.

The preparation of such ferrites has been reported by Dyson[208] and Roth[209] (beta) and Rooymans *et al.*[210] (beta"). The electrical conductivity was measured by Roth[209]. Both ionic and electronic components were apparent, the electronic contribution resulting from the presence of Fe^{2+} ions. The electronic component in $K_{1+x}Fe_{11}O_{17}$ was measured as a function of x by Dudley *et al.*[211] who reported a nearly linear increase in electronic conductivity with increasing x in the range x = 0.09-0.65, consistent with an enhancement of $[Fe^{2+}]$ required for charge compensation. The ionic conductivity and chemical diffusion coefficients in this material were measured by Dudley and Steele[212] who noted that an ordering process occurred at the composition x = 1.7, which presumably reflects an increase in the number of triply-occupied mirror planes. Takahashi *et al.*[213] reported that the electronic conductivity was lowered by the addition of ZnO, MgO or NiO. Potassium ferrite is completely miscible with potassium gallate in all

proportions[214,215] and conductivity measurements on such mixed materials have been reported by Kuwabara and Takahashi[214]

The Fe^{3+} sites in potassium ferrite have been characterised by Mössbauer measurements[216,217] and similar experiments on mixed Fe-Ga and Fe-Al materials are reported by Howe and Dudley[218]. Hever[219] examined the material $K_xNa_{1-x}Fe_7O_{11}$ and found that whereas the Na^+ ions were relatively immobile, the K^+ ions could be exchanged in sodium nitrate melts which may represent one of the first examples of 'co-ionic' behaviour[86,88].

The alkali ferrites and gallates are structurally very similar to the beta aluminas. In the magneto-plumbite structure of $PbFe_{12}O_{19}$, the material again consists of spinel blocks, $(Fe_{11}O_{16})^+$, but the connecting layers must now accommodate a '$PbFeO_3^-$' unit. This is achieved by the Pb and Fe occupying the BR and aBR sites respectively, while the three oxygens are situated on 6h sites about the normal spacer oxygen position. This is a well-ordered arrangement. There is no scope for ionic mobility and the c-axis constant is decreased with respect to the beta aluminas. The material $LaAl_{11}O_{18}$ apparently has a structure intermediary between the beta alumina and magneto-plumbite types[220,221].

It is clear from this introduction, which is by no means exhaustive, that the beta alumina family has been subjected to close scrutiny by a wide range of techniques. In recent years, it has probably been one of the most extensively studied materials in solid state chemistry, but in the subsequent chapters we shall find that explanations for some of its

properties still prove elusive. There is yet a lot to be learnt about beta aluminas.

CHAPTER 4

DEUTERIUM BETA ALUMINAS

4.1 Introduction

Hydrogen-containing beta aluminas have been discussed in the Introduction (section 3.5). A preliminary structural study of deuterium beta alumina[73,181] suggested two interesting possibilities. Firstly, that the system had the stoichiometric composition $DAl_{11}O_{17}$. Secondly, that while at 4.2K the deuterium was bonded to the spacer oxygen (O(5)) in a hydroxyl linkage, at 823K the deuterium was delocalised in the mirror plane. This was taken to be indicative of possible proton mobility.

Conductivity measurements on the hydrated material, hydronium beta alumina ($H_{1.24}Al_{11}O_{17.12}\cdot 1.3H_2O$) revealed a low conductivity of $\sim 10^{-11}\Omega^{-1}cm^{-1}$ at 20°C[83]. However, the conductivity of the analogous hydronium beta" alumina ($H_{1.68}Al_{10}Mg_{0.84}O_{16.68}\cdot 2.8H_2O$) was found to be $5 \times 10^{-3}\Omega^{-1}cm^{-1}$ at 25°C[92], although more recent measurements on single crystals have given a lower value of $\sim 5 \times 10^{-5}\Omega^{-1}cm^{-1}$[89]. The difference between the beta and beta" materials is striking in view of the basic similarity between their structures.

In this chapter, the results of powder neutron diffraction (PND) measurements on deuterium beta alumina at the four temperatures 4.2K, 298K, 573K and 720K are presented. In addition, a PND study of deuterium beta" alumina at 4.2K is described.

4.2 Sample Preparation*

a) Deuterium beta alumina

The starting material was MONOFRAX sodium beta alumina,

* *The preparations were performed by Mr. C.F. Sampson of A.E.R.E. Harwell, for whose cooperation I am very grateful.*

of approximate composition $Na_{1.3}Al_{11}O_{17.15}$, which was ground to less than 37μm particle size. It was converted, by repeated exchange in molten silver nitrate at ∿300°C, to silver beta alumina which was washed and dried under vacuum at ∿350°C. Reduction was effected by deuteration (D_2 Air Products >99.9%) in a sealed silica system. The deuterium was rapidly absorbed with silver metal plating out on the surface of the crystallites to give the previously white powder a brown colouration. Moisture evolution was observed during the exchange. The liberation of water was also noted in the earlier preparation[73] In both cases, the silver beta alumina was thoroughly dried, and thus, in conjunction with the results of structure analysis, this provides strong evidence for the formation of anhydrous stoichiometric $DAl_{11}O_{17}$ according to:

$$Ag_{1.3}Al_{11}O_{17.15} + 0.65D_2 \rightarrow DAl_{11}O_{17} + 0.15D_2O + 1.3Ag$$

The evolved D_2O was pumped off and fresh D_2 admitted. The sample was then transferred, in a dry glove box, into a 12mm diameter vanadium can which was tightly sealed with a gold O-ring. With the first sample of $DAl_{11}O_{17}$[73] this type of seal proved ineffective and, on heating to 823K, D_2 gas was lost with the concomitant re-introduction of silver into the structure (see Chapter 5). In air, this reverse exchange occurs at ∿570K, but in the experiments described here, the sample can proved to be gas-tight.

b) Deuterium beta" alumina

The starting material was British Rail Li-stabilised sodium beta" alumina. The results of elemental analysis (I in Table 4.1) are consistent with several formulae. The first

three correspond to complete location of Li^+ within the spinel blocks and hence not subject to exchange. However, the Li/Al ratio is observed to decrease after the exchange. It is therefore possible that some Li^+ is located in the conducting plane and is subsequently lost in the exchanges.

From the above starting material, conversion to potassium beta" alumina was accomplished using gas phase exchange with KCl at 1000°C after the method described by Tennenhouse[222] The product was treated with 2M HCl at 80°C to give hydrated hydrogen beta" alumina which was then exchanged in molten silver nitrate at ∿300°C. The resulting silver beta" alumina was washed, dried <u>in vacuo</u> and reduced with deuterium gas (D_2 Air Products >99.9%) at 450°C. No significant pressure drop was apparent when the deuterium was introduced but silver metal did appear and some moisture evolution was observed. The subsequent analysis is given as II in Table 4.1. The sample was then transferred under dry N_2 into a 15mm diameter vanadium can which was sealed with a gold O-ring.

In a second preparation, completed later and which followed the same course as that outlined here, the deuterium gas was admitted at the lower temperature of 200°C. In this case, a significant pressure drop was found on admittance of D_2, but no significant evolution of water was seen. The elemental analysis of this second sample is given under III in Table 4.1. In studies of the thermal stability of 'ammonium' beta" alumina, Farrington and Briant[85] have observed the following reactions:

$$(NH_4)_{1.00}(H_3O)_{0.67}Al_{10.33}Mg_{0.67}O_{17} \underset{230°C}{\overset{330°C}{\rightleftharpoons}} H_{1.67}Al_{10.33}Mg_{0.67}O_{17} \qquad (1)$$

TABLE 4.1

ELEMENTAL ANALYSIS OF BETA" ALUMINA SAMPLES

Sample		Na	Al	Li	K
I	Weight%	7.065	45.35	0.3445	-
	Atom%	0.3073	1.6808	0.0496	-

Ratio Li/Al 0.0295

Formula* $Na_{1.769}Al_{10.639}Li_{0.314}O_{17}$, $Na_{1.935}Al_{10.584}Li_{0.312}O_{17}$

$Na_{1.954}(Al_{10.684}Li_{0.316})O_{17.161}$, $Na_{1.959}Li_{0.029}(Al_{10.713}Li_{0.287})O_{17.207}$

		Na	Al	Li	K
II	Weight%	0.06	37.9	0.261	⟨0.01
	Atom%	0.00026	1.4047	0.0376	⟨0.00026

Ratios K/Al ⟨0.0002 Na/Al 0.00019 Li/Al 0.0268

		Na	Al	Li	K
III	Weight%	0.06	37.0	0.252	⟨0.01
	Atom%	0.00026	1.3713	0.0363	⟨0.00026

Ratios Na/Al 0.00019 Li/Al 0.0265

* *The analyses are not sufficiently self-consistent to enable the exact formula to be derived. In addition, we do not know whether vacancies in the spinel block and/or additional oxygen may be present.*

$$H_{1.67}Al_{10.33}Mg_{0.67}O_{17} \xrightarrow{420\text{-}500°C} H_{0.33}Al_{10.33}Mg_{0.67}O_{16.33} \quad (2)$$

The temperature of our first preparation (450°C) falls within the range of reaction (2) and it is likely that our observations stem from this decomposition. The loss of hydrogen as water implies concomitant loss of oxygen, either from the conduction plane (O(5)) or from the spinel blocks. Bovin[51] has directly observed the formation of close-packed slabs across the conduction planes in sodium beta" alumina, albeit under the specialised conditions in an electron microscope. This collapse occurs via sodium loss which is prompted by the electron beam. If this type of decomposition were occurring here, the re-organisation of the spinel blocks implied by the extent of reaction (2) would be apparent in subsequent structure analysis. If, on the other hand, oxygen were lost from spinel block sites, the beta" structure could be largely maintained.

For the second sample, the different observations during preparation suggest that the product differs and presumably corresponds to a deuterium beta" alumina with nearly two protons (deuterons) in each conduction plane. Structure analysis of this second material is not described in this thesis.

4.3 Powder neutron diffraction experiments

Powder neutron diffraction (PND) measurements were performed on the PANDA diffractometer at A.E.R.E. Harwell. A mean wavelength of 1.5172Å was selected from the [511] planes of a Ge monochromator at a take-off angle of 88°. The wavelength was accurately calibrated by a peak-fitting of the 111, 200, 220 and 311 reflections from a standard Ni sample. For the liquid helium temperature scans, the samples were loaded into a

TBT associates cryostat in which the sample cans are immersed in 1.He. At room temperature, the sample can was mounted on goniometer arcs and accurately aligned at the centre of the diffractometer circle by means of a free-standing telescope. For temperatures above ambient, the sample container was mounted in an evacuable furnace with a Ta element. The evacuation is necessary to prevent degradation of the vanadium can by oxygen. For all of these runs, the height of the sample and the collimating slits of the incident beam were adjusted with reference to polaroid photographs taken with the through beam. The position of the sample was clarified by strips of Cd attached to the top and bottom of the can.

The region of 2θ, available to the low-angle counter, from 6° - 104.5° was then scanned, with counts being recorded every 0.1°. The measurement time at each point was determined by the time taken for a fission counter placed in the direct beam to record a preset number of counts. The counting times for each run are given, in chronological order, in Table 4.2.

TABLE 4.2 COUNTING STATISTICS FOR THE PND MEASUREMENTS ON PANDA

Sample	Can diameter	Temperature	Monitor Count x 10^{-3}	Total time hours	App. time per pt. secs.
D beta" alumina	15mm	4.2K	517	50	160
D beta alumina	12mm	4.2K	750	66	220
D beta alumina	12mm	298K	460	45	140
D beta alumina	12mm	573K	750	66	220
D beta alumina	12mm	720K	750	66	220

The experimental arrangement on the Panda diffractometer is such that the counters are susceptible to occasional bursts

of increased extraneous radiation[223] and to enable the resulting spurious points in the PND pattern to be recognised and corrected, the data from each of the three central counters were plotted individually. For each of the runs, the data from these three equatorial counters were then collated to yield the complete profile in the range $6° \leqslant \theta \leqslant 114.5°$. The data were analysed using the profile refinement techniques which were outlined in the Introduction (section 2.3).

Scattering lengths of 0.345 for Al, 0.583 for O and 0.667 for D (all x 10^{-14}m) were taken from Bacon[13]. During refinement, the region $2\theta < 25°$ or 30° was omitted from the calculations because the peak shapes at low angles show marked deviations from ideal gaussians. The areas within which reflections from the silver metal contribute appreciable intensity were also excluded ($\sim$5° in all). For the runs at 573K and 720K, three peaks are also observed from the Ta element of the furnace, necessitating the exclusion of a further 1.5° (see Figure 4.7).

4.4 Results

a) Deuterium beta alumina at 4.2K

Previous work[73] suggested that the position(s) of the deuterium in the structure would be indicated by $/F_{obs}/$ Fourier syntheses based on a phasing model of the atomic coordinates of the spinel block atoms and of the spacer oxygen, O(5). Initial refinements then involved the scale, cell and instrumental parameters together with these atomic coordinates. With R_P = 0.2183, R_{WP} = 0.1813, an $/F_{obs}/$ Fourier synthesis was calculated. Little positive scattering density was apparent in the mirror plane (z = 0.25) save for at the O(5) position. However, peaks

were found close to O(5) but lying off the mirror plane and, on the assumption that these reflected genuine occupation, a deuterium atom was entered at this position (0.25 0.5 0.275 12k). Subsequent refinement of atomic parameters, including the occupation number of this site, did converge to an improved agreement R_P = 0.2077, R_{WP} = 0.1686. The deuterium coordinates were 0.2164 2x 0.28717 although the occupation number was considerably less than unity at 0.55.

Later analyses showed that this model was artificial, but, at this stage, this was only indicated by the low site occupation and by the behaviour of O(5). When displaced from the 1/3 $\bar{1}$/3 $\frac{1}{4}$(2c) site to the more commonly occupied x $\bar{x}$ 1/4 (6h) position, refinements diverged even with the application of shift factors. This behaviour was taken to indicate the occupation by deuterium of sites within the mirror plane. Indeed, when a deuterium was placed at 0.5202 0.5673 1/4 (12j), the position reported by Tofield et al.[73], and its occupation refined together with that of the false 12k site, an improved agreement was obtained with R_P = 0.2045, R_{WP} = 0.1558. After further least-squares adjustment of all atomic parameters, it became apparent that all the deuterium was localised in the mirror plane, close to the x $\bar{x}$ 1/4 (6h) site with x ≃ 0.5.

These initial stages of structure solution and refinement have been detailed here to indicate the limitations of Fourier syntheses based on structure factors derived from the profile refinement of PND data. Indeed, although such Fourier methods have twice been quoted as a tool for structure solution [73,224], in very few of the powder experiments described here have they been helpful in initial structure elucidation. In later stages, when the deconvoluted structure factors more

nearly represent the true $/F_{obs}/$, Fourier and difference Fourier syntheses may give a more accurate representation of the structure or indicate minor irregularities in the derived model.

Following the correct location of the deuterium, iterative least-squares procedures were used to improve all the atomic and instrumental parameters. A preferred orientation correction was considered in several refinements, but the varied parameter (Equation 17, Chapter 2) converged to a low value in both this and the other data sets collected at higher temperatures and the correction was subsequently discarded. The structural parameters which emerged were in agreement with those reported by Tofield et al.[73]. Although our starting composition was slightly less sodium-rich, a deuterium occupation of close to 1.0 was apparent. To gauge the sensitivity of this occupation to changes in other parameters, anisotropic temperature factors were introduced and the residuals improved from R_P=0.1480, R_{WP}= 0.1182 to R_P= 0.1341, R_{WP} = 0.1048. No instability occurred in these refinements and both O(5) and D had large β_{11} and β_{12} components as compared with the spinel-block atoms. However, the O(5)-D bond length was long at 1.19Å. Displacement of either/both O(5) or/and D from the 3-fold 6h to 12j positions which are separated by the $x\bar{x}$ mirror plane gave less good agreements. In addition, many of these refinements were unstable and, in some, the D-O(5) bond length was increased. At this stage, O(5) was close to the position normally found in metal beta aluminas with $x < 1/3$. Figure 4.1 shows a representation of the mirror plane at $z = 0.25$. It is clear that a reduction in D-O(5) separation is achieved by a change in x of O(5) from $x < 1/3$ to $x > 1/3$, without recourse to the more general 12j sites.

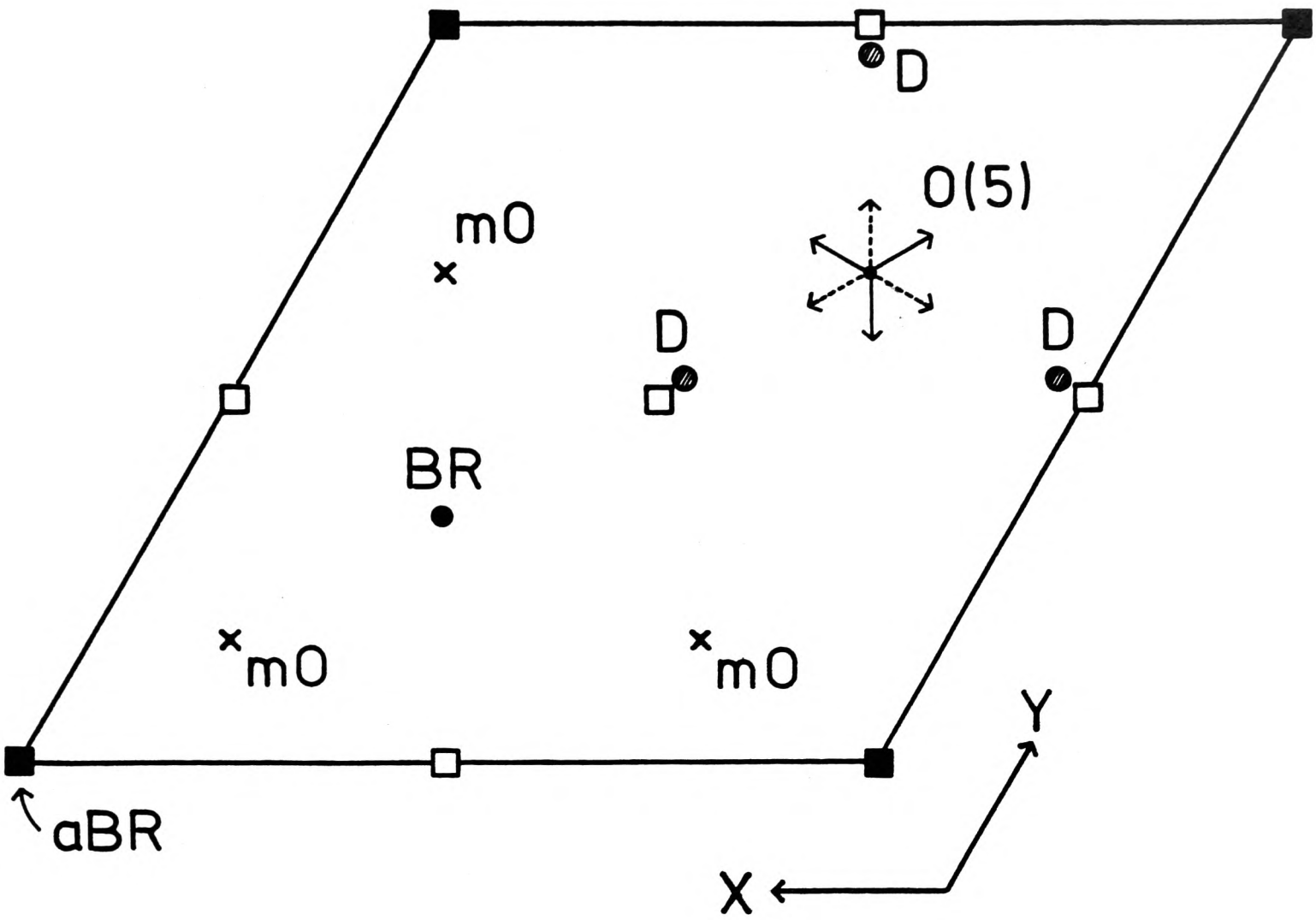


Figure 4.1. A representation of the mirror plane in $DAl_{11}O_{17}$. *The projections of the bordering O(2) (○) and O(4) (●) atoms and the two possible displacements of O(5) to 6h sites (solid and dashed lines) are indicated.*

This displacement was then tested in refinement. The residuals were essentially identical for x = 0.2965 (R_P = 0.1330, R_{WP} = 0.1018) and for x = 0.3712 (R_P = 0.1329, R_{WP} = 0.1018). The D-O(5) bond length was then 1.06Å and it is this model which is presented in the tables. Finally, when these best residuals had been obtained, a 12j displacement of deuterium was again considered. The least-squares process diverged.

In all of the successful refinements, the deuterium occupation remained close to 1.0 and, further, there was no evidence for occupation of any other mirror-plane sites. For example, the occupation number of a silver atom placed at the stoichiometric silver position (see Chapter 5) -0.2237 $\bar{x}$ 1/4 (6h) converged to a value of 0.07(7). In the final refinements there

was a total of 48 variable parameters. Final instrumental and atomic parameters are given in Tables 4.3-5, with bond lengths and angles in Tables 4.6-7. Figure 4.2 displays the z = 0.25 sections of $/F_{obs}/$ and $/F_o - F_c/$ Fourier syntheses using structure factors derived from the final refinements. In contrast to the $/F_{obs}/$ syntheses mentioned above, the deuterium position is now clear. No significant features were apparent in any of the difference Fourier sections, although the errors inherent in the derived structure factors are such that it is unlikely that, say, slight occupation of the interstitial aluminium site would be evident in such a synthesis. The final observed and calculated diffraction profiles are shown in Figure 4.3 and observed and calculated reflection intensities are given in Appendix I.

b) Deuterium beta alumina at 298K

The course of structure solution and refinement paralleled that for the 4.2K data. The initial $/F_{obs}/$ Fourier synthesis suggested occupation of a 12j site 0.380 -0.225 1/4, but this is chemically unreasonable and refinements revealed that the deuterium again occupied the 6h site x $\bar{x}$ 1/4 with x $\sim$ 0.5. Refinement then followed the course outlined above, with anisotropic temperature factors being introduced in later stages. Displacements of O(5) and D to 12j positions were also considered. Such a shift for O(5) always gave slightly worse agreements and, for D, a similar situation occurred, with the deuterium coordinates converging close to the 6h position. A displacement away from the mirror plane to a 12k position, x $\bar{x}$ z, also gave poorer fits. The 6h sites were therefore again taken to represent most accurately the actual situation within the

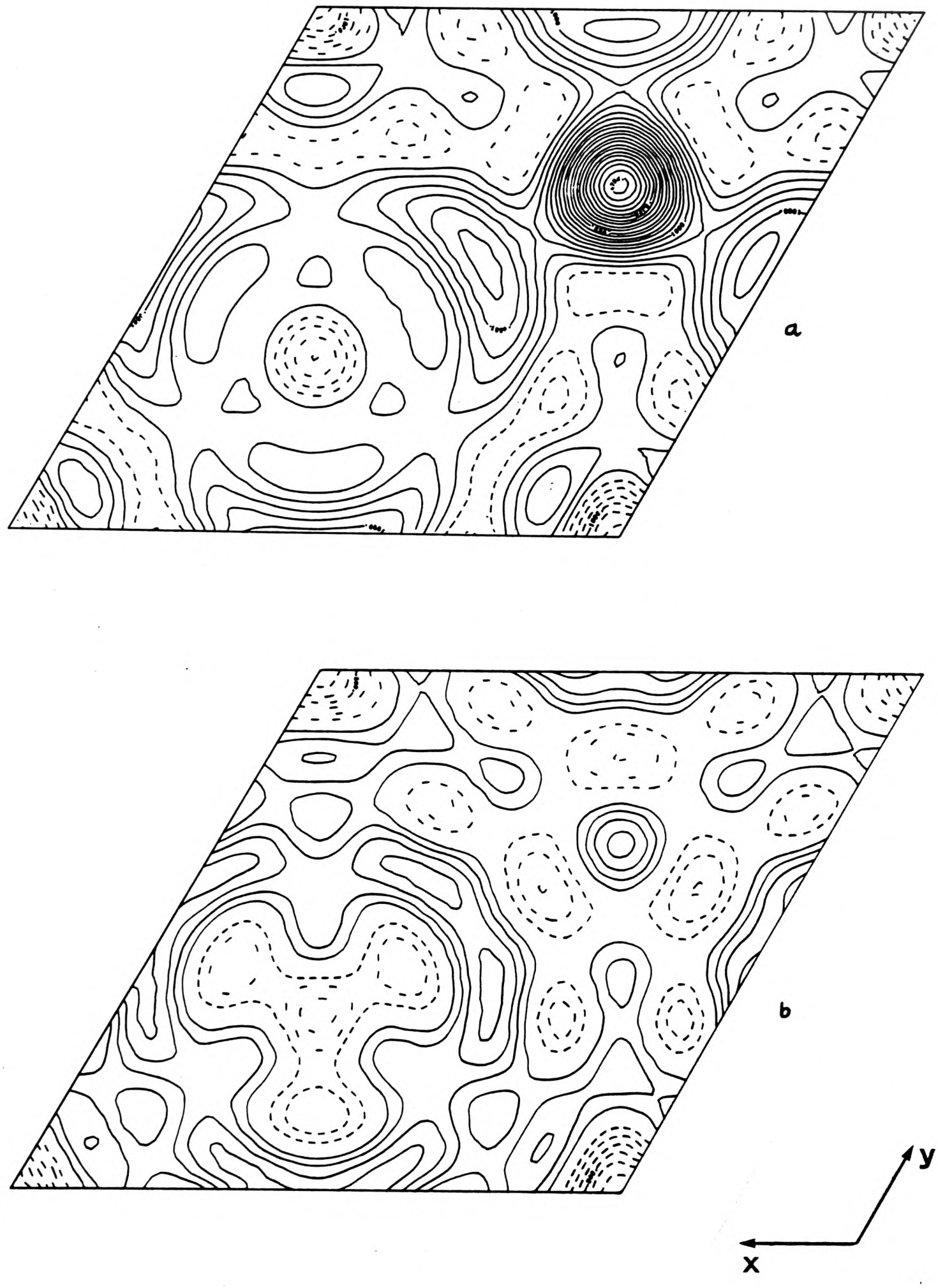


Figure 4.2. The z = 1/4 sections of final /F_{obs}/ (upper) and /F_{obs}-F_{calc}/ (lower) Fourier syntheses derived from the PND data refinements of $DAl_{11}O_{17}$ at 4.2K.

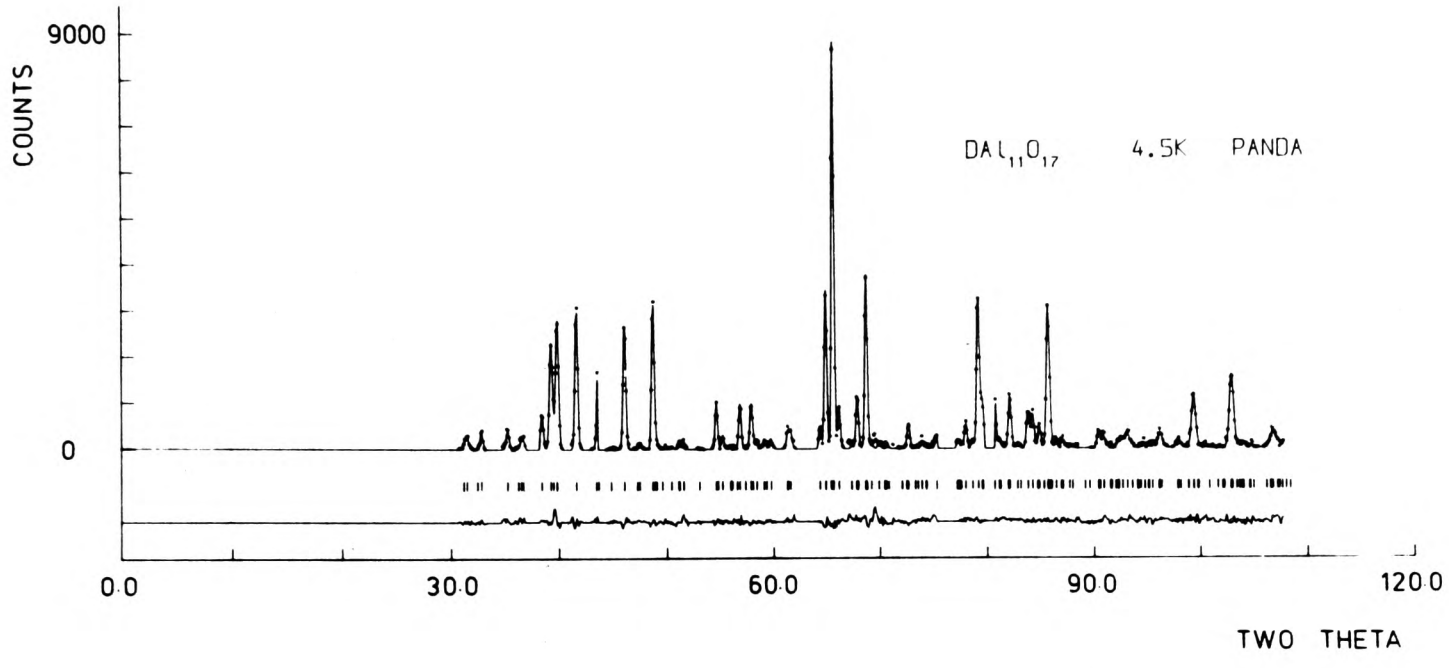


Figure 4.3. Final observed (dots), calculated (continuous line) and difference (lower) diffraction profiles for $DAl_{11}O_{17}$ at 4.2K (PANDA diffractometer). Reflection positions are marked by bars.

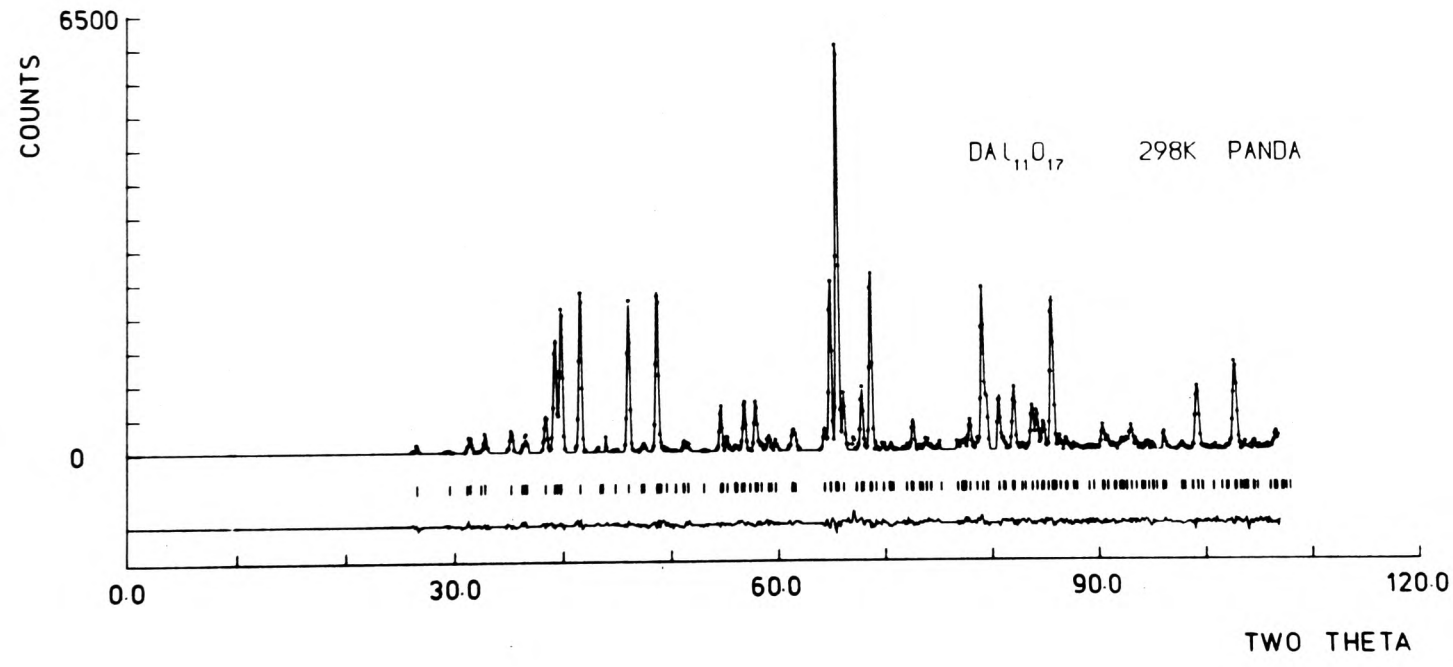


Figure 4.4. Final observed, calculated and difference diffraction profiles for $DAl_{11}O_{17}$ at 298K. (Legend as above.)

structure.

The final observed and calculated profiles are displayed in Figure 4.4, final instrumental and atomic parameters are given in Tables 4.3-5 with bond lengths and angles in Tables 4.6-7. The observed and calculated reflection intensities are listed in Appendix I. The final residuals, R_P = 0.1161, R_{WP} = 0.0924 (Table 4.3) are slightly better than those obtained with the other data sets. This is despite the shorter time spent in data collection (Table 4.2) which is manifested in the greater R_E for this data set. This probably reflects the improvement in data quality which results when the incident and diffracted beams do not have to pass through the apparatus which is required for temperature control. It is customary, in PND experiments, to collect data at liquid He temperature, where appropriate, to minimise thermal vibration. The results described here suggest that improved structure definition, for relatively refractory materials, would be obtained if data were collected under ambient conditions.

The z = 0.25 sections of $/F_{obs}/$ and $/F_o - F_c/$ Fourier syntheses are depicted in Figure 4.5. The definition is striking. This is a further consequence of the improved quality of the observed data set. The deuterium is clearly seen to lie on the x $\bar{x}$ mirror plane, the 6h site. The atomic arrangement will be discussed shortly, but, from the course of the refinements outlined above, it would appear that the atomic distributions at 4.2K and 298K are essentially identical. The improved residuals for the 298K data set therefore suggest that Figure 4.5(a) depicts this distribution more accurately than the corresponding section derived from the 4.2K data set (Fig. 4.2(a))

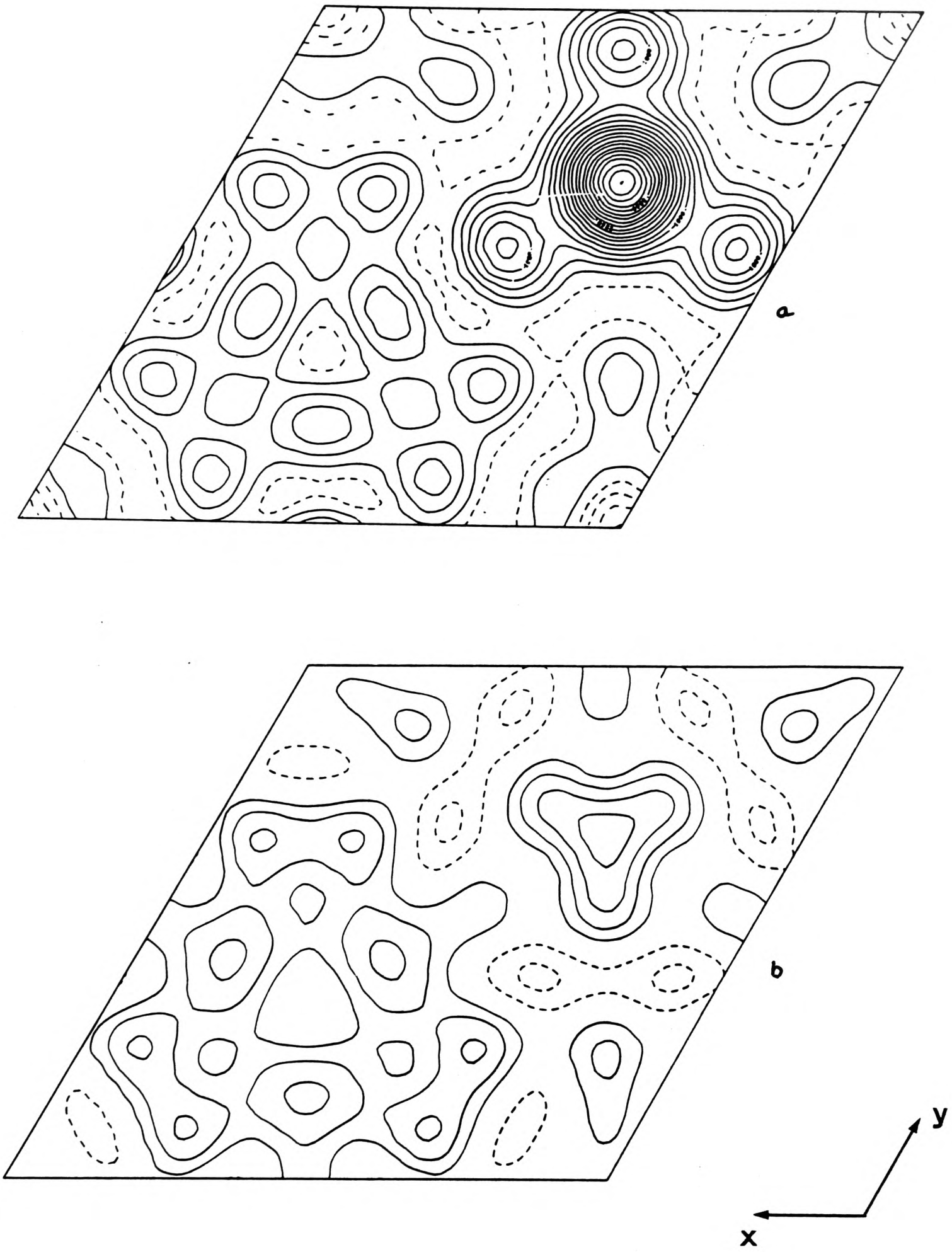


Figure 4.5. The z = 1/4 sections of final /F_{obs}/ (upper) and /F_{obs}-F_{calc}/ (lower) Fourier syntheses derived from the PND data refinements of $DAl_{11}O_{17}$ at 298K.

c) $\underline{DAl_{11}O_{17}}$ at 573K and 720K

Analysis of the data collected at 573K and 720K followed the same paths as those for the earlier data sets. The silver metal reflections were still apparent and were of similar relative intensities to those observed at 4.2K and 298K. The back exchange to $AgAl_{11}O_{17}$ had therefore been avoided. Two differences between the high and low temperature data were, however, apparent.

Firstly, the lattice constants which displayed only a slight expansion from 4.2K to 298K, have increased substantially (see Table 4.3). The data sets were collected consecutively, with no alteration in instrumental configuration save for the apparatus necessary for temperature control. Good significance can therefore be attached to these values (the consistency is exemplified by the zero-point errors which are constant to within 0.025° (Table 4.3)). The variations in the lattice constants as a function of temperature are displayed in Figure 4.6. The form of these plots, with small expansivity at low temperatures followed by an increase above ∿270K, is typical of relatively refractory materials. From the linear regions above 300K, the thermal expansion coefficients, α, may be calculated. The derived values of $\alpha_a = 5.9 \times 10^{-6}K^{-1}$, $\alpha_c = 3.5 \times 10^{-6}K^{-1}$ are lower than those for sodium beta alumina ($\alpha_a = 8.0 \times 10^{-6}K^{-1}$, $\alpha_c = 8.1 \times 10^{-6}K^{-1}$ (225)) which probably reflects the differing atomic arrangements within the mirror planes.

Secondly, in addition to those reflections resulting from silver metal and the furnace, further peaks were apparent in the $(I_{obs} - I_{calc})$ difference profiles at both 573K and 720K. These additional peaks could be satisfactorily indexed

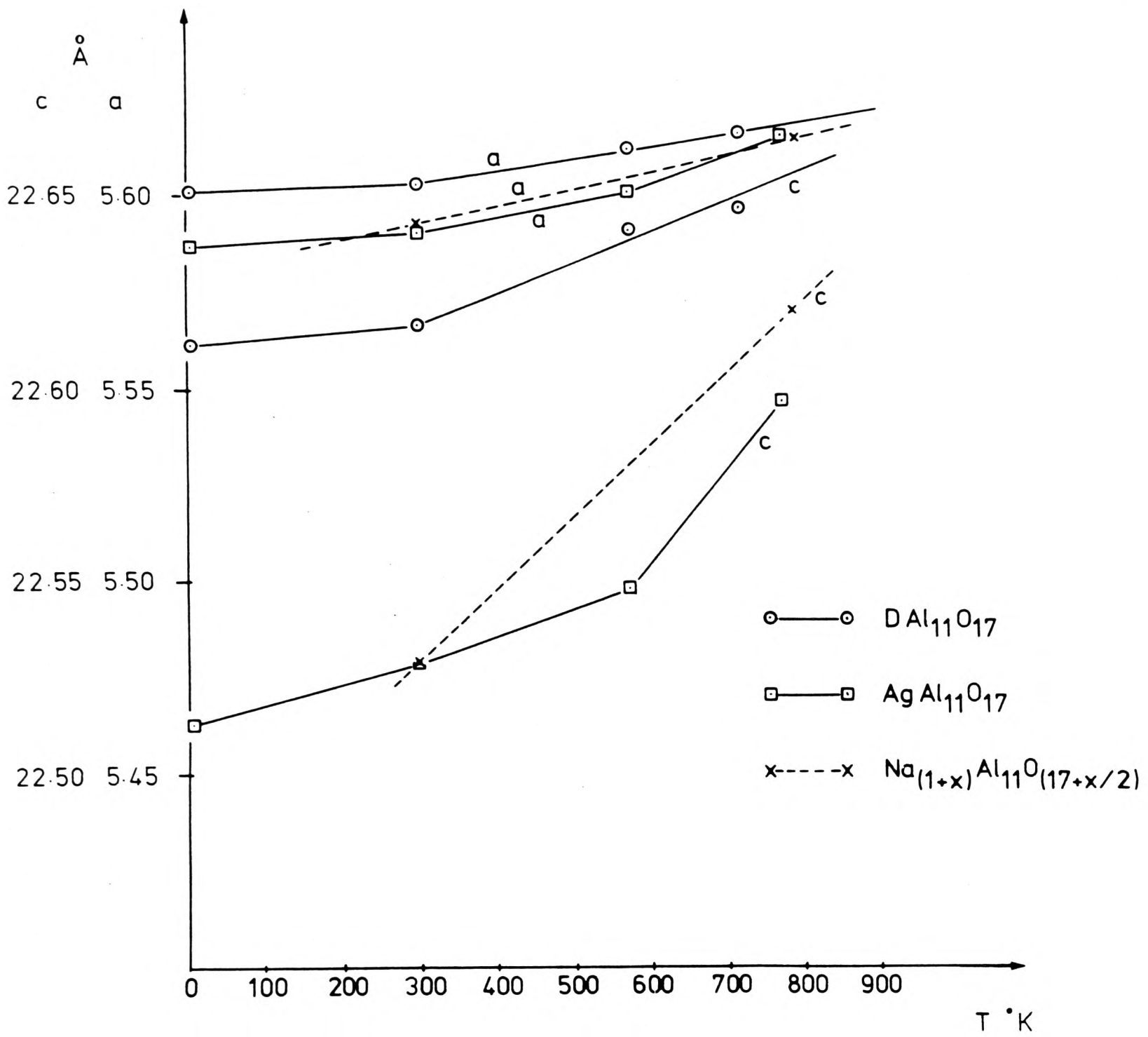


Figure 4.6. The lattice constants of $DAl_{11}O_{17}$ and $AgAl_{11}O_{17}$ (see Chapter 5) as a function of temperature. The dashed lines indicate the behaviour of the non-stoichiometric sodium compound calculated from the data of Peters et al.[43] *and May and Henderson*[225].

on the unit cell of corundum, α-Al_2O_3 (Figure 4.7). This assignment was confirmed by an intensity fit to these peaks. Thus, when the structure of $DAl_{11}O_{17}$ at 573K had been completely refined (with exclusion of the 3.8° to which α-Al_2O_3 reflections contributed significant intensity), the entire profile was re-calculated. From the resulting values of $(I_{obs} - I_{calc})$ at each point, a partial observed profile for α-Al_2O_3 could be determined. This was analysed by profile refinement. Atomic

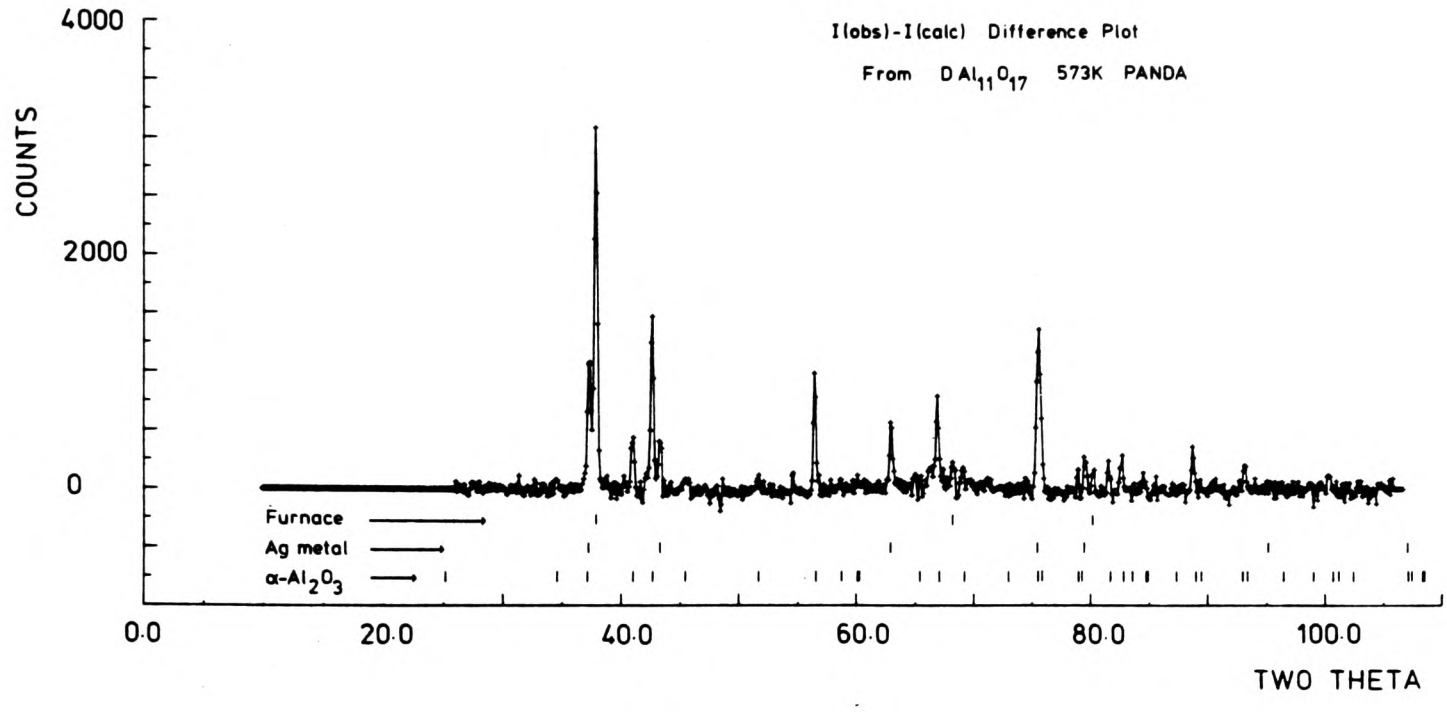


Figure 4.7. Plot of the difference between the observed and final calculated profile for $DAl_{11}O_{17}$ at 573K. The positions and assignments of the additional reflections are marked.

parameters were taken from Newnham and De Haan[226], but only the unit cell constants were refined because of the limitations of the data set. Values of a = 4.765(2)Å and c = 13.015(4)Å were obtained and a listing of observed and calculated reflection intensities is given in Appendix I. Peaks from α-Al_2O_3 were not observed in either of the lower temperature scans (Figures 4.3 and 4.4).

The deuterium location and iterative structure refinement were achieved in the manner outlined above. Isotropic temperature factors were employed until a satisfactory convergence was attained. Anisotropic parameters were then introduced for O(5) and D and subsequently for all atoms. For the 637 (720K data) data points and 182 independent reflections there was a total of 50 variable parameters in the final cycles, of which 43 corresponded to atomic parameters. The ratio of the number of reflections to the number of atomic variables was thus greater than 4.

In the earlier stages, the possibility of occupation by D of sites other than close to x $\bar{x}$ 1/4 (6h) with x ≃ 0.5, and that of partial reverse exchange to (Ag/D)$Al_{11}O_{17}$ were explored. There was no evidence for the former, but occupation numbers greater than zero could be obtained for silver entered at the stoichiometric position x $\bar{x}$ 1/4 (6h) with x = -0.236 (see Chapter 5). The maximum values realised were 0.24(9) at 573K and 0.15(8) at 720K.

The profile refinement technique is relatively insensitive to occupancies of this sort of magnitude. While some reverse exchange will undoubtedly occur, with the liberation of D_2, the reaction will be limited by the pressure of this D_2 gas which is contained by the sample can. The low occupation numbers for Ag (scattering length, b = 0.60 x 10^{-14}m), the values obtained for D (b = 0.667 x 10^{-14}m) and the observation of the Ag_m reflections in the diffraction profile suggest that the extent of this process is slight. The silver site was therefore not included in the later stages of refinement.

In contrast to the behaviour at lower temperatures, there was now evidence that displacements of deuterium from the x $\bar{x}$ 1/4 (6h) sites were significant. At 573K, for example, residuals of R_W = 0.1336, R_{WP} = 0.0979 were obtained for deuterium located on the 6h site with x = 0.463. However, the corresponding D-O separation was 0.87Å. At 720K this 'bond length' was even shorter. For both D and O(5) on 6h sites, with x_D = 0.456 and x_O = 0.377, the residuals were R_P = 0.1304 R_{WP} = 0.0981, with a D-O distance of 0.77Å. When the deuterium was allowed to relax in the more general x y 1/4 (12j) sites, refinement immediately produced an appreciable shift away from the x $\bar{x}$ mirror plane. A comparable refinement at 298K had

given deuterium coordinates very close to those derived for the 6h site, while at 4.2K such refinements had been unstable. The deuterium occupancy was little affected by this displacement and the residuals were also essentially unchanged, R_P = 0.1314, R_{WP} = 0.0974. The deuterium coordinates were x = 0.381, y = 0.473, the D-O separation being 0.83Å. This distance is, of course, sensitive to the sense of the displacement of O(5). When this was altered such that x_O < 1/3, refinement gave the residuals R_P = 0.1314, R_{WP} = 0.0974, and a more reasonable bond length of 0.96Å.

There is, of course, a fourth possibility. For deuterium on the 6h site, the sense of the O(5) displacement can be reversed such that x_O < 1/3. Refinement of this model gave R = 0.1303, R_{WP} = 0.0981 and a D-O distance of 1.04Å. Clearly, the diffraction data provides little distinction between these four possibilities. The slightly better residuals for both models involving the 12j sites could be anticipated on the basis of the increase, by 2, in the number of variable parameters. No adequate significance tests have yet been derived for powder data refinements and the parameters derived from the last-mentioned model are presented in the Tables. This model is selected on the basis of the lower number of variables with respect to those involving 12j sites, the reasonable D-O bond length and because of the continuity this allows with the data collected at other temperatures. Thus, inspection of Table 4.4 reveals that the x-parameter and thermal motion coefficients of deuterium vary in continuous sense from 298K to 720K.

The situation was very similar for the 573K data set. All of the above possibilities were tested, but the model which contains both D and O(5) on 6h sites, with x_O < 1/3, is presented

in the Tables. Fourier and difference Fourier sections at z = 1/4 are given in Figures 4.8 (573K) and 4.9 (720K), observed and calculated profiles in Figures 4.10-11, with final observed and calculated reflection intensities in Appendix I.

The appearance of the $/F_{obs}/$ Fourier sections are somewhat perplexing. At both 720K and 573K, the density distributions suggest that the deuterium is displaced away from the $x\bar{x}$ mirror plane. However, as discussed above, the least-squares analyses do not show such a marked preference. The misleading arrangement apparent in the Fouriers probably derives from series-termination errors* and/or inaccuracies in some of the 'observed' structure factors which result from overlap with regions which were excluded because of the impurities. The former explanation was confirmed by the calculation of $/F_{calc}/$ syntheses, based on the model in which deuterium occupies the 6h sites. The z = 1/4 sections were very similar in appearance to those in the $/F_{obs}/$ syntheses.

The results of our structure analyses thus indicate that, although the thermal motion of the deuterium becomes more pronounced as the temperature is raised, up to at least 445°C it remains closely bonded to the spacer oxygen with only limited delocalisation in the mirror planes.

d) Deuterium beta" alumina

Initial atomic parameters were taken from Bettman and Peters[49]. Refinement of positional and isotropic thermal

* *We may note that in addition to the errors deriving from the use of powder samples, neutron diffraction data is more susceptible to series-termination errors than X-ray data. For neutrons, the nuclear scattering power shows no tail-off with $\sin\theta/\lambda$ so that the number of reflections which have appreciable intensity and which therefore should be included in Fourier syntheses (Equation 2.7) is large.*

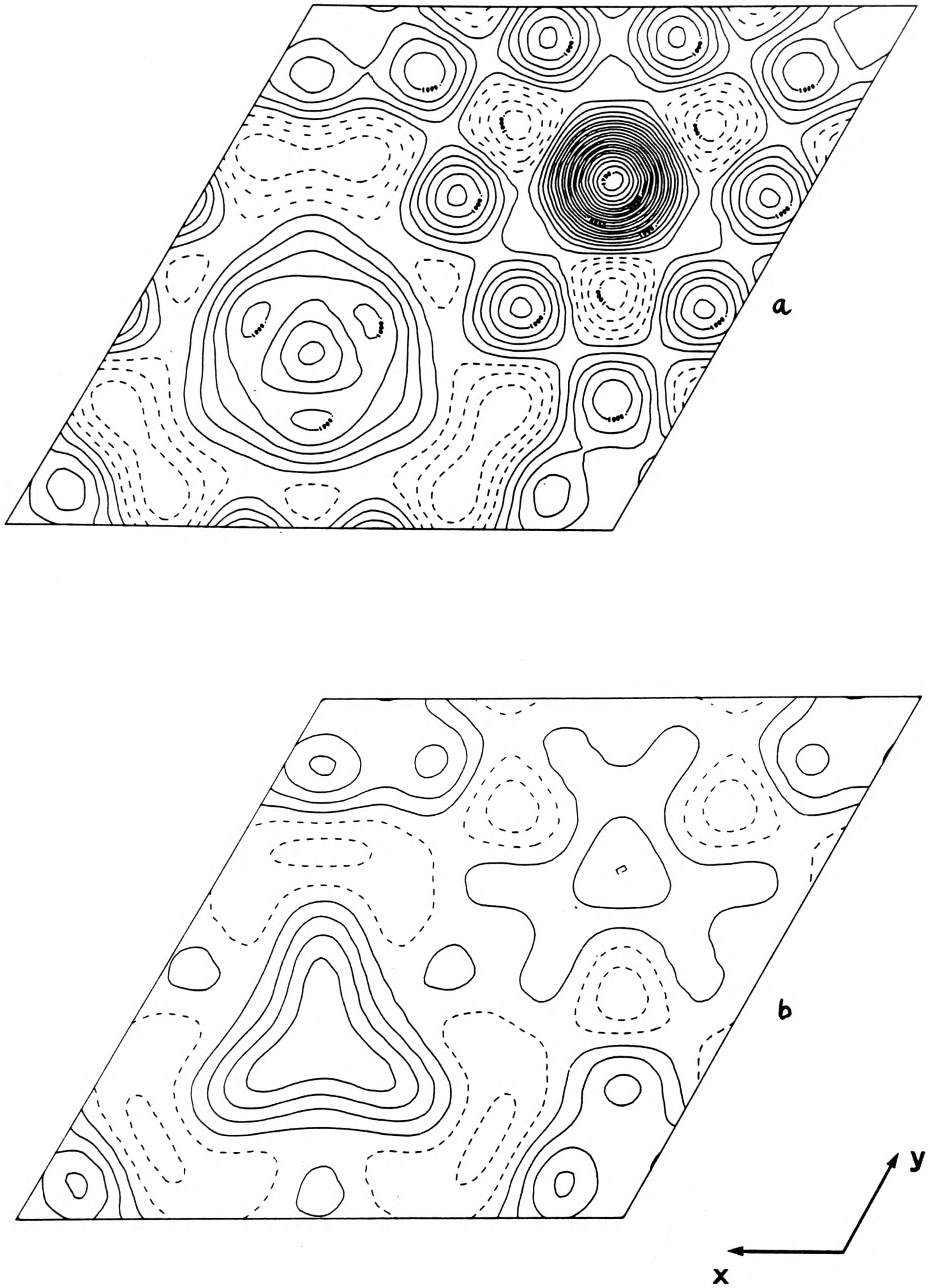


Figure 4.8. The z = 1/4 sections of final /F_{obs}/ (upper) and /F_{obs} - F_{calc}/ (lower) Fourier syntheses derived from the PND refinements of $DAl_{11}O_{17}$ at 573K.

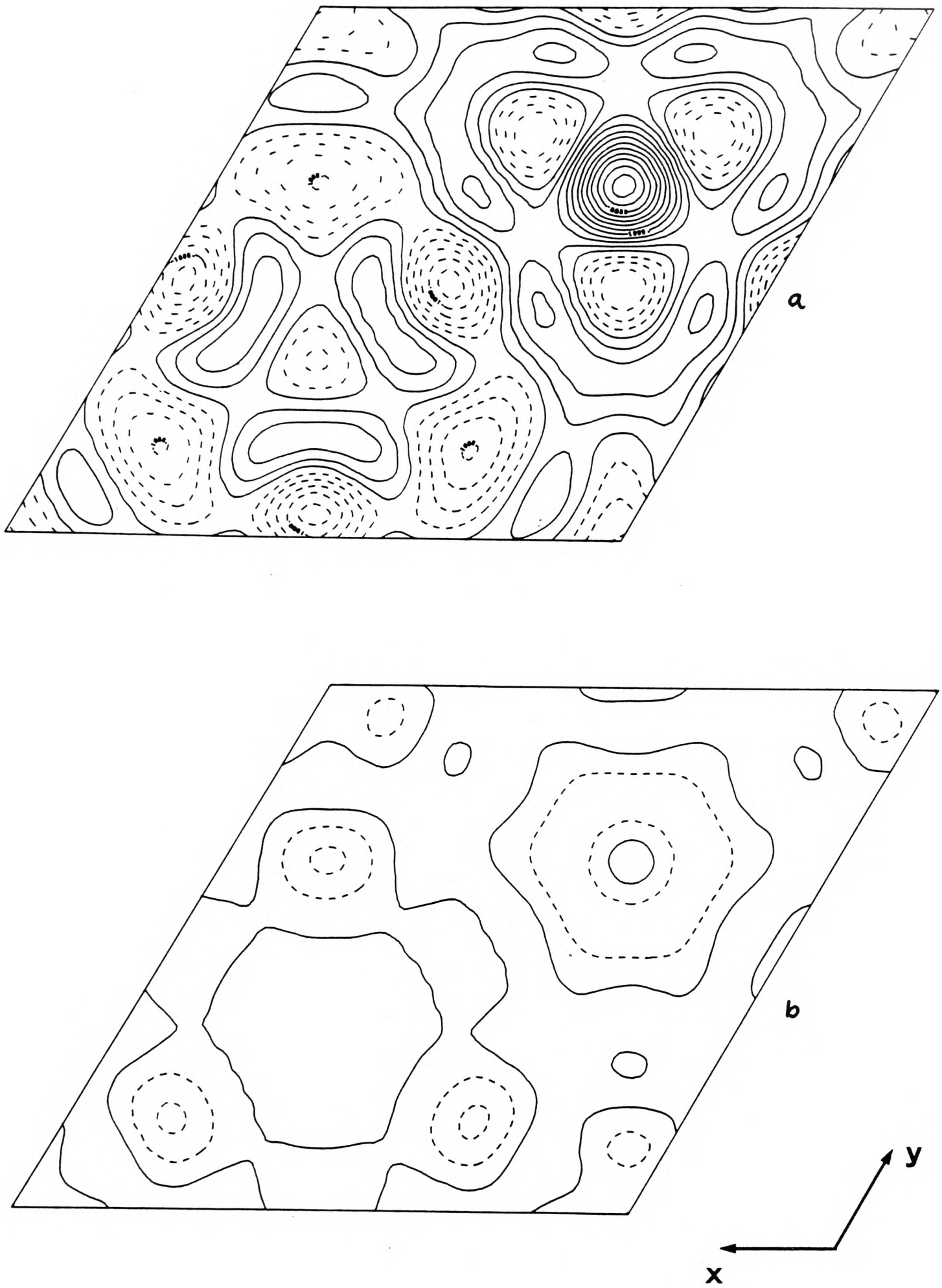


Figure 4.9. The z = 1/4 sections of final $/F_{obs}/$ (upper) and $/F_{obs}-F_{calc}/$ (lower) Fourier syntheses derived from the PND data refinements of $DAl_{11}O_{17}$ at 720K.

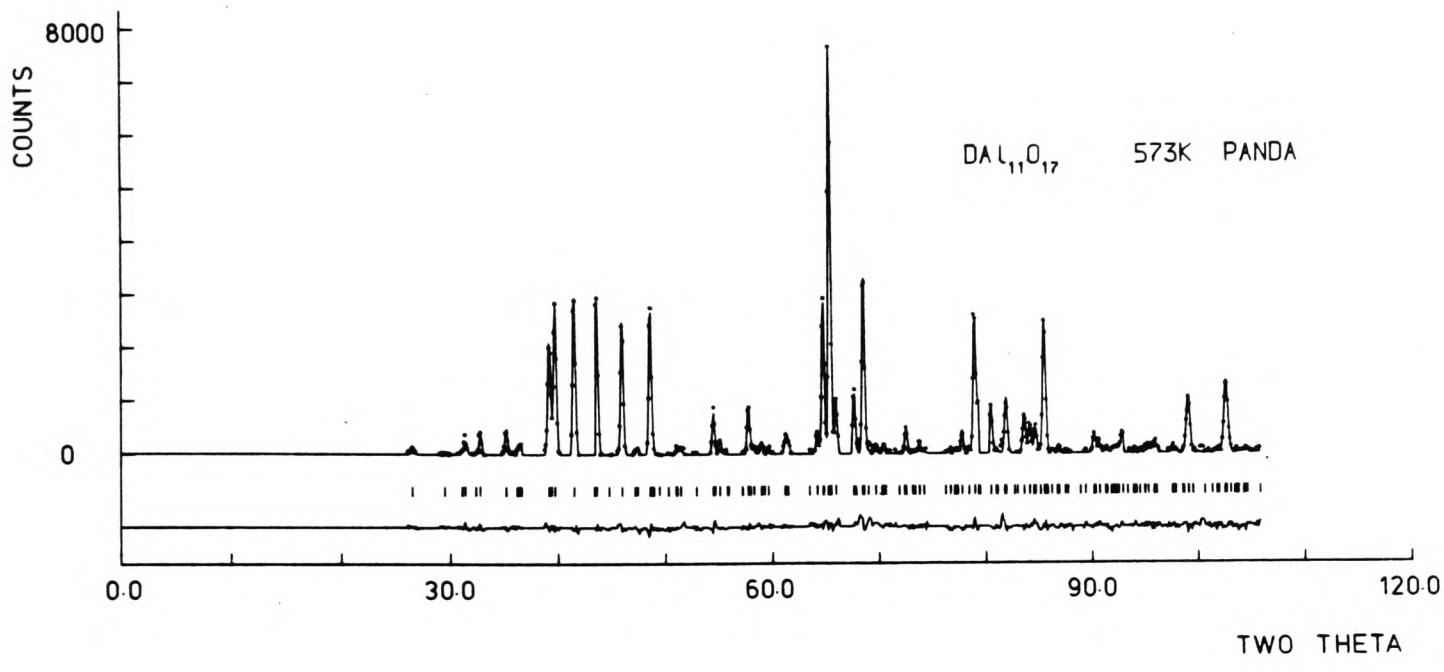


Figure 4.10. Final observed (dots), calculated (continuous line) and difference (lower) diffraction profiles for $DAl_{11}O_{17}$ at 573K (PANDA diffractometer). Reflection positions are marked as bars.

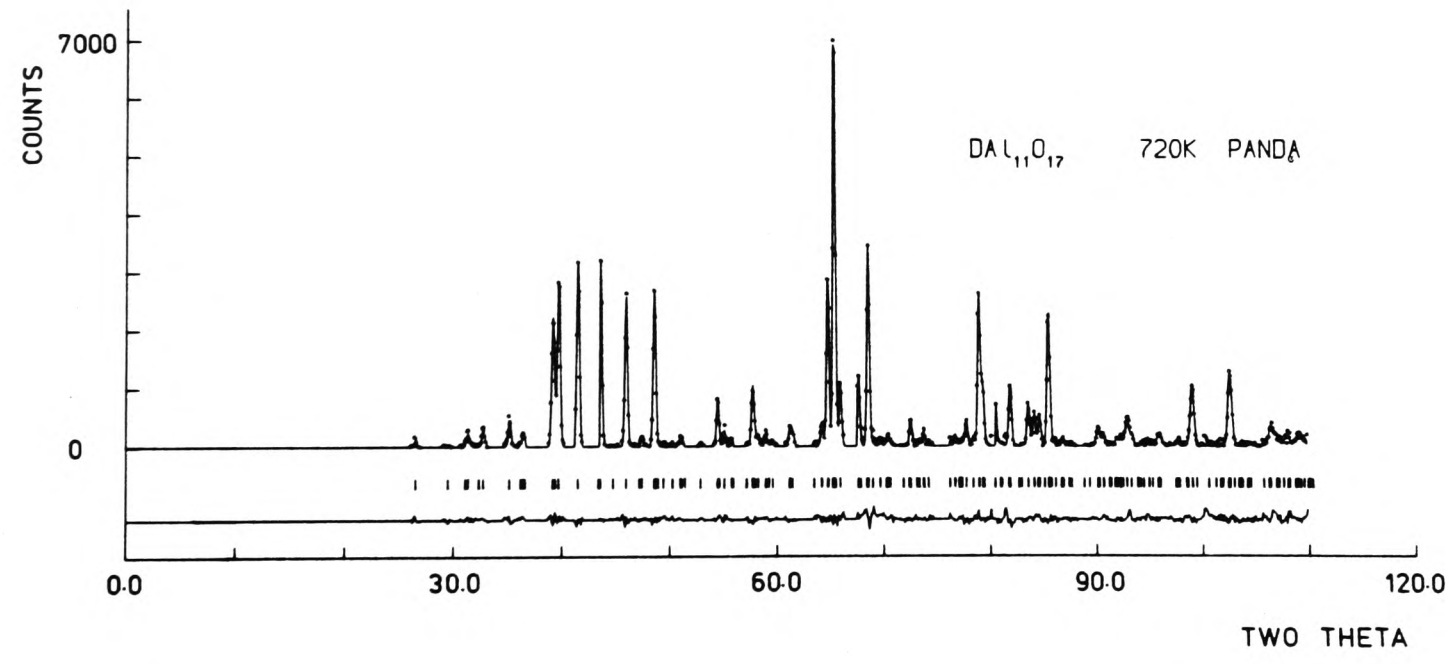


Figure 4.11. Final observed, calculated and difference diffraction profiles for $DAl_{11}O_{17}$ at 720K (legend as above).

parameters converged at R_P = 0.4355, R_{WP} = 0.3133. An $/F_{obs}/$ Fourier synthesis was then calculated and two areas of positive density, ½ 0 ½ (9d) and 1/3 $\bar{1}$/3 0.54 (6c) were included in least-squares refinement. The occupancies of these sites settled at 2.2 and 3.2 respectively (note that to maintain a distinction with the beta materials, the occupation numbers are expressed in terms of the content of one complete unit cell). The second of these sites is that occupied by Ag^+ in silver beta" alumina[93]. However, in the light of the results described above for $DAl_{11}O_{17}$, neither of these sites is likely for deuterium.

An extensive series of positions and of combinations of positions for deuterium was then examined in least-squares. In keeping with earlier refinements, the region $2\theta < 30°$ and those regions containing appreciable intensity from silver metal reflections were excluded. No impurity other than silver was apparent. Unfortunately, the distinction between all of these models was slight in terms of agreement between observed and calculated profiles.

The independent thermal parameters were replaced by single values for spinel block O and Al respectively and a correction for preferred orientation was introduced. There were indications of a deuterium bonded to O(5) at either -0.095 0.095 0.5 (18h) or 0.15 0.15 0.5 (18g), whose occupancy refined, typically, to ca. 2.0. When the occupations of both these sites were varied simultaneously, that of the 18g position fell to a low value. In terms of coordination, the 18h site is indeed more favourable, with a shorter separation of 2.08Å from the adjacent O(2). In addition to this location, however, there was evidence for the occupation of sites well-removed from O(5),

in particular, the 0.55 -0.55 0.5 (18h) and 0.31 0.31 0.5 (18g) positions. In the absence of definitive results from the diffraction data, such sites must be considered in terms of their chemical reasonability. The possibilities include:

(1) Occupation by deuterium. Without additional oxygen in the conduction planes, this is unlikely as it would imply minimum D-O separations of at least 1.7Å.

(2) The presence of Ag^+ ions. In the final round of refinements the occupation number of the 6c silver site had a maximum value of 1.1(3). Further, the intensity of the observed silver metal reflections excludes the possibility of extensive incorporation of silver in this material.

(3) Partial collapse of the structure across the conduction planes as outlined in sections 4.1 and 3.2. This would seem unlikely for three reasons. Firstly, the parameters defining the spinel block atoms were well-behaved throughout refinement. Secondly, this type of occurrence would imply that sites adjacent to the z = ½ plane other than that of Al(3) would be occupied by aluminium, for which there was no evidence. Thirdly, the distribution of oxygen required by the formation of such close-packed slabs would involve conduction-plane sites different from those which are found to be occupied.

(4) Partial occupation by water or hydronium ion species. Inspection of Figure 4.12 reveals that this makes good chemical sense. Were the peak at 0.55 -0.55 0.5 (18h) to correspond to an oxygen, O(21), and that at 0.31 0.31 0.5 (18g) to deuterium, D(21), a water molecule becomes apparent, with a D(21)-O(21) bond length of 1.19Å. The deuteriums form hydrogen bonds to O(5), with D(21)-O(5) equal to 1.73Å, and further, they lie between two O(2) atoms, which are 2.50Å away. The D(21)-O(21)-

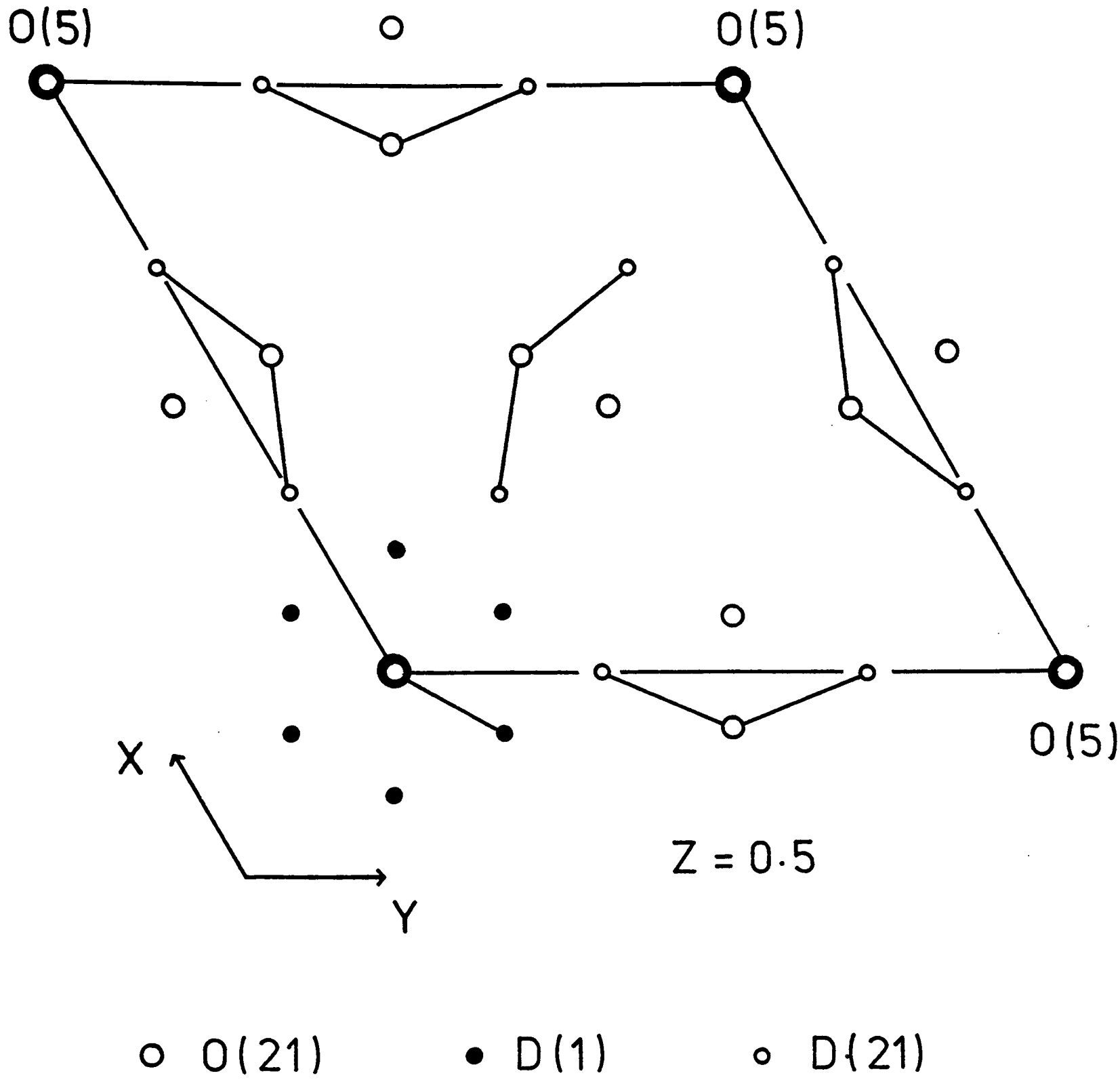


Figure 4.12. A possible interpretation of the atomic distribution in the z = ½ plane in 'deuterium beta" alumina'. The positions of the deuterium bonded to O(5) and of the water molecules are indicated.

D(21) angle is somewhat large at 128.6°, but such an increase from a more typical value of 105° might be justified in terms of the strong D(21)-O(5) interaction. This interpretation, however, is not in good agreement with the derived atomic parameters. The occupancies which are presented in Table 4.8 show that Occ(O(21)) > Occ(D(21)) whereas, for a water molecule, a ratio of 1:2 is anticipated.

It is clear that from this data set, we are unable to

derive a valid model for the distribution within the conduction planes, and, in addition, some other aspects of the structure remain ill-defined. Li^6 has a negative scattering length, b = -0.214×10^{-14}m, and so the location of the lithium which was added to stabilise the beta" phase would be indicated by an apparent reduction in the population of the aluminium site involved. Which of the four aluminium sites was thus affected, however, did not become clear during refinement. In magnesium-stabilised beta" alumina, Mg^{2+} substitutes mainly at the Al(2) position[15,53]. We have alluded to the possibility of D_2O being present within the conduction planes, although we have no independent evidence for this. The sample is still sealed in the vanadium can and has not been subjected to spectroscopic scrutiny. However, if D_2O is incorporated in the structure or was lost from the material during preparation, then oxygen must be derived from sites within the basic structure. In refinement of the oxygen occupations and from the behaviour of their temperature factors, the O(3) site appeared to be under-populated. This position is, however, considerably removed from the z = ½ plane. A more reasonable location for oxygen vacancies is the O(4) site whose occupancy also refined to lower than the ideal value.

A large number of questions are thus posed by this system and, unfortunately, the observed data set enables none of them to be answered with certainty. The parameters presented in Tables 4.3 and 4.8 correspond to the model which was described above and displayed in Figure 4.12. The observed and calculated diffraction profiles are plotted in Figure 4.13 and the corresponding z = ½ $/F_{obs}/$ Fourier section is shown in Figure 4.14. Reflection intensities are given in Appendix I.

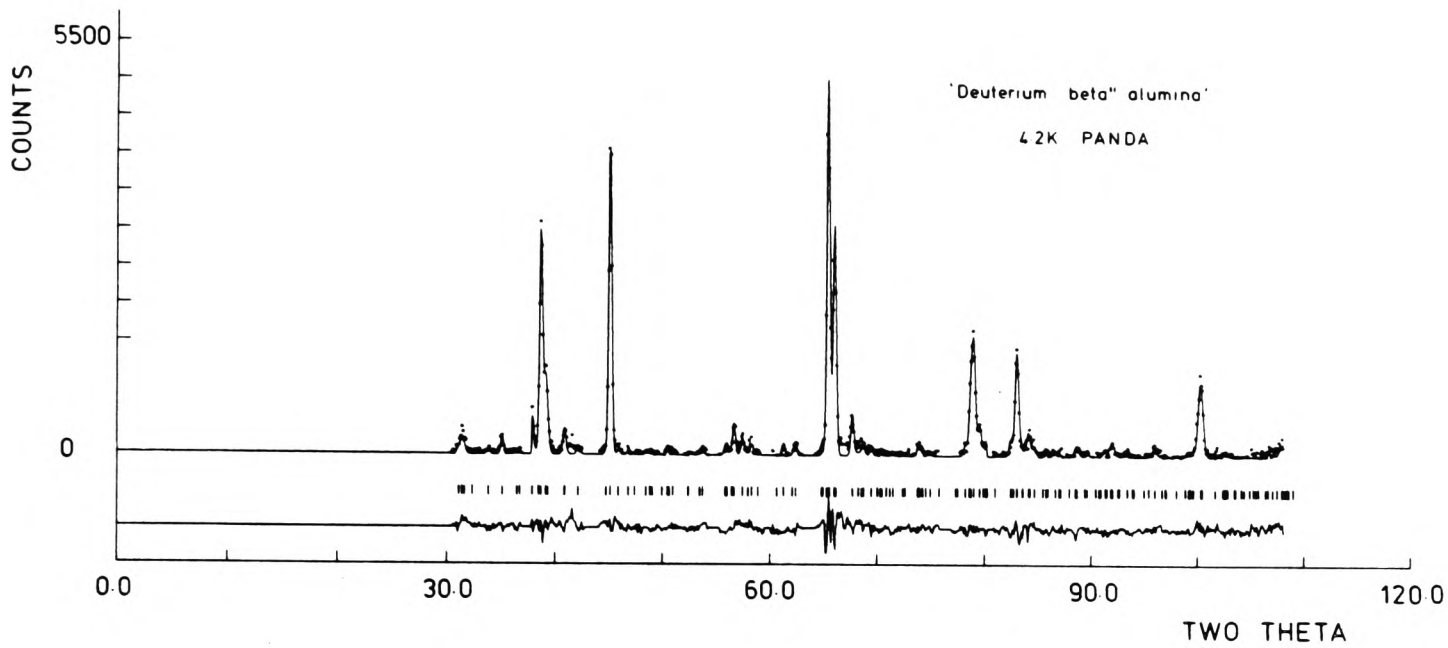


Figure 4.13. Final observed (dots), calculated (continuous line) and difference diffraction profiles for 'deuterium beta" alumina' at 4.2K (PANDA diffractometer). Reflection positions are indicated by bars.

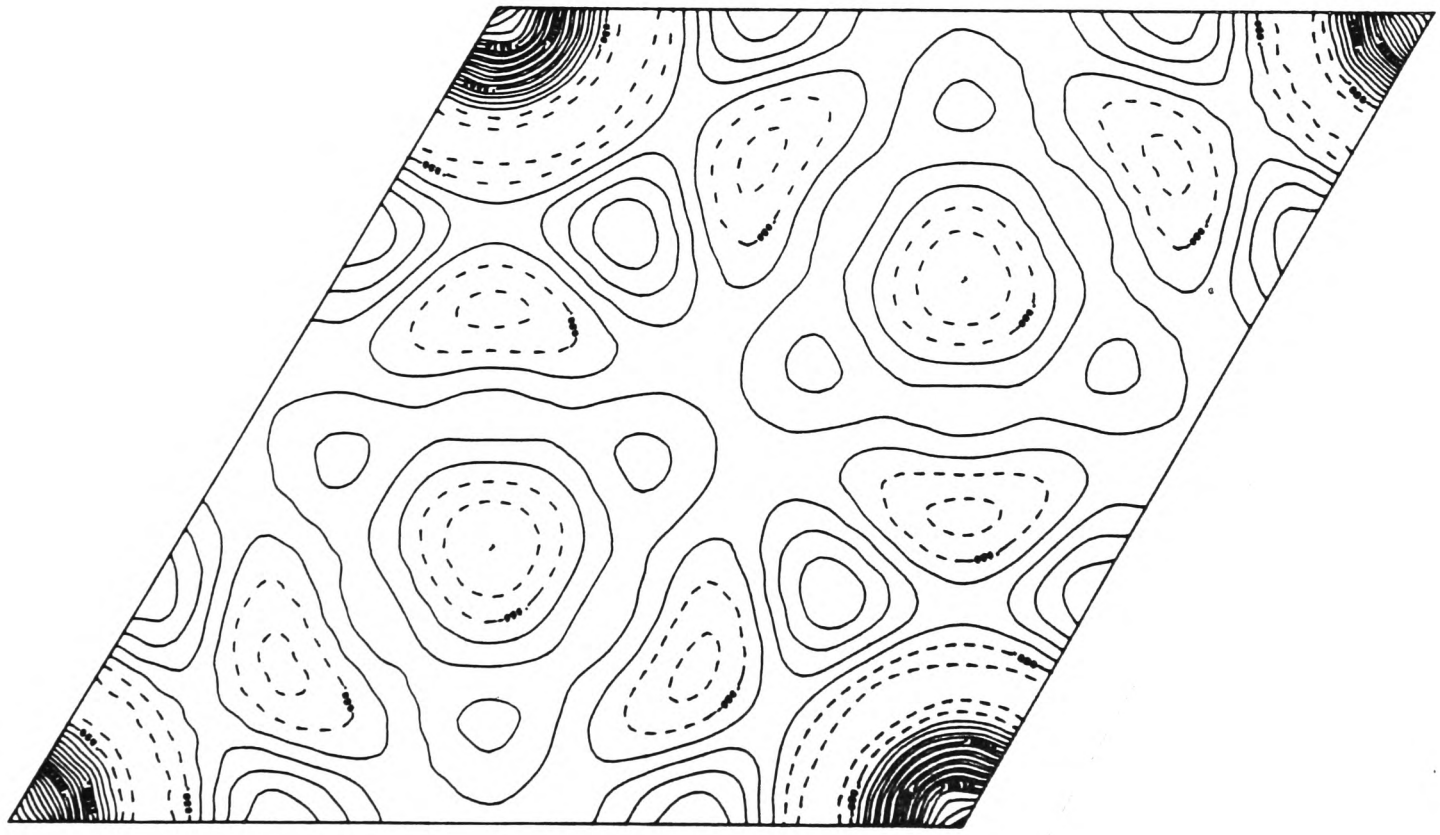


Figure 4.14. The z = 1/4 section of a final /F_{obs}/ Fourier synthesis derived from the PND data refinements of 'deuterium beta" alumina' at 4.2K (compare with Figure 4.12).

4.5 Conclusion

We have seen that reduction of polycrystalline non-stoichiometric silver beta alumina by D_2 gas at 450°C affords anhydrous stoichiometric deuterium beta alumina, $DAl_{11}O_{17}$. The product which is formed from silver beta" alumina undergoes partial decomposition under the same experimental conditions. The latter material has been only poorly characterised, but it appears that the atomic distribution within the conduction planes bears little resemblance to that in the well-ordered deuterium beta alumina.

In $DAl_{11}O_{17}$ at 4.2K, the deuterium is closely bonded to the spacer oxygen in a hydroxyl linkage. It is well-localised in 3-fold sites about the 2c position, this arrangement being favoured by weak electrostatic interactions between the deuterium and the two neighbouring O(2) ions at a distance of 2.4Å. The deuterium is not subject to displacement away from the z = 1/4 mirror plane and all the sites which are normally occupied by cations in metal beta aluminas are vacant. At 298K, this distribution is essentially unchanged. At temperatures above ambient, 573K and 720K, there is some evidence for slight delocalisation of deuterium away from the 6h sites, for the temperature factors of deuterium on this 6h site, particularly those components within the mirror plane, are increased substantially. The strong hydroxyl linkage to O(5) is, however, maintained and it therefore seems unlikely that this material will support appreciable protonic conductivity.

While no gross structural modifications occur in the range 4.2 - 720K, some trends are apparent. Firstly, for the 6h deuterium site x $\bar{x}$ 1/4, the value of x decreases in a continuous

fashion (Table 4.4). The variation is such that in the interpretation of the diffraction data, we were obliged to consider the O(5) displacements at 573K and 720K in an opposite sense to those at 4.2K and 298K in order to maintain a D-O separation of ca. 1Å. The diffraction data does not allow a distinction between this possibility and that of a continuous change in D-O bond length with temperature. We note, too, that the Al(3)-O(2) distance decreases as the temperature is raised (Table 4.6). Even at 4.2K, this bond length is shorter than that found in metal beta aluminas, in further comparison with which the Al(3)-O(5) separation in $DAl_{11}O_{17}$ (and in the H_3O^+ material studied by Kato and Saalfeld[74]) is increased which probably reflects the existence of the strong O(5)-D bond. A reduction in the Al(3)-O(2) distance then maintains an average Al(3)-O contact of ca. 1.76Å[73]. Another interpretation is that, in the absence of cation density around the BR position, there is little attractive influence on O(2) away from positions which are closer to Al(3). In stoichiometric $DAl_{11}O_{17}$ the net cation density in the mirror planes is reduced and, further, as the deuterium becomes more susceptible to thermal vibration, the strength of the D-O(2) interaction will be diminished. A contraction in O(2)-Al(3) therefore results as the temperature is raised. The Al(1)-O(4) distance is also susceptible to such an influence, albeit to a lesser extent, and a slight reduction in this bond length with respect to other beta aluminas is found, particularly at the lower temperatures. We must not neglect the interstitial aluminiums which are present in the non-stoichiometric[53] but presumably absent in the stoichiometric materials. These species will exert a further attractive influence on O(2) away from Al(3). However, their concentration is small so that

their effect on the atomic parameters derived for the bulk material is unlikely to be large.

Another interesting feature of the refinements at 573K and 720K was the observation of a limited amount of α-Al_2O_3. This is presumably formed by the reaction:

$$2DAl_{11}O_{17} \rightarrow D_2O + 11Al_2O_3$$

This decomposition apparently occurred at 573K, although the intensity of α-Al_2O_3 reflections did not change significantly as the sample was maintained at 573K and then 720K for several days. (The extent of the reaction will be limited by the pressure of $(D_2O)_g$ within the sample can and the effectiveness of the sealing system was evidenced by the limited extent of back-exchange to $AgAl_{11}O_{17}$.) In the absence of further data, we can merely record our observations and suggest that the production of '$HAl_{11}O_{17}$' by high temperature routes, such as the decomposition of the ammonium compound, may be accompanied by a similar degradation to α-Al_2O_3.

Finally, we may summarise the successes and failures of the use of profile refinement techniques with these systems. For $DAl_{11}O_{17}$, in contrast to the work previously reported for the same material using a similar data set[73], anisotropic temperature factors were successfully introduced without instability in the refinements. However, for the more disordered deuterium beta" alumina derivative, the measured data did not allow an adequate description of the structure to be obtained. Fourier techniques were completely unsuccessful in structure elucidation and, further, such calculations were so subject to series-termination errors that even $/F_{calc}/$ syntheses gave misleading descriptions of the models which had been employed

in the computation of structure factors.

TABLE 4.3

Final overall parameters, with estimated standard deviations, derived from the PND data refinements of deuterium beta and deuterium beta" aluminas.

	4.2K	298K	573K	720K	4.2K(β")
R_I	0.0703	0.0759	0.0677	0.0795	0.1510
R_P	0.1329	0.1161	0.1341	0.1303	0.2558
R_{WP}	0.1018	0.0924	0.0982	0.0981	0.1674
R_E	0.0921	0.0966	0.0931	0.0978	0.1242
a Å	5.6013(3)	5.6038(2)	5.6135(3)	5.6173(3)	5.6085(13)
c Å	22.6115(8)	22.6177(7)	22.6423(9)	22.6480(8)	33.9445(33)
V Å^3	614.3(1)	615.1(1)	617.9(1)	618.9(1)	924.7(7)
zθ[a]	18.3(3)	17.6(2)	17.2(2)	15.8(2)	18.2(5)
U	3525(208)	2253(151)	2533(198)	2558(194)	3643(531)
V	-4258(269)	-2637(201)	-2989(255)	-3001(248)	-3687(633)
W	2040 (86)	1536 (65)	1649 (80)	1660 (78)	2040(185)

[a] The counter zero-point error, zθ, U, V and W are expressed in units of one hundredth of a degree in 2θ.

TABLE 4.4

Final atomic parameters, with estimated standard deviations, derived from the PND data refinements of $DAl_{11}O_{17}$.

		x	y	z	Occn.
O(1)	4.2K	0.1575(9)	$\bar{x}$	0.0498(2)	6.0
12k[a]	298K	0.1560(6)		0.0496(2)	
m[b]	573K	0.1594(10)		0.0498(3)	
	720K	0.1571(8)		0.0493(2)	
O(2)	4.2K	0.5028(9)	$\bar{x}$	0.1448(2)	6.0
12k	298K	0.5010(7)		0.1454(2)	
m	573K	0.5019(11)		0.1453(2)	
	720K	0.4983(8)		0.1455(2)	
O(3)	4.2K	-1/3	1/3	0.0566(6)	2.0
4f	298K			0.0563(4)	
3m	573K			0.0551(6)	
	720K			0.0564(5)	
O(4)	4.2K	0	0	0.1422(6)	2.0
4e	298K			0.1403(5)	
3m	573K			0.1405(6)	
	720K			0.1422(6)	
O(5)	4.2K	0.371(5)	$\bar{x}$	0.25	1.0
6h	298K	0.367(9)			
mm	573K	0.298(3)			
	720K	0.292(2)			
Al(1)	4.2K	-0.1663(17)	$\bar{x}$	0.1066(3)	6.0
12k	298K	-0.1634(13)		0.1062(2)	
m	573K	-0.1678(17)		0.1066(3)	
	720K	-0.1678(15)		0.1070(3)	

[a] Wyckoff notation [b] site symmetry

Cont. overleaf.

TABLE 4.4 cont.

		x	y	z	Occn.
Al(2)	4.2K	1/3	-1/3	0.0242(6)	2.0
4f	298K			0.0235(6)	
3m	573K			0.0247(7)	
	720K			0.0248(6)	
Al(3)	4.2K	1/3	-1/3	0.1696(8)	2.0
4f	298K			0.1715(7)	
3m	573K			0.1692(8)	
	720K			0.1690(8)	
Al(4)	4.2K	0	0	0	1.0
2a	298K				
$\bar{3}$m	573K				
	720K				
D	4.2K	0.4800(54)	$\bar{x}$	1/4	1.05(15)
6h	298K	0.4678(37)			1.14(15)
mm	573K	0.4624(46)			0.84(18)
	720K	0.4552(31)			1.20(24)

TABLE 4.5

Final anisotropic thermal parameters, with estimated standard deviations, derived from the PND data refinements of $DAl_{11}O_{17}$.

		β_{11}	β_{22}	β_{33}	β_{12}	β_{13}	β_{23}*
O(1)	4.2K	0.001(2)	β_{11}	0.0003(1)	-0.001(3)	-0.0015(4)	$-\beta_{13}$
12k	298K	0.003(2)		-0.0000(1)	0.004(2)	-0.0010(3)	
m	573K	0.016(3)		0.0007(1)	0.016(4)	-0.0002(4)	
	720K	0.015(2)		0.0008(1)	0.016(3)	0.0004(3)	
O(2)	4.2K	0.001(2)	β_{11}	0.0003(1)	-0.002(4)	0.0010(3)	$-\beta_{13}$
12k	298K	0.002(2)		0.0004(1)	0.003(3)	0.0001(3)	
m	573K	0.011(3)		0.0002(1)	0.009(4)	0.0001(5)	
	720K	0.007(2)		0.0007(1)	0.005(3)	0.0004(3)	
O(3)	4.2K	0.001(4)	β_{11}	0.0007(3)	$\beta_{11/2}$	0	0
4f	298K	-0.001(3)		0.0007(2)			
3m	573K	0.001(4)		0.0003(3)			
	720K	0.007(3)		-0.0002(2)			
O(4)	4.2K	0.008(4)	β_{11}	-0.0001(2)	$\beta_{11/2}$	0	0
4e	298K	0.004(3)		0.0005(2)			
3m	573K	0.006(4)		0.0006(3)			
	720K	0.026(4)		0.0000(3)			
O(5)	4.2K	0.008(18)	β_{11}	-0.0002(5)	0.018(10)	0	0
6h	298K	0.063(41)		-0.0001(4)	0.053(26)		
mm	573K	0.056(29)		0.0014(9)	0.050(22)		
	720K	0.028(23)		0.0021(8)	0.038(17)		
Al(1)	4.2K	0.005(3)	β_{11}	0.0003(2)	0.003(5)	0.0008(6)	$-\beta_{13}$
12k	298K	0.003(3)		0.0003(2)	-0.000(4)	0.0006(4)	
m	573K	0.007(4)		0.0006(2)	0.011(6)	0.0006(6)	
	720K	0.012(3)		0.0004(2)	0.012(5)	-0.0003(5)	

Cont.

* Temperature factors expressed in the form:

$$\exp\{-(\beta_{11}h^2 + \beta_{22}k^2 + \beta_{33}l^2 + 2\beta_{12}hk + 2\beta_{13}hl + 2\beta_{23}kl)\}$$

TABLE 4.5 cont.

		β_{11}	β_{22}	β_{33}	β_{12}	β_{13}	β_{23}
Al(2)	4.2K	0.010(4)	β_{11}	-0.0010(2)	$\beta_{11/2}$	0	0
4f	298K	0.001(3)		0.0006(3)			
3m	573K	-0.002(4)		0.0004(4)			
	720K	-0.009(3)		0.0004(3)			
Al(3)	4.2K	-0.010(3)	β_{11}	0.0013(4)	$\beta_{11/2}$	0	0
4f	298K	0.006(4)		0.0007(3)			
3m	573K	0.007(5)		-0.0001(4)			
	720K	0.011(5)		0.0006(4)			
Al(4)	4.2K	-0.012(5)	β_{11}	0.0006(5)	$\beta_{11/2}$	0	0
2a	298K	-0.015(4)		0.0011(5)			
$\bar{3}$m	573K	0.004(6)		0.0004(6)			
	720K	0.009(6)		0.0015(6)			
D	4.2K	0.116(26)	β_{11}	-0.0004(5)	0.093(27)	0	0
6h	298K	0.082(20)		0.0029(8)	0.056(20)		
mm	573K	0.126(42)		0.0031(14)	0.120(38)		
	720K	0.153(37)		0.0063(18)	0.156(32)		

TABLE 4.6

Calculated bond lengths (Å) for deuterium beta and 'deuterium beta"' aluminas

	Number of bonds	4.2K	298K	573K	720K	4.2K(β")
Octahedra						
Al(1)-O(1)	2	2.030	2.010	2.046	2.053	1.988
-O(2)	2	1.823	1.855	1.830	1.843	1.867
-O(3)	1	1.976	1.998	1.987	1.977	2.105
-O(4)	1	1.803	1.763	1.803	1.816	1.775
av. Al(1)-O		1.914	1.915	1.924	1.931	1.932
Al(4)-O(1)	6	1.898	1.885	1.917	1.893	1.942
Tetrahedra						
Al(2)-O(1)	3	1.801	1.820	1.784	1.802	1.806
-O(3)	1	1.827	1.806	1.807	1.838	1.665
av. Al(2)-O		1.808	1.816	1.790	1.811	1.771
Al(3)-O(2)	3	1.738	1.732	1.726	1.691	1.680
-O(5)	1	1.855	1.804	1.863	1.878	1.956
av. Al(3)-O		1.767	1.750	1.760	1.738	1.749
Deuterium Contacts						
D-O(5)		1.056	0.979	1.122	1.044	1.167
-O(2)		2.389	2.388	2.402	2.405	
-Al(3)		2.308	2.202	2.219	2.184	

TABLE 4.7

Calculated bond angles (°) for deuterium beta and 'deuterium beta"' aluminas

	4.2K	298K	573K	720K	4.2K(β")
Octahedra					
O(1)-Al(1)-O(1)	81.4	81.4	82.0	80.3	84.5
-O(2)	89.9	90.1	89.3	89.2	89.2
-O(3)	88.9	88.9	88.3	88.6	86.5
-O(4)	84.8	84.7	83.6	84.2	85.5
O(2)-Al(1)-O(2)	98.1	97.3	98.6	100.6	96.1
-O(3)	84.2	83.9	85.6	85.6	86.4
-O(4)	101.2	101.6	101.3	100.3	100.8
O(3)-Al(1)-O(4)	171.7	171.6	169.3	170.6	169.2
O(1)-Al(4)-O(1)	88.4	88.1	88.9	88.8	87.0
Tetrahedra					
O(1)-Al(2)-O(1)	110.2	101.0	110.3	111.0	108.6
-O(3)	108.7	109.0	108.6	107.9	110.3
O(2)-Al(3)-O(2)	110.1	108.9	110.7	110.5	114.9
-O(5)	114.2	114.9	119.0	120.7	103.3
-O(5)'	97.4	99.6	102.7	101.9	
Deuterium Contacts					
Al(3)-O(5)-D	101.4	100.4	92.7	92.2	106.3

TABLE 4.8

Atomic parameters with estimated standard deviations derived from the PND data refinement of 'deuterium beta" alumina'.

Atom	Position	Site Symmetry	x	y	z	Occn.	B
O(1)	18h	m	0.1589(14)	$\bar{x}$	0.0347(3)	18.0	0.75(11)
O(2)	18h	m	0.1651(17)	$\bar{x}$	0.2357(4)	16.7(6)	"
O(3)	6c	3m	0	0	0.3005(9)	4.6(4)	"
O(4)	6c	3m	0	0	0.0948(8)	6.0	"
O(5)	3b	$\bar{3}$m	0	0	0.5	3.0	0.28(69)
Al(1)	18h	m	-0.1626(24)	$\bar{x}$	0.0710(5)	18.0	0.81(21)
Al(2)	6c	3m	0	0	0.3496(11)	6.0	"
Al(3)	6c	3m	0	0	0.4424(11)	6.0	"
Al(4)	3a	$\bar{3}$m	0	0	0	3.0	"
D(1)	18h	m	-0.115(9)	$\bar{x}$	0.510(4)	1.8(5)	1.5
O(21)	18h	m	0.551(4)	$\bar{x}$	0.505(2)	3.1(4)	0.5
D(21)	18g	2	0.692(14)	x	0.5	2.0(3)	0.5

CHAPTER 5

SILVER BETA ALUMINAS

5.1 Introduction

A summary of the limited available information on stoichiometric beta aluminas was presented in the Introduction, section 3.6. Boilot *et al.*[196] and Collongues[195] reported the production of stoichiometric beta aluminas via the thermal decomposition of the ammonium compound[75] and a room-temperature X-ray diffraction study of stoichiometric silver beta alumina has been reported recently[230]. However, this preparative route can apparently lead to a range of stoichiometries around the composition $MAl_{11}O_{17}$[227] and it is difficult experimentally to halt the reaction at the 'stoichiometric $HAl_{11}O_{17}$' stage. We have seen in the preceding chapter, that at elevated temperatures this material is liable to further decomposition and in the following chapter we describe the macroscopic deterioration in crystal quality which accompanies deammoniation.

An interesting feature of the work of Boilot *et al.*[196] on $AgAl_{11}O_{17}$ is the observation of a superlattice at low temperatures. At ∿300K this superlattice disappears and X-ray diffuse scattering measurements reveal that the silver ions then adopt a two-dimensional quasi-liquid arrangement. In non-stoichiometric materials at low temperatures, limited short-range ordering has been reported[112,123,124] but there is evidence that the average distribution of conducting ions does not change dramatically even down to 4.2K[121,122]. Several questions are then raised in connection with stoichiometric materials:-

(1) Does the distribution of conducting ions differ from that in the non-stoichiometric (NS) parent and, more pertinently, are they *conducting* ions? Modelling studies suggest that no

diffusive motion will occur in the stoichiometric (S) sodium compound[175]. Were the S-materials to adopt similar conducting-ion configurations to those in the NS-counterparts (as suggested by Colomban[52] - see Table 3.2), then the ionic conductivity might be enhanced, despite the reduced population of mobile species, because of the loss of the interstitial oxygens which block the conducting pathways.

(2) Will such materials display the type of order-disorder transition which generally occurs in other fast-ion conducting systems?

(3) In what fashion will the c-axis constant reflect the reduction of atomic density within the mirror planes?

(4) What becomes of the Al_i interstitials which coordinate to the additional oxygens within the conducting planes? Radiation-induced spinel-block defects require vigorous conditions for their removal[46].

In this chapter, we present the results of powder neutron diffraction (PND) experiments on stoichiometric silver beta alumina, $AgAl_{11}O_{17}$, at 4.2K, 298K, 573K and 773K. In addition, the structure of non-stoichiometric silver beta alumina, as determined by single crystal neutron diffraction, is described.

5.2 Single crystal neutron diffraction study of $Ag_{1.25}Al_{11}O_{17.125}$

A crystal (ca. 5 x 11 x 3mm) of a sufficiently large size for neutron diffraction measurements was cut from a cylindrical boule of sodium beta alumina, $Na_{1.25}Al_{11}O_{17.125}$. It was converted to the silver material by exchange in molten silver nitrate at ∿300°C and subjected to a flow of H_2 gas (Air Products) at 450°C over a period of several hours. In contrast

to the behaviour of the polycrystalline samples, which was detailed in Chapter 4, the reduction proceeded slowly. Silver metal (Ag_m) plates out on the surface of the crystal and presumably hinders the incorporation of further hydrogen. This Ag_m was removed in nitric acid, reduction recommenced and the whole process was repeated. It became clear that the time required for complete exchange to hydrogen beta alumina would be prohibitively long. Even after these treatements, the extent of reduction was slight. Figure 5.1 shows a plot of the c-parameter, as a function of the distance across the crystal, measured on the APEX goniometer. The central portion of the

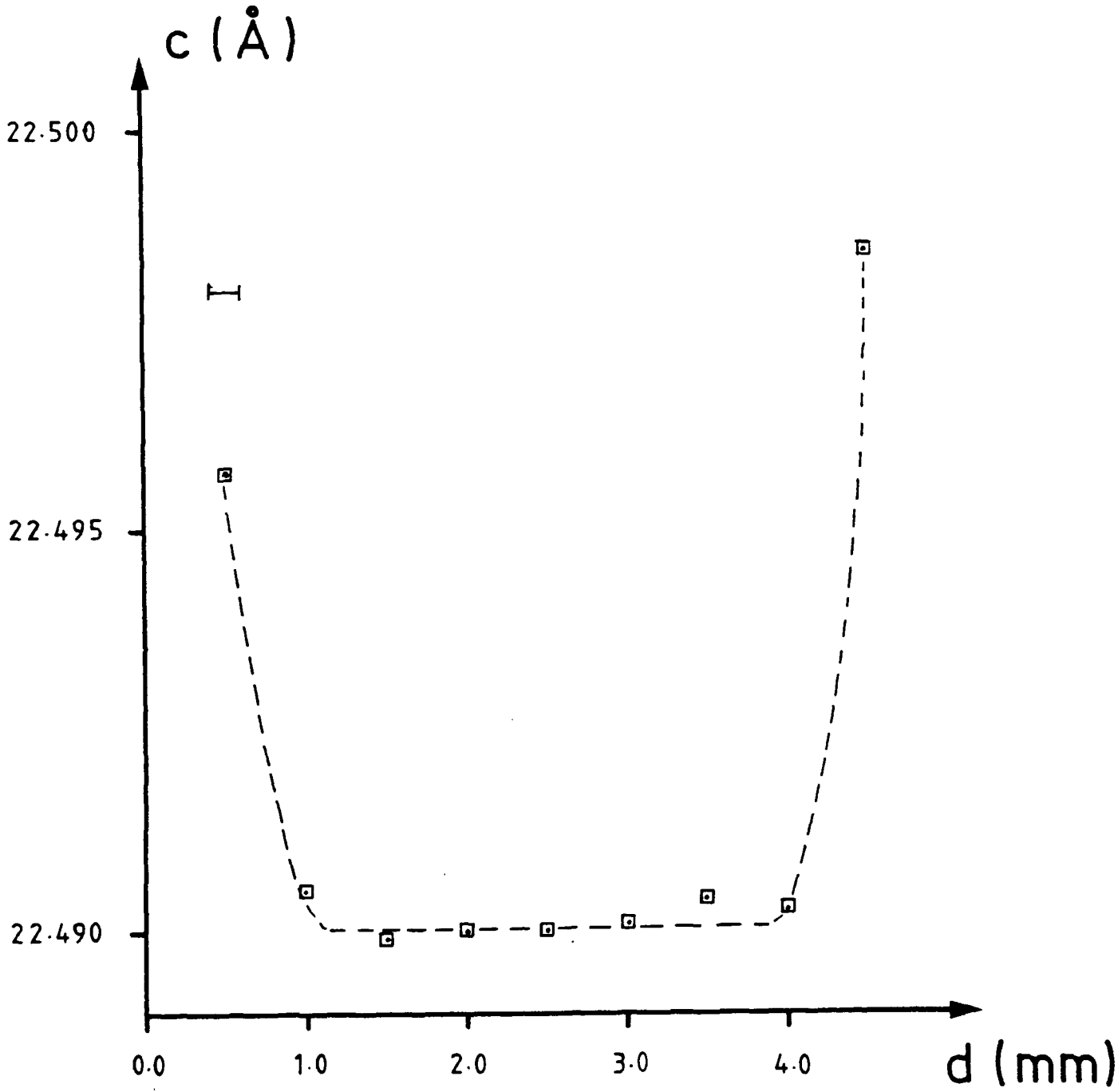


Figure 5.1. The c-axis constant of the partially-reduced crystal of $Ag_{1.25}Al_{11}O_{17.125}$ *measured, as a function of the distance, d, across the crystal, on the APEX goniometer. The beam diameter at the specimen is indicated by the bar.*

crystal has the value reported for silver beta alumina[71] and it is only at the extremities that the lattice constant is increased (we may recall that for $DAl_{11}O_{17}$ at 25°C, c = 22.62Å). Clearly, the major part of the crystal corresponds to the silver compound, although there is the possibility that interstitial oxygen had been lost from a larger proportion of the crystal than that suggested by the lattice constant scan. The mobility both of Ag^+ ions and of water in the mirror planes at 450°C was demonstrated in the preceding chapters.

The crystal was mounted on a goniometer and aligned, using transmission Laue techniques, so as to rotate about the $<11\bar{2}0>$ direction. It was then transferred to the Mark VI Channel I diffractometer and set-up in the standard fashion. The orientation matrix was defined by the angular coordinates of the 330 and 0 0 24 reflections. The lattice constants were checked from the observed positions of reflections of the h h $\overline{2h}$ 0 and 0 0 0 l types assuming a wavelength of 1.1803Å. Values of a = 5.598Å and c = 22.494Å were obtained, that of c being in reasonable agreement with the values recorded in the X-ray scan (Figure 5.1). Automatic data collection was effected by means of ω-2θ scans in bisecting geometry. The complete range of each reflection was stepped in units of 0.08° so that counts were recorded at ca. 30 points for each peak. Background counts were measured at 12 points on either side of this range. The time for measurement at each point was determined by the time taken for a fission counter to record a preset number of counts. Typically, 30 mins. were required per reflection. A total of 377 reflections were measured in the range $\theta < 50°$. The observed data were reduced on the IBM370 at Harwell, with the application of Lorentz corrections, and the resulting

structure factor moduli were analysed on the Oxford University 1906A computer using the CRYSTALS package[6]. The data for each reflection were checked manually to locate spurious points or accidental overlap in the background regions. For those reflections which were thus affected, structure factors were calculated by hand. All observations were used in the data merge which yielded 233 independent structure amplitudes. In the refinements described below neutron scattering lengths of 0.345, 0.583 and 0.60 (all x 10^{-14}m) were employed for Al, O and Ag respectively.

Initial coordinates for spinel block atoms and O(5) were taken from Roth[71] and full matrix least-squares techniques were used for refinement. The distribution of scattering matter within the mirror planes was elucidated by a combination of Fourier and least-squares calculations. As suggested above, it became rapidly clear that the hydrogen content of the crystal was small and, in the later stages of refinement, no hydrogen was included.

The main silver site was found to be of the 6h type, x $\bar{x}$ 1/4, with x ≃ -0.26. In common with other analyses of the silver material (Table 3.2), appreciable occupation of the anti Beevers-Ross site was also apparent. In principle, such an arrangement resembles that given by Roth[71], but when Roth's parameters for silver were tested in least-squares the refinements diverged. Similar instability also occurred when the model derived by Reidinger[44], from a re-analysis of Roth's data, was considered. It would therefore appear that the cation distribution in this particular crystal does differ somewhat from those which were found in other non-stoichiometric silver beta aluminas. This may reflect an inherent disparity between the substrates,

or may arise from a slight reduction in the level of cation excess, as outlined above.

The latter possibility was also suggested by the behaviour of the interstitial aluminium, Al_i, which was included, at -0.1655 0.1655 0.1765 (12k), in the later stages of refinement. The sum of the occupancies of this site and that of Al(1) was held at 6.0. The positional parameters of Al_i were also fixed because, when allowed to vary, the calculated shifts were large. The occupancy for Al_i was always low, the final value being 0.12(7). This contrasts with the occupation numbers found by Reidinger (0.20)[44] and Colomban (0.225)[52]. Both of these authors also obtained satisfactory refinements of the Al_i co-ordinates, further indicating that the occupancy is genuinely lower in the material described here.

Unit weights were employed throughout refinement and a correction for secondary extinction[6,7] was included in the later stages. Final residuals of $R = 0.0593$, $R_W = 0.0567$ were obtained. The derived atomic parameters are presented in Table 5.1 with bond lengths and angles listed in Tables 5.7 and 5.8. Figure 5.2(a) shows the appearance of the $z = 1/4$ section in a difference Fourier which was based on structure factors calculated without any contribution from Ag and Figure 5.2(b) is the corresponding final difference Fourier section. Final observed and calculated structure factors are given in Appendix II.

It is clear from Figure 5.2(b) that there is no apparent occupation of the mO position and we can therefore present no direct evidence for the occurrence of charge-compensating additional oxygen. In Colomban's analysis[52,230], such a site was included although it is poorly defined and does not provide an unequivocal demonstration of the existence of such O_i(mO)

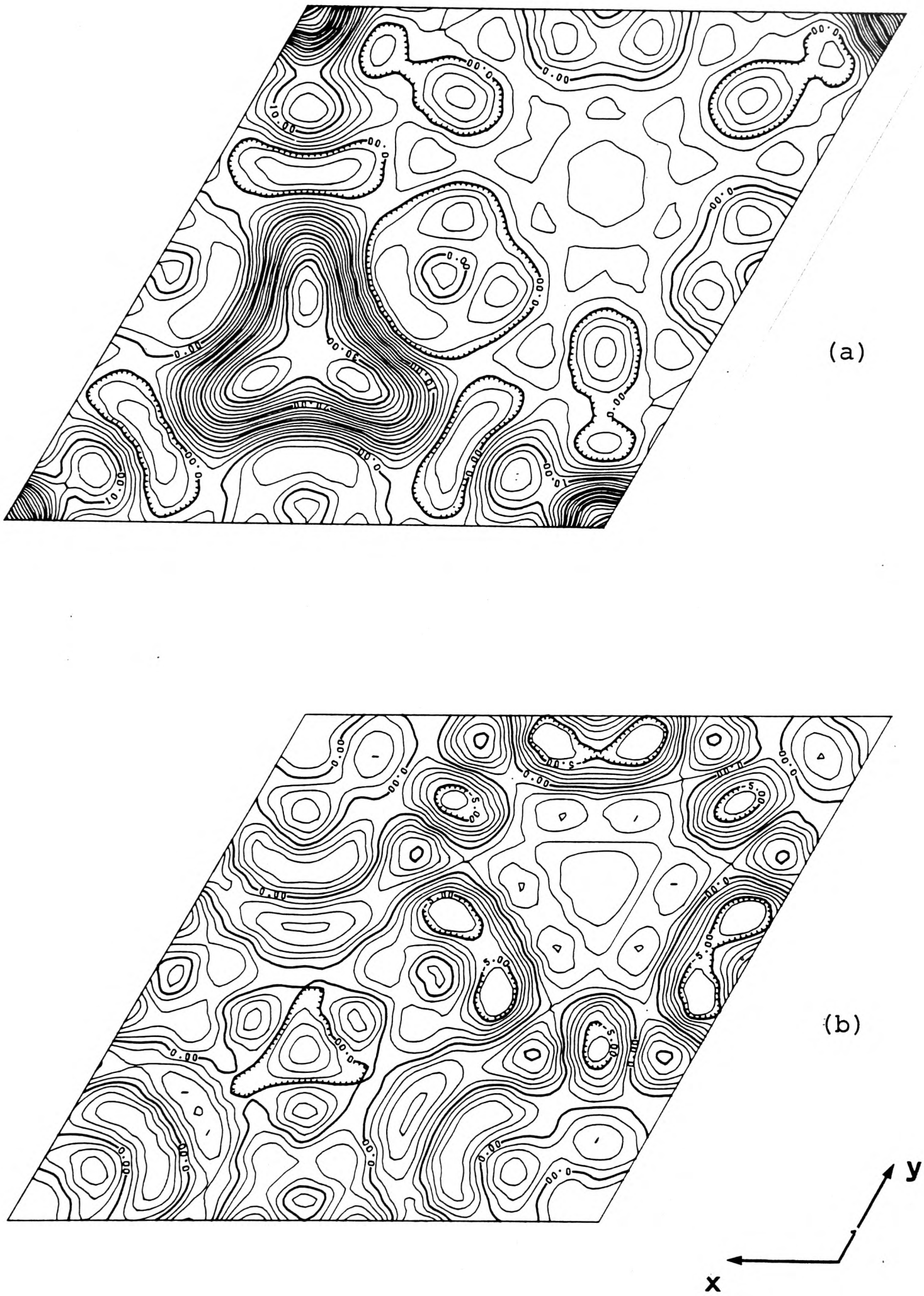


Figure 5.2. The z = 1/4 sections of difference Fourier syntheses calculated from the single crystal neutron diffraction data on $Ag_{1.25}Al_{11}O_{17.125}$. *The upper section is derived from calculated structure factors which contain no contribution from silver and the lower section is the corresponding final difference Fourier section(arbitrary units).*

species[227]. The sum of the derived silver occupation numbers gives rise to a formula $Ag_{1.31}Al_{11}O_{17.15}$, which is close to the starting composition as derived from chemical analyses, although the corresponding esd's are large.

In conclusion, the material examined here displays the main features common to other studies of non-stoichiometric silver beta alumina. There is some evidence, however, that the level of cation excess was reduced by the treatment with hydrogen at 450°C. The lattice constant, c = 22.490Å, is close to that given by Roth[71] and appreciable occupation of the anti Beevers-Ross site is apparent. However, the occupancy of the Al_i site is lower than that reported elsewhere and the distribution about the Beevers-Ross position is more reminiscient of that found in the stoichiometric material which is described below.

5.3 Polycrystalline $AgAl_{11}O_{17}$ - Experimental details

The sample* was derived from the highly non-stoichiometric material $Na_{1.45}Al_{11}O_{17.225}$[73]. This was converted to $DAl_{11}O_{17}$, via the non-stoichiometric silver compound, in the manner described in Chapter 4. The silver metal which is liberated in the reduction is retained by the powder as a surface coating. The material was studied at 4.2K using PND[73] and then heated to 550°C in an evacuated furnace. Although it was not realised at this time, D_2 was lost from the sample can under these conditions, resulting in the reverse exchange:-

$$2DAl_{11}O_{17} + 2.9Ag \rightarrow 2AgAl_{11}O_{17} + D_2 + 0.9Ag$$

The interstitial oxygens responsible for charge compensation were removed, as D_2O, in the formation of $DAl_{11}O_{17}$ and in

** The sample was kindly supplied by W.A. England.*

the above reaction there is no possibility for such oxide ions to be re-incorporated. In air, the reverse exchange to $AgAl_{11}O_{17}$ occurs at ∿300°C. The sample maintains a slightly brown coloration due to the excess of silver metal. Infra-red spectroscopic measurements of the sample showed no evidence of hydrogen (deuterium)-oxygen vibrations in the near IR region and the far IR spectrum was similar to that of stoichiometric silver beta alumina prepared by other routes[52].

The sample was not transferred from the original vanadium can (15mm diameter) and it was thus already suitably contained for the PND measurements. Data was collected on the D1A diffractometer at the temperatures 4.2K, 298K (25°C) and 773K (500°C) as set out in Table 5.2. The procedure for sample alignment and data measurement was as described in Chapter 4. The incident neutron wavelength for each of the runs was calibrated from reflections recorded from a standard nickel sample. For the runs on D1A, the data from each of the nine counters were plotted individually so that spurious points might be recognised. Data from those counters which appeared to be abnormally noisy were rejected. The relative counter efficiencies and separations were derived from a peak-fitting procedure and the data were then collated[228] to give the complete diffraction profile in the range $4° \leqslant 2\theta < 160°$. The summed patterns contained contributions from 7, 8 and 6 separate counters for the data at 4.2K, 25°C and 500°C respectively. The instrumental geometry and the use of vanadium for the tail of the cryostat and the furnace element ensured that the only peaks apparent in the observed profiles are those due to $AgAl_{11}O_{17}$ and Ag_m. For the PANDA run at 300°C, an evacuable furnace with a tantalum element was employed so that three additional Ta peaks were observed (as

noted in Chapter 4). For this run, the data from the three equatorial counters were used in collation. In refinement, those regions to which Ag_m (or Ta) reflections contributed significant intensity were excluded from the calculations. The low-angle regions were also omitted because of the asymmetrical deviations of the peak shapes from gaussian in these areas.

5.4 Polycrystalline $AgAl_{11}O_{17}$ at 4.2K - Results

The procedure followed for structure solution and refinement was similar to that detailed for $DAl_{11}O_{17}$ in Chapter 4. After Fourier methods had failed to reveal the distribution of scattering matter in the mirror planes, a series of possible sites for silver was tested in least-squares refinement. A 6h site near the BR position was found to have substantial occupation. The parameters describing this site were refined together with those of the other atomic species. Anisotropic temperature factors were introduced for this silver and the spacer oxygen, O(5), and subsequently for all atoms. These refinements converged quickly without instability. Corrections for preferred orientation and peak asymmetry were included in the early stages, but they were subsequently discarded because of their low magnitudes. There was no evidence for occupation of any mirror plane sites other than those of the single silver close to the BR position and that of O(5), both of the x $\bar{x}$ 1/4 (6h) type. For example, occupancies of -0.01(1)* (aBR), -0.05(1) (BR) and a maximum value of 0.10(3) for the site adopted by deuterium in $DAl_{11}O_{17}$ were obtained. Further, the occupancy of the silver site was always close to unity. The mO site (-0.1667 0.1667, 1/4,

* *The quoted estimated standard deviations are as derived from the Rietveld refinements and it is likely that they are slightly underestimated (262).*

6h) lies close to that of Ag(1) and in refinement, as anticipated, an occupancy of greater than zero was found for this position, with a corresponding reduction in the thermal components within the plane. However, the sum of the silver occupancies of 0.79(2) (Ag(1)) and 0.21(3) (mO) remained unity. Occupation numbers for Al(1) and Al_i of 5.93(6) and 0.01(4) were found and the latter species was therefore not included in the final refinement.

The extent of the possible delocalisation of Ag or O(5) away from the 6h sites was also probed. Refinements involving the more general 12j or 12k sites were normally unstable, but where refinement was possible the derived coordinates were close to those of the 6h positions. Final overall and atomic parameters are presented in Tables 5.2 and 5.3 respectively, with bond distances and angles in Tables 5.7 and 5.8. The final observed and calculated profiles are shown in Figure 5.3, while Figure 5.4 depicts the final observed and difference mirror-plane Fourier sections. Observed and calculated reflection intensities for this data set and for those collected at the higher temperatures are listed in Appendix II.

The results of this analysis reveal that the structure of stoichiometric silver beta alumina is well-ordered at 4.2K, with a single silver site between the BR and mO positions. There is no occupation of the often-called 'ideal' BR site. Occupation of the aBR position is also not an intrinsic feature of the stoichiometric material and, in the absence of such occupation, the c-axis constant is increased relative to the NS-counterpart. The value c = 22.5131(2)Å at 4.2K compares with c = 22.49Å for the non-stoichiometric material at 298K.

The confidence with which the lattice parameters given in Table 5.2 represent their absolute magnitudes is limited by

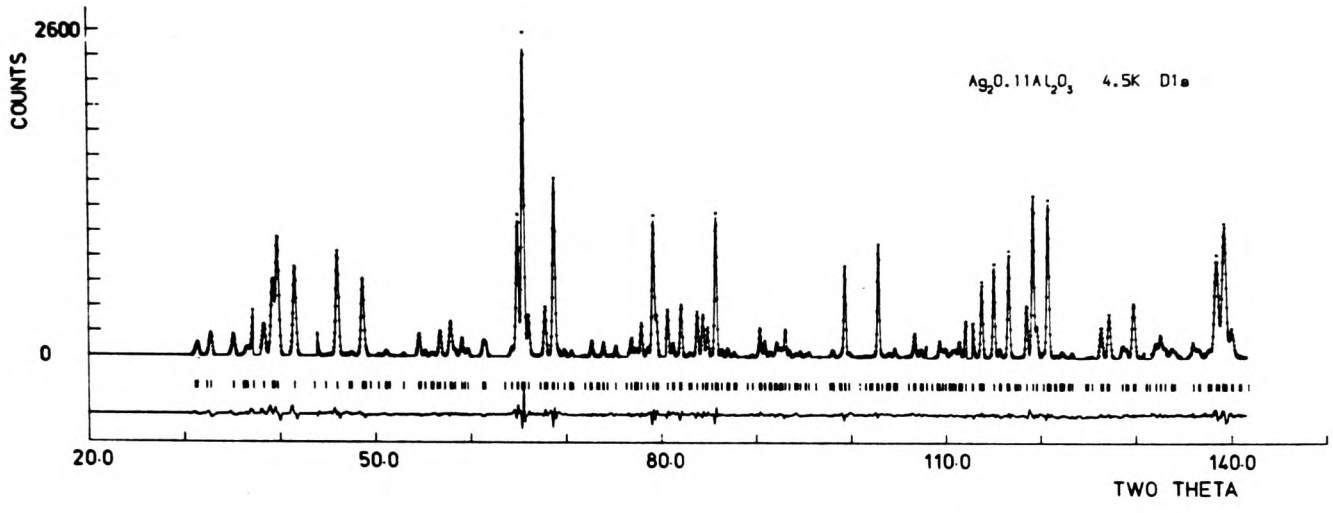


Figure 5.3(a). The final observed(dots),calculated (continuous line) and difference (lower) diffraction profiles for $AgAl_{11}O_{17}$ at 4.2K (D1a diffractometer).The reflection positions are marked as bars.

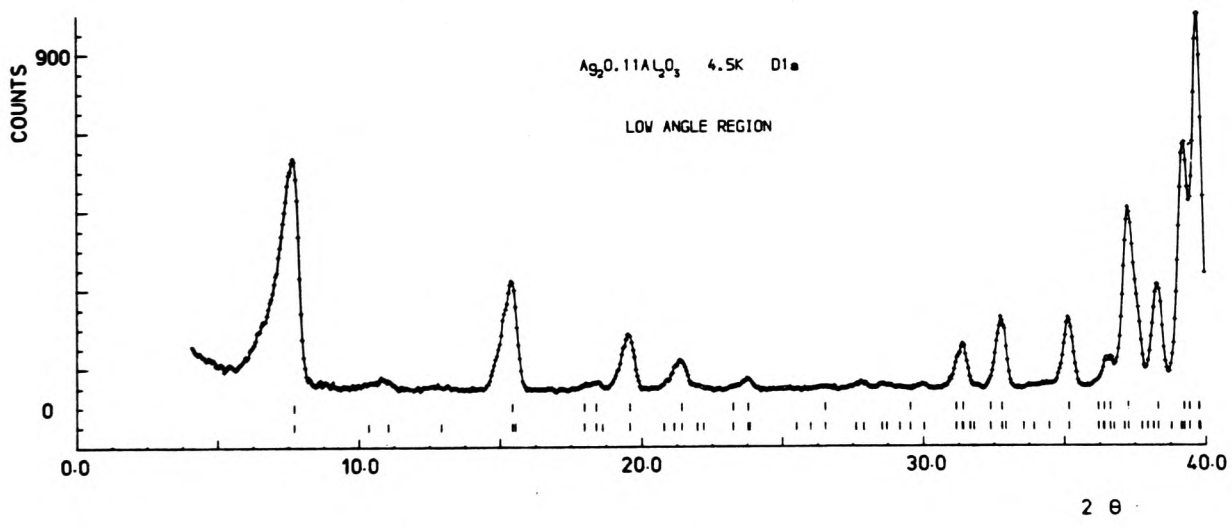


Figure 5.3(b). The low angle region of the observed PND profile for $AgAl_{11}O_{17}$ at 4.2K. The upper reflection bars indicate the positions of reflections from the normal beta alumina sub-cell whereas the lower bars indicate the positions of allowed superlattice reflections.

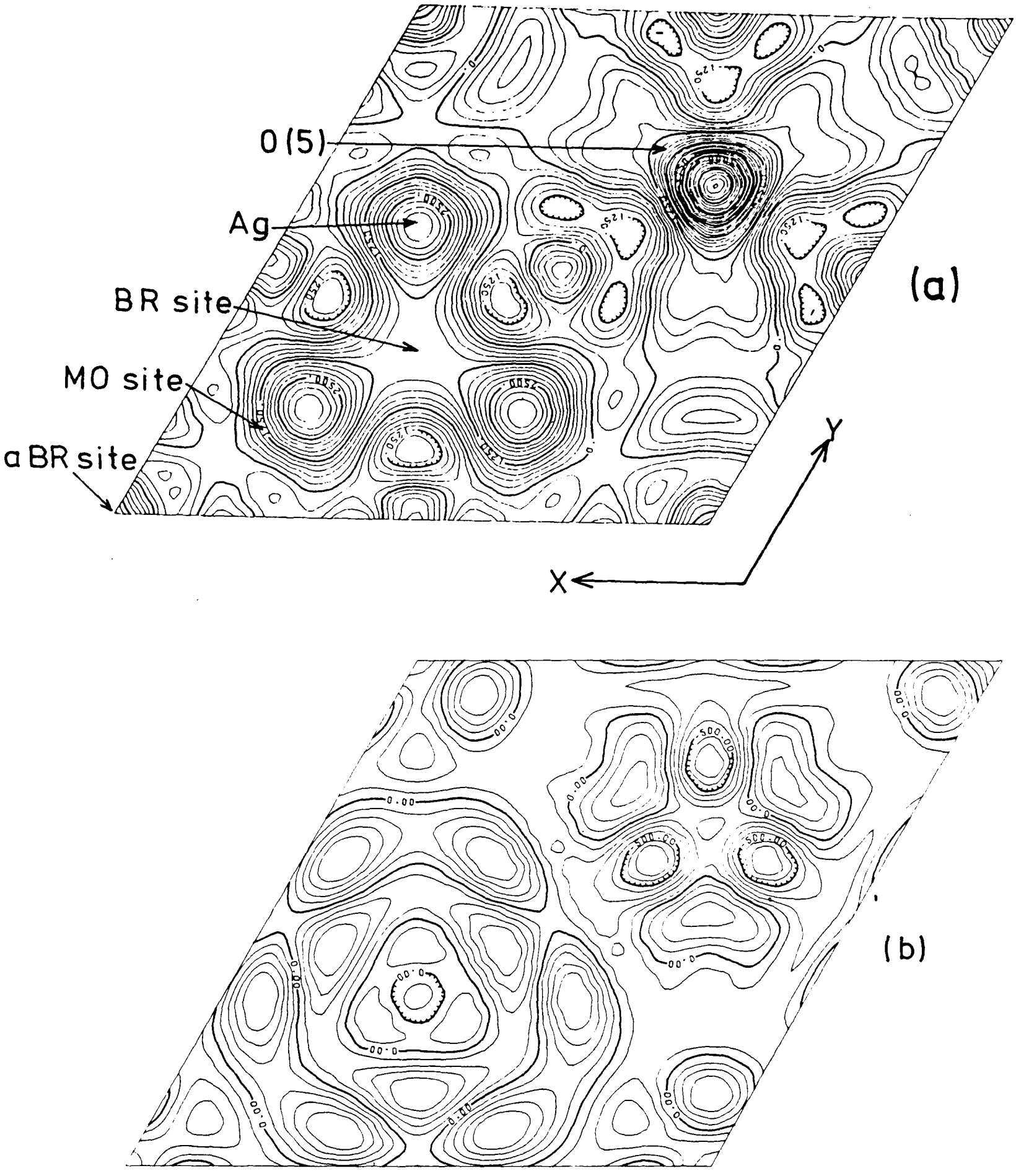


Figure 5.4. The z = 1/4 sections of final /F_{obs}/ (upper) and /F_{obs}-F_{calc}/ (lower) Fourier syntheses calculated from the PND data on stoichiometric silver beta alumina at 4.2K. The positions of the Beevers-Ross (BR) ,anti-Beevers-Ross (aBR) and mid-oxygen (mO) sites are indicated.The contours are scaled in arbitrary units.

the accuracy with which we know the incident neutron wavelength. This was defined, as outlined above, by the use of a standard Ni sample. In addition, we may use the small quantity of excess silver metal as an internal calibrant. The silver metal regions were extracted from the observed pattern and employed in powder profile refinement. In addition to the scale factor, the variable parameters were the cell constant, counter zero-point error and the temperature factor for silver*. Final values of a_o = 4.0663(5)Å, $z\theta$ = -0.082(14)° and B_{Ag} = 0.56(15)Å² were obtained and a list of reflection intensities is given in Appendix II. The lattice constant agrees well with that derived by extrapolation from the values given in International Tables[1]. The zero-point error agrees to within 0.01° of that obtained in refinement of the bulk pattern (Table 5.2). Clearly, good significance can be attached to the value c = 22.513Å for $AgAl_{11}O_{17}$ at 4.2K.

Inspection of Figure 5.5 (overleaf) reveals the reason why the silver ions occupy this particular site. This location brings the silver ions as close as possible (2.727Å) to four O(2) atoms above and below the mirror plane (cf. O(2) - BR 2.827Å, O(2) - mO 2.841Å). The coordination may be improved still further by an in-plane cooperative movement of O(5) atoms. In refinement, these spacer oxygens are found to occupy the 3-fold 6h sites. There are thus three possible O(5) sites per mirror plane, as indicated by the arrows in Figure 5.5. If, for each silver site, the displacement of O(5) is chosen which minimises the Ag-O(5) distance, then the distribution in Figure 5.5 and the indicated superlattice are created. The dimensions of

* *This refinement also indicates that the face-centred cubic phase of Ag_m is maintained at 4.2K.*

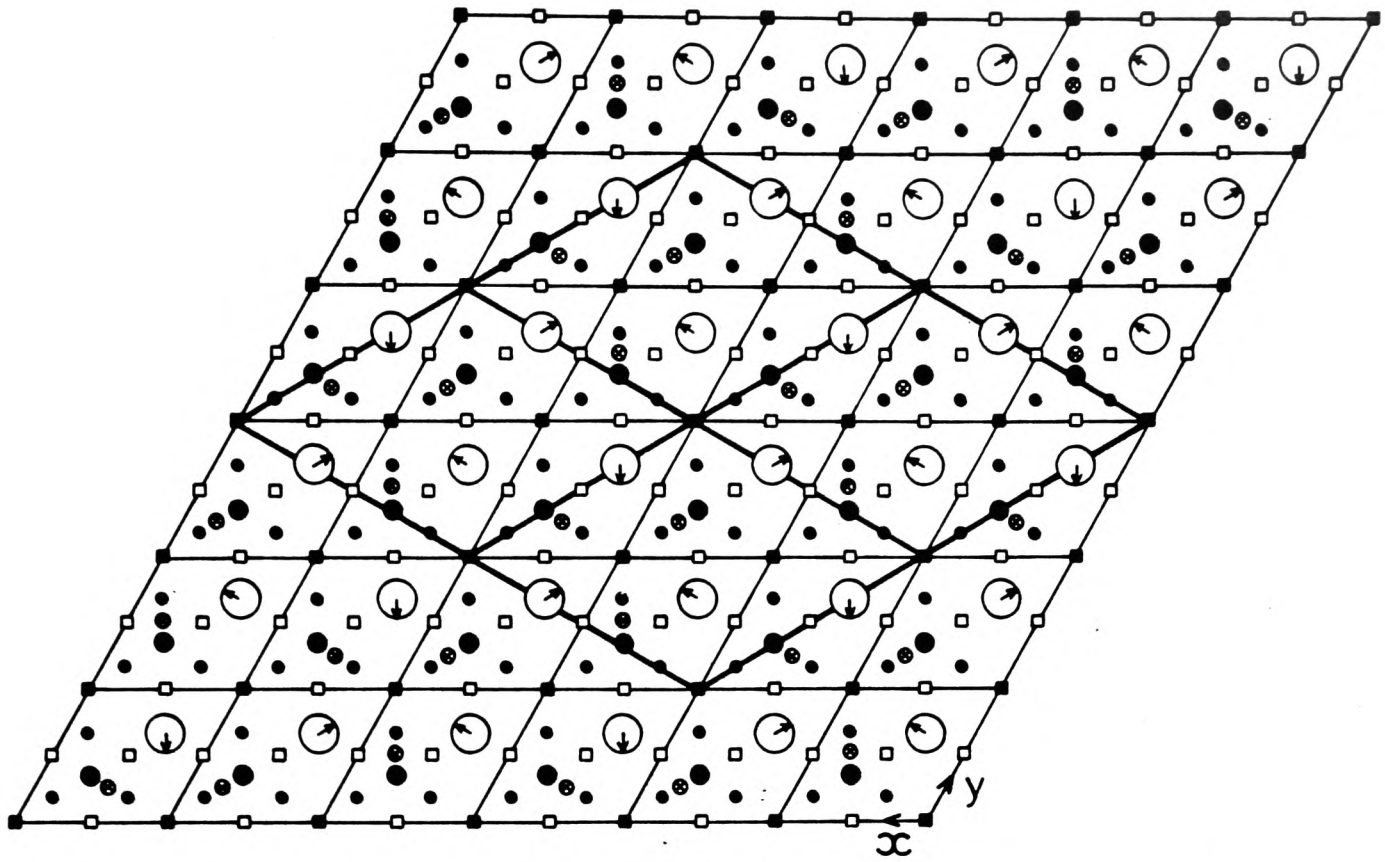


Figure 5.5. Superlattice of Stoichiometric Silver Beta Alumina.
• Silver, ● BR site, ○ O(5), • MO position
▪ ABR site and projection of O(4) position
▫ Projection of O(2) position

this supercell, a√3 x a√3 are identical to those reported by Boilot et al.[196]. However, though we have deduced this arrangement for a particular conduction plane, we have no direct information on how the other planes, separated by increments in the c-direction, are related.

The presence of the 6_3 screw axis in the subcell implies that the supercell will have a c-axis of the same length. Collin et al.[230] report that their X-ray data on the supercell manifests hexagonal symmetry with the systematic absences 0 0 0 ℓ ℓ = 2n+1, although other members of h h $\overline{2h}$ ℓ, and h $\bar{h}$ 0 ℓ, series for ℓ = 2n+1 are present. These observations are consistent with the space groups $P6_3$, $P6_3/m$ or $P6_322$. However, they also find the intensity relationship I(hkℓ) = I(khℓ) which implies that the Laue symmetry is 6/mmm, or a sub-group such as 622, which restricts the space group to $P6_322$. In Figure 5.5, we see that the silver sites correspond to x y 1/4 (6h) in $\underline{P6_3/m}$ with

x = 0.45 and y = 0.11. The spacer oxygens are also at such 6h positions, with x = 0.37 and y = 0.33. The coordinates are such that these two pairs of sites are, to a reasonable approximation, related by the symmetry elements of $P6_322$. That is, a single atomic species at 0.4 0.1 1/4 (12i) in this space group would give rise to occupation of both the three silver and the three oxygen positions. However, for X-rays, the scattering powers of silver and oxygen are markedly different so that this arrangement does not, in itself, explain the observed intensity distribution. A second interpretation is that the silver ions (and O(5)) adopt the 12i sites in $P6_322$. This would imply six equivalent, half-occupied silver sites in each supercell z = 1/4 plane, with the silvers subject to slight displacements from z = 1/4 so that their locations do not correspond exactly to the x y 1/4 (12j) sites of $P6_3/mmc$. Although such displacements might be favoured by a reduction in two Ag-O(2) contacts, there is no evidence for such behaviour in the atomic parameters derived from our analysis of the subcell. In the room temperature X-ray study of Colomban[52,230], the U_{33} components of the major silver species are approx. twice as large as those of O(5) and the spinel block atoms. However, at room temperature, the structure already displays a decrease in the extent of order within the mirror planes (Section 5.5 and ref. 230) and an accurate description of the supercell arrangement will probably require an analysis of X-ray data collected at low temperature.

The existence of the supercell implies the possibility of crystallographically distinct O(2) and O(4) ions. Thus, for one third of the O(4) sites there are silver ions at shorter separations than for the remaining two-thirds (see Figure 5.5).

A similar situation accrues to the O(2) sites. Were such a distinction between the respective O(2) and O(4) species significant, we might have anticipated slight anomalies in the behaviour of their atomic parameters in refinement and, in particular, their β_{33} thermal components. Table 5.3 reveals no such abnormality, however, which implies that these oxygen atoms are little influenced by changes in the atomic distribution within the mirror plane.

The analysis outlined above derives from a consideration solely of the <u>average</u> structure, employing only subcell reflections and no appreciable disparities are seen in the difference plot given in Figure 5.3(a). The intensity of superlattice reflections derives from the cooperative displacement of one silver and one oxygen per $AgAl_{11}O_{17}$ unit. The relative neutron scattering lengths are such that this involves only 8.3% of the total scattering power and hence superlattice reflections are of low intensity. Figure 5.3(b) displays the low angle region of the observed profile (the region $2\theta < 25°$ had been excluded from the calculations because of the asymmetry of the Bragg peaks). Some peaks of limited intensity, at positions of allowed superlattice reflections are discernible. Their intensities are of the right order of magnitude if it is assumed that they arise solely from the AgO unit, as above. These minor fluctuations above background disappear at higher temperatures (compare with Figures 5.10(b) and 5.11).

5.5 Polycrystalline $AgAl_{11}O_{17}$ at 25°C - Results

Figure 5.6(a) displays the final z = 1/4 $/F_{obs}/$ Fourier section obtained from this data set. A comparison with Figure

5.2(a) demonstrates the change in silver distribution effected by the increase in temperature from 4.2K to 25°C*, a difference which was evidenced in the least-squares refinements. The predominant silver site was again found to be of the 6h type, with the value of x close to that obtained at 4.2K, and refinement progressed as for the data collected at that temperature, with anisotropic thermal parameters being introduced for all atoms in the later stages. The thermal components of the silver within the mirror plane are considerably increased relative to those at 4.2K and, further, even with this considerable thermal delocalisation, the occupancy of the 6h site refined to less than unity. A series of models including other sites was then considered. Firstly, schemes for a more extended delocalisation about this 6h site, involving a second silver at or close to -0.19 0.19 1/4 (6h) with independent temperature factors, were tested in least squares. Such refinements converged to reasonable residuals (R_P = 0.0837, R_{WP} = 0.0933) when the total occupancy was constrained to be unity. The individual occupancies were 0.51 and 0.49 respectively, but the β_{11} component of the former site was 0.25(2). As subsequent refinements converged to slightly lower residuals, with the β_{11} component of the major silver site a factor of 5 lower, we do not elaborate on this particular model. However, we must stress that the use of PND data does not allow us to probe accurately the type of schemes that have been derived from single crystal X-ray data[52,71,230] where, for X-rays, the scattering power of the silver is relatively much greater. The other models which were tested involved the mO, BR and aBR positions. Of these three, the former two were un-

* *It is worth noting that series-termination errors are of lower magnitude for D1A data compared with that from the PANDA diffractometer because a larger range of 2θ is measured.*

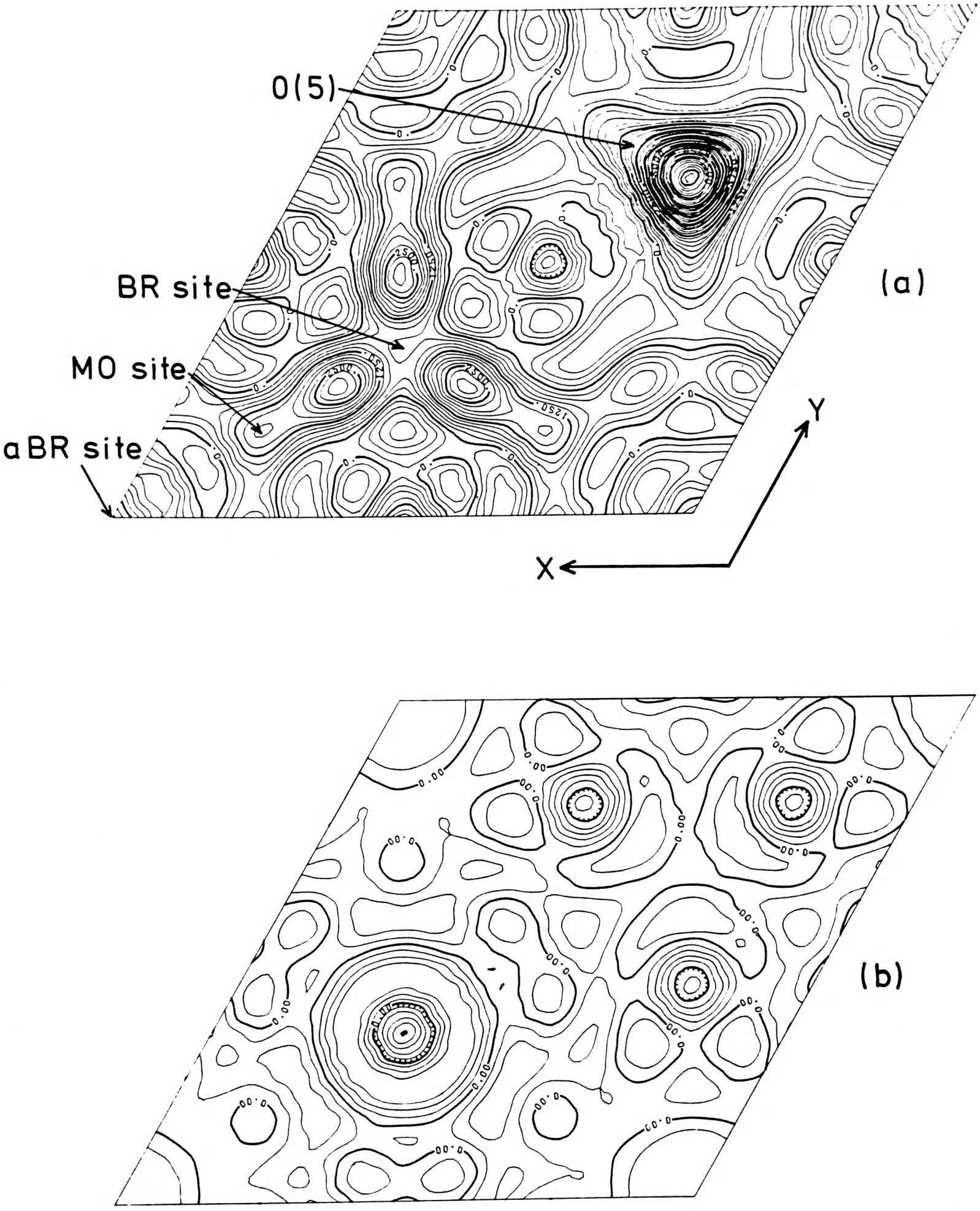


Figure 5.6. The z = 1/4 sections of final $/F_{obs}/$ (upper) and $/F_{obs}-F_{calc}/$ (lower) Fourier syntheses calculated from the PND data on stoichiometric silver beta alumina at 298K (25°C).The positions of the Beevers-Ross (BR), anti Beevers-Ross (aBR) and mid oxygen sites are indicated.The contours are scaled in arbitrary units.

satisfactory in that the β_{11} components of silver on these sites adopted extremely large values (1.2(2) and 0.8(1) respectively). The aBR site gave improved agreements and it is this model that we present in the tables. Even for this site, the β_{11} and β_{12} components are large which probably indicates that some static disorder also occurs, but the limited occupancy and the diffuse nature of this position would not enable sensible refinements, involving slight displacements from the aBR site to be obtained. When allowed to vary, the occupancies of the interstitial aluminium site, Al_i, and of Al(1) converged to values of 0.02(4) and 5.91(5) respectively. The observed and calculated profiles are displayed in Figure 5.7(a) and reflection intensities are listed in Appendix II.

This analysis reveals the onset of a transformation in the structure of $AgAl_{11}O_{17}$. The ordered distribution which was apparent at 4.2K is no longer found and the major silver site is subject to large-amplitude thermal vibration, although about a position still close to that which optimises the silver co-ordination. There is, however, evidence for limited occupation by silver of the aBR site suggesting that the activation energy for conduction will be small. The lattice constant is still increased relative to the non-stoichiometric parent. In the low angle region of the observed PND profile (Figure 5.7(b)), the superlattice reflections are now of reduced intensity, manifesting the breakdown of the long-range ordering scheme although our analysis indicates that the silver does not yet adopt a quasi-liquid distribution such as that apparent at 500°C (section 5.6). The spinel-block atomic parameters are in good agreement with those of Colomban et al.[52,230], although the details of the mirror plane distributions differ somewhat. We have found

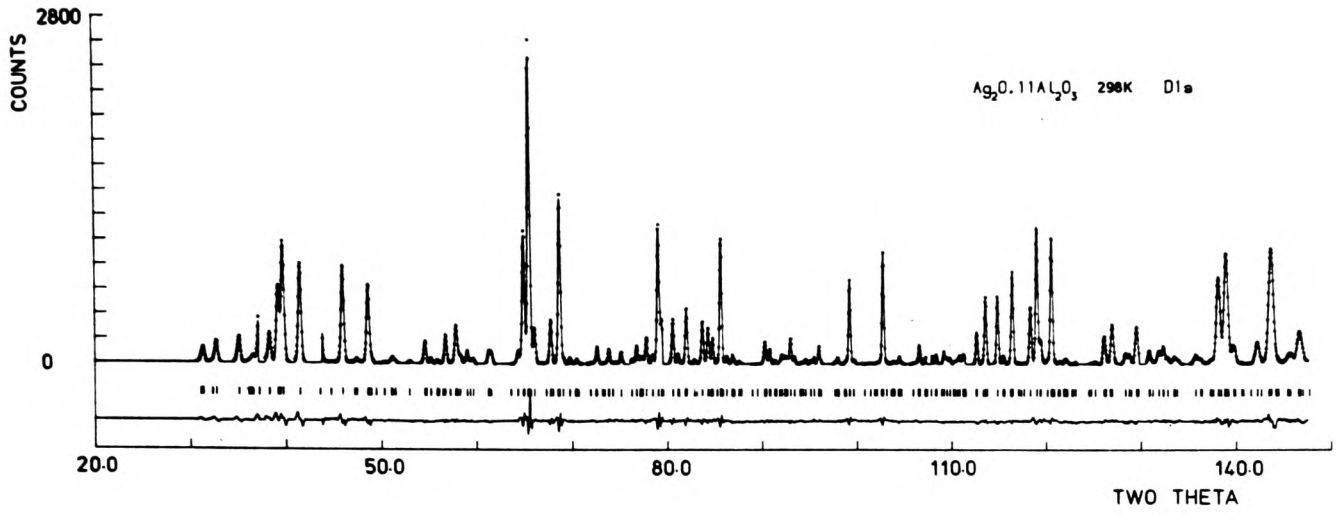


Figure 5.7(a). The final observed (dots), calculated (continuous line) and difference (lower) diffraction profiles for $AgAl_{11}O_{17}$ at 25°C (D1a diffractometer). The reflection positions are marked as bars.

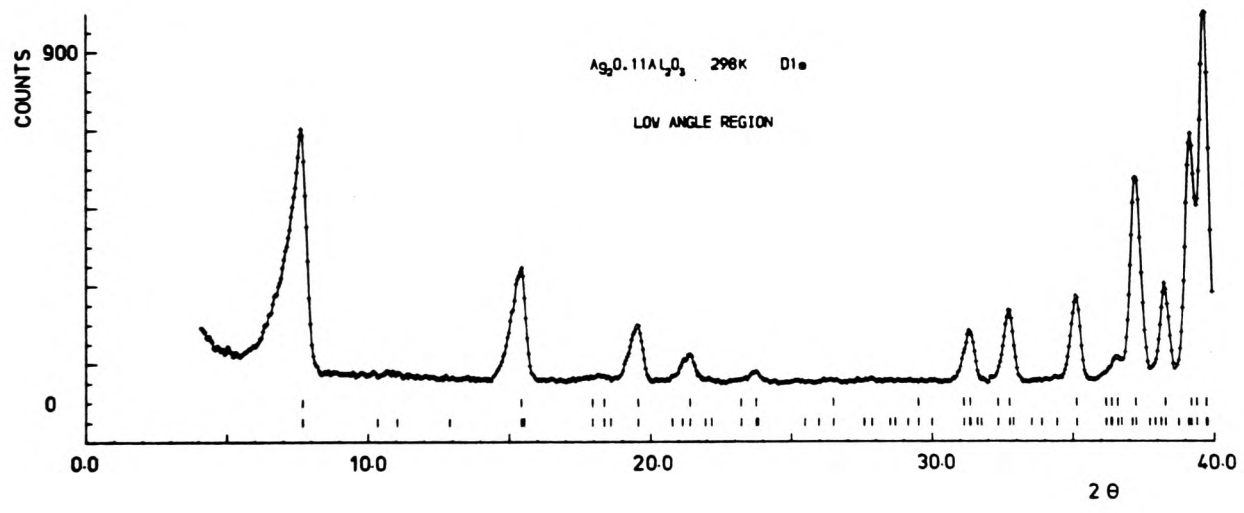


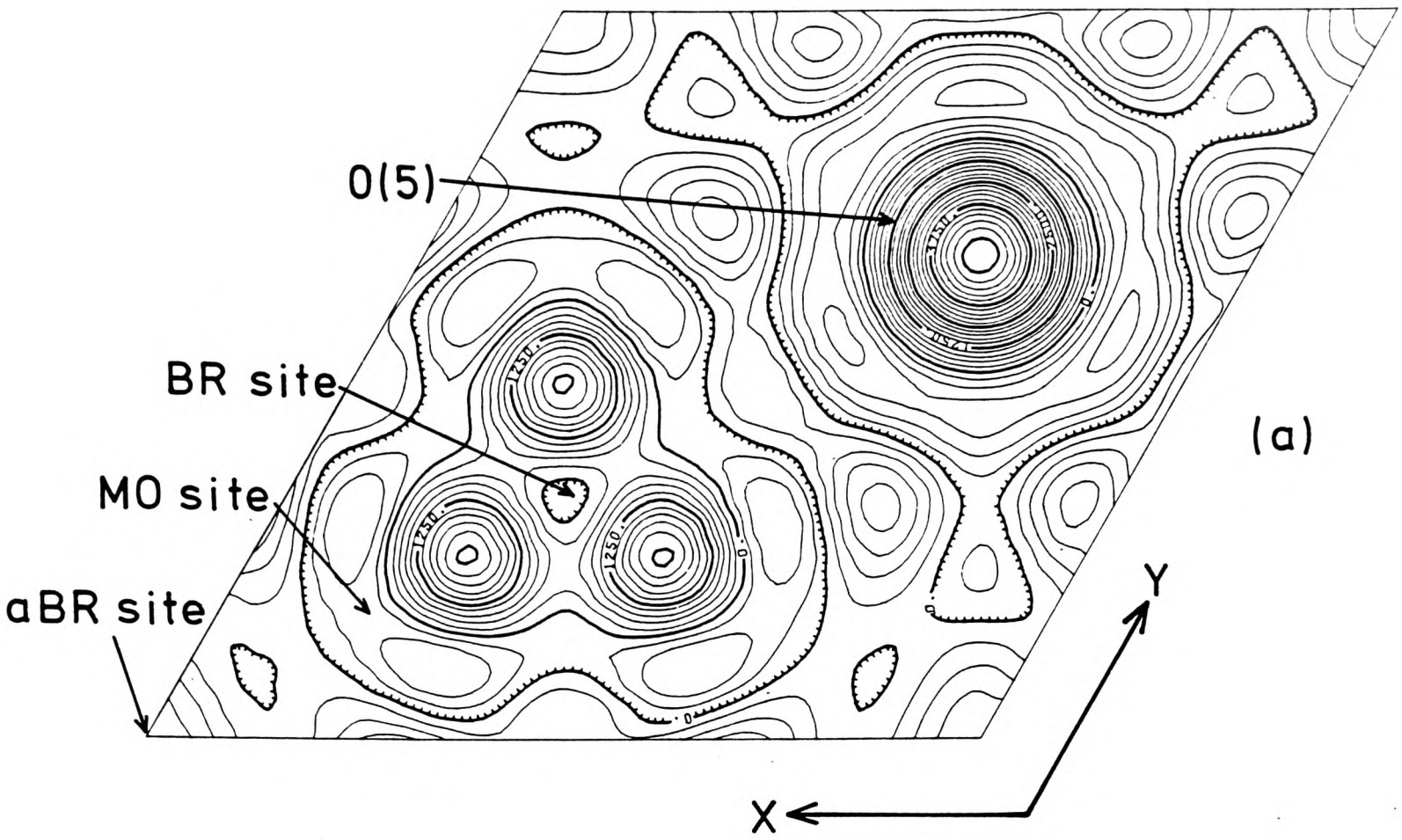
Figure 5.7(b). The low angle region of the observed PND profile for $AgAl_{11}O_{17}$ at 25°C.The upper bars indicate the positions of reflections from the nromal beta alumina sub-cell and the lower bars indicate the positions of allowed superlattice reflections.

no evidence for occupation of sites close to the BR position, but we do find some indication of aBR occupancy. Colomban et al.[52,230] also report a significant population of interstitial aluminiums. These disparities probably arise from the different preparative routes and we consider the deammoniation of ammonium beta alumina, the route which they used to prepare stoichiometric materials, in the following chapter.

5.6 Polycrystalline $AgAl_{11}O_{17}$ at 300°C and 500°C - Results

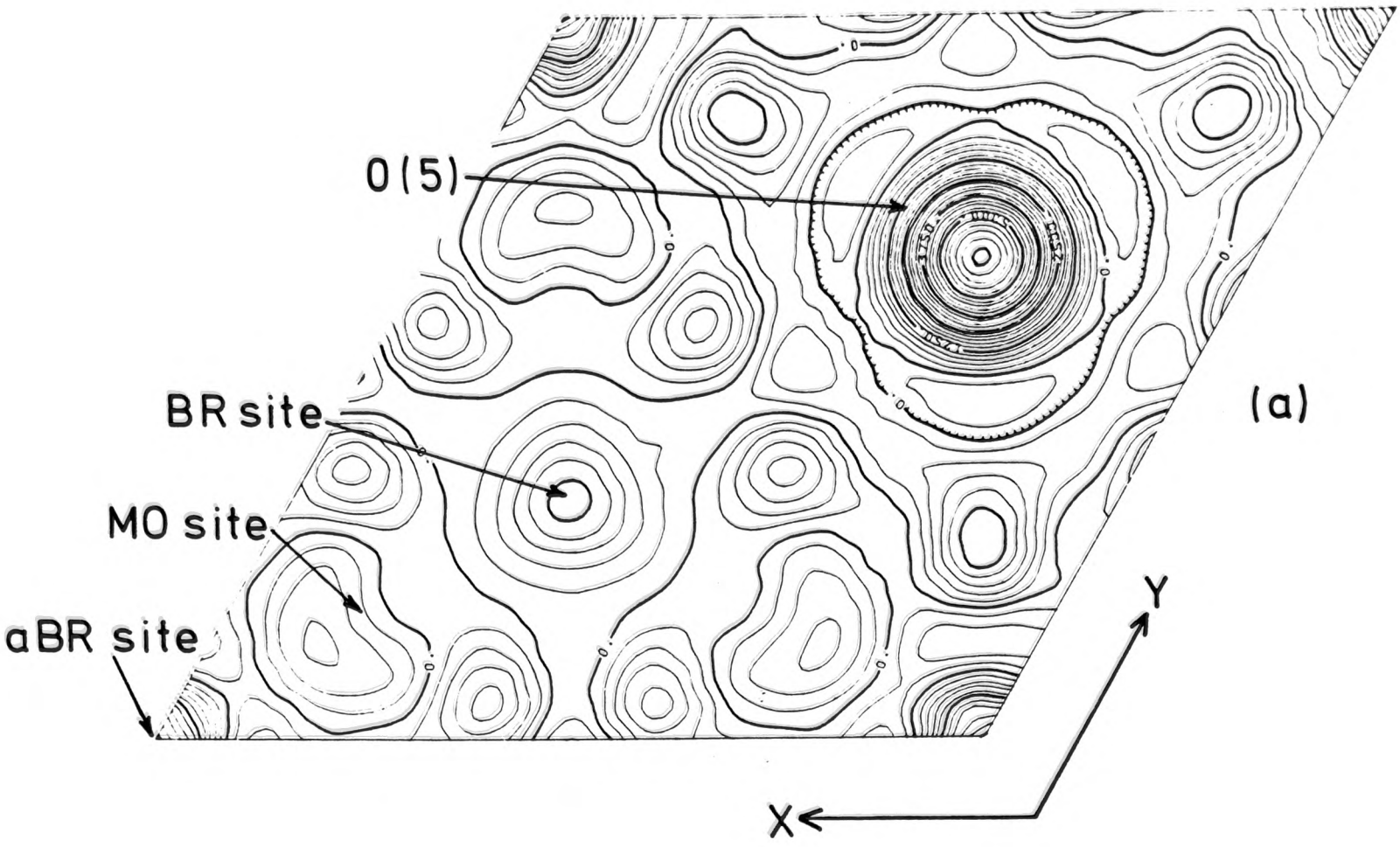
Least-squares refinement of these two data sets proceeded in the manner described above for that collected at 25°C. The final derived parameters are presented in the tables; the corresponding z = 1/4 $/F_{obs}/$ and $/F_{obs} - F_{calc}/$ Fourier sections are displayed in Figures 5.8 (300°C) and 5.9 (500°C), with final observed and calculated profiles in Figure 5.10. Reflection intensities are listed in Appendix II. At 300°C, the structure definition is limited by the poorer quality of the data set which is consequent on the use of the PANDA diffractometer. In particular, the temperature factors are not as reliable as those determined from the D1A data sets. However, the atomic parameters broadly reflect the trend in structure evolution as the temperature is raised.

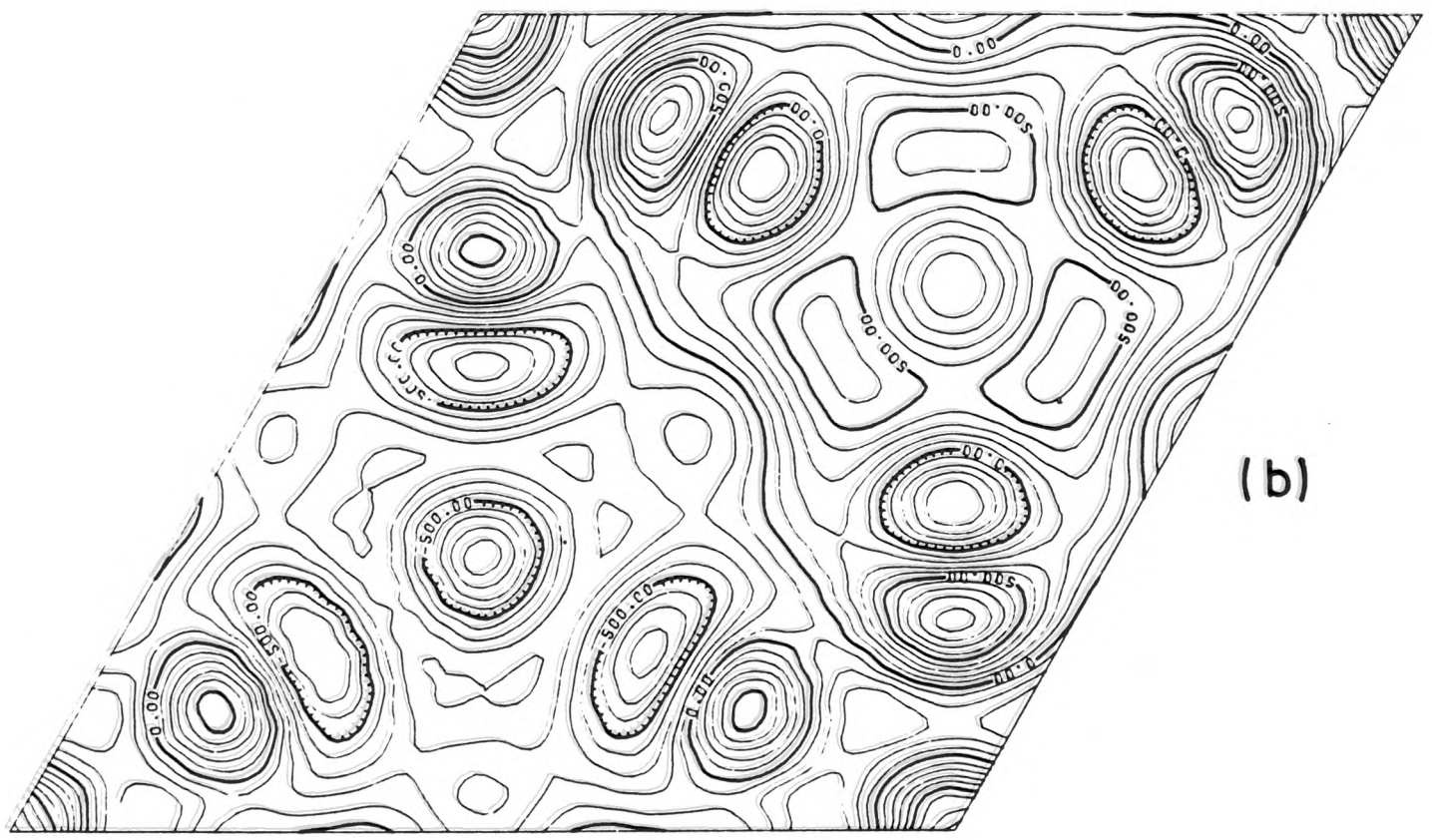
In the z = 1/4 $/F_{obs}/$ Fourier section obtained from the 500°C data (Figure 5.9(a)) no silver density is resolved and the final atomic parameters are indicative of the quasi-liquid distribution which was deduced from X-ray diffuse scattering studies[196]. The weak superlattice reflections have now completely disappeared from the low-angle region of the observed profile (Figure 5.11). It is interesting to compare this model with that derived by Reidinger for non-stoichiometric (NS) sodium



Ag $Al_{11}O_{17}$ 573 K

Figure 5.8. The z = 1/4 sections of final /F_{obs}/ (upper) and /F_{obs}-F_{calc}/ (lower) Fourier syntheses calculated from the PND data on stoichiometric silver beta alumina at 573K (300°C).The positions of the Beevers-Ross (BR), anti Beevers-Ross (aBR) and mid oxygen (mO) sites are indicated.The contours are scaled in arbitrary units.





Ag Al_{11} O_{17} 773 K

Figure 5.9. The z = 1/4 sections of final /F_{obs}/ (upper) and /F_{obs}-F_{calc}/ (lower) Fourier syntheses calculated from the PND data on stoichiometric silver beta alumina at 773K (500°C).The positions of the Beevers-Ross (BR), anti Beevers-Ross (aBR) and mid oxygen (mO) sites are indicated.The contours are scaled in arbitrary units.

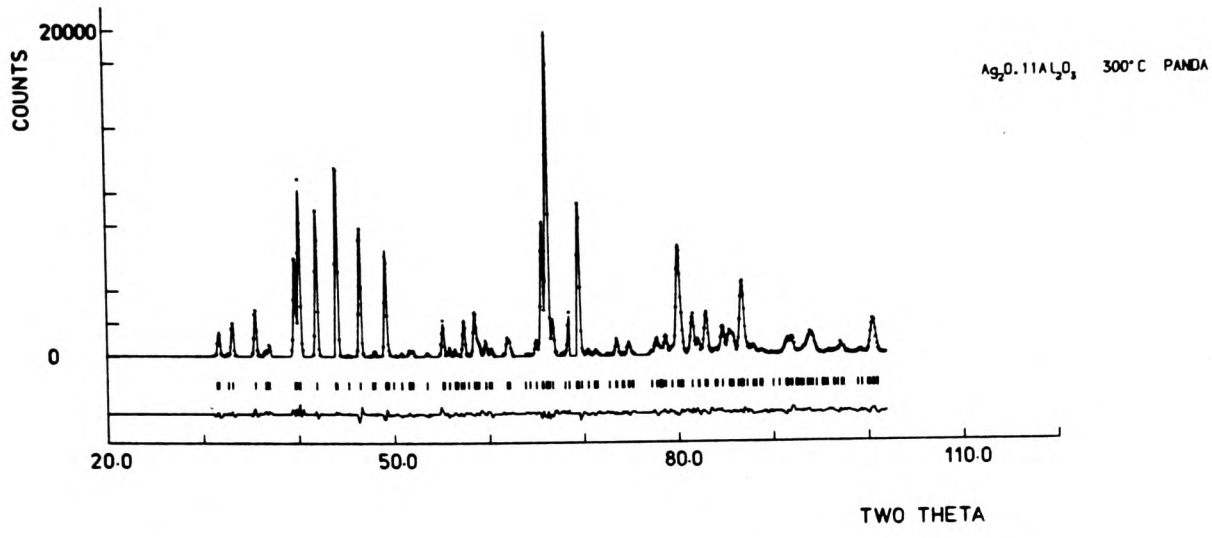


Figure 5.10(a). The final observed (dots), calculated (continuous line) and difference (lower) diffraction profiles for $AgAl_{11}O_{17}$ *at 300°C (PANDA diffractometer). The reflection positions are marked as bars.*

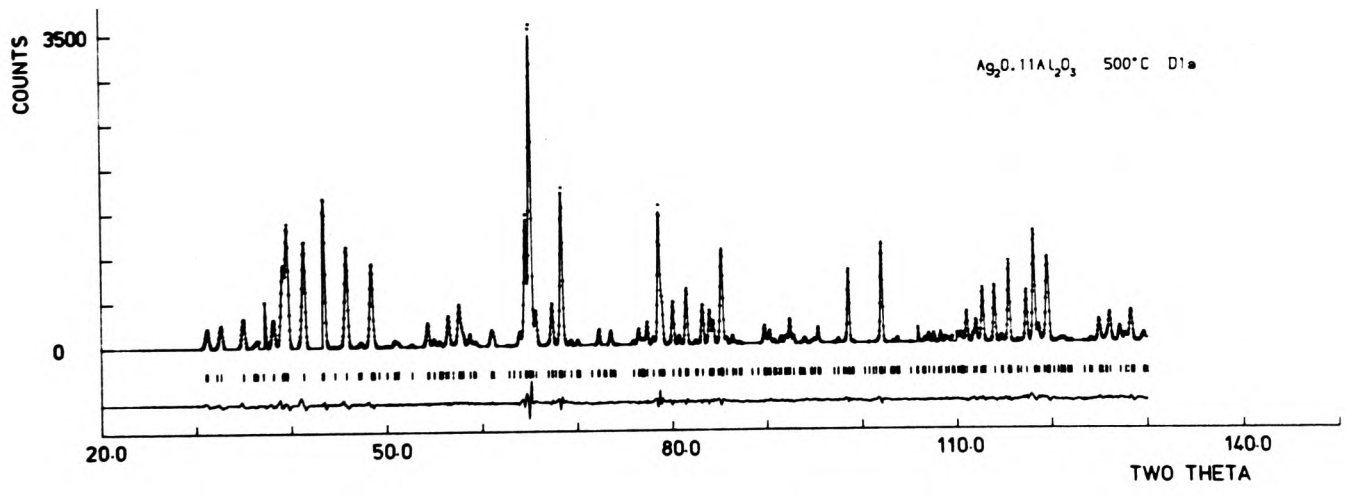


Figure 5.10(b). The final observed (dots), calculated (continuous line) and difference (lower) diffraction profiles for $AgAl_{11}O_{17}$ *at 500°C (D1a diffractometer). The reflection positions are marked as bars.*

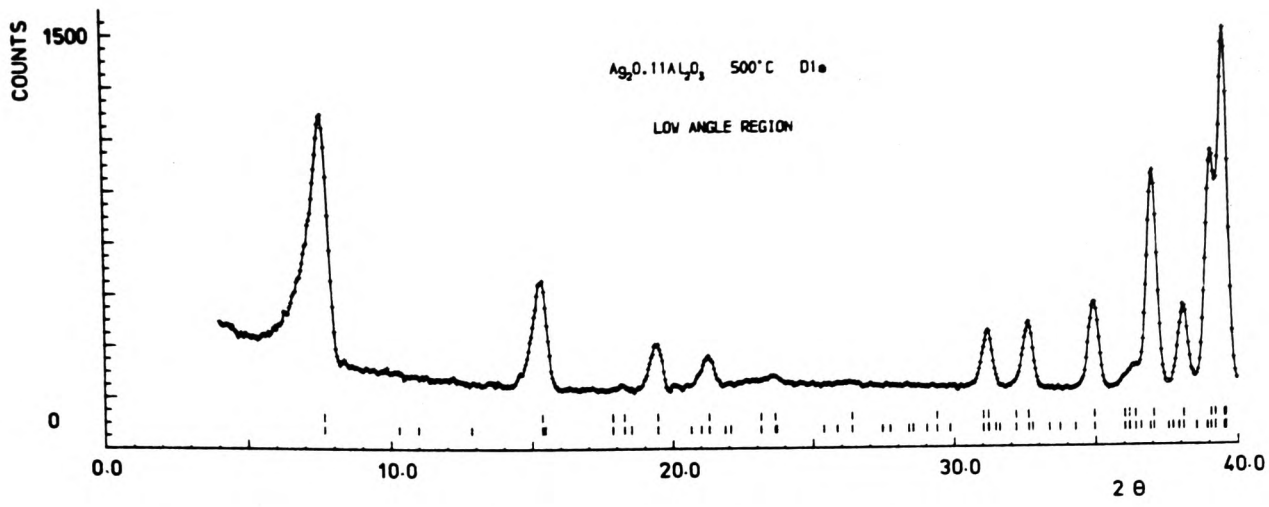


Figure 5.11. The low angle region of the observed PND profile of $AgAl_{11}O_{17}$ at 500°C (D1A). The bars indicate the calculated positions of normal (upper) and superlattice (lower) reflections.

beta alumina at 500°C[44]. In that material, the degree of thermal motion increases and the distribution between BR, mO and aBR sites is altered as the temperature is raised from 80K to 500°C, but the sodium density remains well-defined. The anisotropic temperature factors do not become excessively large, even at 500°C. The X-ray diffuse data on NS-sodium beta alumina[125] does not display the quasi-liquid scattering which is found for both NS-[124] and S-silver[196] materials and because of this disparity, we cannot directly gauge the effect of the absence of interstitial oxygens on the cation distribution in S-materials at elevated temperatures. It would be interesting to examine, as a function of temperature, the structure of the S-sodium compound which may be prepared by the exchange of polycrystalline $AgAl_{11}O_{17}$ in molten sodium nitrate[231].

Examination of the atomic coordinates and bond lengths as a function of temperature reveals that the spinel block atoms are little affected by the order-disorder transition whch occurs within the mirror planes. This is consistent with the description of the superlattice observed at 4.2K as deriving solely from the silver location and the cooperative displacement of O(5). As the silver becomes more delocalised, the strength of the Ag-O(5) interaction diminishes and the extent of the dis-

placement of O(5) away from the 2c site decreases. This is manifested by an increase in the O(5) x-parameter from 4.2K - 25°C - 500°C. At these three temperatures, the Al(3)-O(5) bond length is increased relative to that in the NS-material; that obtained in the single crystal neutron study described in section 5.2 is intermediate between the two. The increase probably reflects the reduced cation density in the mirror planes which is therefore less able to shield the O-O repulsions across these planes. Such an effect is probably also partly responsible for the expansion, with respect to the NS-compound, in the c-axis constants.

5.7 Conclusion

We have prepared stoichiometric $AgAl_{11}O_{17}$ by a new route and we have presented evidence that the level of stoichiometry in metal beta aluminas may be lowered by partial reduction with hydrogen. Our structural study of stoichiometric silver beta alumina has demonstrated the existence of a well-ordered phase at 4.2K. As the temperature is raised, the thermal motion of the silver ions increases and, at 25°C, we observe the onset of a transformation to an atomic distribution in which the long-range order is destroyed and the silver ions become delocalised within the conducting planes. By 500°C, this change is complete; our diffraction results are indicative of a highly diffuse silver distribution, although the spinel block atoms are hardly affected by the transition. The behaviour of the stoichiometric material is thus in contrast to that of the non-stoichiometric parent.

TABLE 5.1. Final atomic parameters derived from the single crystal neutron diffraction study of $Ag_{1.25}Al_{11}O_{17.125}$ with estimated standard deviations in parentheses.

Atom	Position	Site symmetry	x[a]	z	Occn.	U_{11}[b]	U_{33}	U_{12}	U_{13}	U_{23}
O(1)	12k	m	0.1561(3)	0.0500(1)	6.0	0.014(1)	0.014(1)	0.009(1)	-0.0008(5)	$-U_{13}$
O(2)	12k	m	0.0528(4)	0.1467(1)	6.0	0.012(1)	0.018(1)	0.005(1)	-0.0002(5)	$-U_{13}$
O(3)	4f	3m	-1/3	0.0552(2)	2.0	0.014(2)	0.008(2)	$U_{11/2}$	0	0
O(4)	4e	3m	0	0.1424(2)	2.0	0.0011(1)	0.010(2)	$U_{11/2}$	0	0
O(5)	6h	mm	-0.301(3)	1/4	1.0	0.044(13)	0.013(5)	0.016(7)	0	0
Al(1)	12k	m	-0.1677(5)	0.1068(2)	5.88(7)[c]	0.013(2)	0.015(2)	0.006(2)	-0.000(1)	$-U_{13}$
Al(2)	4f	3m	1/3	0.0248(3)	2.0	0.006(2)	0.014(3)	$U_{11/2}$	0	0
Al(3)	4f	3m	1/3	0.1764(3)	2.0	0.014(3)	0.001(3)	$U_{11/2}$	0	0
Al(4)	2a	$\bar{3}$m	0	0	1.0	0.009(3)	0.002(4)	$U_{11/2}$	0	0
Ag(1)	6h	mm	-0.268(4)	1/4	0.80(7)	0.087(16)	0.025(9)	0.012(16)	0	0
Ag(2)	2b	$\bar{6}$m2	0	1/4	0.15(13)	0.01(6)	0.09(13)	$U_{11/2}$	0	0
Ag(3)	6h	mm	-0.07(2)	1/4	0.36(11)	0.087(16)[d]	0.025(9)	0.012(16)	0	0

Cont.

TABLE 5.1, cont.

$R = 0.0593 \quad R_W = 0.0567$

Extinction Parameter = 1.7(2)

[a]For all sites $y = -x$ and $U_{11} = U_{22}$

[b]Temperature factors are given in the form of Equation 6, Chapter 2, where:

$$B_{11} = 8\pi^2 U_{11}, \text{ etc.}$$

[c]The occupancy of the interstitial aluminium, Al_i, was constrained with that of Al(1) such that the total was 6.0. The thermal components of Al_i were equivalenced with those of Al(1) (see text).

[d]The thermal components of Ag(3) were constrained to equal those of Ag(1).

TABLE 5.2

Lattice constants and Instrumental Parameters for the PND studies of $AgAl_{11}O_{17}$, with estimated standard deviations in parentheses.

	4.2K	298K (25°C)	573K (300°C)	773K (500°C)
Instrument	D1A	D1A	PANDA	D1A
Apparatus	V-tailed cryostat	-	Ta-element furnace	V-element furnace
Wavelength Å	1.5118(1)	1.5118(1)	1.5279(5)[a]	1.5110(5)
a Å	5.5871(1)	5.5913(1)	5.6026(6)	5.6169(1)
c Å	22.5131(2)	22.5293(2)	22.5489(10)	22.5973(2)
U Å^3	608.62(2)	609.96(2)	613.0(2)	617.42(4)
Zeropoint[b]	-8.90(8)	-8.04(7)	12.4(2)	-3.03(8)
U	893(14)	896(11)	6014(346)	1045(24)
V	-2288(35)	-2266(29)	-5366(384)	-2596(52)
W	2080(20)	2016(17)	1893(100)	2222(24)

[a]Calculated from the profile refinement of the silver metal diffraction pattern which was extracted from the observed profile

[b]Counter zeropoint, U, V and W expressed in units of hundredths of a degree in 2θ.

TABLE 5.3. Final atomic parameters for $AgAl_{11}O_{17}$ at 4.2K with estimated standard deviations in parentheses.

Atom	Position	Site Symmetry	x	z	Occn.	β_{11} [a]	β_{33}	β_{12}	β_{13}	β_{23}
O(1)	12k	m	0.1576(2)	0.0501(1)	6.0	0.0031(6)	0.00023(3)	0.0023(7)	-0.0000(1)	$-\beta_{13}$
O(2)	12k	m	0.5029(3)	0.1460(1)	6.0	0.0052(6)	0.00012(3)	0.0051(9)	-0.0001(1)	
O(3)	4f	3m	-1/3	0.0548(2)	2.0	-0.0002(8)	0.00020(5)	$\beta_{11/2}$	0	0
O(4)	4e	3m	0	0.1415(1)	2.0	0.0018(9)	0.00016(6)	$\beta_{11/2}$	0	0
O(5)	6h	mm	0.2972(10)	0.25	1.0	0.021(5)	0.00006(13)	0.012(3)	0	0
Al(1)	12k	m	-0.1665(5)	0.1066(1)	6.0	0.0006(7)	0.00028(4)	-0.001(1)	0.0005(1)	$-\beta_{13}$
Al(2)	4f	3m	1/3	0.0251(2)	2.0	-0.0021(7)	0.00017(9)	$\beta_{11/2}$	0	0
Al(3)	4f	3m	1/3	0.1754(3)	2.0	0.0017(9)	0.00032(9)	$\beta_{11/2}$	0	0
Al(4)	2a	$\bar{3}$m	0	0	1.0	-0.0002(14)	0.00014(11)	$\beta_{11/2}$	0	0
Ag	6h	mm	-0.2237(10)	0.25	1.02(5)	0.014(4)	0.00020(20)	-0.005(3)	0	0

$R_I = 0.0511$ $R_P = 0.0861$ $R_{WP} = 0.0977$ Expected R = 0.1108

[a] Thermal parameters are expressed in the form:- $\exp\{-(\beta_{11}h^2 + \beta_{22}k^2 + \beta_{33}l^2 + 2\beta_{12}hk + 2\beta_{13}hl + 2\beta_{23}kl)\}$ and for each site $x = -y$ and $\beta_{11} = \beta_{22}$.

Correlations greater than 70%: O(1) β_{11}-β_{12} 0.87; O(2) β_{11}-β_{12} 0.92; Al(1) β_{11}-β_{12} 0.89.

BLE 5.4. Final atomic parameters for $AgAl_{11}O_{17}$ at 25°C (D1A) with estimated standard deviations in parentheses

om	Position	Site Symmetry	x	z	Occn.	β_{11}	β_{33}	β_{12}	β_{13}	β_{23}
1)	12k	m	0.1569(2)	0.0500(1)	6.0	0.0060(5)	0.00030(2)	0.0042(7)	-0.0003(1)	$-\beta_{13}$
2)	12k	m	0.5021(3)	0.1459(1)	6.0	0.0062(5)	0.00044(3)	0.0037(7)	0.0002(1)	β_{13}
3)	4f	3m	-1/3	0.0551(1)	2.0	0.0044(8)	0.00030(5)	$\beta_{11/2}$	0	0
4)	4e	3m	0	0.1421(1)	2.0	0.0052(8)	0.00021(6)	$\beta_{11/2}$	0	0
5)	6h	mm	0.3058(17)	0.25	1.0	0.026(6)	0.00026(11)	0.015(3)	0	0
(1)	12k	m	-0.1665(4)	0.1067(1)	6.0	0.0027(6)	0.00047(4)	0.0006(10)	0.0004(1)	$-\beta_{13}$
(2)	4f	3m	1/3	0.0254(2)	2.0	0.0019(7)	0.00026(8)	$\beta_{11/2}$	0	0
(3)	4f	3m	1/3	0.1753(2)	2.0	0.0077(10)	0.00019(8)	$\beta_{11/2}$	0	0
(4)	2a	$\bar{3}$m	0	0	1.0	0.0075(15)	0.00044(13)	$\beta_{11/2}$	0	0
(1)	6h	mm	-0.2383(22)	0.25	0.74(5)[a]	0.050(7)	0.00044(30)	-0.032(6)	0	0
(2)	2b	$\bar{6}$m2	0	0.25	0.26(5)	0.46(12)	0.0010(12)	$\beta_{11/2}$	0	0

$R_I = 0.0417$ $R_P = 0.0834$ $R_{WP} = 0.0927$ Expected R = 0.1164

rrelations greater than 70%:- O(1) β_{11}-β_{12} 0.86; O(2) β_{11}-β_{12} 0.91; O(5) x - β_{11} 0.88; Al(1) β_{11}-β_{12} 0.91.

The sum of the silver occupancies was constrained to equal 1.0.

TABLE 5.5. Final atomic parameters for $AgAl_{11}O_{17}$ at 300 °C (PANDA) with estimated standard deviations in parentheses.

Atom	Position	Site Symmetry	x	z	Occn.	β_{11}	β_{33}	β_{12}	β_{13}	β_{23}
O(1)	12k	m	0.1557(6)	0.0495(2)	6.0	0.001(2)	-0.0001(1)	0.002(2)	-0.0007(3)	$-\beta_{13}$
O(2)	12k	m	0.5025(6)	0.1467(2)	6.0	0.003(2)	0.0001(1)	0.003(3)	0.0004(2)	β_{13}
O(3)	4f	3m	-1/3	0.0559(5)	2.0	-0.002(3)	0.0013(3)	$\beta_{11/2}$	0	0
O(4)	4e	3m	0	0.1416(6)	2.0	0.008(3)	0.0017(4)	$\beta_{11/2}$	0	0
O(5)	6h	mm	0.2983(17)	0.25	1.0	-0.010(11)	0.0003(3)	0.021(8)	0	0
Al(1)	12k	m	-0.1657(13)	0.1066(3)	6.0	0.004(3)	0.0005(1)	-0.005(5)	-0.0011(6)	$-\beta_{13}$
Al(2)	4f	3m	1/3	0.0241(6)	2.0	0.023(4)	-0.0002(3)	$\beta_{11/2}$	0	0
Al(3)	4f	3m	1/3	0.1791(5)	2.0	0.009(4)	-0.0008(3)	$\beta_{11/2}$	0	0
Al(4)	2a	3m	0	0	1.0	-0.013(5)	0.0025(6)	$\beta_{11/2}$	0	0
Ag(1)	6h	mm	-0.262(4)	0.25	0.66(9)[a]	0.003(15)	0.003(1)	-0.017(11)	0	0
Ag(2)	2b	$\bar{6}$m2	0	0.25	0.34(9)	0.48(13)	-0.002(1)	$\beta_{11/2}$	0	0

$R_I = 0.0519$ $R_P = 0.0914$ $R_{WP} = 0.0824$ Expected R = 0.0434

Correlations greater than 70%:- O(1) β_{11}-β_{12} 0.90; O(2) β_{11}-β_{12} 0.92; O(5) x-β_{11} 0.83; O(5) x-β_{12} 0.80; O(5) β_{11}-β_{12} 0.96; Al(1) β_{11}-β_{12} 0.85.

[a] The sum of the silver occupancies was constrained to equal 1.0.

TABLE 5.6. Final atomic parameters for $AgAl_{11}O_{17}$ at 500°C (D1A) with estimated standard deviations in parentheses.

Atom	Position	Site Symmetry	x	z	Occn.	β_{11}	β_{33}	β_{12}	β_{13}	
O(1)	12k	m	0.1577(2)	0.0501(1)	6.0	0.0112(5)	0.00056(3)	0.0086(7)	-0.0005(1)	-
O(2)	12k	m	0.5026(3)	0.1460(1)	6.0	0.0081(5)	0.00075(3)	0.0019(8)	0.0005(1)	-
O(3)	4f	3m	-1/3	0.0553(2)	2.0	0.0111(9)	0.00054(6)	$\beta_{11/2}$	0	
O(4)	4e	3m	0	0.1422(2)	2.0	0.0095(9)	0.00070(8)	$\beta_{11/2}$	0	
O(5)	6h	mm	0.311(5)	0.25	1.0	0.043(11)	0.00024(11)	0.029(6)	0	0
Al(1)	12k	m	-0.1679(4)	0.1071(1)	6.0	0.0099(8)	0.00059(5)	0.0077(11)	0.0003(1)	$-\beta_{13}$
Al(2)	4f	3m	1/3	0.0253(2)	2.0	0.0059(9)	0.00067(9)	$\beta_{11/2}$	0	0
Al(3)	4f	3m	1/3	0.1752(2)	2.0	0.0120(12)	0.00040(10)	$\beta_{11/2}$	0	0
Al(4)	2a	$\bar{3}$m	0	0	1.0	0.0056(13)	0.00087(16)	$\beta_{11/2}$	0	0
Ag(1)	6h	mm	-0.246(6)	0.25	0.83(8)[a]	0.27(6)	0.0010(4)	-0.22(7)	0	0
Ag(2)	2b	$\bar{6}$m2	0	0.25	0.17(8)	0.28(12)	0.0002(14)	$\beta_{11/2}$	0	0

$R_I = 0.0386$ $R_P = 0.0796$ $R_{WP} = 0.0778$ Expected R = 0.1086

Correlations greater than 70%:- O(1) β_{11}-β_{12} 0.89; O(2) β_{11}-β_{12} 0.86; O(5) x-β_{11} 0.96, x-β_{12} 0.74; β_{11}-β_{12} 0.86; Al(1) β_{11}-β_{12} 0.92; Ag(1) β_{11}-β_{12} 0.97, β_{11}-Ag_{occ} 0.76.

[a] The sum of the silver occupancies was constrained to equal 1.0.

TABLE 5.7

Bond distances (Å) calculated from the final coordinates for $AgAl_{11}O_{17}$ and $Ag_{1+x}Al_{11}O_{17+\frac{1}{2}x}$.

	Stoichiometric					Non-stoichiometric	
	4.2K	25°C	300°C	500°C	550°C[a]	25°C[b]	25°C[c]
Octahedra							
Al(1)-O(1)	2.021	2.023	2.024	2.044	2.040	2.026(4)	2.017
-O(2)	1.829	1.832	1.846	1.828	1.843	1.832(4)	1.839
-O(3)	1.991	1.991	1.989	1.991	1.986	1.981(5)	1.973
-O(4)	1.792	1.799	1.791	1.816	1.822	1.811(5)	1.821
Average	1.914	1.917	1.920	1.925	1.929	1.918	1.918
Al(4)-O(1)	1.897	1.891	1.879	1.906	1.898	1.885(3)	1.893
Tetrahedra							
Al(2)-O(1)	1.792	1.796	1.816	1.799	1.806	1.809(4)	1.806
-O(3)	1.800	1.812	1.804	1.820	1.828	1.799(9)	1.800
Average	1.794	1.800	1.813	1.804	1.811	1.807	1.804
Al(3)-O(2)	1.769	1.764	1.797	1.774	1.756	1.772(4)	1.762
-O(5)	1.716	1.703	1.636	1.705	1.716	1.686(9)	1.675
Average	1.756	1.749	1.757	1.757	1.746	1.750	1.740
Silver Contacts							
Ag(1)-O(2)	2.727	2.724	2.710	2.726	-	2.70(1)	2.720
-O(5)	2.595	2.695	2.736	2.766	-	2.77(3)	-
Ag(2)-O(4)	-	2.431	2.443	2.436	-	2.421(4)	2.424
-O(5)	-	2.961	2.894	3.026	-	2.91(3)	3.117
Ag(3)-O(4)	-	-	-	-	-	2.51(5)	-
-O(5)	-	-	-	-	-	2.64(11)	-

[a] Reference 73.

[b] Single-crystal neutron diffraction study (section 5.2)

[c] Reference 71.

TABLE 5.8

Bond Angles (°) calculated from the final atomic coordinates of $AgAl_{11}O_{17}$ and $Ag_{1+x}Al_{11}O_{17+\frac{1}{2}x}$.

	Stoichiometric					Non-stoichiometric	
	4.2K	25°C	300°C	500°C	550°C[a]	25°C[b]	25°C[c]
Octahedra							
O(1)-Al(1)-O(1)	81.62	81.17	80.56	81.06	80.0	80.6(2)	-
-O(2)	90.23	90.17	91.00	90.02	90.1	90.8(1)	90.70
-O(3)	88.40	88.45	88.75	88.37	88.7	88.7(2)	89.19
-O(4)	84.14	84.40	84.39	83.89	83.9	83.9(2)	84.04
O(2)-Al(1)-O(2)	97.20	97.76	96.71	98.23	98.5	97.3(2)	-
-O(3)	85.39	85.35	85.05	85.66	86.0	85.9(2)	86.09
-O(4)	101.05	100.78	100.85	100.92	100.2	100.4(2)	-
O(1)-Al(4)-O(1)	88.25	88.18	88.28	88.36	88.3	88.0(1)	92.06
Tetrahedra							
O(1)-Al(2)-O(1)	110.61	110.92	110.53	110.75	111.1	110.6(2)	110.37
-O(3)	108.30	107.99	108.39	108.16	107.8	108.3(2)	108.56
O(2)-Al(3)-O(2)	106.90	106.76	104.62	107.07	107.4	106.7(2)	107.55
-O(5)	105.73	107.36	107.59	107.99	-	106.5(5)	111.33
Silver Contacts							
O(5)-Ag(1)-O(5)	147.46	144.27	132.72	142.68	-	132(2)	-
-O(2)	62.90	62.08	61.18	61.66	-	60.8(3)	-

[a] Reference 73

[b] Single-crystal neutron diffraction study (section 5.2)

[c] Reference 71.

CHAPTER 6

AMMONIUM BETA ALUMINA AND ITS DERIVATIVES

6.1 Introduction

A summary of the reported work on the preparation, properties and structure of ammonium beta alumina was presented in section 3.5. In the work described here, the structure of $(NH_4)_{1.25}Al_{11}O_{17.125}$, prepared by the exchange of $Na_{1.25}Al_{11}O_{17.125}$ in molten ammonium nitrate, was examined by single crystal X-ray and neutron diffraction. The results obtained are considered in relation to the nuclear magnetic resonance (NMR), infra-red (IR) and structural studies available in the recent literature. Secondly, single crystal neutron studies of two derivatives of ammonium beta alumina, which were prepared by the heat treatment of $(NH_4)_{1.25}Al_{11}O_{17.125}$, are described. These structural studies have been helpful in understanding the behaviour of $(NH_4)_{1+x}Al_{11}O_{17+\frac{1}{2}x}$ and the related $(H_3O)_{1+x}Al_{11}O_{17+\frac{1}{2}x}$; in particular, we discuss the mechanism by which stoichiometric beta aluminas may be formed.

6.2 Sample preparation*

The starting material consisted of two single crystal boules of sodium beta alumina (Union Carbide) of approximate composition $Na_{1.25}Al_{11}O_{17.125}$. These boules were approx. 12cm long and 1.5 and 2.5cm in diameter respectively, with the crystallographic c-direction perpendicular to the long axis. Using a platinum wire support to prevent fragmentation, slices were cut from the boules to give cylindrical plates 1-5mm thick. Ion exchange was then achieved in molten NH_4NO_3 at 210°C. To ensure complete conversion, the melt was refreshed 11 times during the exchange which was allowed to continue over 78 days.

* *I am again indebted to C.F. Sampson of A.E.R.E. Harwell for the bulk of this work.*

The melt bath was contained in a furnace which was open to the atmosphere. The final observed weight loss was in the range 1.0 - 1.2% which is consistent with the formation of either $(NH_4)_{1.25}Al_{11}O_{17.125}$ (1.04% theoretical) or $(NH_4)(H_3O)_{0.25}Al_{11}O_{17.125}$ (1.00% theoretical). Elemental analysis gave N 3.665 wt.%; Al 48.15 wt.%, with no residual sodium, which corresponds to the composition $(NH_4)_{1.251}Al_{11}O_{17.125}$.

In addition to the diffraction experiments described here, similar samples have been used in conductivity measurements[84,68], analysis of thermal stability[84], IR spectroscopy[232] and inelastic neutron scattering experiments[191]. The same starting material was used in the investigation of ammonium exchange in $Ag_{1.25}Al_{11}O_{17.125}$[68].

On removal of the mechanical support, the slices of the completely exchanged material cleave readily perpendicular to the c-axis. From the batch of long crystals which resulted, two were selected and cut to more manageable proportions on a circular saw. The crystals were protected during this operation by an araldite surround which was subsequently removed in $CHCl_3$. The chosen crystal of ammonium beta alumina was then of appropriate dimensions (2.8 x 2.2 x 9.5mm) for the single crystal neutron study on the Mark VI diffractometer. The sample from which crystals for the prior X-ray structure analysis were selected, was derived from an earlier exchange performed under similar conditions.

The single crystals prepared in the above fashion are entire. However, on heating above 460°C, the temperature around which substantial weight loss is recorded by thermo-gravimetric analysis (tga)[84], the crystals tend to flake apart perpendicular to the c-axis. Electron microscopy of the resulting material

indicates that, although macroscopic degradation has occurred, on a microscopic level the beta alumina structure remains intact. The specimens which result are thus no longer truly single crystals, but as the relative orientations of the respective plates are largely maintained, they prove amenable to structure analysis by single crystal techniques. We were therefore able to undertake structural analyses of two such crystals which were obtained under different preparative conditions.

In a first preparation, several crystals of ammonium beta alumina were cut to 3-6mm square perpendicular to the c-axis, along which they measured between 2 and 4.5mm. These were subjected to a flow of H_2 gas at 600°C (16 hours) and then 620°C (16 hours). A selection of the resulting crystals (termed #1) were chosen for the subsequent D9 and D12 experiments. The uptake of atmospheric moisture by this material, as monitored by weight gain, was slow at room temperature, although weight increases were observed after several hours exposure to moist Ar at temperatures above ambient and some of the resulting partially hydrated crystals (#2) were also examined on D12. This batch of materials was not subjected to chemical analysis, although similar crystals were examined by IR spectroscopy[232].

In the second preparation, the sodium beta alumina substrate was exchanged in molten NH_4NO_3 at 210°C over 18 days, the bath being renewed 8 times during this period. Elemental analysis of a portion of the resulting ammonium beta alumina gave Al 49.0 and 49.6 wt.%; Na 0.58 and 0.56 wt.% which indicates that the exchange was 88% complete (Boilot *et al.*[227] have suggested that a small amount of residual sodium helps to prevent further decomposition when ammonium beta alumina is converted to stoichiometric '$HAl_{11}O_{17}$' at 500°C[230]). The sample

(#3) was held in a mechanical clamp and heated at 295°C (16 hours) and then 619°C (15 hours) under a flow of dry H_2. Weight loss of 2.27 wt.% was found for an unclamped piece of similar material under such treatment (this corresponds to loss of $0.66(NH_3)$ + $0.125(H_2O)$). The selected crystal (ca. 3 x 4 x 19mm) was mounted, in air, on a glass fibre and sealed within a quartz cap prior to the neutron diffraction experiment.

6.3 Single crystal X-ray diffraction study of ammonium beta alumina

Crystal Data: $(NH_4)_{1.25}Al_{11}O_{17.125}$ Hexagonal $P6_3/mmc$ a = 5.601(1)Å c = 22.882(4)Å Z = 2 D_c = 3.14gcm^{-3} Mo-Kα radiation, λ = 0.71069Å μ = 10.2cm^{-1}.

Crystals of a suitable size for X-ray work were obtained by cleavage of the larger specimens described above. After preliminary photographic work, a selected crystal (ca. 0.3 x 0.3 x 0.1mm) was set-up on an Enraf-Nonius CAD-4F diffractometer which was prepared for data collection in a standard manner. The orientation matrix and the above cell constants were optimised by least-squares refinement employing 25 reflections with $\theta > 12°$. 3621 reflections, comprising slightly more than one octant of the limiting sphere with $\theta \leqslant 40°$, were collected in bisecting geometry using ω-nθ scans (n = 1.67). Lorentz and polarisation corrections were applied although, because of the regular shape of the crystal and the low value of the linear absorption coefficient, no absorption correction was necessary. All those reflections flagged as weak[32] and those which had uneven backgrounds were rejected and the data were then merged. The merging R-factor[6] of 0.049 was rather high and on further examination

of the data, systematic discrepancies were apparent. For the 1 0 $\bar{1}$ ℓ series of reflections, 1 0 $\bar{1}$ ℓ, $\bar{1}$ 0 1 ℓ, 1 $\bar{1}$ 0 ℓ and $\bar{1}$ 1 0 ℓ were in good agreement but the 0 1 $\bar{1}\ell$ and 0 $\bar{1}$ 1 ℓ generally differed, although such disparities were not found in the single crystal neutron diffraction data (section 6.3). The latter pairs of reflections were excluded and the merging R-factor improved to 0.038. There remained 547 independent structure amplitude amplitudes with $I > 3\sigma(I)$ where $\sigma(I)$ was derived from the counting statistics. Initial atomic coordinates for the spinel block and O(5) were taken from Colomban et al.[75] and refined by full-matrix least-squares techniques. The population of sites within the mirror planes and the possibility of defects within the spinel blocks were monitored throughout refinement by repeated $/F_{obs}/$ and $/F_{obs} - F_{calc}/$ Fourier syntheses. In agreement with Colomban et al.[75], it was found that nitrogen predominantly occupies the Beevers-Ross site (BR; $\bar{1}/3$, 1/3, 1/4) although when slight displacements from this site to a 6h (x $\bar{x}$ 1/4) position were considered, refinements diverged. There was no appreciable occupation of the anti-Beevers-Ross site (aBR; 0 0 1/4). The other mirror plane site which is occupied by nitrogen is of the 6h type, x $\bar{x}$ 1/4 with x = 0.9, which lies between the mid-oxygen (mO) and aBR positions, separated from the BR site by 2.24Å. Such a short distance excludes the possibility of occupation of both sites within the same mirror plane (by "mirror plane" we refer to the z = 1/4 section of a single unit cell). The non-stoichiometry is accommodated by the occurrence of mirror planes which contain two or three ammonium ions on the N(2) (6h) sites.

Colomban et al.[75] had a starting composition $Na_{1.3}Al_{11}O_{17.15}$ which after complete exchange yields an average of

$(NH_3)_{1.3}O_{0.15}$ per mirror plane, in addition to the spacer oxygen O(5) which has unit occupation. The final occupancies which they obtained were 0.915 (N(1), BR), 0.275 (N(2)) and 0.09(N(3), aBR). The large value for N(1) is too high for there to be a sufficient number of doubly- or triply-occupied mirror planes to accommodate the occupancies of the other sites, an inconsistency which is due, they suggest, to neglect of the scattering power of the protons on the NH_4^+ function. However, the sum of the nitrogen occupations is 1.280, which is already less than that anticipated from the initial composition.

In this work, a similar picture emerged. With the exclusion of 8 reflections which were in gross disagreement, these being the 2 2 0 (extinction), 0 0 2 and 0 0 4 (low angle reflections) and six of the 0 k ℓ type, residuals of R = 0.0364 and R_W = 0.0584 were obtained. The occupancies were 0.91 for N(1) and 0.471 for N(2). The interstitial aluminium (Al_i or Al(11)), which had been indicated in difference Fourier syntheses, was also included at this stage and in refinement its occupation was constrained with that of Al(1) such that the sum was 6.0. Hydrogens were then added at the positions determined in the single crystal neutron study (section 5.4) with occupations related to those of the nitrogens such that the composition NH_4 would be obtained at each site. After refinement the residuals, R = 0.0363 and R_W = 0.0589, were not significantly improved, but the ammonium ion occupancies fell to 0.81 (N(1), BR) and 0.43 (N(2)). In the final cycles, the hydrogen coordinates were refined subject to a series of bond length and angle constraints. A correction for secondary extinction was applied and a three term Chebyshev series was employed as the weighting scheme. The final residuals were R = 0.0304, R_W = 0.0517. Atomic coordinates

are presented in Table 6.1, bond lengths and angles in Tables 6.5 and 6.6 and structure factors are listed in Appendix III. The final $/F_{obs}/$ and $/F_{obs} - F_{calc}/$ Fourier sections at $z = 1/4$ are displayed in Figure 6.1. Atomic scattering factors were taken from Cromer and Mann[8] and Spagna[9] (H only).

6.4 Single crystal neutron study of ammonium beta alumina

The chosen crystal (2.8 x 2.2 x 9.5mm) of ammonium beta alumina was mounted in air on a stiff glass fibre and aligned so as to rotate about <1 0 $\bar{1}$ 0> on an X-ray precession camera. Values for the cell constants of a = 5.6011Å, c = 22.8817Å were taken from the X-ray analysis (section 6.3). The crystal and goniometer were then transferred to the Mark VI Channel I diffractometer. The orientation matrix was defined by the angular coordinates of the 0 0 32 and 4 2 10 reflections which were accurately centred by repeated step-scans in each of the four diffractometer circles. This matrix was checked by a comparison of the calculated positions of 15 reflections with those observed and later, throughout the data collected, by examination of the measured reflection profiles. A wavelength of 1.1803Å was assumed. Automatic data collection was implemented using ω-2θ scans in bisecting geometry. Initially, an octant of the limiting sphere with $\theta < 50°$, defined by h = 0-6, k = 0-6, ℓ = -1-29, was collected in successive shells. When this was complete, further reflections in the -ve h, -ve k, +ve ℓ octant were measured. The parameters controlling the measurement of reflection and background points were the same as detailed in section 5.2, so that $\sim$30 mins were required per reflection. The data were reduced on the IBM 370 at A.E.R.E. Harwell to give an intensity and standard deviation for each reflection. Subsequent

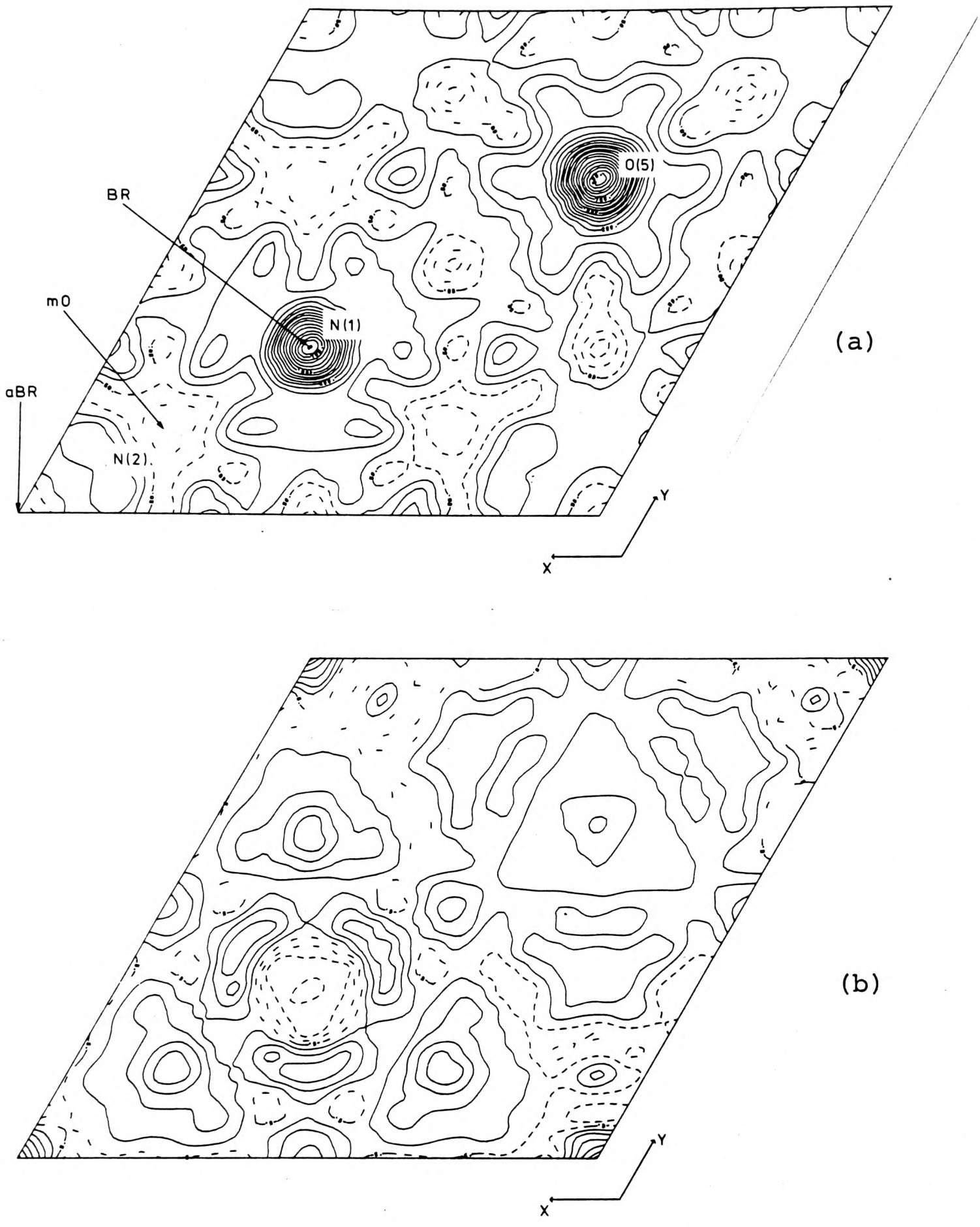


Figure 6.1. The z = 1/4 sections of final /F_{obs}/ (upper) and /F_{obs}-F_{calc}/ (lower) Fourier syntheses (arbitrary units) calculated from the single crystal X-ray data on $(NH_4)_{1.25}Al_{11}O_{17.125}$. The two sections are on the same scale, but the contour levels in the difference plot are at 0.1× the spacings in the /F_{obs}/ plot. The maximum feature in the former has an intensity of 3% that in the latter.

analysis was accomplished on the Oxford 1906A computer. Firstly, all the measured data were checked manually and reflections which were off-centre or whose backgrounds could not be reasonably determined were rejected (14 in all). For all reflections in which there were spurious points or slight overlap in the background regions, an intensity and standard deviation were calculated by hand ($\sim$100 in all). Lorentz corrections were applied to the resulting total of 1207 observed intensities and the data were merged, with retention of all reflections, to give 308 independent structure amplitudes. The merging R-factor was 0.0752. The magnitude of this residual resulted principally from those reflections at large values of the Bragg angle, θ. During part of the data collection the blind-spot data had been erroneous so that the controlling software could not recognise when the diffractometer machinery, in particular the χ-circle, interfered with the incident or diffracted beams. For this reason, in the later stage of refinement, only the 258 structure factor moduli with $\theta < 45°$ were employed in the calculations.

Structure analysis and refinement followed the same course as that for the X-ray study. For both this and the subsequent data sets discussed in this chapter, scattering lengths of 0.345, 0.583, 0.940, 0.360 and -0.374 (all x 10^{-14}m) were assumed for Al, O, N, Na and H respectively. After refinement of the spinel block atoms and O(5), a large peak of positive density was found at the BR position and calculations with a nitrogen included at this site converged to R = 0.19. Difference Fourier syntheses then indicated occupation of the same N(2) (6h) site as found in the X-ray analysis. Further, appreciable negative scattering density corresponding to hydrogen was found around N(1) (BR). The geometry of the distribution is such that

three-fold disordered tetrahedra are generated (see Figures 6.2 - 6.4). The NH_4^+ group on the BR site lies with a 2-fold rotation axis lying along x $\bar{x}$ 1/4, but the crystallographic $\bar{6}$-axis does not coincide with any of the molecular symmetry elements. In any one of the three tetrahedra generated by the $\bar{6}$-axis, two protons lie in the mirror plane close to, say, x_2 $\bar{x}_2$ 1/4 and x_2 $2x_2$ 1/4 with the remaining pair on the 12k sites x_1 $\bar{x}_1$ 1/4+z and x_1 $\bar{x}_1$ 1/4-z, which are related by the z = 1/4 mirror plane. Inspection of Figure 6.4 reveals that this arrangement optimises the coordination of the NH_4^+ group, with all four protons being involved in hydrogen bonds. H(11) is directed towards O(2), at a separation of 1.9Å, and H(12) is 2.1Å away from the spacer oxygen in the adjacent unit cell (Figure 6.4). Both protons are little removed from the line joining N(1) to the respective oxygen (Table 6.6). Such a distribution had been envisaged by Colomban et al.[75] using IR data and Gourier and Sapoval suggested a similar orientation for the major NH_4^+ species in their NMR analysis[189].

With the configuration about N(1) on the BR site clarified, there remains the similar question of that around the second nitrogen site, N(2). In refinements, which included the positional and thermal parameters of H(11) and H(12) bonded to N(1), the occupation numbers of both $(NH_4)_1$ and N(2) were allowed to vary. They converged to values of $\sim$0.7 and $\sim$0.5 respectively. A computed difference Fourier synthesis then revealed areas both of positive density at the interstitial aluminium position and of negative density around N(2). The peaks of negative intensity were at x 0 1/4 (12j) with x $\approx$ 0.3 and close to 0 0 z (4e) with z $\approx$ 0.22. The hydrogens, H(22) and H(21), to which these areas correspond define the orientation of the $(NH_4)_2$ tetrahedron which

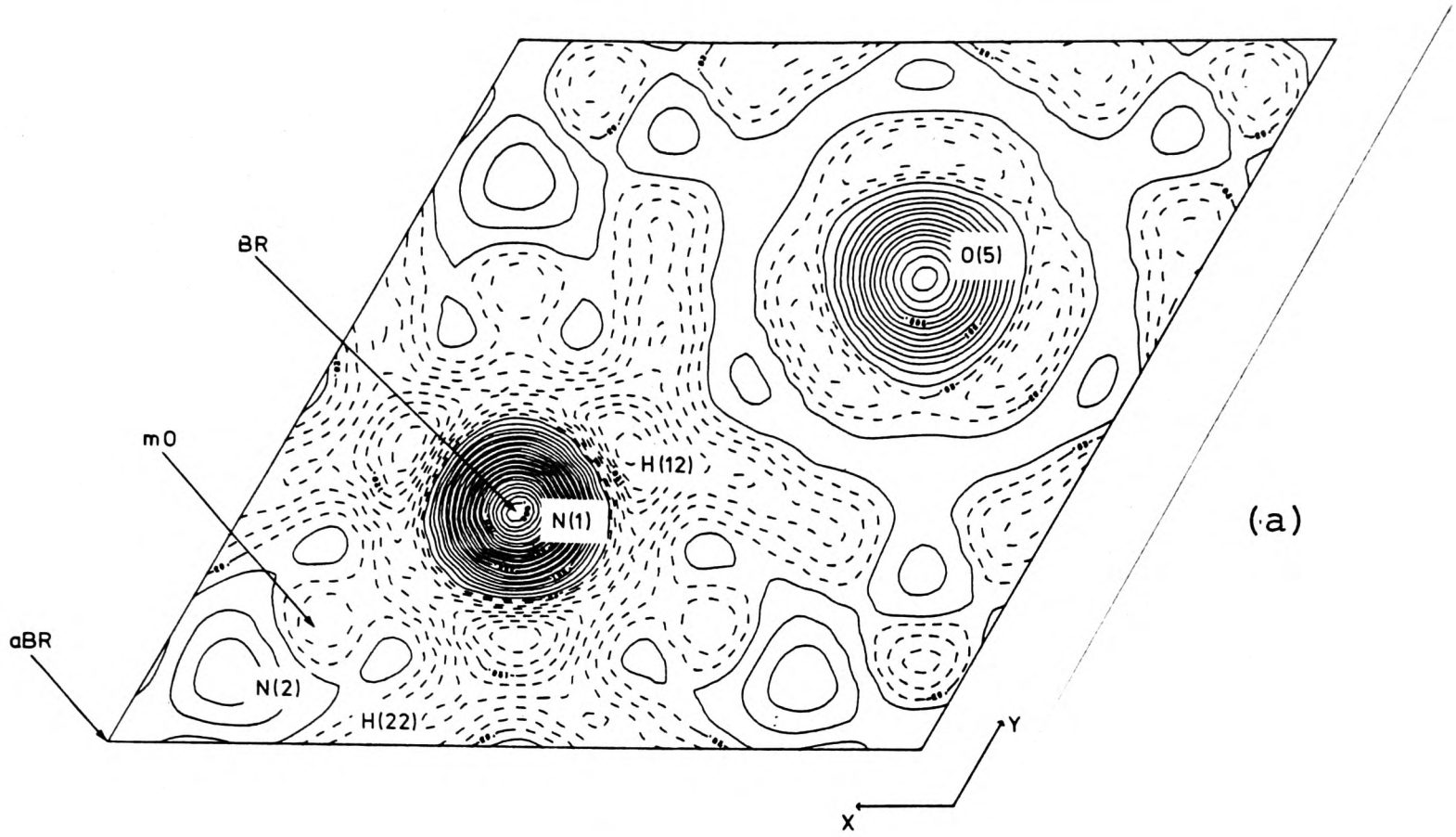


Figure 6.2. The z = 1/4 sections of final $/F_{obs}/$ (upper) and $/F_{obs}-F_{calc}/$ (lower) Fourier syntheses (arbitrary units) calculated from the single crystal neutron data on $(NH_4)_{1.25}Al_{11}O_{17.125}$. The $/F_{obs}/$ synthesis is scaled to a maximum of 999 with contour spacings of 40 (positive) and 20 (negative). The difference plot is computed at 10× this scale with contour spacings of 10. The maximum feature of the difference section is -1.2 % of that in the $/F_{obs}/$ section.

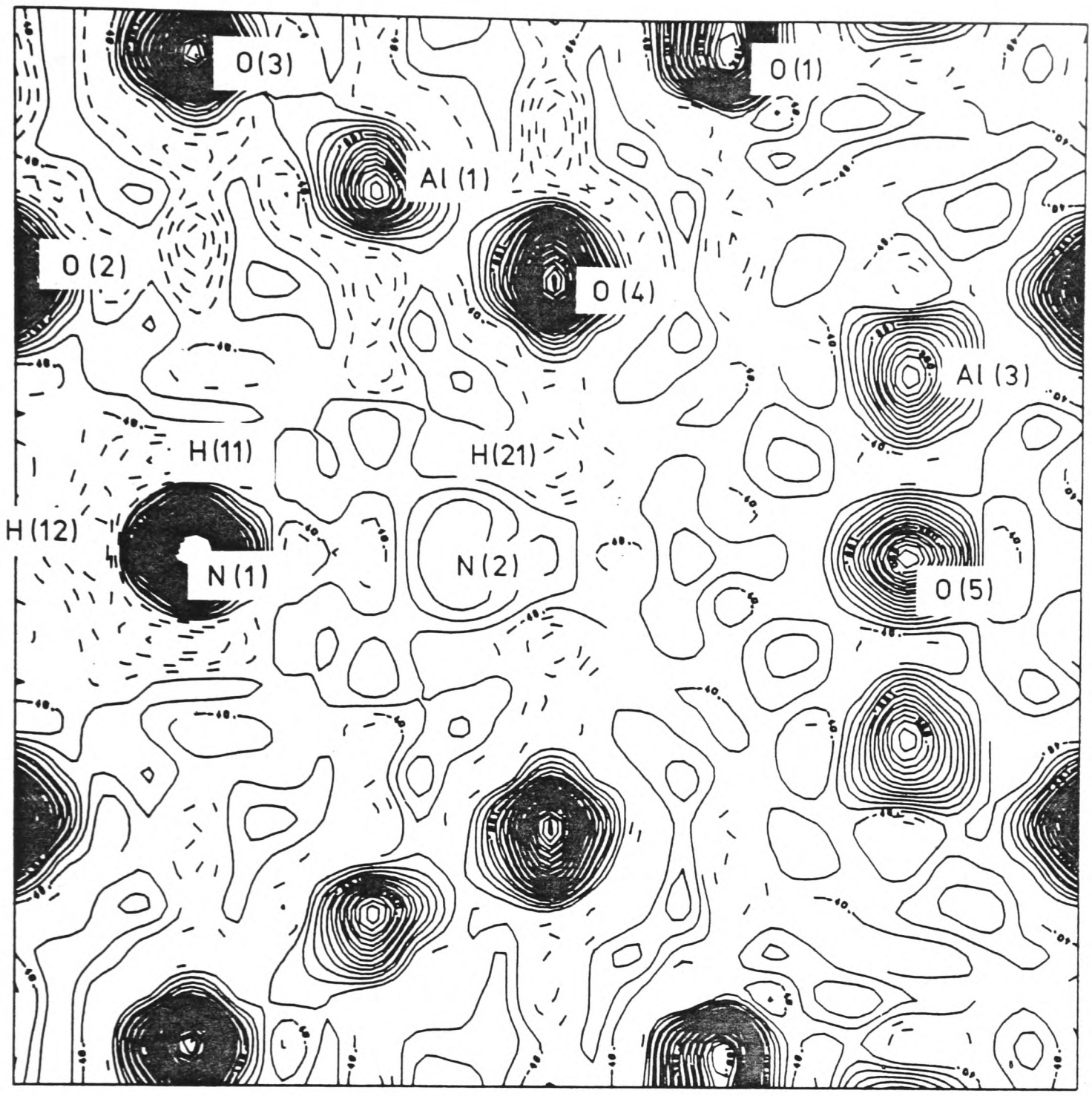
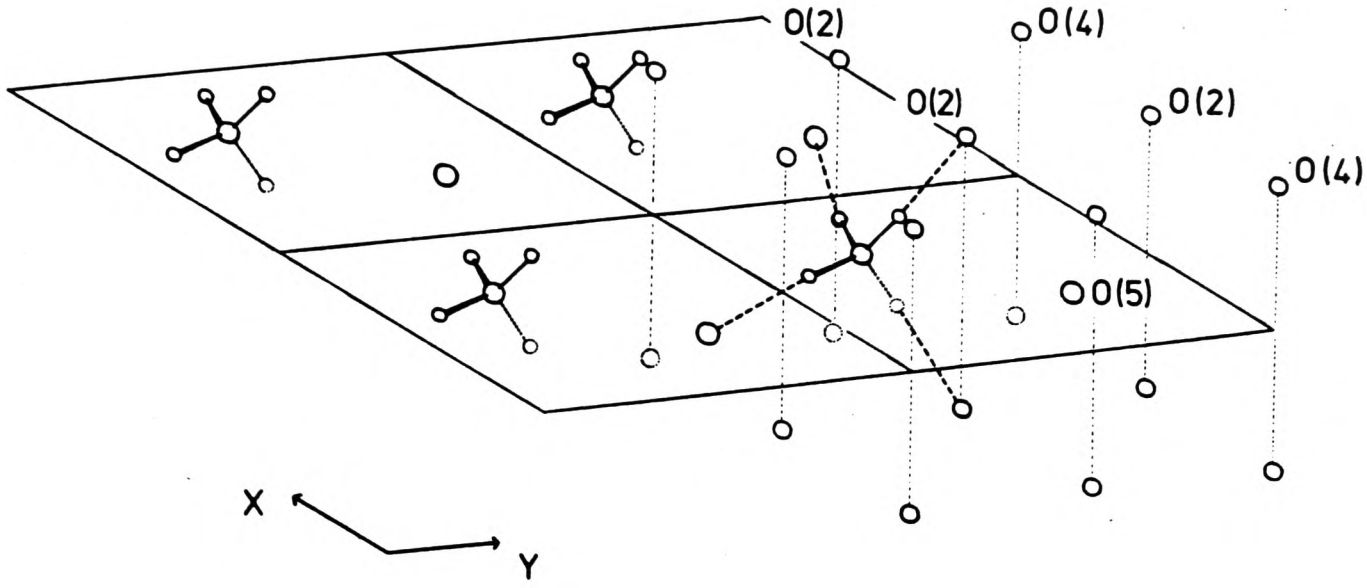
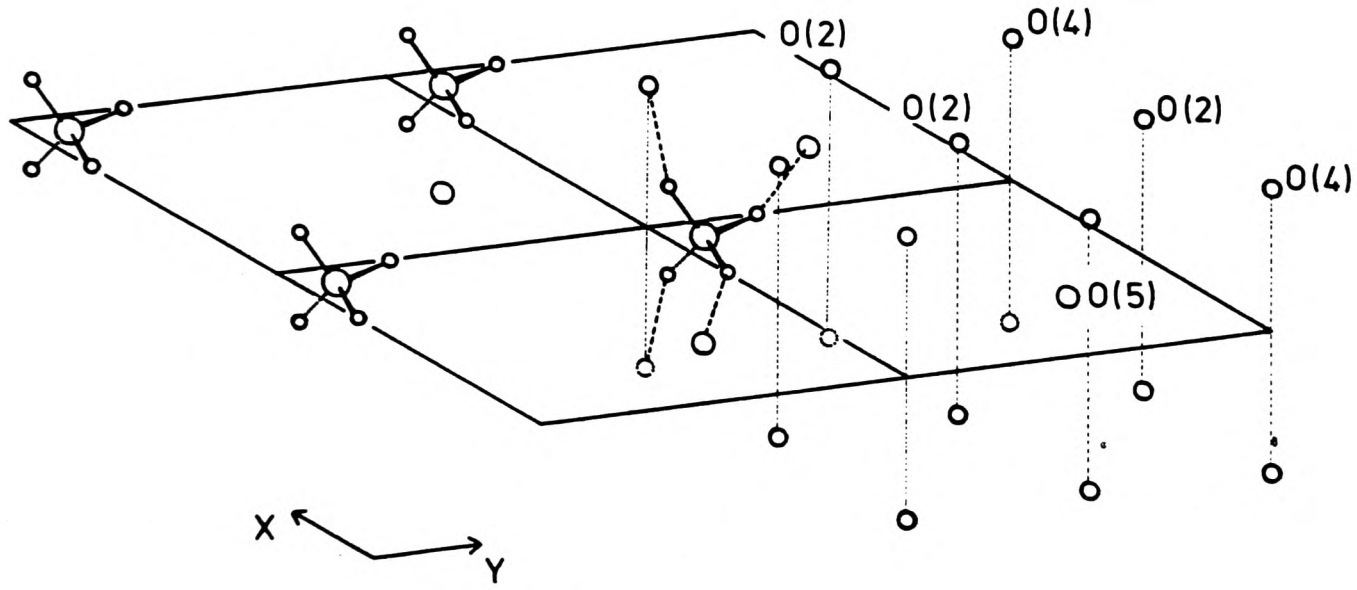


Figure 6.3. Scattering density in the x $\bar{x}$ z plane as calculated in a final /F_{obs}/ slant Fourier synthesis (arbitrary units) using the single crystal neutron diffraction data on ammonium beta alumina. Only the portion adjacent to the z = 1/4 mirror plane (which contains H(12),N(1), and O(5)) is included.



N(1) Position (Beevers-Ross site)



N(2) Position

Figure 6.4. A depiction of the hydrogen-bonding arrangements for the NH_4^+ *ions at each of the two distinct sites in ammonium beta alumina. N(1) (upper) has three equivalent orientations,with hydrogen bonds to two O(5) and two O(2) atoms. For each N(2) site, there is only one distinct orientation which allows hydrogen-bonding with two O(4) and two O(5) atoms.*

like $(NH_4)_1$, is favourably coordinated. Thus, the H(22)'s at $\bar{x}$ 0 1/4 and 0 x 1/4 have short contacts (1.8Å) to the spacer oxygen in adjacent cells and, further, they lie near the centre of the square defined by two O(2) and two O(4) atoms, albeit at longer separations (2.7Å to O(2)). The two protons, H(21), which complete the tetrahedron are even more favourably situated, being directed towards O(4) at a separation, O(4) - H(21), of only 1.7Å. Here then is the explanation why neither the mO or aBR site is occupied by nitrogen. Neither of these two sites would enable such propitious coordination about nitrogen to be achieved. With displacement of N(2) towards aBR, the hydrogen bonds to O(5) are stretched and, conversely, with movement towards mO the contacts to O(4) are increased.

These protons were then included in the least-squares calculations in which the occupation numbers of both (NH_4^+) functions, that of the interstitial aluminium (with the constraint that the sum of Al(1) and Al(11) occupancies was 6.0), all atomic coordinates and fully anisotropic thermal parameters were treated as variables. For regular tetrahedral geometry to be achieved about N(1), H(12) cannot occupy the 6h sites but rather must be slightly displaced to the 12j positions. When this displacement was included, a series of Waser-type constraints on bond-lengths and angles about nitrogen were applied to both NH_4^+ functions. For the 258 reflections there was a total of 72 variables, with 10 constraints. In the final cycles of refinement a three-term Chebyshev polynomial was employed as the weighting scheme[4] and final residuals of $R = 0.0500$, $R_W = 0.0525$ were obtained (the residuals calculated from this model using all 308 reflections, including those with $\theta > 45°$, were $R = 0.1148$ and $R_W = 0.2145$). The corresponding atomic parameters are given in Table 6.2, bond

lengths and angles in Tables 6.5 and 6.6 respectively and structure factor tables appear in Appendix III. The maximum feature found in a difference Fourier, of which Figure 6.2(b) represents the z = 1/4 section, had a height of 0.016 times the maximum in the corresponding $/F_{obs}/$ synthesis. The contour levels in Figure 6.2(b) have been exaggerated to indicate the absence of evidence for additional oxygen at the mO position (compare with Figure 6.1(b)).

6.5 Single crystal neutron diffraction study of ammonium/hydrogen beta alumina

The crystal examined here (#3) was derived from the second heat treatment of $(NH_4)_{1.25}Al_{11}O_{17.125}$ as described in section 6.2. The experimental conditions were chosen to minimise crystal degradation and, as we shall see, this was successful to the extent of allowing the preparation of a new derivative of ammonium beta alumina.

The chosen crystal (∿3 x 4 x 19mm) was sealed in a quartz cap and aligned so as to rotate about $<1\bar{1}00>$ on an X-ray precession camera. The goniometer was then transferred to the Mark VI Channel I diffractometer and set-up in the manner described earlier. The orientation matrix was defined by the positions of the 0 0 24 and 3 3 0 reflections. Values for the lattice constants of a = 5.601Å, c = 22.660Å and for the wavelength of 1.1803Å were assumed. The accuracy of these parameters and of the orientation matrix were checked by examination of the profiles of the measured reflections. Automatic data collection was accomplished using ω-2θ scans in bisecting geometry, the other scan parameters being similar to those described

earlier (section 5.2). Slightly more than one octant of the limiting sphere defined by $\theta < 50°$ was measured. These data were reduced on the IBM 370 at A.E.R.E. Harwell and subsequently analysed on the Oxford University 1906A computer. In the initial manual checking, off-centre and poorly defined reflections were rejected and structure factors were calculated by hand for those in which minor overlap occurred. There remained 965 observed intensities to which Lorentz corrections were applied and the data were merged, using unit weights, to give 278 independent structure amplitudes. The merging R-factor was 0.031 and all reflections were employed in the subsequent calculations. While the large size of the crystal improved the counting statistics, it became clear during refinement that its length had exceeded the width of homogeneity of the incident beam. In bisecting geometry, therefore, at low values of the Bragg angle, θ, the extremities of the crystal contributed less to the observed diffracted intensity than the central portion. At higher values of ω and θ, where the long axis of the crystal is less close to perpendicular to the incident beam, this effect is reduced. The result is that the crystal appears to have an increase in scattering power with $\sin\theta/\lambda$ which counteracts the reduction due to thermal vibration. In refinement, therefore, though we can have reasonable confidence in the atomic coordinates and occupancies, the thermal components are generally much lower than anticipated (Table 6.3).

Isotropic and subsequent anisotropic refinement of the spinel block atoms and O(5), which was fixed on the 1/3 $\bar{1}$/3 1/4 (2c) site, gave residuals R = 0.215, R_W = 0.254. A difference Fourier synthesis computed at this stage revealed, somewhat surprisingly, a large peak at the Beevers-Ross ($\bar{1}$/3 1/3 1/4, 2d)

position. When an oxygen atom was entered at this location, the residuals improved to R = 0.135 and R_W = 0.194 and a subsequent $/F_{obs} - F_{calc}/$ Fourier calculation indicated both further positive density at the BR site and surrounding areas of negative density similar to those found in the above analysis of $(NH_4)_{1.25}Al_{11}O_{17.125}$. It was therefore clear that the BR site was occupied by $(NH_4)^+$ ions indicating that a considerable proportion of such ions had been retained in the structure during the heat treatment. N(1), H(11) and H(12) were then included in subsequent refinement subject to a series of Waser-type constraints on the hydrogen positions and, after several cycles, the residuals were reduced to R = 0.077 and R_W = 0.069. The $(NH_4)_1$ occupation was 0.87(13).

There was no evidence of any appreciable positive density at any other mirror plane sites. For example, the occupation number of nitrogen entered at the N(2) position refined to -0.03(3), but difference Fourier syntheses did indicate two regions of negative density, both at 6h positions, x $\bar{x}$ 1/4, with x = 0.18 and x = 0.46 respectively. The latter corresponds to that occupied by deuterium in $DAl_{11}O_{17}$ while the former is related to this site by a C_6^1 rotation about an axis passing through 1/3 $\bar{1}$/3 1/4 (2c). Hydrogens, H(31) and H(32), at these positions were included in refinements and several models were tested in an attempt to describe accurately the distribution of O(5). For reasonable separations O(5)-H(31) and O(5)-H(32), considerable displacements from the 2c site are expected. However, many of the refinements involving 6h sites with x > 1/3 or x < 1/3 or a combination of both, or both 6h and 2c, or 12j sites were unstable and, in terms of agreement between observed and calculated structure factors, there was little distinction

between models involving x < 1/3 and x > 1/3 displacements. Clearly, the average O(5) distribution is dictated by the predominance of mirror planes which contain NH_4^+ species and if there is a small number of cells in which displacements are significant, their effect is probably included in the average thermal components of O(5). The result is that the apparent O(5)-H(31), H(32) bond lengths are long (Table 6.5).

In the later stages of refinement, the interstitial aluminium site, which had again been indicated in difference Fourier syntheses, and a contribution from sodium to allow for the incomplete exchange (section 6.2), were included. Two sodiums were entered at the positions and with the relative occupations given by Reidinger[44], the total being calculated so as to allow for a 88% level of exchange. The first, Na(1), is close to $(NH_4)_1$, at the BR site and the only varied parameter was the occupancy of Na(2) which lies near the mO site. If there were there a significant population of additional oxygens at mO, this occupancy would be expected to increase, particularly as the scattering length of O (0.583×10^{-14}m) is greater than that of Na (0.36×10^{-14}m). The final value obtained (Table 6.3) is 0.03(10) which contrasts with the value of 0.08 calculated assuming 12% of residual sodium. The final atomic parameters are given in Table 6.3, bond lengths and angles in Tables 6.5 and 6.6 and structure factors in Appendix III. The z = 1/4 sections of $/F_{obs}/$ and $/F_{obs} - F_{calc}/$ Fourier syntheses based on this final model are shown in Figure 6.5.

6.6 Single crystal neutron diffraction study of 'hydrogen beta alumina'

a) Photographic neutron diffraction experiment



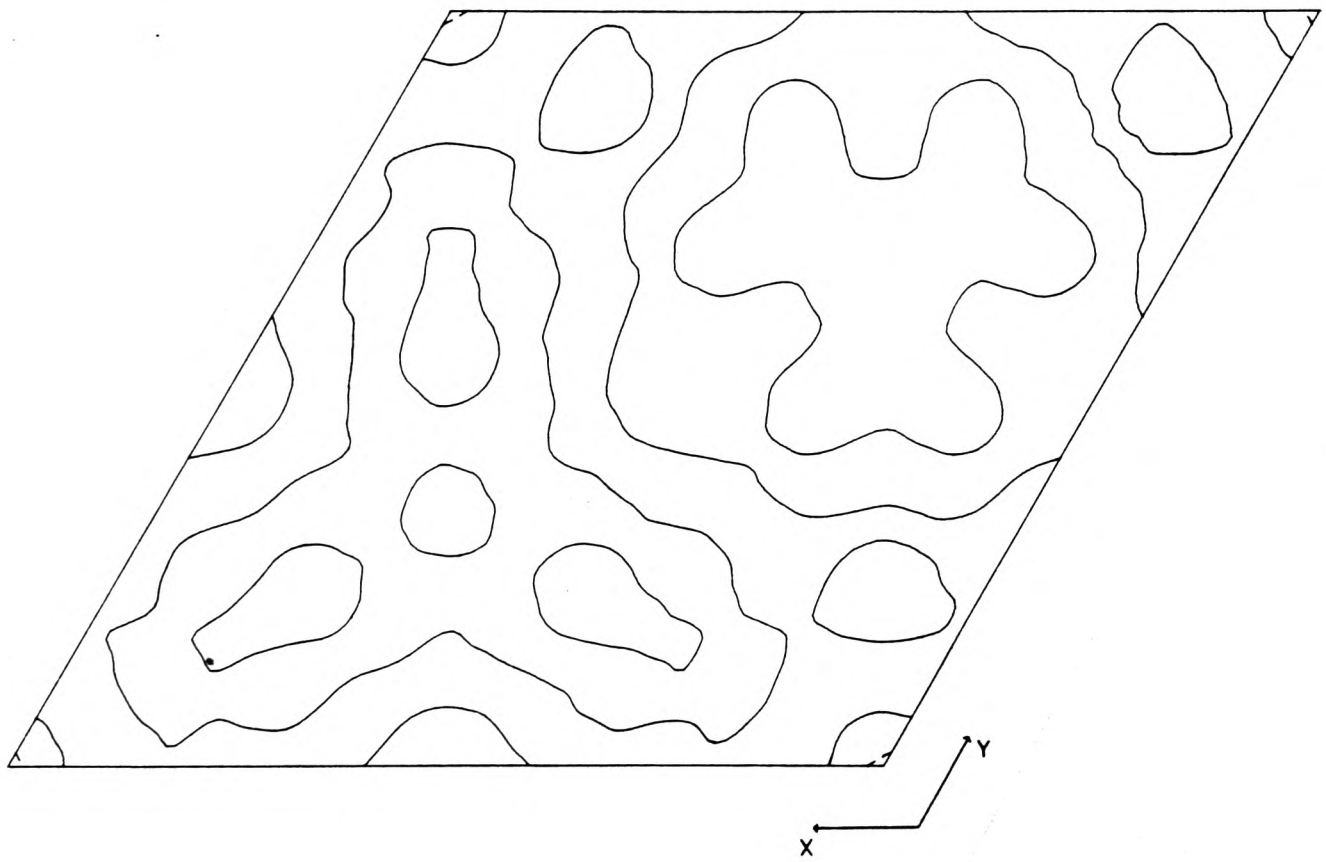


Figure 6.5. The z = 1/4 sections of final /F_{obs}/ (upper) and /F_{obs} - F_{calc}/ (lower) Fourier syntheses (arbitrary units) calculated from the single crystal neutron data on $(NH_4)_{0.78}H_{0.25}Al_{11}O_{17}$. The /$F_{obs}$/ synthesis is scaled to 1000 with contour spacings of 50. The difference synthesis is on the same scale and has the same contour levels. The maximum feature in the difference section has a height of -6.5% that in the /F_{obs}/ section.

Crystals (#1 and #2) derived from the first heat treatment of $(NH_4)_{1.25}Al_{11}O_{17.125}$ were initially examined by photographic neutron diffraction techniques on D12A and D12B[233]. This experiment was aimed at determining whether the protons in these systems are subject to long-range ordering over more than one unit cell. Such an ordering would manifest itself in the form of superlattice reflections. Crystals (#2) of partially hydrated 'hydrogen beta alumina' were examined at room temperature using standard equi-inclination Weissenberg techniques at a wavelength of 1.596Å and, for comparison, the zero and higher a*b* nets of 'hydrogen' (#1) and sodium beta aluminas were recorded. Three anti-equi-inclination zero layers were also taken to monitor the effects of absorption by the sample. A chosen crystal of the partially hydrated species was then transferred to the vertical-axis Weissenberg camera (D12B) on which zero- and upper-level exposures of the a*b* nets were recorded at 85K using normal-beam geometry. All these photographs were successfully indexed, but no evidence for superlattice ordering was found. However, the signal-to-noise ratio in many of these exposures, particularly those taken at low-temperature, was poor and it is therefore probable that if superlattice reflections (which are expected to be of low intensity) were present, they would not be resolved above background.

D12A was also used to screen the selection of crystals (#1) which was available for the subsequent diffractometer experiment on D9. Figure 6.6 displays two oscillation pictures taken from such crystals. Because of the 'leafing' perpendicular to the c-axis which occurred when the sample was prepared, the reflections are very broad, particularly in the upper photograph and, for D9, a crystal was chosen which produced relatively

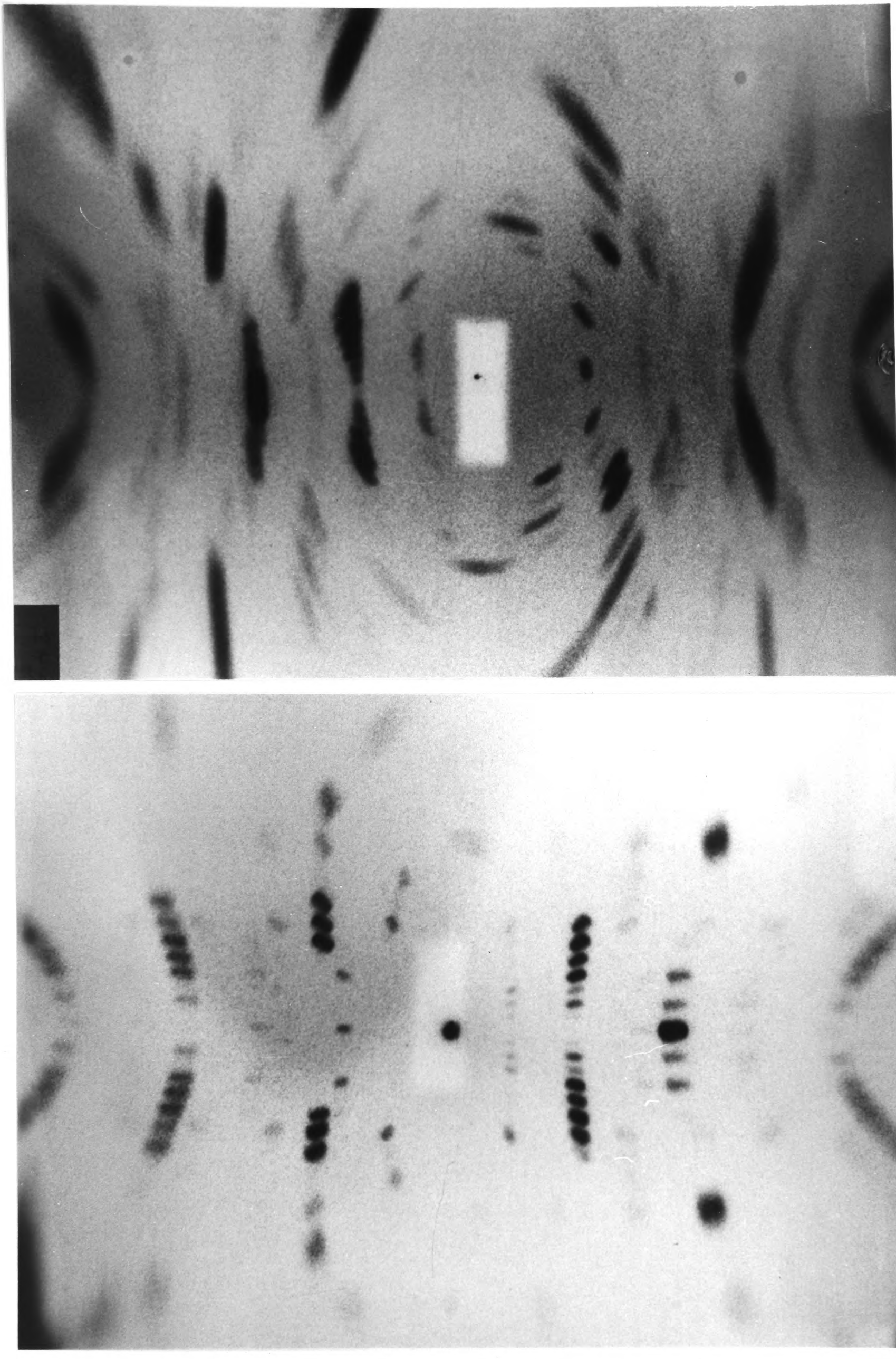


Figure 6.6. Oscillation photographs (neutrons, λ = 1.596A) of two crystals of '$HAl_{11}O_{17}$'. Both crystals are rotating approximately about the c-axis

sharp reflections.

b) Neutron diffraction experiment on the D9 diffractometer

The selected crystal (∿4 x 4.5 x 1mm) was mounted on the D9 four-circle diffractometer which was prepared for data collection in a standard manner. A mean wavelength of 0.8323Å was selected from the (200) planes of a Cu monochromator at a take-off angle of ∿27° and accurately determined in least-squares calculations using the coordinates of 10 reflections measured from a standard KCl crystal. This value, which is close to the long-wavelength limit for D9, was chosen to optimise the resolution of reflections in real space. The cell constants and orientation matrix were optimised by least-squares using the angular coordinates of 12 reflections. Values of a = 5.601(3)Å, c = 22.657(9)Å were obtained; that for c compares with 22.618Å ($DAl_{11}O_{17}$, Chapter 4), 22.62Å ($(H_3O)Al_{11}O_{17}$[75]), 22.76Å ($(H_3O)_{1+x}Al_{11}O_{17+½x}$[66]) and 22.70Å ($H_{0.61}(H_3O)_{0.39}Al_{11}O_{17}$[74]).

The resolution curve measured on the instrument is displayed in Figure 6.7; it clearly shows the greater width of the 0 0 0 ℓ series which reflects the macroscopic 'leafing' that occurred during preparation of the crystal. Data collection was implemented using ω-nθ scans in bisecting geometry, where n was determined at each value of the Bragg angle from an empirical curve, but the mode was later changed to ω-scans because of instrumental malfunction. In all, 1027 reflections were measured in the range $\theta < 45°$ over a period of 30 days. Initial data reduction was accomplised at the ILL using the program COLL5N[234] and the derived data set was then analysed using the CRYSTALS system[6]. The data were twice checked manually to eliminate off-centre reflections and those which

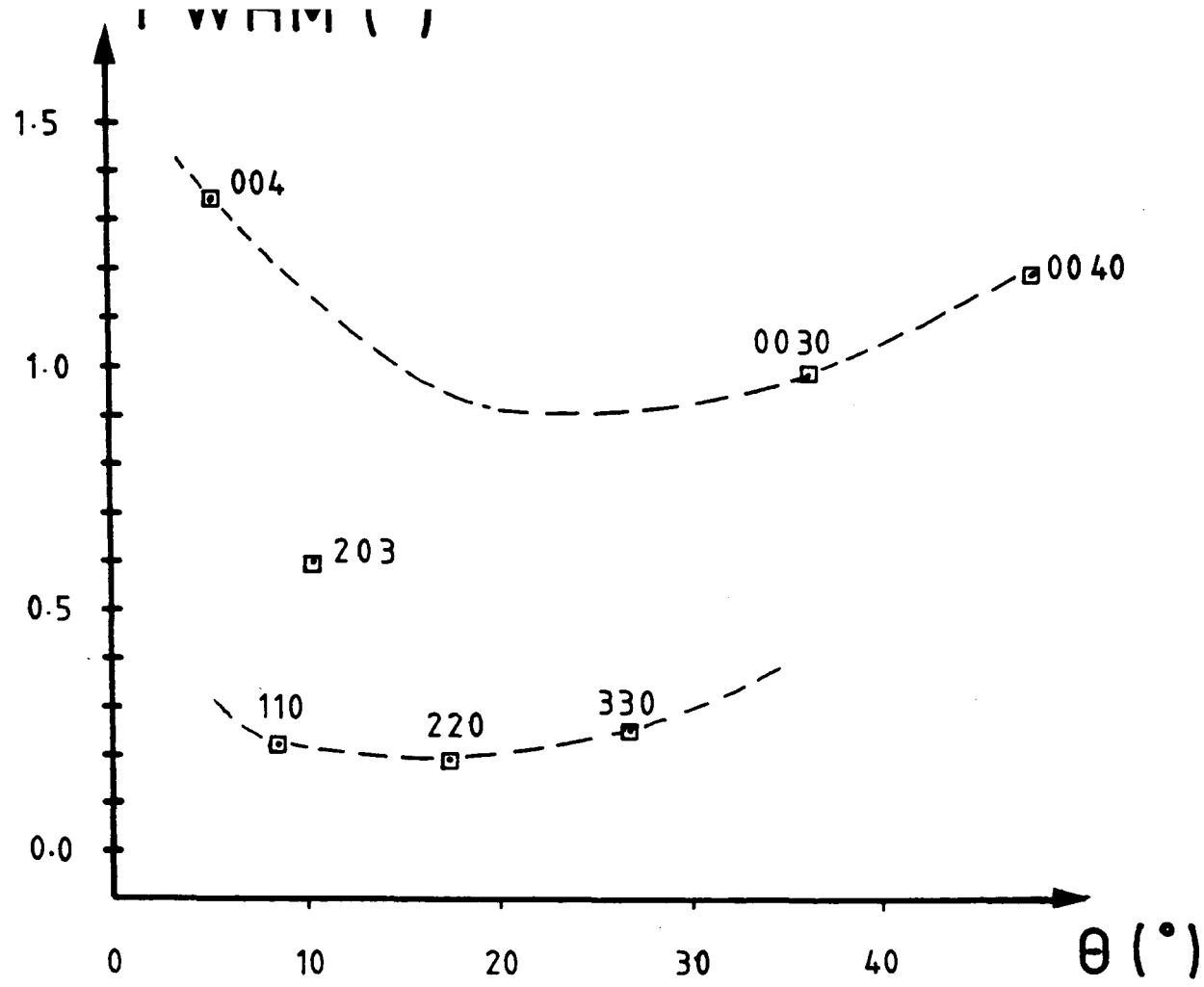


Figure 6.7. The full width at half-height (FWHM) of Bragg reflections plotted as a function of Bragg angle, θ. The data were measured on the D9 diffractometer from a crystal of '$HAl_{11}O_{17}$'.

suffered from overlap. All the 0 0 0 ℓ series measured in the ω-scan mode were rejected and the remaining 884 reflections were merged using unit weights. The merging R-factor was 0.0592 and there remained 472 independent structure amplitudes with $I \geqslant 0$.

The course of structure analysis was similar to that outlined above although after anisotropic refinement of the spinel block atoms and O(5), the residuals, R = 0.22 and R_W = 0.23, were large and they were not appreciably improved by any of the subsequent models. The poor agreement reflects several sources of inaccuracy in the observed data set. For example, the large width of the reflections, particularly at higher values of ℓ, makes background estimation and the recognition of overlap difficult and further, it limited the accuracy of the derived orientation matrix. In addition to the macroscopic deterioration in crystal quality which accompanied the preparation, we noted in Chapter 4 that $DAl_{11}O_{17}$ was liable to partial decomposition at elevated temperatures. In single crystals, this decomposition

occurs via an intermediate phase in which a correspondence with the beta alumina sturcture is retained[66] and it is possible that some such degradation has occurred within the crystal studied here.

While the structure definition allowed by this data set is limited, it does enable some important questions to be answered. No population of the BR site was apparent in $/F_{obs}/$ or $/F_{obs} - F_{calc}/$ Fourier syntheses and when the occupation number of a nitrogen entered at this position was refined, it converged to -0.01(17). The main peaks found in the Fourier calculations were at 0 0 0.083 (4e), 0.489 0.485 0.177 (24ℓ), 0.113 -0.113 0.25 (6h) and 0.5 -0.5 0.25 (6h), the last being of negative intensity and presumably corresponding to hydrogen. All of these sites were examined in least-squares refinement, with oxygen atoms being introduced at the first three positions and hydrogen at the last. The residuals were slightly improved and occupancies greater than zero were derived for all sites, although those of the hydrogen and of O(21) at 0.481 0.467 0.1757 attained the highest values of 1.0(1) and 0.7(1) respectively. The hydrogen site is close to that found for deuterium in $DAl_{11}O_{17}$ (Chapter 4) and an occupancy of near unity is consistent with the reports of Colomban et al.[75]. However, the other sites bear no similarity with those described in any other beta alumina materials and they presumably either reflect errors in the observed data or derive from the effects of the aforementioned partial decomposition. We present in Table 6.4, the atomic parameters derived from refinements in which these secondary sites were ignored. The bond lengths and angles (Tables 6.5 and 6.6) and listed structure factors (Appendix III) also correspond to this model, as do the z = 1/4 $/F_{obs}/$ and $/F_{obs} - F_{calc}/$

Fourier sections displayed in Figure 6.8.

In the list of bond lengths (Table 6.5), the respective Al(3)-O(5) distances indicate a higher value for this material in comparison with the two precursors, which probably reflects the presence of the O(5)-H(31) linkage. However, this distance does not approach that found in $DAl_{11}O_{17}$ (Chapter 4) and further, the c-axis constant of the latter material (22.62Å) is less than that of the '$HAl_{11}O_{17}$' (22.66Å) described here. Both c-parameter values are accurately reproducible so that this disparity reflects a genuine difference between the two materials. Our ambitious single-crystal experiment on '$HAl_{11}O_{17}$' does not provide an explanation for this distinction, but it does indicate firstly that the proton distribution is similar to that in $DAl_{11}O_{17}$ and secondly that the '$HAl_{11}O_{17}$' is probably liable to further degradation under the conditions required for its formation.

6.7 Discussion and Conclusion

In ammonium beta alumina, the NH_4^+ ions occupy discrete, well-defined sites of two types and determination of the proton positions by neutron diffraction has revealed favourable hydrogen-bonding schemes for both of these sites. Structure analyses of two different crystals, prepared independently, have given occupation numbers for N(1) at the Beevers-Ross site of 0.83(X-ray) and 0.84(neutron) respectively (in the case of neutrons, the large scattering length of nitrogen allows reasonable confidence to be attached to the derived occupancies). There remain 0.16 mirror planes in which to accommodate the residual 0.41 ammonium ions so that this distribution implies

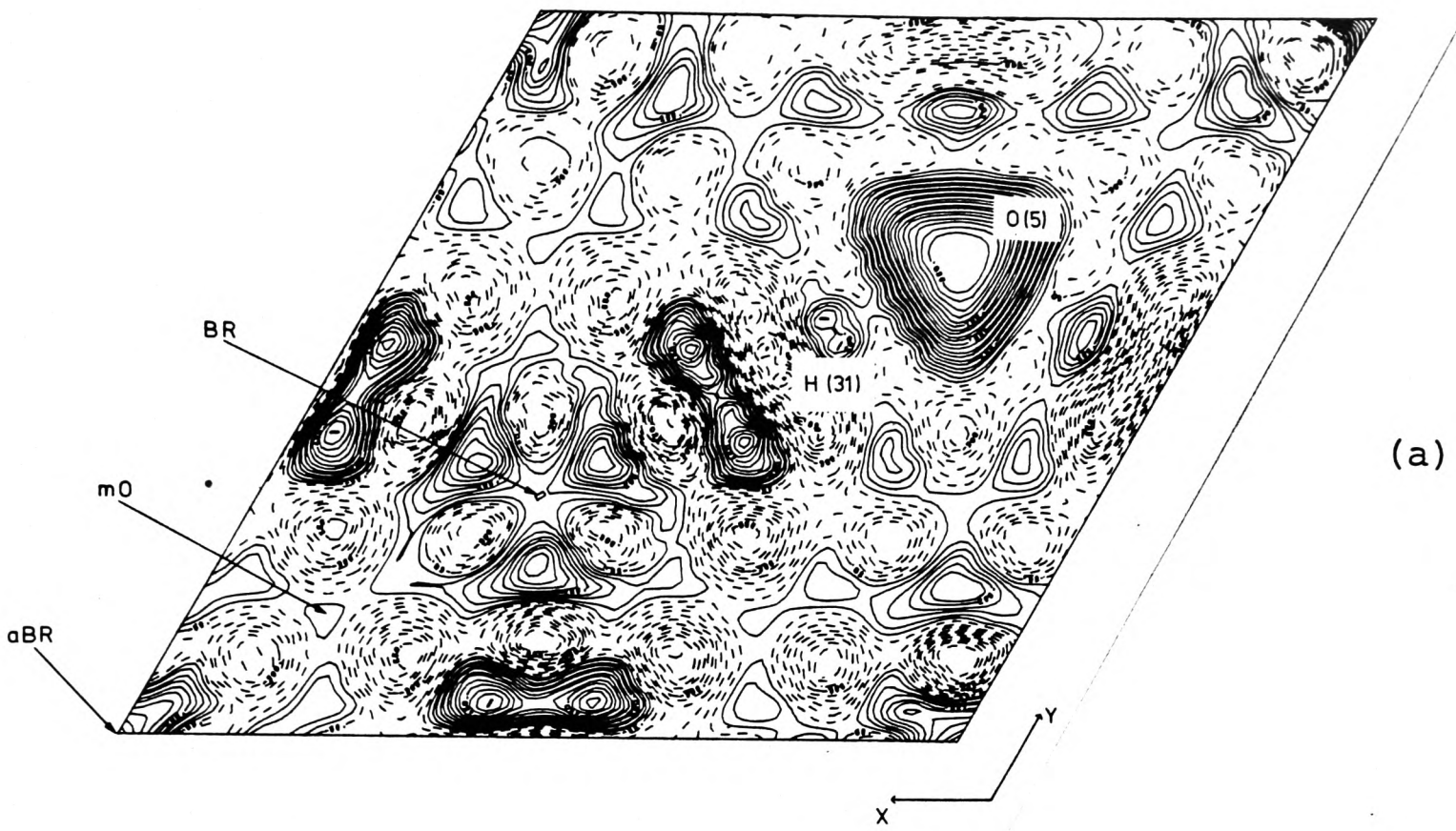


Figure 6.8. The z = 1/4 sections of final /F_{obs}/ (upper) and /F_{obs}-F_{calc}/ (lower) Fourier syntheses (arbitrary units) calculated from the single crystal neutron data on '$HAl_{11}O_{17}$'. The /F_{obs}/ synthesis is scaled to 999 with contour spacings of 50.The difference section is on the same scale and has the same contour levels. The maximum feature in the difference section has a height of 0.47× the maximum in the /F_{obs}/ section

a certain number of triply-occupied mirror planes. The mO site, which is that reported to be occupied by the additional oxygens required for charge compensation[15,44,52], is near that of N(2) and neither site will be populated in a mirror plane* which already contains N(1). There are three mO and N(2) sites per mirror plane and the derived N(1) occupancy yields a total of 3 x 0.16 = 0.48 possible locations for such species. The N(2) requirement is 0.41 and there is therefore an insufficient number of sites to accommodate the anticipated number of oxygen interstitials (0.125). We have found only limited evidence for population of the mO site itself and, as the sum of nitrogen occupancies approaches that implied by the chemical composition, it seems unlikely that any oxygen is incorporated at the N(2) site. However, we have found a significant population of interstitial aluminiums (Al_i) and the preparation of stoichiometric beta aluminas via hydrogen-containing systems strongly suggests that interstitial/additional oxygen is predominantly responsible for charge-compensation in the non-stoichiometric materials.

The proximity of a given N(2) site to those in two of the adjacent unit cells (Figure 6.9) restricts the way in which N(1) and N(2) populations may be accommodated in the extended structure. However, there are several schemes by which this can be achieved and a combination of these is presumably responsible for the absence of superlattice ordering in this system.

N(1) has $\bar{6}$m2 site symmetry which implies that the ammonium ion has three distinct energetically-equivalent orientations. The $(NH_4)_1$ hydrogen-bonding scheme (Figure 6.4) suggests that the most likely rotation mode for this ion is that about the $\bar{6}$

* *By 'mirror plane' we refer to the z = 1/4 section of one unit cell.*

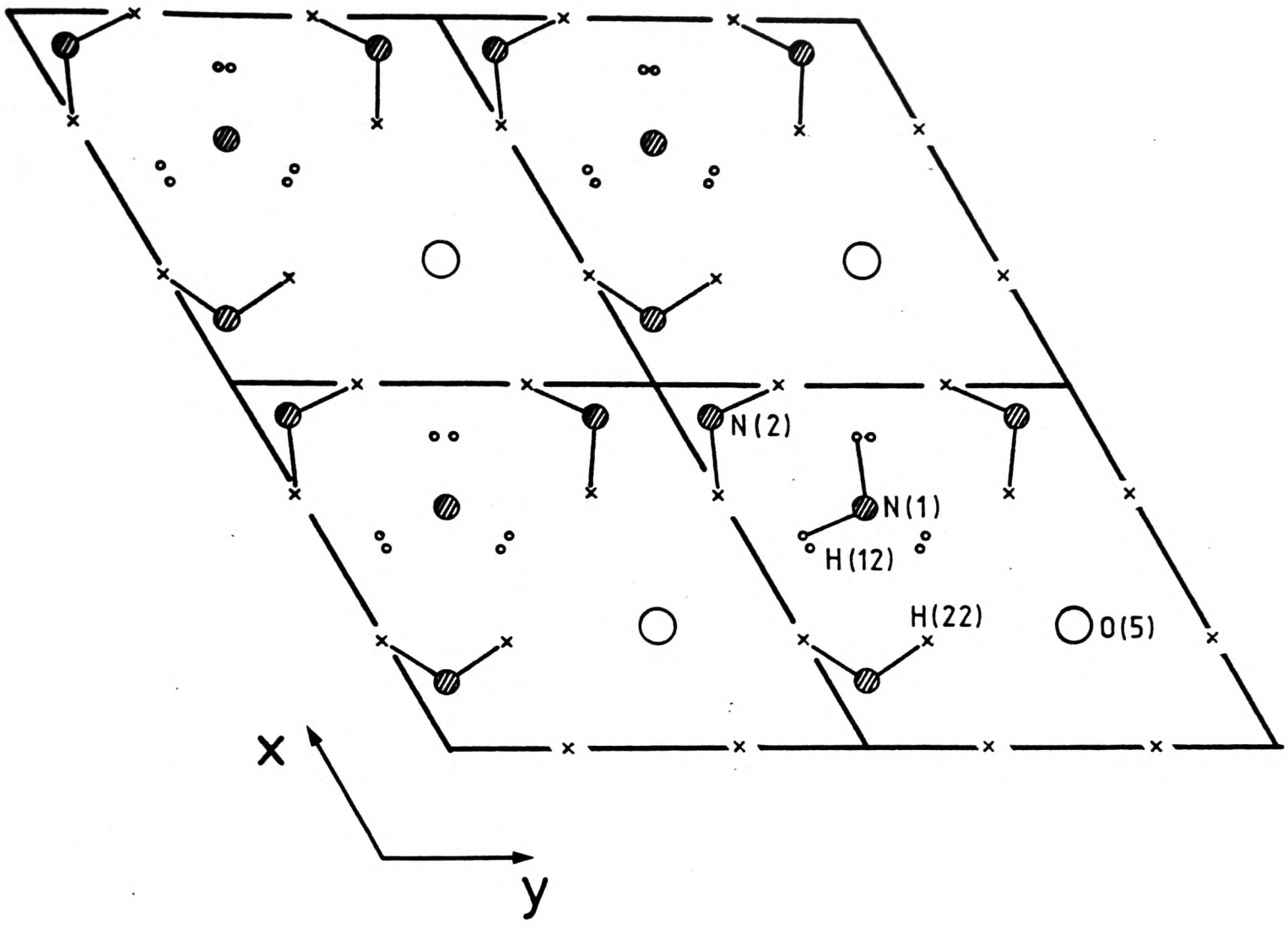


Figure 6.9. A representation of the z = 1/4 sections of four unit cells of ammonium beta alumina. The average structure, as derived in the crystallographic analyses, is displayed.

crystallographic axis and not that corresponding to tetrahedron inversion, implying that assumptions based on the latter may be misleading. Indeed, recent inelastic neutron scattering experiments[191] favour a more complicated scheme for the motion of the ammonium ions than that initially presented by Axe et al.[190]. In comparison with N(1), for each N(2) site, of symmetry mm, there is only one distinct orientation which gives rise to the propitious H-bonding arrangement. Further, the H(21)-O(4) and H(22)-O(5) contacts (Table 6.5) are shorter than the corresponding contacts involving H(12) and H(11) so that rotation of $(NH_4)_2$ is likely to be a process of higher energy than that for $(NH_4)_1$. This is in accord with spectroscopic results[189,192]. In relation to the higher frequency IR and Raman absorptions, the proton distribution and accurate values for atomic coordinates

and separations enable N-H stretching frequences to be estimated with some precision[235] which should simplify the interpretation of vibrational spectra.

The N(2)-O(4) distance of 2.66Å compares with the shortest value reported for a N-H···O linkage of 2.63Å in nicotinium salicylate[263,235]. Any contraction in the c-axis would reduce this separation unless N(2) were to move toward, say, the BR site. However, such movement will expand the N(2)-H(22)-O(5) linkage and is also likely to be limited by the presence of other $(NH_4)_2$ groups within the same mirror plane. We are therefore not surprised to find a large value of 22.88Å for the c-axis constant.

By heating a crystal of ammonium beta alumina to 620°C we have prepared a first derivative in which the N(2) site is vacant, but the occupancy for N(1) at the BR position remains close to that in the parent material. The use of a mechanical clamp during the heat treatment and a small amount of residual sodium probably facilitated the preparation of this intermediate phase. In the absence of N(2) the c-parameter is reduced to 22.66Å even though the majority of mirror planes still contain ammonium ions. This validates our explanation for the length of the c-axis in $(NH_4)_{1.25}Al_{11}O_{17.125}$. The N(1)-O(2) contact distance which is correlated with the c-parameter, is now shortened (Table 6.5). This is likely to limit the mobility of $(NH_4)_1$ in this intermediate phase and alter the appearance of the corresponding vibrational spectra. However, the existence of this phase has not yet been recognised by other workers so that, as yet, no spectroscopic data is available.

The macroscopic deterioration in crystal quality is clearly allied to the loss of the N(2) species. However, tga

and lattice-constant measurements[236] indicate that even formation of this intermediate phase is not a simple process. On heating ammonium beta alumina at 350°C for extended periods, weight loss (0.70%) close to that corresponding to 0.24(NH_3) (0.69%) is observed, but the lattice constant decreases only slightly from 22.88Å to 22.86Å. A value of 22.66Å is only obtained when the temperature is raised above 400°C. This behaviour probably reflects the limited mobility, particularly at lower temperatures, both of NH_4^+ ions and of the H^+ ions which result from the loss of ammonia and implies that other intermediate phases, in addition to those described here, might be isolated.

We have demonstrated in the introduction (Chapter 3) and in Chapter 4 that water molecules are relatively mobile in beta aluminas at temperatures above ambient and our experiments, together with those of others, indicate that comparable mobility accrues to the neutral species, NH_3. The fact that the $(NH_4)_2$ species are lost on heating before those on BR sites probably derives from a combination of several factors. Firstly, the process of deammoniation presumably occurs by proton transfer from an $(NH_4)^+$ ion to an oxygen, either O(5) or perhaps initially O(2) or O(4). The ammonia molecule which results is then lost, although the remaining proton may participate in the mechanism by which further NH_3 is transported. The initial transference is likely to be most facile for the shortest N-H···O linkage. (The behaviour at 350°C, which was noted above, may relate to such a mechanism in which a proton is initially transferred to O(4), but on further heating an increase in proton mobility enables this H^+ to adopt the presumably more favourable hydroxyl linkage with O(5)). Secondly, thermal agitation will have a less

dramatic effect on $(NH_4)_1$ than $(NH_4)_2$. The former rests at the centre of a cage defined by six O(2) atoms (Figure 6.4) so that even with extensive molecular rotation it is likely to remain close to the BR site. For the latter, as we have already indicated, such rotation destroys the favourable H-bonding scheme and the $(NH_4)_2^+$ species will then be influenced by longer-range interactions. Thirdly, the $(NH_4)_2^+$ ions exist in doubly- or triply-occupied mirror plances which presumably also contain (or are adjacent to those which contain) O_i interstitials. This crowded environment will be conducive to proton transfer. Finally, the proximity of $(NH_4)_2$ to adjacent cells is further likely to facilitate the loss of $(NH_4)_2^+$ compared with the predominant $(NH_4)_1^+$ species.

The structure analysis of the H/NH_4 beta alumina intermediate phase reveals that $(NH_4)_1$ has an identical orientation to that in the parent material and indicates the distribution of the protons which remain when $0.47(NH_3)$ is lost. H(31) is at the same location as deuterium in $DAl_{11}O_{17}$ (Chapter 4) and H(31) in '$HAl_{11}O_{17}$'. H(32), which is the major species, does not have an analogue in other systems. For an isolated mirror plane the H(31) site is preferred because of the weak interaction this allows with the neighbouring O(2) atoms, but where NH_4^+ ions occur in adjacent unit cells (see Figure 6.10) such sites involve short H(31)-H(12) contacts and the H(32) sites are favoured. When, in '$HAl_{11}O_{17}$', no cells contain NH_4^+ ions the protons revert to the H(31) positions.

We arrive finally at the question of stoichiometry. The limited information which we obtained on '$HAl_{11}O_{17}$' is consistent with the stoichiometric composition as described by other authors[75,89,195]. In the intermediate phase,

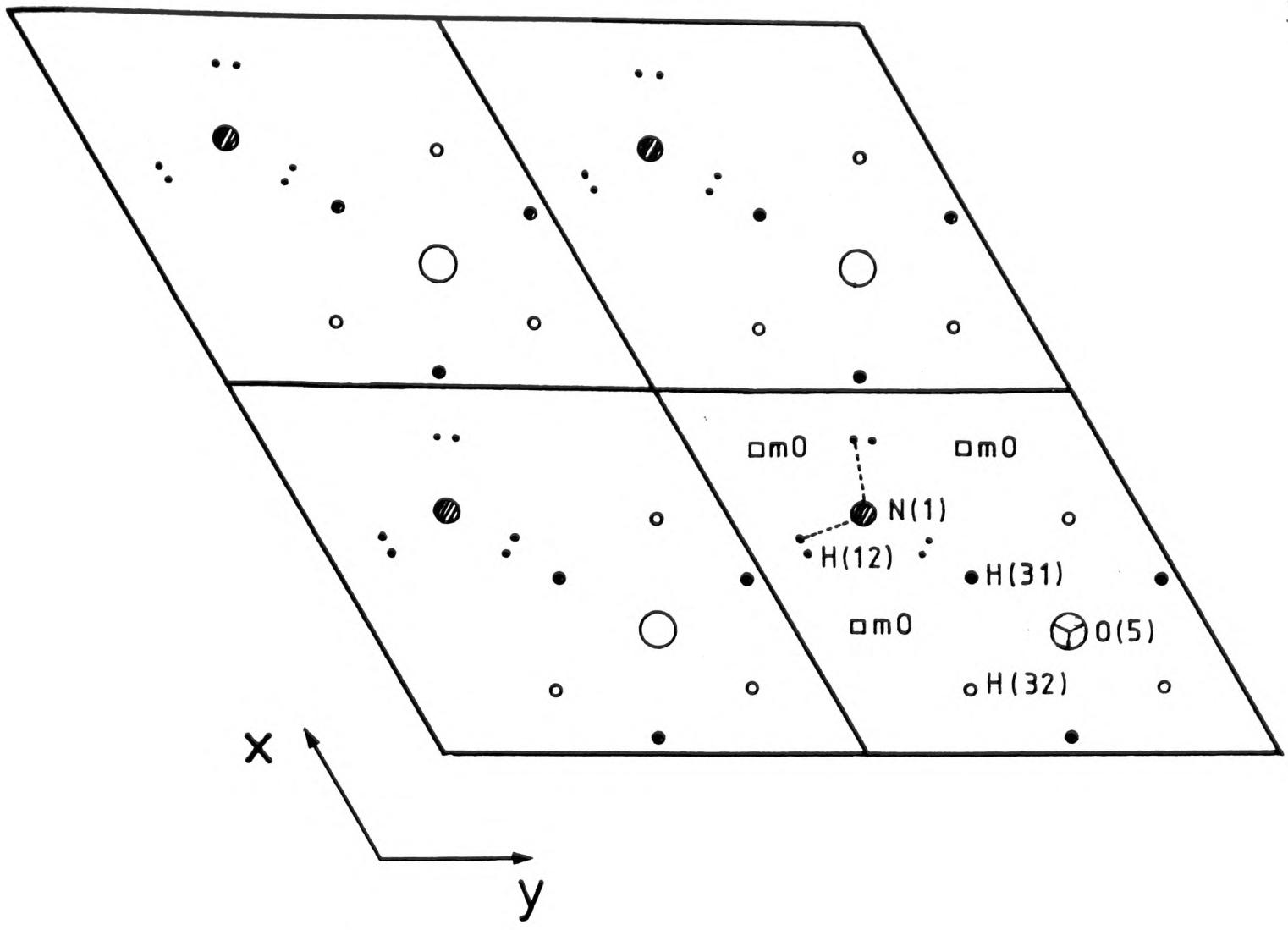


Figure 6.10. A representation of the z = 1/4 sections of four unit cells of ammonium/hydrogen beta alumina.

'$H/NH_4Al_{11}O_{17}$', we have deduced a population of aluminium interstitials which is little reduced from that in the parent ammonium compound. The occupancies of H(31) and H(32) are small and they are, as a result, poorly defined in refinement. In particular, that of H(31) oscillated about a near-zero value in the later stages and its final value (Table 6.3) is no larger than the associated standard deviation. This behaviour indicates that there is only a low concentration of H(31) species and the sum of the remaining cations in the mirror plane of 1.03 is favourably close to the stoichiometric (S) composition. Although Colomban et al.[75,230] and Collongues[195] have not considered the possibility of this type of intermediate, for the preparation of S-materials they report that best results are obtained when ammonium beta alumina, containing a small quantity of residual sodium, is heated at 500°C. In the light of our results, it is likely that these conditions will give rise to a considerable

proportion of the H/NH_4 intermediate, implying that stoichiometry has, indeed, been attained in this phase.

We can depict the evolution in ammonium beta alumina in terms of the changes that occur within the average mirror plane as set out in Scheme I. We assume that charge compensation is entirely achieved by additional oxygen, although we are not concerned here with the nature of the sites which these species occupy. In the light of this scheme, we can suggest that the '$H/NH_4Al_{11}O_{17}$' material described above corresponds to phase II, but in which a small amount of further decomposition to III has occurred. We do not, as yet, have sufficient experimental data to confirm the exact details of this scheme, but it would appear that this representation conveys more useful information than the corresponding empirical formulae. It further prompts us to consider the hydronium beta alumina system in a similar fashion (Scheme II).

The thermal evolution in hydronium beta alumina has been studied in detail by several authors (section 3.5) and we have chosen to consider the composition quoted by Roth et al.[185]. The general features of this scheme are consistent with the reported work, although Roth et al.[184,185] do not find a distinct weight loss corresponding to the formation of '$HAl_{11}O_{17}$'. The weight loss found for step I at ∿220°C is close to $\frac{1}{2}H_2O$[185] and the composition, $2.6H_2O.11Al_2O_3$, for the 'H^+-H_3O^+' intermediate phase approaches that indicated in the scheme. Kato and Saalfeld reported details of the structure of a material of nominal composition $1.79H_2O.11Al_2O_3$[74] and aspects of this crystallographic analysis indicate the presence of a H-O(5) linkage. IR measurements[186,75] reveal a characteristic band at $3510cm^{-1}$ and although this was initially inter-

preted in terms of an O-H stretch in an (H_3O^+) function, it is now clear that it derives from an O(5)-H vibration. The experimental evidence therefore suggests that the intermediate phase I, corresponds to stoichiometric $(H_3O)Al_{11}O_{17}$ in which there is a water molecule of unit occupancy at the Beevers-Ross position and a single proton involved in a hydroxyl-linkage with O(5).

No X-ray or neutron diffraction measurements have been reported for the as-prepared hydronium beta alumina and the IR spectra[186] display several bands which may be assigned to O-H stretching modes. It is therefore difficult to determine the nature of the species which occupy the mirror planes. However, if the BR sites are completely populated, it is possible that species such as $H_5O_2^+$ and $H_7O_3^+$ will occur in the doubly- and triply-occupied unit cells. It would be interesting to use neutron diffraction to determine the positions of the hydrogens in this system. Such an analysis might indicate whether $H^+(H_2O)_n$ species do occur or whether all the protons are involved either in hydroxyl linkages with O(5) or as neutral water molecules, H_2O_i. We may also note that this system appears to offer a low-temperature route to stoichiometric beta aluminas. The non-stoichiometric to stoichiometric transformation is further considered elsewhere[237,238].

In conclusion, we have found that even in unfavourable circumstances structural analyses, particularly using neutron diffraction data, can yield invaluable insight into the chemical and physical behaviour of these beta alumina systems.

SCHEME I

Thermal evolution in the structure of ammonium beta alumina

$(NH_4^+)_{0.84} + (NH_4^+)_{0.41} + O_{i\,0.125}^{2-} + O(5)^{2-}$ $(+ Al_{11}O_{16}^+)$

$\equiv (NH_4)_{1.25}Al_{11}O_{17.125}$

$\downarrow$ $-0.41(NH_3)$, $\sim 350°C$

$(NH_4^+)_{0.84} + H^+_{0.41} + O_{i\,0.125}^{2-} + O(5)^{2-}$

$\downarrow$ $>400°C$, $-0.125H_2O$, rearrangement

Intermediate Phase I
c = 22.84 - 22.86Å

$(NH_4^+)_{0.84} + H^+_{0.16} + O(5)^{2-}$

$\downarrow$ $\sim 600°C$, $-0.84(NH_3)$

Intermediate Phase II
$H/NH_4Al_{11}O_{17}$
c = 22.66Å

$H^+ + O(5)^{2-}$

$'HAl_{11}O_{17}'$
c = 22.66Å

$\downarrow$ $\sim 800°C$, $-\frac{1}{2}H_2O$

$O(5)^{2-}_{0.5}$ $(+ Al_{11}O_{16}^+) \equiv Al_2O_3$ Disordered phase

$\downarrow$ $\sim 1000°C$

α-Al_2O_3

SCHEME II

Thermal evolution in the structure of hydronium beta alumina.

$'H_3O^+' + (H_3O^+)_{0.3} + O_{i\,0.15}^{2-} + O(5)^{2-}$ $(+ Al_{11}O_{16}^+) \equiv (H_3O)_{1.3}Al_{11}O_{17.15}$, or $3.9H_2O.11Al_2O_3$

rewrite ↓

$'H_3O^+' + (H_2O)_{0.45} + O(5)^{2-}$

220°C
$-0.45H_2O$ ↓

$'H_3O^+' + O(5)^{2-}$ — Intermediate Phase I

>700°C (?) ↓
$-H_2O$

$'H^+\text{-}H_3O^+$ beta alumina'
$3H_2O.11Al_2O_3$

$H^+ + O(5)^{2-}$ — $'HAl_{11}O_{17}'$ or $H_2O.11Al_2O_3$.

∿800°C ↓
$-\frac{1}{2}H_2O$

$O(5)_{0.5}^{2-}$ $(+ Al_{11}O_{16}^+) \equiv Al_2O_3$ disordered phase

∿1100°C ↓

$\alpha\text{-}Al_2O_3$

TABLE 6.1

Final atomic parameters derived from the single crystal X-ray study of $(NH_4)_{1.25}Al_{11}O_{17.125}$ with estimated standard deviations in parentheses.

Atom	Position	Site Symmetry	x	y	z	Occn.
O(1)	12k	m	0.1571(1)	$\bar{x}$	0.04904(6)	6.0
O(2)	12k	m	0.5019(2)	$\bar{x}$	0.14441(7)	6.0
O(3)	4f	3m	-1/3	1/3	0.05451(11)	2.0
O(4)	4e	3m	0	0	0.13957(10)	2.0
O(5)	6h	mm	0.327(5)	$\bar{x}$	1/4	1.0
Al(1)	12k	m	-0.16783(3)	$\bar{x}$	0.10445(3)	5.77(1)
Al(11)	12k	m	-0.1627(19)	$\bar{x}$	0.1756(8)	0.23(1)
Al(2)	4f	3m	-1/3	1/3	0.02455(5)	2.0
Al(3)	4f	3m	-1/3	1/3	0.17451(5)	2.0
Al(4)	2a	$\bar{3}$m	0	0	0	1.0
N(1)	2d	$\bar{6}$m2	-1/3	1/3	1/4	0.83(2)
N(2)	6h	mm	-0.090(3)	$\bar{x}$	1/4	0.47(3)
H(11)	12k	m	-0.392(4)	$\bar{x}$	0.215(2)	1.66(4)
H(12)	12j	mm	-0.420(6)	0.452(7)	1/4	1.66(4)
H(21)	12k	m	-0.033(5)	$\bar{x}$	0.216(2)	0.94(6)
H(22)	12j	m	0.300(9)	0.296(10)	1/4	0.94(6)

$R = 0.0304$ $R_W = 0.0517$

Extinction Parameter = 1.0(1)

Cont.

TABLE 6.1, cont.

Atom	U_{11} or U(iso)	U_{33}	U_{12}	U_{13}	U_{23}
O(1)	0.0072(4)	0.0059(5)	0.0047(5)	-0.0002(2)	$-U_{13}$
O(2)	0.0062(4)	0.0097(5)	0.0025(4)	0.0000(2)	$-U_{13}$
O(3)	0.0060(6)	0.0071(9)	$U_{11/2}$	0	0
O(4)	0.0056(6)	0.0052(9)	$U_{11/2}$	0	0
O(5)	0.020(2)	0.008(2)	-0.003(11)	0	0
Al(1)	0.0061(2)	0.0057(3)	0.0034(2)	0.0001(1)	$-U_{13}$
Al(11)	"	"	"	"	"
Al(2)	0.0046(3)	0.0037(4)	$U_{11/2}$	0	0
Al(3)	0.0079(3)	0.0035(4)	$U_{11/2}$	0	0
Al(4)	0.0050(4)	0.0054(6)	$U_{11/2}$	0	0
N(1)	0.030(2)	-0.003(2)	$U_{11/2}$	0	0
N(2)	0.024(8)	0.023(11)	0.005(9)	0	0
H(11)	0.05 (U(iso))				
H(12)	0.05				
H(21)	0.05				
H(22)	0.05				

TABLE 6.2

Final atomic parameters derived from the single crystal neutron study of $(NH_4)_{1.25}Al_{11}O_{17.125}$ with estimated standard deviations in parentheses.

Atom	Position	Site Symmetry	x	y	z	Occn.
O(1)	12k	m	0.1570(2)	$\bar{x}$	0.04921(8)	6.0
O(2)	12k	m	0.5015(2)	$\bar{x}$	0.14431(9)	6.0
O(3)	4f	3m	-1/3	1/3	0.05460(14)	2.0
O(4)	4e	3m	0	0	0.13975(16)	2.0
O(5)	6h	mm	0.313(7)	$\bar{x}$	0.25	1.0
Al(1)	12k	m	-0.1680(4)	$\bar{x}$	0.10464(14)	5.83(6)
Al(11)	12k	m	-0.174(14)	$\bar{x}$	0.178 (6)	0.17(6)
Al(2)	4f	3m	1/3	-1/3	0.0238(2)	2.0
Al(3)	4f	3m	1/3	-1/3	0.1745(2)	2.0
Al(4)	2a	$\bar{3}$m	0	0	0	1.0
N(1)	2d	$\bar{6}$m2	-1/3	1/3	1/4	0.84(6)
H(11)	12k	m	-0.393(2)	$\bar{x}$	0.2134(8)	1.69(11)
H(12)	12j	m	-0.420(6)	0.452(8)	0.25	1.69(11)
N(2)	6h	mm	-0.088(2)	$\bar{x}$	0.25	0.42(5)
H(21)	12k	m	-0.027(5)	$\bar{x}$	0.2124(13)	0.84(9)
H(22)	12j	m	0.295(7)	0.301(6)	0.25	0.84(9)

$R = 0.0500$ $R_W = 0.0525$

Cont.

TABLE 6.2, cont.

Atom	U_{11}	U_{22}	U_{33}	U_{12}	U_{13}	U_{23}
O(1)	0.0104(8)	U_{11}	0.0126(10)	0.0061(8)	-0.0001(4)	$-U_{13}$
O(2)	0.0090(8)	U_{11}	0.0225(12)	0.0046(7)	0.0000(4)	$-U_{13}$
O(3)	0.0107(11)	U_{11}	0.0089(17)	$U_{11/2}$	0	0
O(4)	0.0075(10)	U_{11}	0.0158(19)	$U_{11/2}$	0	0
O(5)	0.017(16)	U_{11}	0.010(3)	0.013(6)	0	0
Al(1)	0.011(1)	U_{11}	0.012(2)	0.006(1)	0.0013(7)	$-U_{13}$
Al(11)	"	"	"	"	"	"
Al(2)	0.012(2)	U_{11}	0.006(2)	$U_{11/2}$	0	0
Al(3)	0.011(2)	U_{11}	0.003(3)	$U_{11/2}$	0	0
Al(4)	0.005(2)	U_{11}	0.016(4)	$U_{11/2}$	0	0
N(1)	0.035(5)	U_{11}	0.002(7)	$U_{11/2}$	0	0
H(11)	0.055(8)	U_{11}	0.014(10)	0.033(8)	-0.015(5)	$-U_{13}$
H(12)	0.046(15)	0.12(4)	0.012(10)	0.044(17)	0	0
N(2)	0.006(8)	U_{11}	0.049(16)	-0.010(7)	0	0
H(21)	0.08(2)	U_{11}	0.05(3)	-0.00(3)	-0.07(2)	$-U_{13}$
H(22)	0.09(4)	0.00(2)	0.06(2)	-0.08(2)	0	0

TABLE 6.3

Final atomic parameters determined from the single crystal neutron diffraction study of 'NH_4/H $Al_{11}O_{17}$' with estimated standard deviations in parentheses.

Atom	Position	Site Symmetry	x	y	z	Occn.
O(1)	12k	m	0.1568(3)	$\bar{x}$	0.0491(1)	6.0
O(2)	12k	m	0.5021(3)	$\bar{x}$	0.1444(1)	6.0
O(3)	4f	3m	-1/3	1/3	0.0552(2)	2.0
O(4)	4e	3m	0	0	0.1401(2)	2.0
O(5)	6h	mm	0.350(6)[a]	$\bar{x}$	0.25	1.0
Al(1)	12k	m	-0.1669(4)	$\bar{x}$	0.1063(2)	5.77(7)[b]
Al(2)	4f	3m	1/3	-1/3	0.0242(3)	2.0
Al(3)	4f	3m	1/3	-1/3	0.1748(3)	2.0
Al(4)	2a	$\bar{3}$m	0	0	0	1.0
N(1)	2d	$\bar{6}$m2	-1/3	1/3	0.25	0.78(7)
H(11)	12k	m	-0.392(3)	$\bar{x}$	0.212(1)	1.57(15)
H(12)	12j	m	-0.417(8)	0.451(8)	0.25	1.57(15)
H(31)	6h	mm	0.485[c]	$\bar{x}$	0.25	0.1(1)
H(32)	6h	mm	0.180(14)	$\bar{x}$	0.25	0.25(9)
Na(1)	6h	mm	-0.293	$\bar{x}$	0.25	0.05
Na(2)	6h	mm	-0.145	$\bar{x}$	0.25	0.03(10)

$R = 0.0732$ $R_W = 0.0732$

[a] In the last cycles of refinement, the spacer oxygen coordinates were fixed. The quoted esd derives from earlier calculations which did not include H(32)

[b] The occupancy of Al(1) was refined together with that of Al_i

Cont.

TABLE 6.3, cont.

Atom	U_{11} or U(iso)	U_{22}	U_{33}	U_{12}	U_{13}	U_{23}
O(1)	0.001(1)	U_{11}	0.012(1)	0.003(1)	-0.001(1)	$-U_{13}$
O(2)	0.000(1)	U_{11}	0.015(1)	-0.001(1)	0.0004(5)	$-U_{13}$
O(3)	-0.000(1)	U_{11}	0.011(2)	$U_{11/2}$	0	0
O(4)	-0.003(1)	U_{11}	0.013(2)	$U_{11/2}$	0	0
O(5)	0.013(4)	U_{11}	-0.001(3)	-0.002(8)	0	0
Al(1)	-0.003(2)	U_{11}	0.000(2)	-0.000(2)	0.0004(7)	$-U_{13}$
Al(2)	-0.007(2)	U_{11}	0.009(3)	$U_{11/2}$	0	0
Al(3)	0.001(2)	U_{11}	0.007(4)	$U_{11/2}$	0	0
Al(4)	-0.008(3)	U_{11}	0.005(5)	$U_{11/2}$	0	0
N(1)	0.032(8)	U_{11}	0.021(9)	$U_{11/2}$	0	0
H(11)	0.06(2)	U_{11}	0.04(2)	0.01(1)	-0.02(1)	$-U_{13}$
H(12)	0.12(7)	0.09(4)	0.04(2)	0.08(3)	0	0
H(31)	0.03 (U(iso))					
H(32)	0.03					
Na(1)	0.04					
Na(2)	0.04					

(placed at -0.1667 $\bar{x}$ 0.1765) with the constraint that the sum was 6.0. The temperature factors of Al_i were constrained to equal those of Al(1).

[c] The coordinates of H(31) were fixed in the final cycles because, when allowed to vary, the calculated shifts were large.

TABLE 6.4

Atomic parameters derived from the single crystal neutron study of '$HAl_{11}O_{17}$' with estimated standard deviations in parentheses.

Atom	Position	Site Symmetry	x	y	z	Occn.
O(1)	12k	m	0.1574(5)	$\bar{x}$	0.0491(2)	6.0
O(2)	12k	m	0.5031(6)	$\bar{x}$	0.1456(3)	6.0
O(3)	4f	3m	-1/3	1/3	0.0556(5)	2.0
O(4)	4e	3m	0	0	0.1412(5)	2.0
O(5)	6h	mm	0.362(3)	$\bar{x}$	0.25	1.0
Al(1)	12k	m	-0.1676(11)	$\bar{x}$	0.1058(5)	6.0
Al(2)	4f	3m	1/3	-1/3	0.0233(7)	2.0
Al(3)	4f	3m	1/3	-1/3	0.1737(7)	2.0
Al(4)	2a	$\bar{3}$m	0	0	0	1.0
H(31)	6h	mm	0.482(2)	$\bar{x}$	0.25	1.18(13)

Atom	U_{11}	U_{33}	U_{12}	U_{13}	U_{23}
O(1)	0.006(1)	0.019(2)	0.004(2)	0.001(1)	$-U_{13}$
O(2)	0.008(1)	0.021(2)	0.004(2)	0.001(1)	$-U_{13}$
O(3)	0.003(2)	0.025(4)	$U_{11/2}$	0	0
O(4)	0.010(2)	0.015(4)	$U_{11/2}$	0	0
O(5)	0.07(3)	0.016(8)	0.06(2)	0	0
Al(1)	0.009(2)	0.026(4)	0.003(3)	0.000(2)	$-U_{13}$
Al(2)	0.011(4)	0.009(6)	$U_{11/2}$	0	0
Al(3)	0.007(3)	0.010(5)	$U_{11/2}$	0	0
Al(4)	0.007(5)	0.019(9)	$U_{11/2}$	0	0
H(31)	0.097	0.027	0.225	0	0

$R = 0.2136 \quad R_W = 0.2132$

TABLE 6.5

Bond distances (Å) calculated from the final refinements of $(NH_4)_{1.25}Al_{11}O_{17.125}$ and its derivatives, with estimated standard deviations in parentheses.

	$(NH_4)_{1.25}Al_{11}O_{17.125}$			'H/NH_4-$Al_{11}O_{17}$'	'$HAl_{11}O_{17}$'	$(H_3O)Al_{11}O_{17}$	
Octahedra	X-ray	Neutron	Ref.75			Ref.74	Ref.75
Al(1)-O(1)	2.025(1)	2.025(3)	2.022	2.037(4)	2.036(9)	2.034(2)	2.039
-O(2)	1.845(1)	1.842(3)	1.834	1.824(3)	1.833(8)	1.829(2)	1.826
-O(3)	1.971(2)	1.970(4)	1.968	1.986(5)	1.970(9)	1.975(2)	1.988
-O(4)	1.816(1)	1.817(4)	1.815	1.792(3)	1.813(11)	1.803(2)	1.808
Av. Al(1)-O	1.921	1.920	1.916	1.917	1.920	1.917	1.921
Al(4)-O(1)	1.893(1)	1.894(2)	1.891	1.885(3)	1.889(5)	1.890(2)	1.905
Tetrahedra							
Al(2)-O(1)	1.799(2)	1.807(3)	1.800	1.803(4)	1.804(7)	1.803(2)	1.798
-O(3)	1.809(3)	1.795(7)	1.811	1.798(9)	1.797(19)	1.812(3)	1.807
Av. Al(2)-O	1.801	1.804	1.803	1.802	1.802	1.805	1.800
Al(3)-O(2)	1.775(2)	1.772(3)	1.778	1.776(4)	1.766(8)	1.753(2)	1.784
-O(5)	1.728(2)	1.739(9)	1.717	1.711(8)	1.752(17)	1.794(2)	1.687
Av. Al(3)-O	1.763	1.764	1.763	1.760	1.762	1.763	1.760
Al(11)-O(2)	1.777(11)	1.76(8)	-	1.763	-	-	-
Nitrogen Contacts							
N(1)-H(11)	0.97(5)	1.01(2)	-	1.02(3)			
-H(12)	1.00(5)	1.00(3)	-	0.98(3)			
N(2)-H(21)	0.97(5)	1.05(4)	-	-	-		
-H(22)	1.00(5)	1.03(2)	-	-			
N(1)-O(5)	3.20(2)	3.14(3)	3.143[a]	3.075		2.646(13)	3.077[a]
-N(2)	2.36(3)	2.38(2)	-	-			
-O(2)	2.897(2)	2.901(2)	2.893[a]	2.876(3)		2.774(6)	2.875[a]
N(2)-O(5)	2.84(5)	2.96(2)	2.908[a]	-			
-O(2)	3.190(8)	3.204(11)	3.209	-			
-O(4)	2.675(10)	2.664(8)	2.636	-			
N(1)-Al(11)	2.37(2)	2.26(13)	-	2.32			
N(2)-Al(11)	1.84(2)	1.85(12)	-	-			

Cont.

TABLE 6.5, cont.

Hydrogen Contacts	$(NH_4)_{1.25}Al_{11}O_{17.125}$ X-ray	Neutron	'H/NH_4-$Al_{11}O_{17}$'	'H$Al_{11}O_{17}$'
H(11)-O(2)	1.93(5)	1.89(2)	1.85(3)	-
-O(5)	2.75(3)	2.70(3)	2.65(3)	-
H(12)-O(5)	2.20(6)	2.14(4)	2.10(3)	-
-O(2)	2.49(1)	2.49(1)	2.47(1)	-
H(21)-O(4)	1.77(4)	1.68(3)	-	-
H(22)-O(5)	1.94(6)	1.77(7)	-	-
-O(2)	2.67(2)	2.67(1)	-	-
H(31)-O(5)	-	-	1.31	1.16(4)
H(32)-O(5)	-	-	1.41	

[a] average value.

TABLE 6.6

Bond angles (°) calculated from the final refinements of $(NH_4)_{1.25}Al_{11}O_{17.125}$ and its derivatives, with estimated standard deviations in parentheses.

	$(NH_4)_{1.25}Al_{11}O_{17.125}$ X-ray	Neutron	'H/NH_4-$Al_{11}O_{17}$'	'HAl_{11}-O_{17}'	(H_3O)-$Al_{11}O_{17}$ (Ref.74)
Octahedra					
O(1)-Al(1)-O(1)	81.37(5)	81.25(14)	80.6(2)	81.0(4)	80.74(6)
-O(2)	90.48(3)	90.28(5)	90.0(1)	90.6(2)	90.08(6)
-O(3)	89.17(6)	89.15(13)	88.4(2)	88.9(5)	88.77(6)
-O(4)	83.89(6)	83.80(15)	83.7(2)	84.2(4)	83.53(7)
O(2)-Al(1)-O(2)	97.24(6)	97.76(17)	98.6(2)	97.1(5)	98.49(7)
-O(3)	86.06(6)	86.09(15)	85.0(2)	85.5(4)	85.54(6)
-O(4)	99.94(6)	99.96(15)	101.6(2)	100.5(5)	-
O(1)-Al(4)-O(1)	88.44(6)	88.27(8)	88.7(1)	88.9(2)	88.37(6)
Tetrahedra					
O(1)-Al(2)-O(1)	110.77(6)	110.2(2)	110.6(2)	110.0(5)	110.59(6)
-O(3)	108.14(6)	108.7(2)	108.3(3)	108.9(5)	108.33(6)
O(2)-Al(3)-O(2)	105.91(7)	105.8(2)	105.9(3)	107.7(6)	107.53(7)
-O(5)	111.8(8)	109.5(1.0)	107.5(2)	101.9(1.2)	98.46(18)
O(2)-Al(11)-O(2)	102.3(9)	105(7)	103.3(1)	-	-
Nitrogen Contacts					
H(11)-N(1)-H(11)	108.5(2.9)	110.0(2.3)	113(4)	-	-
-H(12)	109.7(1.0)	109.0(1.2)	109(1)	-	-
H(12)-N(1)-H(12)	109.6(2.9)	109.8(4.1)	109(5)	-	-
H(21)-N(2)-H(21)	109.1(2.9)	110.6(3.0)	-	-	-
-H(22)	109.6(1.0)	108.5(1.2)	-	-	-
H(22)-N(2)-H(22)	109.4(2.9)	112.2(4.1)	-	-	-
Al(3)-O(5)-H(31)	-	-	95	99(1)	-
-H(32)	-	-	92	-	-
Angles about hydrogen					
N(1)-H(11)-O(2)	176(2)	179(2)	180(3)		
N(1)-H(12)-O(5)	174(2)	177(3)	169(3)		
N(2)-H(21)-O(4)	155(2)	154(3)			
N(2)-H(22)-O(5)	149(3)	149(3)			

CHAPTER 7

SODIUM AND SILVER ORTHOPHOSPHATES

7.1 Introduction

In this and the subsequent chapter we consider orthophosphates and sulphates of monovalent cations which are exemplary of a large group of salts in which the anions adopt tetrahedral geometry. This group includes such species as PO_4^{3-}, SO_4^{2-}, BF_4^-, BH_4^-, ClO_4^- and IO_4^-. Many anhydrous tertiary systems containing these ions exist as well-ordered low-temperature phases which transform, at varying temperatures, to phases in which the anions are rotationally disordered. For M_nAX_4, the temperature of the transition probably depends on the charge n- of the anion, the A-X distance and on the identity of the cation. Although conductivity for these types of system are sparse, appreciable cation mobility has been observed in II-Na_3PO_4 (γ)[239]*, II-Ag_3PO_4[239], α-Ag_2SO_4[240] and α-Li_2SO_4[241]. In contrast to the beta aluminas, the ionic conductivity in these materials is 3-dimensional and the initial results suggest that this flexible series of salts will prove rewarding to further study[242]. In order to obtain information about the structural basis for fast-ion conduction in oxyacid salts and to probe the possible relationship between the high-temperature phases and the fluorite structure, we have studied some representative examples using diffraction techniques.

Sodium orthophosphate is tetragonal at room temperature with a = 10.81Å and c = 6.84Å[243], although no structural details have yet been reported and even the space group is not known with certainty. On heating, this low-temperature form,

* *We propose a common nomenclature for the compounds discussed here. The low-temperature phases are designated I-, the label II- referring to the high-temperature form. The designation which has been previously used in the literature occurs in parentheses after the formula at its first few incidences.*

I-Na_3PO_4 (α), undergoes a transition which is complete by 300°C to a phase, II-Na_3PO_4 (γ), which possesses face-centred cubic (FCC) symmetry[243]. The sodium ion conductivity in II-Na_3PO_4 (γ) is $5 \times 10^{-3}\Omega^{-1}cm^{-1}$ at 300°C[239]. The addition of small amounts of $AlPO_4$ to Na_3PO_4 apparently stabilises this FCC phases at room temperature[243] although conductivity measurements on $Na_{3(1-x)}Al_x\square_{2x}PO_4$, where $\square$ represents a vacancy, demonstrate that such additions do not enhance the cation mobility at 300°C[239]. At this temperature the variation of ionic conductivity with dopant level displays an unusual relationship. There is a sharp minimum at $x = 0.025$, with $\sigma \sim 10^{-4}\Omega^{-1}cm^{-1}$, a broad maximum at $x = 0.2$ ($\sigma \sim 3 \times 10^{-3}\Omega^{-1}cm^{-1}$) and the conductivity diminishes quite rapidly as x is increased above 0.3 (see Figure 6 in ref. 239).

The room temperature phase of silver orthophosphate, I-Ag_3PO_4, has been the subject of two recent papers. The first of these[244] confirmed the early analysis of Helmholz[245] in which the silver, phosphorus and oxygen atoms occupy the 6d, 2a and 8e special positions, respectively, in space group $P\bar{4}3n$. The second analysis[246] revealed that the silver ions are displaced slightly from $\frac{1}{4}$ 0 $\frac{1}{2}$ (6d) to x 0 $\frac{1}{2}$ (12h) sites with $x = 0.231(1)$. This static displacement had been considered by Helmholz[245] but he had obtained a more satisfactory agreement merely by allowing the silver ions to vibrate anisotropically about the 6d special positions. On heating, Ag_3PO_4 transforms reversibly at 520°C to a system which, like II-Na_3PO_4, has face-centred cubic symmetry[244]. The ionic conductivity of the high temperature phase is not known, but even in the low temperature form, I-Ag_3PO_4, appreciable cation mobility has been found[239].

We describe here a single crystal X-ray study of I-Ag_3PO_4 and powder neutron diffraction (PND) experiments on I-Ag_3PO_4 (at 375°C), I-Na_3PO_4 (25°C), II-Ag_3PO_4 (650°C), II-Na_3PO_4 (400°C) and the solid solutions $Na_{3(1-x)}Al_x\square_{2x}PO_4$ (25°C) at the two compositions x = 0.025 and x = 0.2.

7.2 Single Crystal X-ray Study of I-Ag_3PO_4

Ag_3PO_4 (BDH) was recrystallised from '0.880' ammonia to yield well-formed yellow cubes.

Crystal data: Ag_3PO_4: M = 418.6, cubic, $P\bar{4}3n$, a = 6.0095(6)Å, U = 217.0Å^3, D_c = 6.41gcm^{-3} for Z = 2. MoKα radiation, λ = 0.71069Å, μ = 132.5cm^{-1}.

After preliminary photography using Weissenberg and precession techniques, which revealed the systematic absences hh1C, l = 2n+1, a selected crystal (∿0.1mm cube) was mounted on an Enraf-Nonius CAD-4F diffractometer. The unit cell and orientation matrix were optimised by the least-squares refinement based on the coordinates of 25 reflections with 15° < θ < 24°. 1012 reflections in the range θ < 40° were then measured in bisecting geometry using ω-nθ scans (n = 1.67). Intensity and orientation checks were performed throughout data collection. Three absorption curves were collected as azimuthal scans on reflections with κ ∿135° (χ_E ∿ 90°)[32], but the small size and regular shape of the crystal resulted in an azimuthal absorption correction being unnecessary.

Lorentz and polarisation corrections were applied and the data merged to yield 116 independent structure amplitudes with $I > 3\sigma_I$ where σ_I is the standard deviation derived from the merging statistics. Initial atomic parameters were taken from Helmholz[245] and were refined by full-matrix least-squares

methods. A four term Chebyshev series was used for the weighting scheme in the later stages of refinement during which corrections for anomalous dispersion and secondary extinction were applied[6, 7]. The final R-factors obtained are presented in Table 7.1 and observed and calculated structure factors are listed in Appendix IV. Atomic scattering factors were taken from Cromer and Mann[8].

In Table 7.1 it is clear that the parameters derived for Model II are in good agreement with those of Ng *et al.*[246]. The improved fit obtained when the Ag^+ ions are displaced from the 6d to the 12h special positions is due partly to the increased number of parameters which may then be used to describe the positions and thermal motion of these ions. Hamilton's test[247] shows that the displacement is significant at the 99.5% level. Further, no substantial changes were observed in an oscillation exposure of a single crystal of Ag_3PO_4 taken at -70°C, suggesting that this disorder may persist to low temperatures. What then is the cause of this irregularity? When the 6d site is occupied, four Ag-O separations of 2.370Å occur. With displacement along the 2 [100] axis, the observed distances become 2.353Å and 2.392Å, there being two incidences of each (Figure 7.1), and the occur-

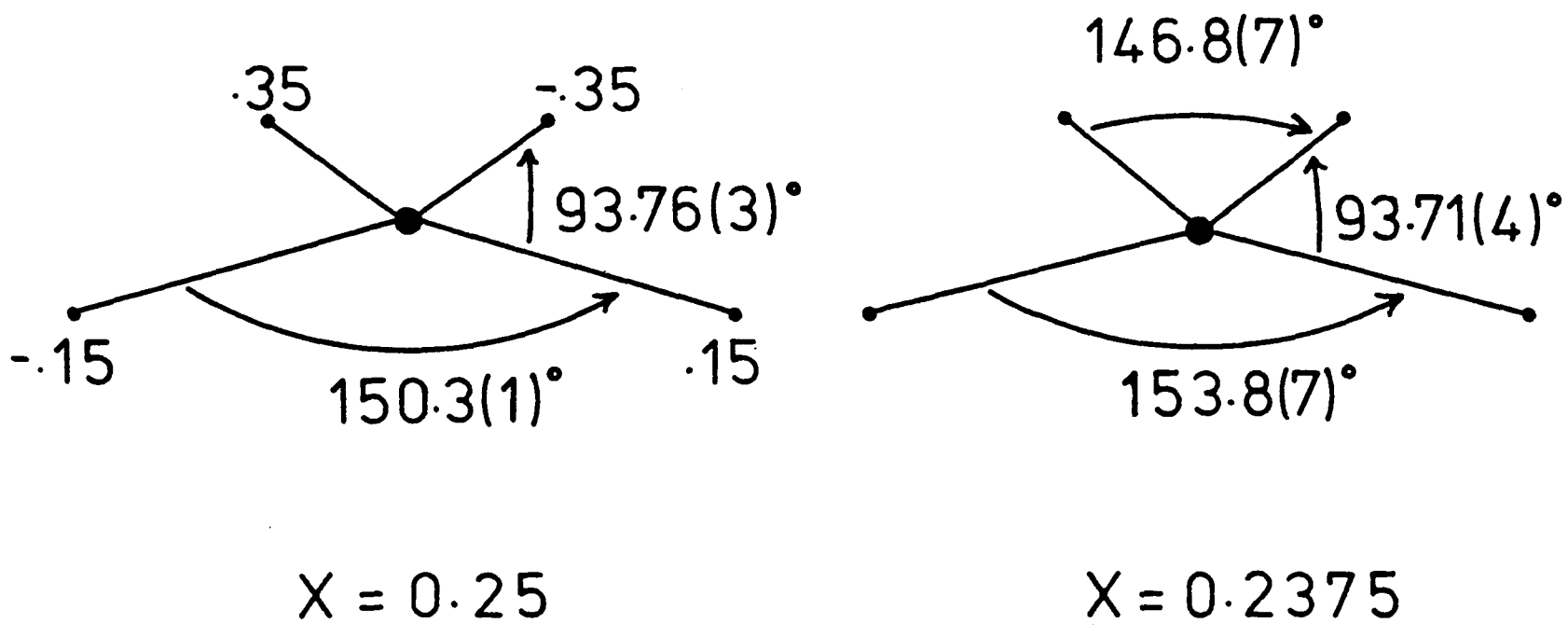


Figure 7.1. The coordination about silver in I-Ag_3PO_4 for the 6d ($\frac{1}{4}$ 0 $\frac{1}{2}$) and 12h (x 0 $\frac{1}{2}$) sites. The silver and oxygen atoms are represented by large and small circles respectively.

rence of the shorter contact is presumably responsible for the observed disorder. There are many instances where Ag^+ ions adopt two anomalously short contact distances to oxygen, as in, for example, silver beta alumina[71] in which such behaviour is rationalised in terms of a covalent interaction.

Model III, which is given in Table 7.1, derives from the appearance of the final difference Fourier (Figure 7.2). In addition to the 'diffraction ripples' around the main silver site, a small peak of similar height is noted at the 0 ¼ ½ (6c) position. On the assumption that this represents genuine occupation, a silver was entered on this site and its occupancy refined with the constraint that the total number of silvers per unit cell was 6.0. The derived occupancy for Ag(2) is small, although Hamilton's test[247] indicates significance at the 75% level. In the absence of Ag-Ag interactions, the 6d and 6c sites would be energetically equivalent, but, if a 6c site on a given face is occupied in an otherwise normal cell, the minimum Ag-Ag distance is 2.1Å. This is restrictively short and use of the 6c site would therefore require the existence of further local perturbations or a more extended domain model. In a normal crystal, a certain amount of imperfection is anticipated and the formation of Frenkel-type defects has been considered by several authors, e.g. Greenwood[248].

7.3 Powder neutron diffraction investigation of I-Ag_3PO_4 at 375°C

A 15mm diameter vanadium can was loaded with dry Ag_3PO_4 (BDH) and sealed with a gold O-ring. This sample was examined on the D2 diffractometer at the ILL, Grenoble. A mean wavelength of 1.2227(16)Å was selected from the (311) planes of a Ge mono-

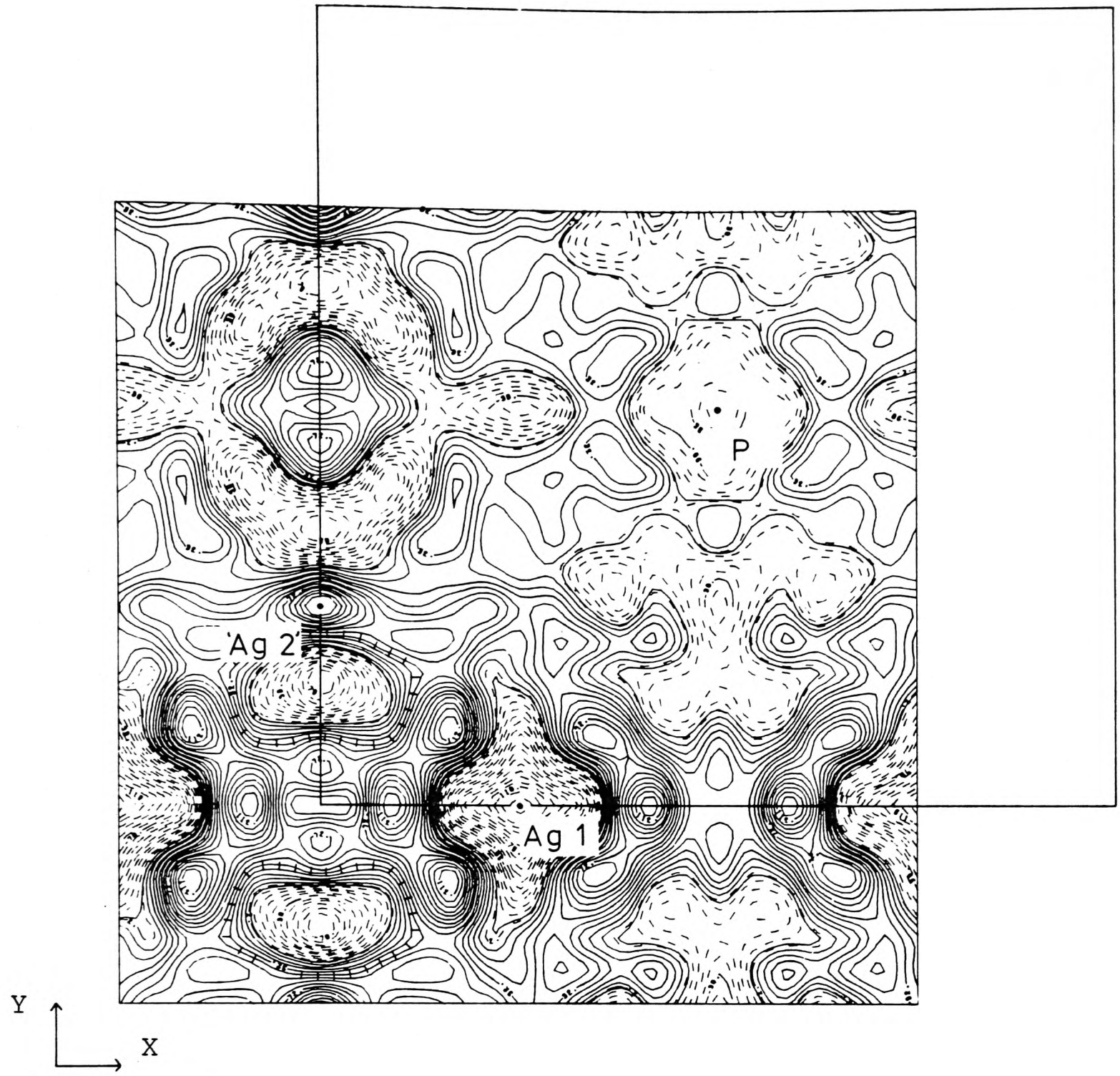


Figure 7.2. The z = 1/4 section of a difference Fourier synthesis calculated on the basis of Model II (Table 7.1). The outline of the unit cell edge is shown as a solid line. The major silver (Ag1) and phosphorus (P) positions are indicated. Some additional positive density is apparent at the 0 1/4 1/2 (6c) site.

chromator and accurately calibrated by the profile refinement[18] of 3 peaks recorded from a standard nickel powder sample. The diffraction profile in the range $2° \leqslant 2\theta \leqslant 75°$ was first recorded at 700°C over a period of 12 hours, the sample being contained in an evacuable furnace with a molybdenum element. This scan showed the same features as that recorded on PANDA (section 7.5) but with an increased background resulting from

diffuse scattering. These data were not used for refinement because of difficulties in correctly determining an integrated intensity for each reflection.

The sample had been at a temperature of 700°C in a beam of incident flux ∿5 x 10^{7}n.$cm^{-2}s^{-1}$ for approximately 20 hours. The temperature was then lowered, below the transition point, to 375°C. When short scans over the low-angle region had indicated that reconversion to I-Ag_3PO_4 was complete, the diffraction profile in the range $0° < 2\theta < 85°$ was measured. The pattern was sampled at intervals of 0.1° with a counting time of ∿25 secs per point and the data from the three operational counters were collated with correct allowance for their relative separations and efficiencies[228]. The room temperature structure was used as an initial model in the least-squares profile-fitting refinements[18] which were carried out on the DEC-10 system at UMIST[28]. The lattice constant derived in these refinements was a = 6.061(1)Å.

Separate isotropic temperature factors were employed, but after convergence to R_{WP}= 0.1266, some considerable disparities were still found in the (y_{obs} - y_{calc}) difference plot. Firstly, some reflections such as the 421 were poorly fitted and so anisotropic thermal components were introduced for silver. Secondly, although no extraneous reflections are apparent in the data recorded on PANDA at 650°C (Figure 7.6 in section 7.5) other than those from the furnace element, there were four peaks significantly above background which could not be ascribed to I-Ag_3PO_4. Two of these were indexed as silver metal (Ag_m). On heating Ag_3PO_4 to above the transition temperature, some decomposition can occur and silver may be observed as dendrites or globules within the sample[229,239]. When both the D2 and PANDA

(section 7.5) samples were examined at the completion of the runs, the insides of the vanadium cans were plated with Ag_m. The remaining bulk had darkened somewhat and it also appeared to have sintered. Several X-ray Guinier exposures of the D2 sample were taken in an attempt to identify any other decomposition products. Faint extra lines were discernible, all of which could be indexed as deriving from silver pyrophosphate, $Ag_4P_2O_7$ [249]. In the measured PND profile, there are only two areas, at 2θ $\sim$20.5° and $\sim$25.3° respectively, in which such reflections are noted and in refinement those regions to which impurity or furnace reflections contributed significant intensity were excluded from the calculations (a total of 5.9° in 2θ). The 110 reflection of I-Ag_3PO_4 was also omitted because of the peak asymmetry at low angles. The final atomic parameters, which gave R_P = 0.1070, R_{WP} = 0.0958, are presented in Table 7.2, the final observed and calculated profiles are shown in Figure 7.3 and a list of reflection intensities appears in Appendix IV.

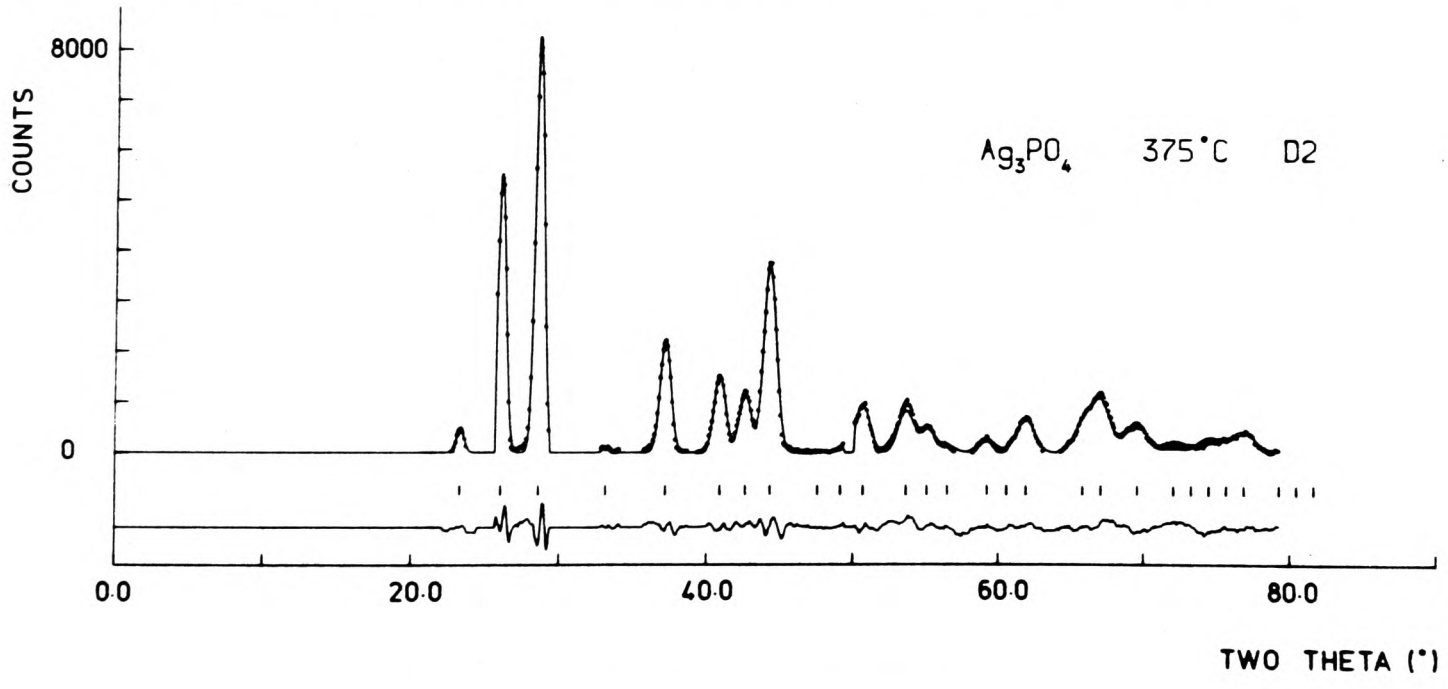


Figure 7.3. The final observed (dots), calculated (continuous line) and difference (lower) PND profiles for I-Ag_3PO_4 at 375°C (D2 diffractometer).

Our analysis reveals that in I-Ag_3PO_4 at 375°C, the extent of the displacement of silver from the 6d site is increased

relative to that at 25°C and the corresponding thermal components are still indicative of pronouncedly anisotropic vibration. The shortest Ag-O contact is now reduced to 2.341Å and this reduction is in accord with the observation that the colour of Ag_3PO_4 deepens from a yellow noted at 25°C to a dark orange as the temperature is raised[250].

7.4 Powder neutron diffraction experiment on I-Na_3PO_4 at 25°C

Sodium orthophosphate occurs in several hydrated forms[251] which undergo complete loss of water of crystallisation below 300°C. Several different methods including flux growth[252] vapour transport and use of non-aqueous solvents, were considered in an attempt to prepare single crystals suitable for X-ray structure analysis. The former two techniques are restricted by the existence of the high-temperature phase and the latter was limited by problems of solubility. Anhydrous Na_3PO_4 is, however, soluble in glacial acetic acid, but crystallisation from this medium affords only well-formed plates of NaH_2PO_4 which derives from proton exchange. Because single crystals of I-Na_3PO_4 (α) could not be obtained, an attempt was made to elucidate the structure by PND techniques.

$Na_3PO_4.xH_2O$ ($x \sim 10$) was dried at 900°C *in vacuo* for 48 hours and loaded under dry N_2 into a 15mm diameter vanadium can which was sealed with a gold O-ring. The PND pattern was recorded on the PANDA diffractometer using a mean wavelength of 1.5456Å taken from the (511) planes of a Ge monochromator. The scan range was sectioned at intervals of 0.1° in 2θ and the data from the three equatorial counters were merged to give the complete profile in the range $14° \leqslant 2\theta \leqslant 114°$ (Figure 7.4). The

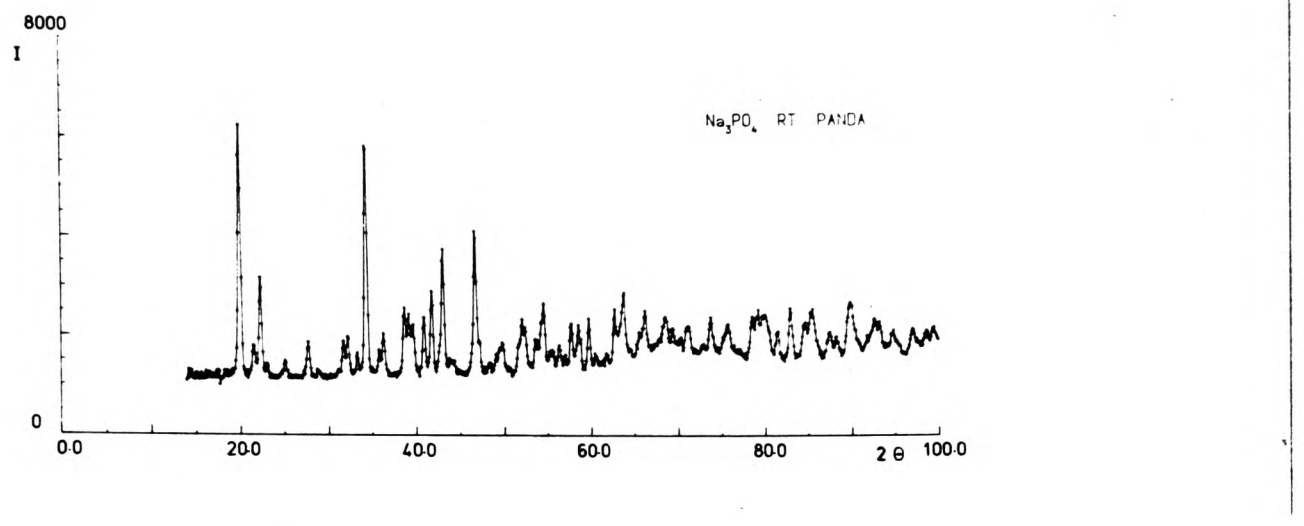


Figure 7.4. The observed PND profile for I-Na_3PO_4 measured at 25°C on the PANDA diffractometer (λ = 1.546Å).

complete profile, save for one small peak at 2θ = 24.1°, is satisfactorily indexed on the basis of a tetragonal unit cell with a = 10.774Å and c = 6.816Å. The cell volume implies a content of 8 formula units for D_c = 2.73gcm^{-3}.

Because of overlap, the systematic absences cannot be defined unambiguously, but the only possible conditions are $hh\ell, \ell$ = 2n; 0 0 ℓ, ℓ = 2n, 4n; h 0 0, h = 2n. A large number of space groups are therefore possible and we attempted to limit the choice by consideration of site-symmetries, interatomic contact distances and the relationship of the tetragonal unit cell to that of II-Na_3PO_4 (γ) (section 7.5). The length of the c-axis imposes severe restrictions on the possible orientations of the PO_4^{3-} groups if they are separated only by ½c, the shortest O-O contact being $\leqslant$2.4Å. Secondly, a simple relationship between low- and high-temperature phases is apparent in the distribution of phosphorus shown in Figure 7.5. In this arrangement, there is no c-glide perpendicular to $(1\bar{1}0)$ and the space group of highest symmetry to which the above considerations then lead is $P\bar{4}2_1m$. An extensive series of models based on this space group was tested in least-squares profile refinements, but, although some encouraging residuals were obtained, we have not

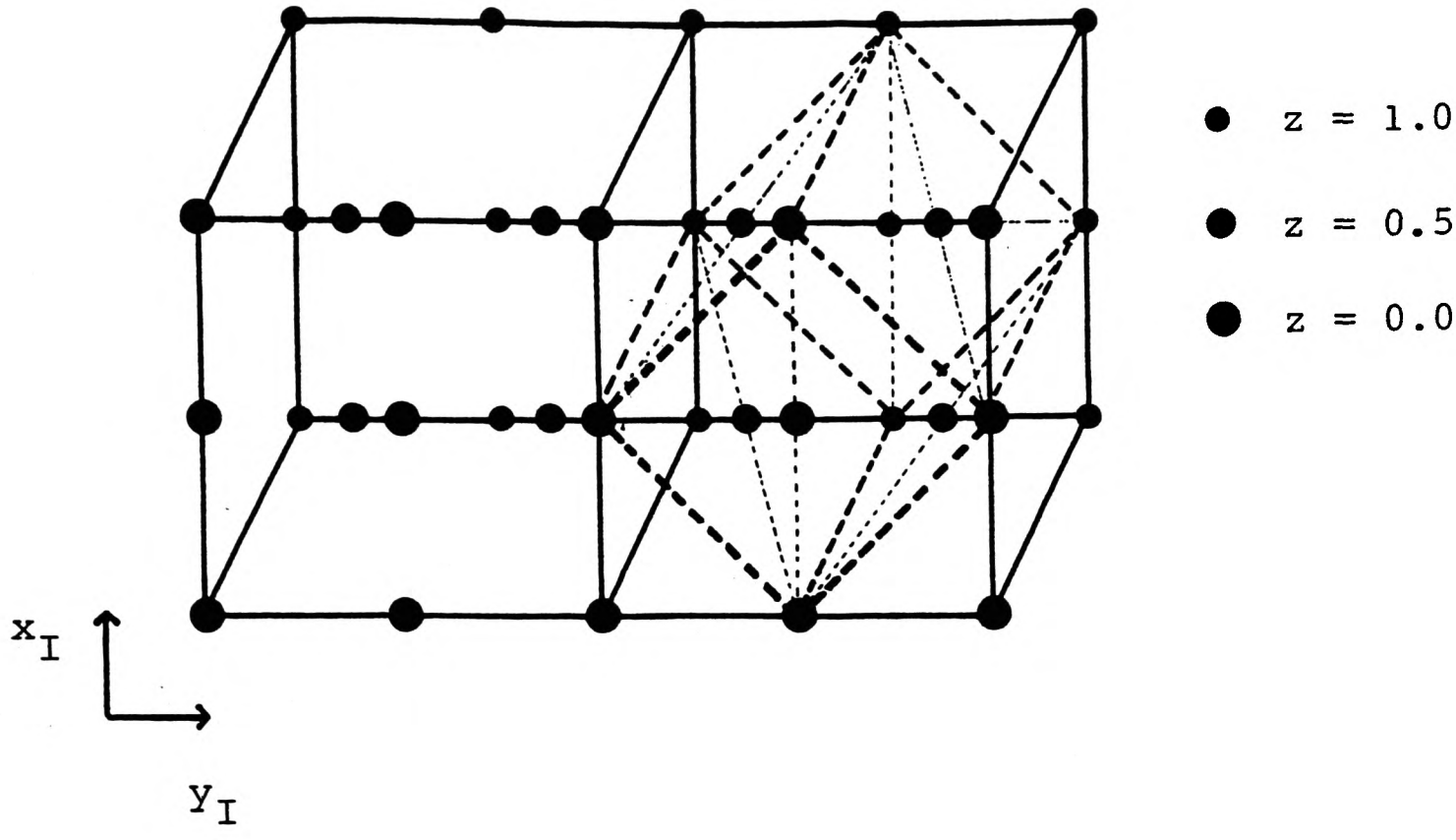


Figure 7.5. A possible relationship between the low- and high-temperature modifications of Na_3PO_4. The filled circles indicate phosphorus atoms, the dashed line indicates the FCC unit cell of II-Na_3PO_4 and the solid outline represents the tetragonal cell of I-Na_3PO_4.

been able to deduce an adequate model for this structure. The unit cell contains 64 atoms and, for profile refinement to be feasible, the majority of these must be defined initially with reasonable accuracy. In conjunction with the space-group ambiguity, therefore, the problem posed by this structure is considerable and it is unlikely to be solved from PND data alone.

7.5 Powder neutron diffraction studies of II-Na_3PO_4 (400°C) and II-Ag_3PO_4 (650°C).

Ag_3PO_4 (BDH) was dried at 250°C for 24 hours before being mounted, under dry conditions, into a 12mm diameter vanadium can. $Na_3PO_4.xH_2O$, x $\sim$10, (HBL Research Reagent) was dehydrated under vacuum at 1000°C for 48 hours (thermogravimetric analysis reveals complete loss of water of crystallisation by 300°C). Under dry

N_2 gas, the sample was then ground to a fine powder and loaded into a 15mm diameter vanadium can. Both sample cans were sealed with gold O-rings to prevent the entry of moisture. The $Na_3PO_4.xH_2O$ probably contained some NaOH impurity[251], but at the temperature of the PND experiment the only peaks significantly above background are those from II-Na_3PO_4 or those due to the tantalum furnace element (see Figure 7.6).

The neutron powder diffraction profiles were measured on the PANDA diffractometer at A.E.R.E. Harwell. A mean wavelength of 1.2562(3)Å was selected from the (511) planes of a Ge monochromator with a take-off angle of ∿70° and calibrated by the profile-refinement[18] of the diffraction pattern of the Ag_3PO_4 sample recorded at room temperature, after the run at 650°C, assuming a = 6.0095Å.

The sample cans were mounted and centred in an evacuable furnace with a tantalum element. The sample temperature was held at 400°C (Na_3PO_4) and 650°C (Ag_3PO_4) for the duration of the runs. The chosen range of 2θ was sampled at intervals of 0.1° with a counting time of ∿250 secs per point and the data from the central three counters were collated to yield the complete profiles in the range $12° < 2\theta < 82°$ (Na_3PO_4) and $12° < 2\theta < 66°$ (Ag_3PO_4). These are displayed in Figure 7.6.

The positions of the observed reflections indicated the symmetry of both systems to be face-centred cubic. When approximately correct structural models had been obtained, the lattice parameters were refined by the Rietveld least-squares profile-fitting routines[18] to give a = 7.512(3)Å for II-Na_3PO_4 and a = 7.722(5)Å for II-Ag_3PO_4. The observed reflections are all well resolved (Figure 7.6) so that an integrated intensity could be determined for each reflection. The observed counts minus an

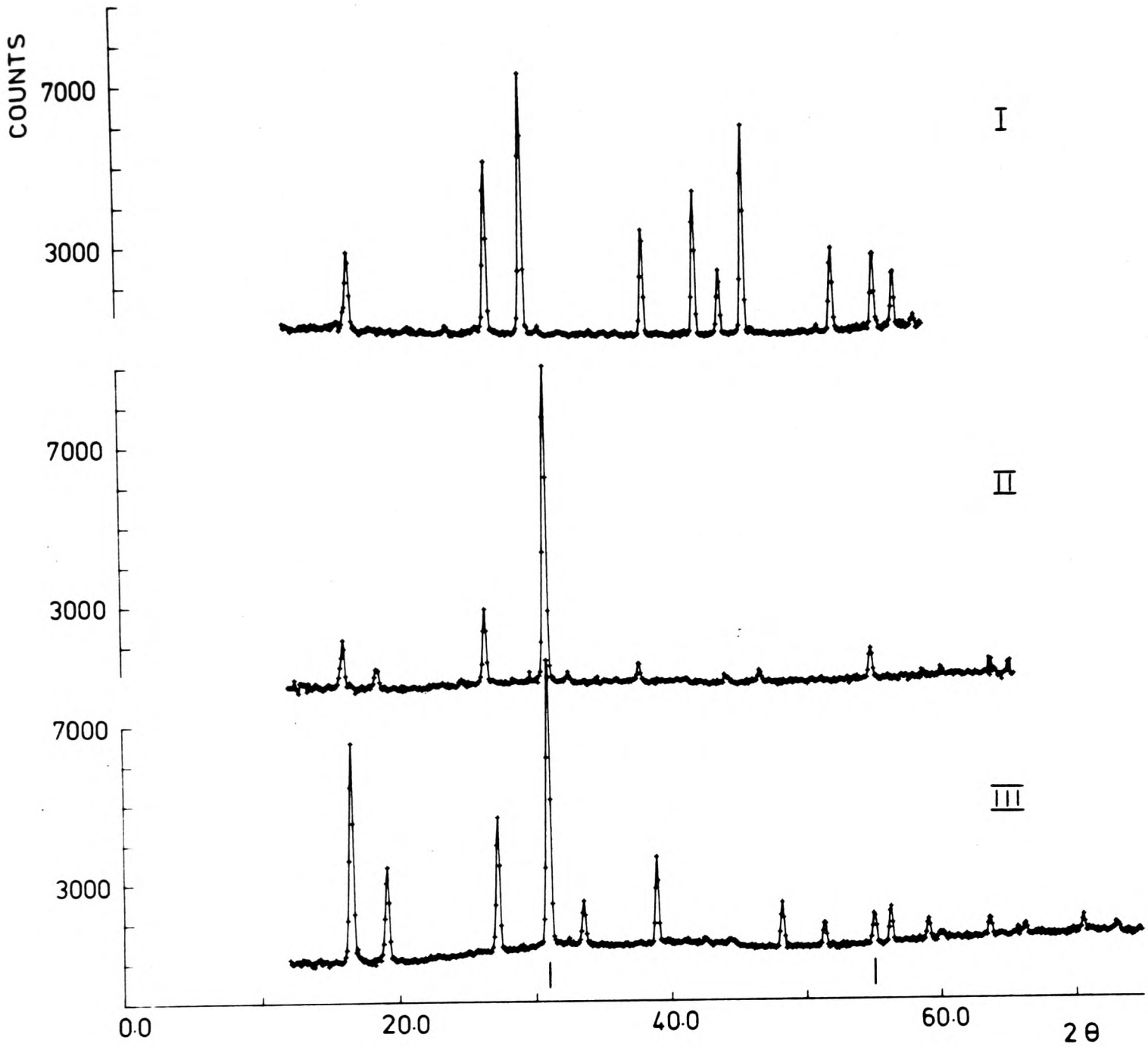


Figure 7.6. The observed PND profiles for I-Ag_3PO_4 at 25°C (Top, I), II-Ag_3PO_4 at 650°C (middle, II) and II-Na_3PO_4 (lower, III), measured on the PANDA diffractometer (λ = 1.256Å). The positions of reflections from the tantalum element of the furnace are marked as bars.

estimated background were summed over the full peak range. The standard deviation was then calculated as $(I+2B)^{\frac{1}{2}}.(4-n)^{\frac{1}{2}}$ where I is the net intensity, B the total estimated background over the peak range and n the number of counters by which the reflection was recorded. The various structural models were then evaluated using the integrated-intensity least-squares refinement program of Wiseman[16].

For the high-temperature phases of both Ag_3PO_4 and Na_3PO_4, there is a rapid diminution in diffracted intensity with $\sin\theta/\lambda$. This is indicative of high thermal motion and/or

static disorder. No systematic absences other than those due to the face-centring condition are apparent (Figure 7.6) and there are thus five possible space groups (F23, F$\bar{4}$3m, F432, Fm3 and Fm3m). Results from similar systems[253] suggest that the PO_4^{3-} groups will be subject to extensive rotational disorder. With disorder of this type, a distinction between the possible space groups is difficult to make and is generally of limited significance. For all of the above space groups, the models for disordered oxygen positions are similar and we thus assumed the group of highest symmetry, Fm3m.

If the PO_4^{3-} groups were rotating more or less freely, the elastic scattering from the oxygens could be described in terms of a spherical form-factor of the type $4b_o(\sin\kappa r/r)$ where κ is $4\pi\sin\theta/\lambda$ and r is the assumed P-O bond length. This is an oscillatory function which has been used successfully in the refinement of the structure of NH_4ClO_4 at room temperature,[254] in refinements of some magnetic structures in which covalency effects imply some distribution of spin-density about the central metal ion[255] and, recently, in refinement of the FCC phase of Li_2SO_4 (α) at 600°C[256]. In the cases of II-Na_3PO_4 and II-Ag_3PO_4, however, we did not obtain reasonable agreement between observed and calculated intensities using a form-factor of this type.

For Na_3PO_4 in Fm3m with Z = 4, a plausible starting model consists of the sodium ions occupying the $\frac{1}{4}\frac{1}{4}\frac{1}{4}$ (8c) and $\frac{1}{2}\frac{1}{2}\frac{1}{2}$ (4b) sites, with oxygen located tetrahedrally about phosphorus at the origin, 000 (4a). This arrangement was considered for O positioned along all of the high-symmetry directions (x00, 0xx, etc.) assuming a P-O separation of 1.55Å. Only for xxx (32f) are regular tetrahedra generated so that the other sites require

further oxygen positions to complete the coordination. None of these models gave a satisfactory agreement between observed and calculated intensities although the x00 (24e) position proved to be the best in this respect. We then considered an extensive series of more-disordered schemes. Reasonable agreements were only obtained with a model containing two oxygens of equal occupancies but whose refined coordinates always gave slightly different 'bond lengths' to the origin.

The first of these oxygens is at 0yz (96j) lying close to the <001> direction, but at ca. 1.65Å from the origin. The second is at the general position xyz (192ℓ) with a separation from the origin of ca. 1.45Å. This arrangement was originally considered suspect, but it was the only model which gave reasonable residuals and it was validated in two ways. Firstly, the refinements were repeated in space group F23. Similar residuals were obtained. Secondly, some reflections were omitted from refinement on the anticipation that if the paucity of data were responsible for the derivation of an artificial model, a reduction in the number of observations would allow this model to relax still further. When re-included, the excluded reflections might then show considerable disparities between their observed and calculated intensities. Such was not the case, and the calculated intensities for those reflections ignored in the refinement of atomic parameters were in good agreement with the observed values. This arrangement can be rationalised in terms of regular tetrahedra which are not centred at the origin, but rather whose centroids lie at the 0yz (96j) position with $y \sim 0.018$ and $z \sim 0.020$ (see Figure 7.12, section 7.6). Such a displacement for phosphorus was therefore included in the model, although the magnitude of the shift from the origin is small and so these

coordinates were not refined. For the final atomic parameters presented in Table 7.3 , the P-O bond lengths are 1.54, 1.53, 1.55 and 1.56Å. The tetrahedra are nearly regular, allowing for the errors on the atomic coordinates.

Apart from the consistency with which this model for oxygen was obtained in refinement of this data set, we have two ways of corroborating our results. Firstly, there are the data from II-Ag_3PO_4 at 650°C. The higher temperature at which these data were collected is responsible for an even sharper tail-off in Bragg intensity with $\sin\theta/\lambda$ (Figure 7.6) so that the number of observations which can be used in refinement is severely restricted. However, a similar series of models was tested in least-squares. The best agreements were obtained with models similar to that derived for II-Na_3PO_4. For II-Ag_3PO_4, however, the disparity between the 'bond lengths' from the two oxygens to the origin was slightly greater, ca. 1.68Å and 1.35Å respectively, indicating slightly larger displacement for phosphorus. Secondly, our results from structure analysis of the solid solution $Na_{2.925}Al_{0.025}PO_4$ at 25°C (section 7.6) are entirely consistent with those derived for II-Na_3PO_4 at 400°C so that we have strong evidence for the validity of our model.

We have thus shown that the PO_4^{3-} groups in II-Na_3PO_4 and II-Ag_3PO_4 are highly rotationally disordered, but apparently not rotating, and that they are, in addition, subject to slight displacements from the origin. One further interesting feature of our analysis of II-Na_3PO_4 was apparent. Whereas the sodium ion on the $\frac{1}{4}\frac{1}{4}\frac{1}{4}$ (8c) site had a Debye-Waller factor of the same order as those of the oxygens, that of the $\frac{1}{2}\frac{1}{2}\frac{1}{2}$ (4a) was considerably higher. This behaviour was apparent in all of the refinements which gave acceptable residuals. We may note that

in anion-excess fluorite systems, the 4a interstitial site is not normally populated[257,258]. The excess fluoride ions occupy sites which are displaced from this position in the <110> or <111> directions. We were therefore not surprised to find evidence for similar behaviour in the systems considered here, particularly in the light of the preferred orientations of the PO_4^{3-} function which result in short Na-O contact distances (Table 7.3). Displacements of Na(2) along the <100>, <110> and <111> directions were considered in least-squares refinements. Of these three, the <110> sense gave the best agreements, although the displacement is poorly defined and with the limited quantity of observed data we cannot accurately distinguish between the xx½ (48i) and xxx (32f) sites, or a combination of the two. For these reasons, we present the final derived parameters for two models in Table 7.3. The first (I) involves the xx½ (48i) sites in which x was allowed to vary but the temperature factors of the two sodium ions were equivalenced. Model II has Na(2) on the ½½½ (4a) site and the sodium Debye-Waller factors were considered independently. The extent of the <110> displacement is sufficient to allow Na(2)-O contacts of <2.2Å to be avoided for any given PO_4^{3-} orientation. The minimum Na(1)-O(1) contact is also short at 2.1Å although only 1/4 of the Na(1) species are thus involved for any PO_4^{3-} orientation and slight displacements of these atoms are probably accounted for by the magnitude of the B-factors. Table 7.5 contains the atomic parameters which were derived for II-Ag_3PO_4. Because of the severe limitations in the quantity of observed data, similar displacements for Ag(2) could not be considered, although, even when allowed to vary independently, the thermal parameters for both silvers were of similar magnitude. The

largerlattice constant for II-Ag_3PO_4 implies an increase in Ag-O separation for a distribution similar to that in II-Na_3PO_4. Tables 7.4 and 7.6 contain the final observed and calculated reflection intensities for II-Na_3PO_4 and II-Ag_3PO_4 respectively.

Figure 7.7 displays projections down the <001> axis of four unit cells of the I-Ag_3PO_4 structure. When drawn in this way, the relationship between the low (I) and high temperature forms (II) is apparent. The II-Ag_3PO_4 modification is derived from I-Ag_3PO_4 by a slight contraction (8.5 → 7.7Å) along two face-diagonals (marked as heavy dashed lines in Figure 7.7), with a net expansion along the perpendicular 001 axis (6.0 → 7.7Å). In this way, each PO_4^{3-} group is subject to only a slight translational movement. The silver ions fall into two groups. The first (e.g. $0\frac{1}{2}\frac{1}{4}$) occupy sites which are already close to those of the high temperature phase, whereas for the second (e.g. $\frac{1}{4}0\frac{1}{2}$) more extended displacements are required, although conductivity measurements have demonstrated that the I-Ag_3PO_4 phase supports appreciable cation mobility[239]. The driving force for the I → II transition is then presumably the effect of the enhanced libration of the PO_4^{3-} function as the temperature is raised.

Does our analysis provide any information about the chemical behaviour of this system? We have already mentioned a relationship with the fluorite structure. Indeed, both II-Na_3PO_4 and II-Ag_3PO_4 may be regarded as <u>cation</u>-excess anti-fluorites, XM_{2+n} with n = 1. In II-Na_3PO_4, we may reduce n by doping with Al^{3+} (section 7.6). For II-Ag_3PO_4 there is a different possibility deriving from the presence of attainable higher valencies Ag^{2+} (d^9) and Ag^{3+} (d^8) and to reduce the level of 'cation-excess' in Ag_3PO_4 we would need to effect the disproportionation:

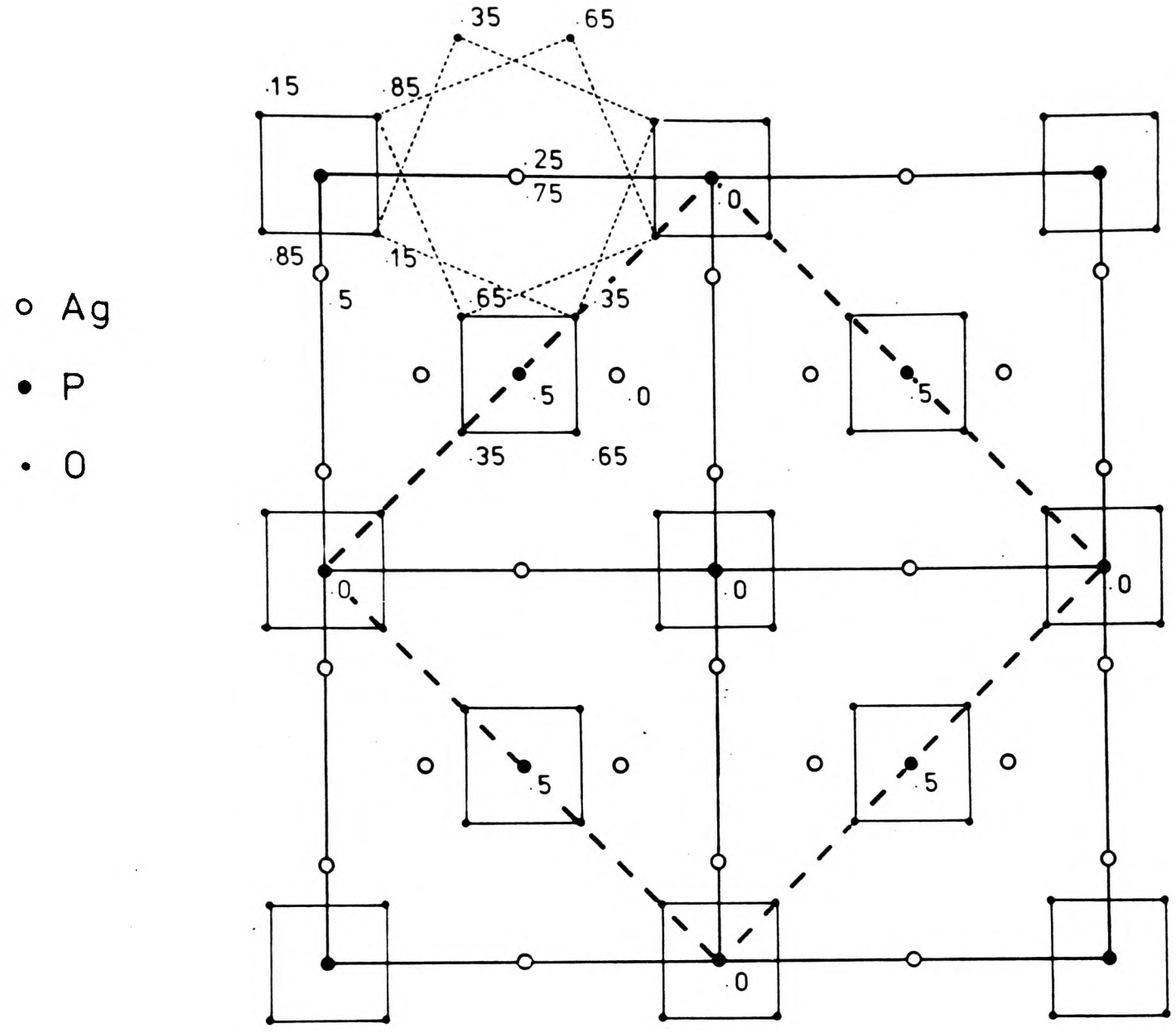


Figure 7.7. The projection of four unit cells of I-Ag_3PO_4 (solid lines) down <001>. The faint solid and dashed lines indicate the tetrahedra about P and Ag respectively and the z-coordinates of selected atoms are marked. The heavy dashed lines indicate the <001> projection of the FCC cell of II-Ag_3PO_4. (After Masse et al.[244].)

$$3Ag^{+} \longrightarrow 2Ag + Ag^{3+}$$

which implies the liberation of silver metal. This is, of course, consistent with our observations, but at this stage we cannot ascribe the formation of silver metal solely to this reaction and we have shown that other decomposition products occur.

The occurrence of a rotationally disordered PO_4^{3-} group implies that the energy separation between different orientations will be slight, although we have seen that in these systems, at least, there is good evidence that the groups are not rotating

freely. This property then enables the PO_4^{3-} function to act as a large polarisable anion, perhaps similar to I^- in AgI. A reasonable mechanism for conduction would then involve a cooperative process in which motion of the cations is accompanied by slight reorientations of PO_4^{3-} as has been suggested for the similar FCC phase of Li_2SO_4 (α)[259,260], although there is a notable distinction between these materials in that the 4a 'interstitial' site is completely vacant in Li_2SO_4 (α)[260].

7.6 Powder neutron diffraction measurements on the solid solutions $Na_{3(1-x)}\square_{x}\square_{2x}PO_4$

a) Experimental

Two preparative methods were examined. In the first, $Na_3PO_4.xH_2O$, x = 9-12 (HBL Research Reagent) was dehydrated *in vacuo* at 1000°C for 24 hours and ground with the correct proportions of dried $AlPO_4$ (BDH) for the compositions x = 0.1, 0.2, 0.3 and 0.5. The mixtures were fired in air at 1000°C for 36 hours, reground and heated again at 1000°C. In the second, $Na_2CO_3.10H_2O$ (BDH) and Al_2CO_3 (BDH) were used as starting materials. They were dried in air at 400°C for 48 hours and finely ground with $NH_4H_2PO_4$ (BDH 'Analar') in the correct ratios for the compositions x = 0.025, 0.2, 0.4 and 0.58. The mixtures were fired in air at 900°C for 24 hours, cooled, reground, submitted to a second firing at 1000°C over 48 hours and finally allowed to cool to *ca*. 150°C in the switched-off furnace before being stored in a dessicator. This method of preparation was repeated for each of the above compositions. The products were characterised by Guinier X-ray powder diffraction and by microprobe X-ray analysis using a JEOL TEMSCAN 100-CX electron micro-

scope. The samples for the PND measurements were taken from the second preparative route because the $Na_3PO_4.xH_2O$ substrate employed in the first undoubtedly contained some NaOH impurity (< 3%)[251].

At the higher concentrations of $AlPO_4$, our preparations resulted in the formation of a glass with only broadly diffuse maxima in the diffraction pattern. For x = 0.4, the products displayed a limited amount of crystallinity, but of insufficient magnitude for viable PND experiments. At the lower concentrations, the Guinier exposures contained several impurity lines which did not correspond to any of the starting materials nor to the phases I-Na_3PO_4 (α) or $Na_3PO_4.xNaOH.(12-x)H_2O$ for which powder X-ray data are available. The same lines were apparent in exposures taken of dehydrated '$Na_3PO_4.xH_2O$' (HBL) and they therefore probably arise from a hydrated form of Na_3PO_4 which results from the uptake of atmospheric moisture during the preparation and exposure of the Guinier sample. Unfortunately, no crystallographic data for $Na_3PO_4.\frac{1}{2}H_2O$, $Na_3PO_4.6H_2O$ or $Na_3PO_4.8H_2O$[251] has been reported so that we are unable to check this directly. However, the PND samples were largely protected from atmospheric moisture and the only peaks significantly above background in the measured profiles are those of the II-Na_3PO_4 phase (Figure 7.8). In the X-ray microprobe analyses, some variation in aluminium concentration from one crystallite to another was noted, but, on the whole, the homogeneity was reasonable. Sodium analysis was limited in accuracy by a tendency for sodium to be lost from the crystallites under the influence of the electron beam so that the corresponding Kα X-ray count rate decreased substantially over the time taken to record a spectrum. This behaviour, which is similar to that

observed in silver beta alumina[128], silver orthophosphate[229] and sodium beta" alumina[51], presumably reflects the mobility of the sodium ions.

Two samples of $Na_{3(1-x)}Al_x\square_{2x}PO_4$ corresponding to the compositions x = 0.025 and x = 0.2 were loaded, under dry N_2, into 15mm vanadium cans which were sealed with gold O-rings. The PND profiles were measured on the D2 diffractometer at the ILL, Grenoble. A mean wavelength of 1.2227(16)Å was taken from the (311) planes of a Ge monochromator and accurately calibrated by the least-squares profile refinement of three peaks recorded from a standard Ni sample, assuming a_o = 3.5238Å[261]. The range 8° < 2θ < 75° was covered by the highest-angle detector, with counts being recorded for ∿22 secs (x = 0.2) and ∿25 secs (x = 0.025) at intervals of 0.1° in 2θ and the data from the three operational counters were then collated[228]. The diffraction pattern of a sample of anhydrous undoped Na_3PO_4 was also measured, at 400°C in an evacuable furnace with a molybdenum element, under the same instrumental conditions. The three resulting observed profiles are displayed in Figure 7.8. In all three runs the background is high and undulating. The variation in background level with (sinθ/λ) does not resemble that produced by the incoherent scattering from hydrogen and it presumably therefore arises either from thermal or defect diffuse scattering. The former will be limited at room temperature, but may contribute significant intensity at 400°C.

At a later date the two aluminium-containing samples were subjected to further heat treatment more conducive to annealing processes. The samples were heated at 800°C (24 hrs), 1000°C (24hrs), 500°C (24hrs), 200°C (12 hrs) and then allowed to cool slowly to 25°C before being stored in a desiccator. The subse-

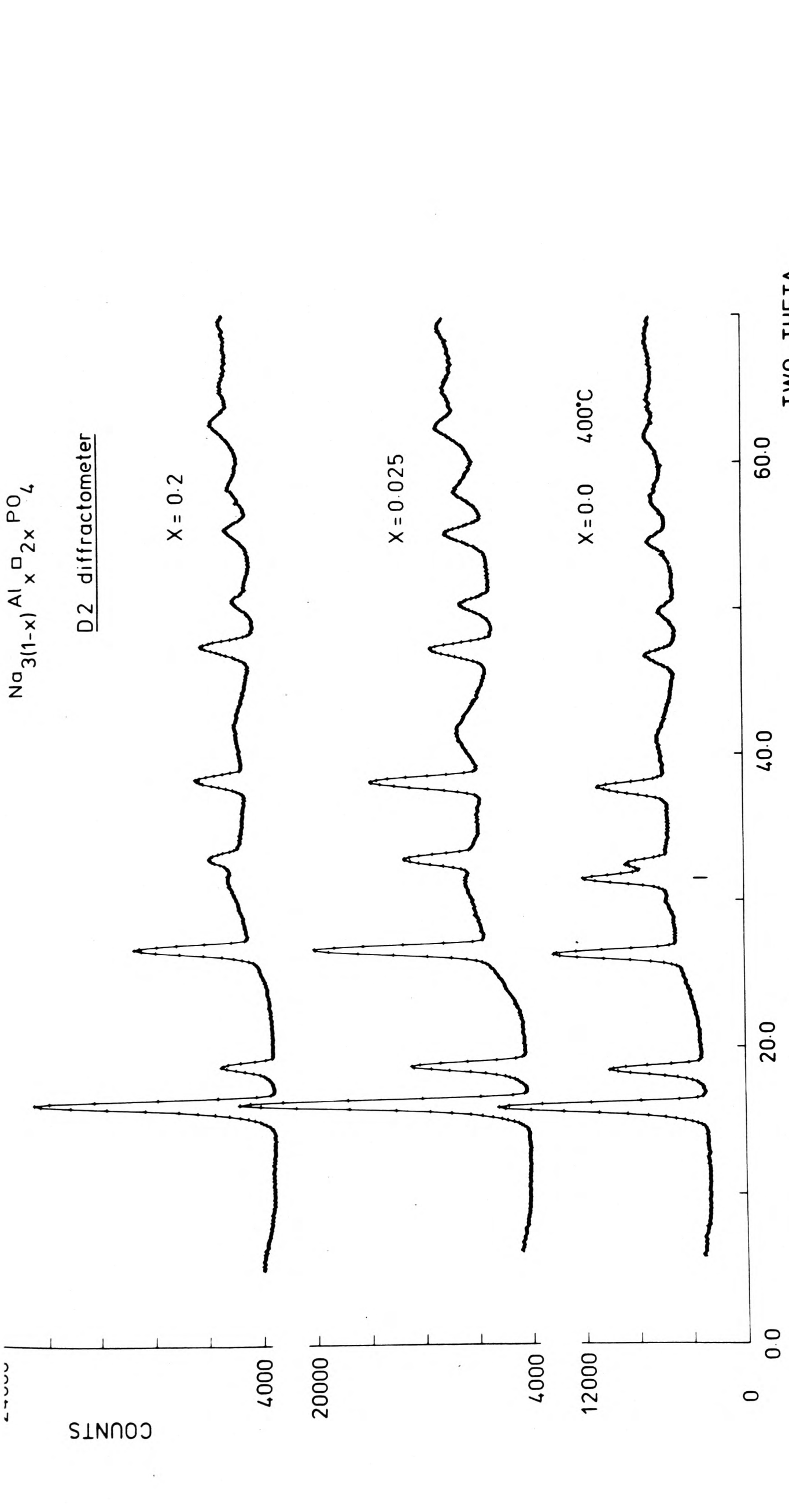


Figure 7.8. The observed powder neutron diffraction profiles for the solid solutions $Na_{3(1-x)}Al_x\square_{2x}PO_4$ at the three compositions x = 0.0 (400°C), x = 0.025 (25°C) and x = 0.2 (25°C) (D2 diffractometer). The position of the 111 reflection from the molybdenum element of the furnace, used for the run on Na_3PO_4 at 400°C, is marked with a bar.

quent PND profiles, which were measured at 25°C on the D2 diffractometer with λ = 1.2213Å, with similar counting times to the above, are displayed in Figure 7.9. For x = 0.025, the further heat treatment has enabled phase segregation to occur, and both I-Na_3PO_4 and II-Na_3PO_4 reflections are now discernible. For x = 0.2, this segregation is more limited and the background still manifests the signs of considerable diffuse scattering. Further analyses of these second data sets will be possible when the structure of the low-temperature phase, I-Na_3PO_4, has been elucidated.

For the earlier data collected from the doped materials, a space group symmetry of Fm3m was assumed and an initial model corresponding to the structure of II-Na_3PO_4 at 400°C was employed in the least-squares profile refinements[18,27,28].

b) Results for the composition $Na_{2.925}Al_{0.025}PO_4$

At this composition the model derived for II-Na_3PO_4 gave a good agreement between observed and calculated profile intensities when only the scale factor had been adjusted. Subsequent refinements then involved the unit-cell and half-width constants, counter zero-point, and the atomic parameters. The temperature factors of all atoms attained lower values than those found for II-Na_3PO_4 at 400°C, although the oxygen coordinates shifted only slightly. In common with the analysis of the undoped material at 400°C, a disparity between the two sodium sites was apparent. The Debye-Waller factor for sodium on the 4b site, B = 8(1)Å^2, was considerably greater than that at the 8c position, B = 3.4Å^2. The analysis of the composition x = 0.2 (section 7.6(c)) revealed that the vacancies created by the incorporation of Al^{3+} ions were concentrated on the 4b site. The occupancy of

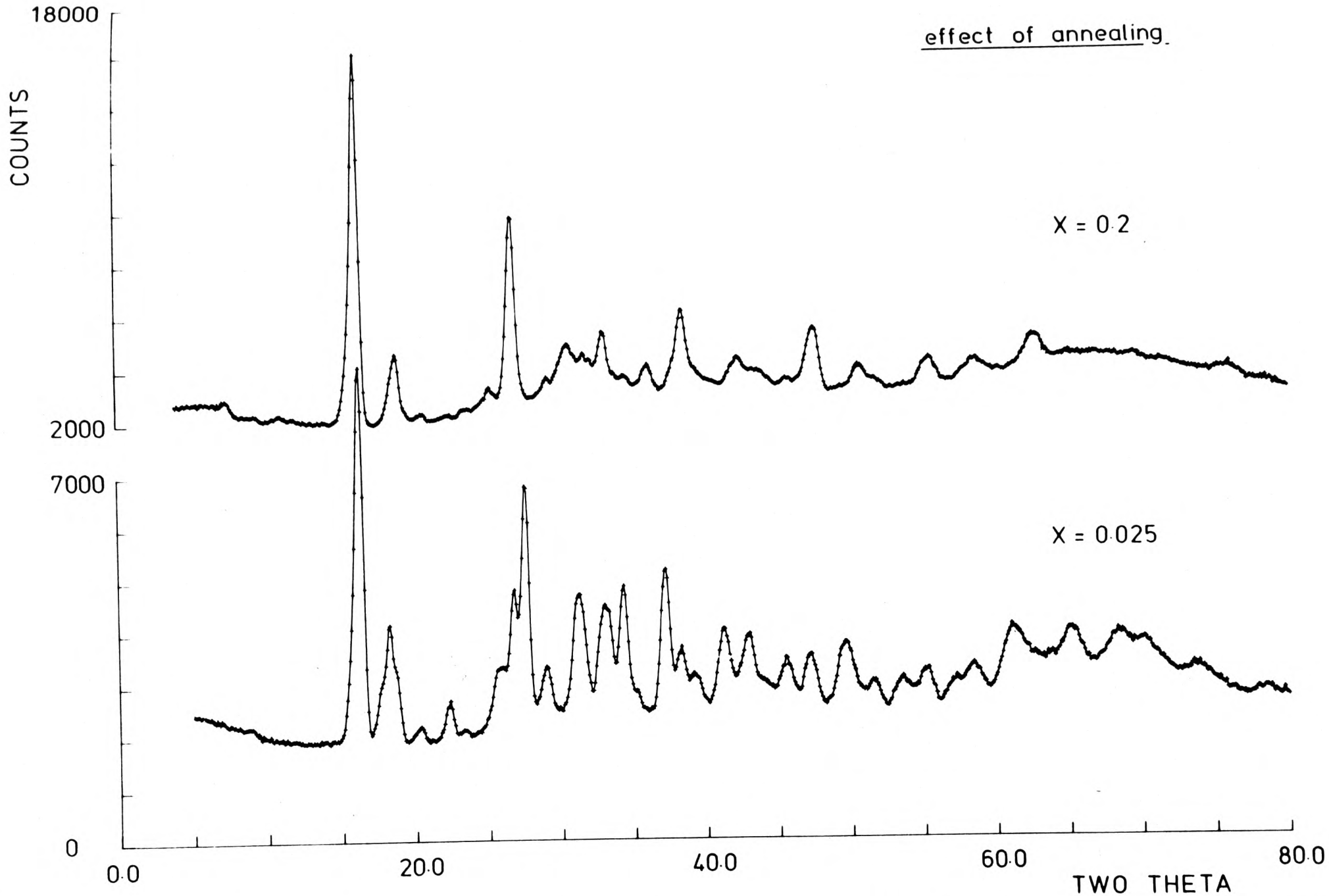


Figure 7.9. The observed powder neutron diffraction profiles (25°C) for the samples of $Na_{3(1-x)}Al_x\square_{2x}PO_4$ *at the compositions* $x = 0.025$ *and* $x = 0.2$ *after they had been subjected to further heat treatment (compare with Figure 7.8)*

this site was then reduced from 4.0 to 3.8 to allow for the limited vacancy population implied by the level x = 0.025 and displacements of the remaining sodium ions along the <100>, <110> and <111> directions were tested in least-squares.

For the x½½ (24e) sites, the value of x refined to 0.49(53) with B = 9(31)Å² and residuals R_P = 0.1645, R_{WP} = 0.1805. The refinements involving either the x x ½ (48i) or the x x x (32f) sites converged to similar residuals and, in common with the analysis of pure II-Na_3PO_4 at 400°C, we cannot accurately distinguish between the two, or a combination of both of them. In Table 7.7 we therefore present the final parameters for the models involving each of these two positions. The final residuals were R_P = 0.1616, R_{WP} = 0.1795 (for xx½) and R_P = 0.1613, R_{WP} = 0.1794 (xxx).

A second question is raised by the oxygen distribution. That good agreement is obtained with a model which is effectively identical to that of II-Na_3PO_4 despite the difference in instrument, temperature, sample preparation and refinement technique, enables us to have considerable confidence in its validity. Figure 7.12 displays this distribution of oxygen and, when drawn in this way, it is clear that the arrangement may be interpreted in terms of PO_4^{3-} tetrahedra which are centred at 0 y z (96j), with y ∿ 0.018 and z ∿ 0.020, rather than at the origin. These coordinates were then assumed for phosphorus but, because of the small extent of the displacement, they were held constant in refinement. The final calculated bond lengths and angles are given in Table 7.7, together with the atomic parameters. The displacement of Na(2) from ½ ½ ½ (4b) in either <110> or <111> directions is sufficient for Na(2)-O contacts of less than 2.2Å to be avoided. The diffuse nature of the Na(2) site

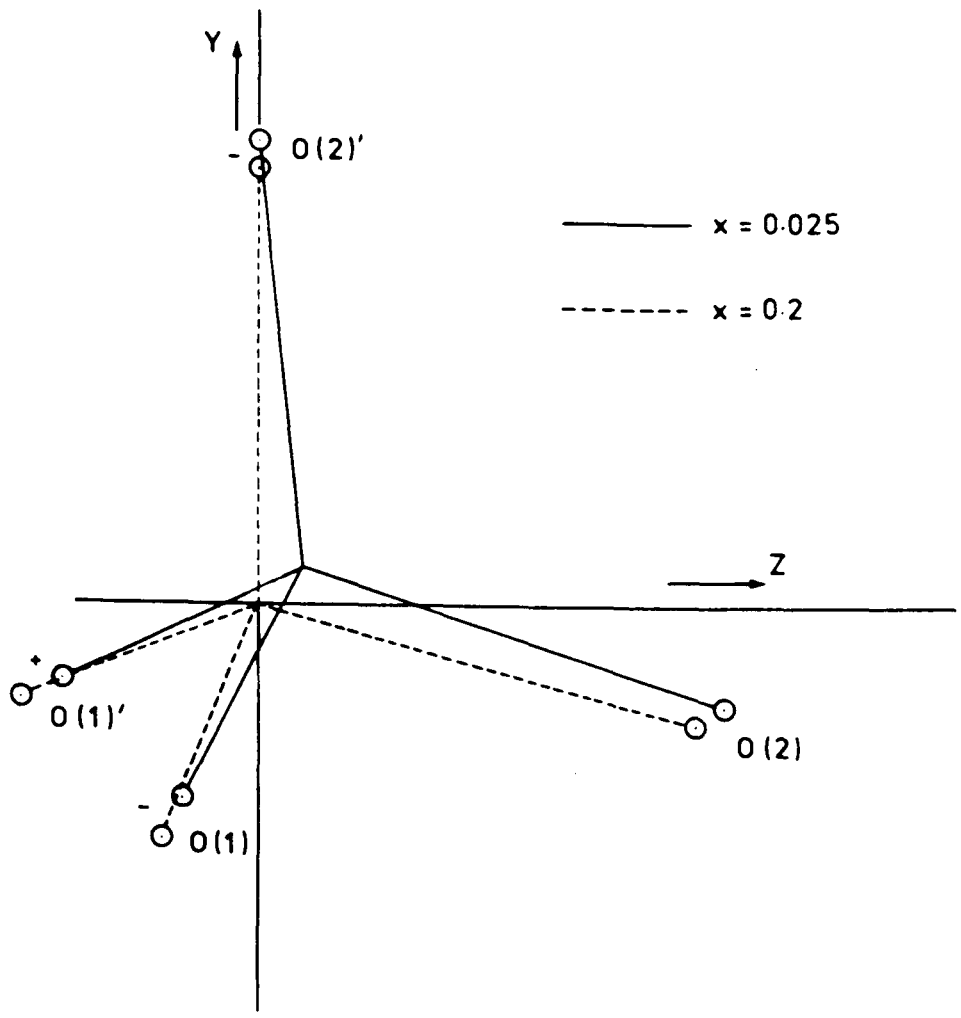


Figure 7.12. The distribution of oxygen about the origin in II-Na_3PO_4 and the solid solutions $Na_{3(1-x)}Al_x\square_{2x}PO_4$. Two equivalent positions for each of the two independent oxygen sites are shown. The PO_4^{3-} tetrahedra are indicated by the solid and dashed lines.

probably derives from such coulombic interactions rather than a tendency towards defect-cluster formation such as that found in the anion-excess fluorites[257].

Final observed and calculated reflection intensities are listed in Appendix IV and the observed, calculated and difference profiles are shown in Figure 7.10. This plot displays a gross disagreement in the fitting of the 111 reflection which arises from the peak asymmetry at low Bragg angles where the radius of the Debye-Scherrer cones is small. This asymmetry is apparent in all three of the profiles depicted in Figure 7.8. The peak-shape, which is accurately gaussian at higher angles, is modified because of the finite height of the detector aperture. No satisfactory analytical expression has yet been reported for coping with this problem and we therefore had the choice either of

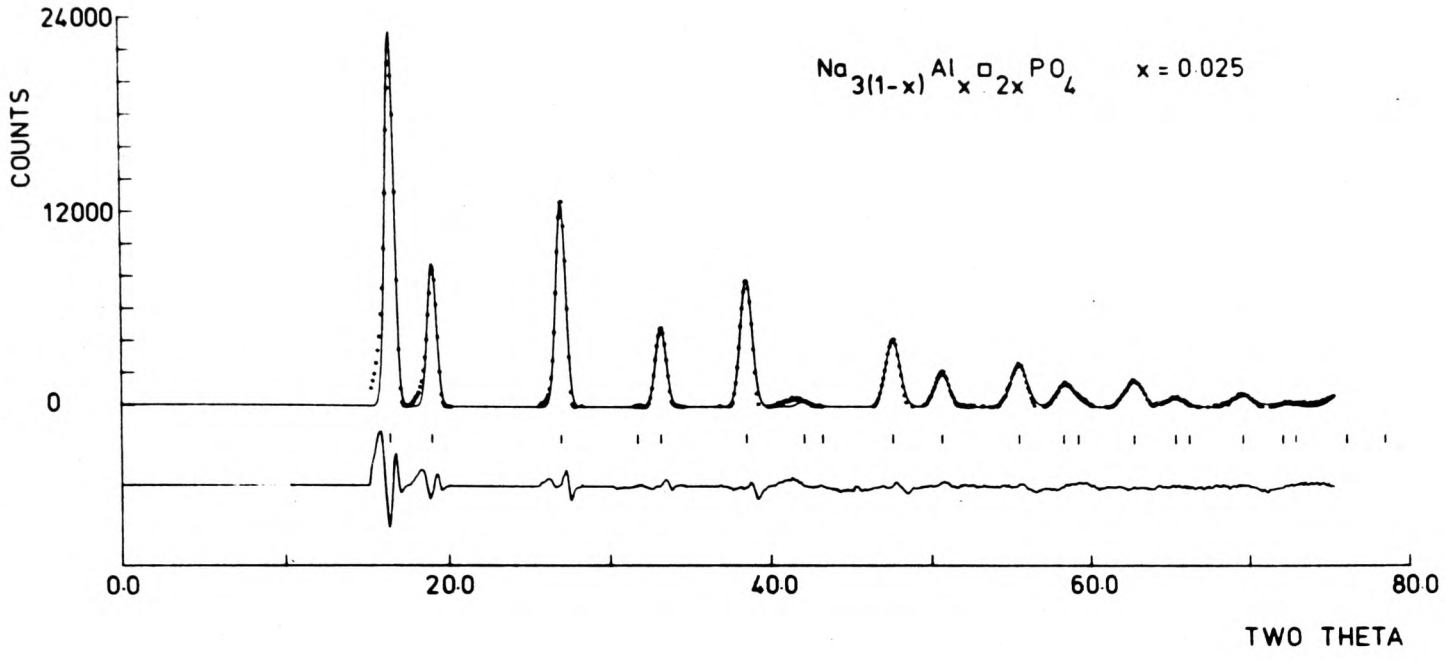


Figure 7.10. Final observed (dots), calculated (continuous line) and difference (lower) profiles for the PND data refinements of $Na_{2.925}Al_{0.25}PO_4$ *(D2 diffractometer).*

excluding the 111 reflection from the calculations or of including it, in the anticipation that the final residuals would consequently be poor. We present, in the tables, the results of the latter course. Refinements in which the region $2\theta < 17°$ was excluded, converged to the lower residuals $R_P = 0.1487$, $R_{WP} = 0.1240$, $R_E = 0.0609$ (for Na(2) on the x x ½ (48i) sites) and $R_P = 0.1499$, $R_{WP} = 0.1244$, $R_E = 0.0609$ (Na(2) at x x x (32f)), although the variable parameters were not significantly changed. The value for the lattice constant, a = 7.424(2)Å was taken from these refinements.

c) Results for the composition $Na_{2.4}Al_{0.2}PO_4$

At this higher concentration of Al^{3+} ions, the refinement of individual temperature factors immediately indicated the location of the concomitant sodium vacancies. The derived values were 0.42 0.42 ½ (48i), B = 41(3)Å²; ¼ ¼ ¼ (8c), B = 3.1(3)Å². The occupation number of the 4b/48i site was therefore included as a variable parameter in the refinements. How-

ever, the correlations between this occupancy and the other atomic parameters, particularly the temperature factors, make it difficult to define the Na(2) site with precision. The temperature factors, Na(2) occupancies and residuals for models involving the ½ ½ ½ (4b), x x ½ (48i) and x x x (32f) sites for Na(2) are given in Table 7.8. The R_{WP} residuals are essentially the same for the different models, a slight reduction being anticipated when the number of variable parameters is increased. We present the atomic coordinates derived from the model in which Na(2) is located at the ½ ½ ½ (4b) site. In this arrangement, the sodium and oxygen temperature factors converged to values close to those found at the lower $[Al^{3+}]$. Further, the Na(2) occupation is 2.8(1) which is in reasonable agreement with the value of 2.4 calculated from the relative proportions of the starting materials. This calculation is based on the assumption that all the Al^{3+} ions substitute for Na^{+} in regular sites. The scattering length of aluminium is close to that of sodium, making a distinction between the two, in a PND experiment, impracticable. However, that vacancies are found solely at the 4b position implies that the 4b site potential is lower than that of the 8c position. It is therefore likely that the incorporated Al^{3+} ions will only be situated at this latter ¼ ¼ ¼ position.

The other feature which became clear during refinement is that the two independent oxygens adopt sites closer to the origin, at distances which are nearly compatible with reasonable P-O bond lengths. This arrangement is displayed in Figure 7.12, in comparison with that derived at the lower Al^{3+} concentration. The two oxygen positions thus form tetrahedra which are now centred close to the 0 0 0 (4a) site. In these refinements, there-

fore, the phosphorus was fixed at the origin. The change in oxygen distribution and the slightly less diffuse nature of the Na(2) site are probably correlated. With a reduction in the separation of O(2) from the origin, the Na(1)-O(2) contact is increased so that the corresponding coulombic interactions are diminished. The somewhat less disordered arrangement at this composition (x = 0.2) is probably also reflected in the reduced level of diffuse scattering in the observed PND profile compared with that for x = 0.025 (Figure 7.8). The final observed and calculated reflection intensities are listed in Appendix IV, with atomic coordinates, bond lengths and angles in Table 7.8. The effect of the asymmetry of the 111 reflection is again apparent in the difference plot (Figure 7.11). Refinements in which this reflection was excluded converged to the residuals R_P = 0.1661, R_{WP} = 0.1244 and R_E = 0.0879. The corresponding atomic parameters remained close to those given in Table 7.8, although the Na(2) occupancy was reduced to 2.04(9). The quoted lattice constant is taken from this refinement.

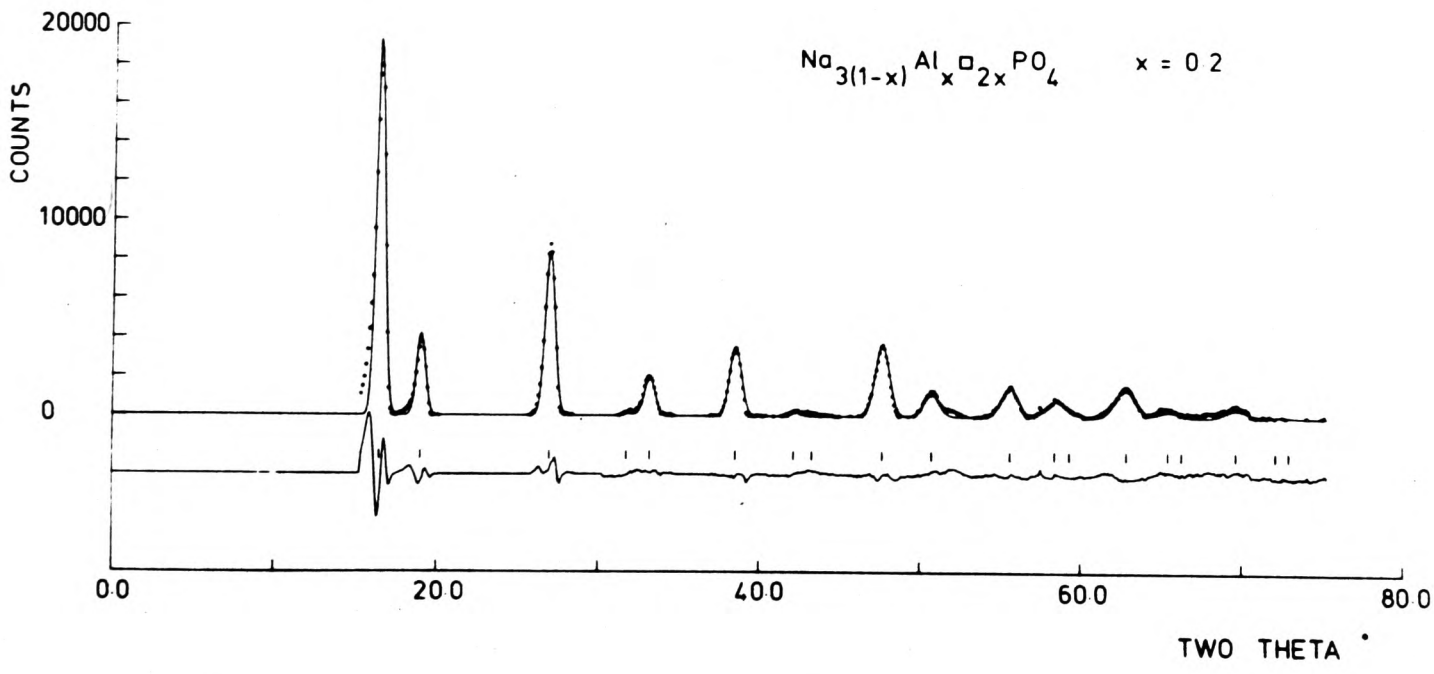


Figure 7.11. Final observed (dots), calculated (continuous line) and difference (lower) PND profiles from the refinements of $Na_{2.4}Al_{0.2}PO_4$ *(D2 diffractometer).*

d) Conclusion

The inherent disorder and the limited number of experimental observations for these materials limit the accuracy with which their structures may be defined. However, the results of our analyses enable some interesting points to be considered.

Firstly, although substitution of Na^+ by the smaller, more highly charged Al^{3+} species might be expected to result in a contraction in the length of the unit cell edge[239], the observed lattice constants at 25°C, a = 7.424(2)Å (x = 0.025) and a = 7.421(2)Å (x = 0.2) show no significant change with increasing $[Al^{3+}]$. These values are close to that reported for an unspecified $[Al^{3+}]$ by Palazzi and Rémy[243] of a = 7.413(2)Å. The results of our structure analyses suggest an explanation for the limited extent of the contraction. For levels up to x = 0.2 at least, the vacancies created by the incorporation of Al^{3+} ions occur predominantly at the octahedral ½ ½ ½ (4b) position so that the ¼ ¼ ¼ (8c) site effectively retains complete occupation. The contacts between this latter site and O(1) are relatively short and any decrease in the length of a would further reduce this separation, with a net increase in coulombic repulsion.

The space group symmetry adopted by these materials is the same as that of the fluorite structure. If the PO_4^{3-} group is considered as a discrete entity, the structures which we have determined correspond closely to an anti-fluorite system XM_{2+n}, in which the excess cations, n, are situated on the octahedral ½ ½ ½ (4b) sites. In II-Na_3PO_4 for which n = 1, this site is fully occupied, but as the level of cation-excess is reduced by the incorporation of Al^{3+}, it becomes depopulated. In the anion-excess fluorites, $(Ca/Y)F_{2+x}$, this ideal interstitial site is not occupied under normal conditions. The excess anions are

displaced from this position along <110> (F') <111> (F") and, in addition, some vacancies are found at the normal ¼ ¼ ¼ (8c) sites[257]. Although the F" positions are not well-defined[258] typical values for the x-coordinates of the x x ½ (48i, F') and x x x (32f, F") positions are 0.38 and 0.42 respectively[257] Clearly, there is an analogy between the solid solutions $Na_{3(1-x)}Al_{x\ 2x}PO_4$ and the anion-excess fluorites, but it is limited by the complexity of the counter-ion. The displacements of sodium away from the 4b sites are probably the result of the coulombic interactions arising from the particular way in which the PO_4^{3-} tetrahedra are accommodated. Further, an enhancement of the $[Al^{3+}]$ apparently alters this oxygen distribution so that we cannot probe directly the variations in structure which are produced solely by an increasing number of cation vacancies.

Do our analyses shed any light on the curious way in which the ionic conductivity varies with dopant level at 300°C? We believe so. We postulated above (section 7.5) that in pure II-Na_3PO_4 at 400°C, conduction would occur by a cooperative mechanism, similar to that proposed for α-Li_2SO_4[259,260], in which the PO_4^{3-} tetrahedra were subject to slight re-orientations. In II-Na_3PO_4, however, the interstitial ½ ½ ½ (4b) site is fully populated so that, in addition to these re-orientations, a crowdion or caterpillar-like process will occur. The incorporation of the more highly-charged Al^{3+} species is likely to limit the PO_4^{3-} re-orientations by stabilising one particular configuration through enhanced coulombic interactions. Further, the mobility of the Al^{3+} ions is likely to be small so that, even at low $[Al^{3+}]$ the crowdion or caterpillar-like process will be hindered. In fluorite systems at elevated temperatures, appreciable anion mobility is found. While there is still considerable discussion

on the subject[264,265], it seems likely that such anion motion occurs via pathways which involve the interstitial ½ ½ ½ (4b) sites either directly or, more probably, indirectly. In II-Na_3PO_4, this <u>cation</u> site is fully populated, but we have seen that, by the introduction of Al^{3+} ions, vacancies are created at this very site. With increasing $[Al^{3+}]$ and vacancy population, we would therefore expect the conductivity, via this type of mechanism, to increase. However, beyond a certain limit (presumably before the composition $Na_{1.5}Al_{0.5}PO_4$ beyond which the ¼ ¼ ¼ (8c) site will become depopulated), the introduction of further $AlPO_4$ will result in a reduction in the number of mobile charge-carriers.

Thus, we can propose three competing processes. At the lowest vacancy concentrations, a cooperative mechanism will occur which will be limited by increasing $[Al^{3+}]$. As this Al^{3+} level is enhanced, however, the increased population of ½ ½ ½ (4b) vacancies will allow a mechanism similar to that found in fluorite systems to operate, although beyond a certain $[Al^{3+}]$, the conductivity will diminish because of the progressive reduction in the concentration of mobile charge-carrying species. In $Na_{3(1-x)}Al_x\square_{2x}PO_4$ at 300°C, the variation of conductivity, σ, with x displays the form which would be anticipated, in qualitative terms, on the basis of these phenomena (see Figure 6, ref. 239, and section 7.1).

Finally, we may add that the way in which the PO_4^{3-} tetrahedra are accommodated in the structure is probably responsible for the formation of glassy phases at higher values of x. Above the composition $Na_{1.5}Al_{0.5}PO_4$, the ¼ ¼ ¼ (8c) site will be depopulated. The electrostatic restrictions on the possible orientations of the PO_4^{3-} groups will then be reduced and they may relax so as

to optimise the interactions with their local environments. This will give rise to a certain short-range ordering, but the basis for a more extended scheme, the cation sublattice, has been removed and a glassy phase results.

7.7 Conclusion

We have used single-crystal X-ray and powder neutron diffraction to investigate the structures of the discrete phases of sodium and silver orthophosphates. Even for materials that are extensively disordered, the latter technique has been reasonably successful in enabling valid structural models to be obtained. These models have been helpful in understanding the physical and chemical behaviour of these systems.

TABLE 7.1 Final atomic parameters for three models for I-Ag_3PO_4, with estimated standard deviations in parentheses.

MODEL 1 R = 0.0241 R_W = 0.0347 Extinction parameter 13(2)

Atom	Site	x	y	z	U_{11}	U_{22}	U_{33}	U_{23}	U_{13}	U_{12}
Ag	6d	0.25	0.0	0.5	0.0418(4)	0.0176(3)	U_{22}	0	0	0
P	2a	0.0	0.0	0.0	0.0099(1)	U_{11}	U_{11}	0	0	0
O	8e	0.3510(5)	x	x	0.0187(9)	U_{11}	U_{11}	-0.006(1)	U_{23}	U_{23}

Distances (Å) P - O 1.551(6) Ag - O 2.370(3),3.317(1) Ag - Ag 3.005(0) Ag - P 3.359(0)

MODEL II R = 0.0192 R_W = 0.0267 Extinction parameter 14(2)

Atom	Site	x	y	z	U_{11}	U_{22}	U_{33}	U_{23}	U_{13}	U_{12}
Ag	12h	0.2374(25)	0.0	0.5	0.036(3)	0.024(2)	0.0122(9)	-0.003(2)	0	0
P	2a	0.0	0.0	0.0	0.0100(4)	U_{11}	U_{11}	0	0	0
O	8e	0.3512(3)	x	x	0.0180(8)	U_{11}	U_{11}	-0.0048(8)	U_{23}	U_{23}

Distances (Å) P - O 1.549(5) Ag - O 2.353(5),2.392(5),3.262(11),3.371(11)

Ag - Ag 0.15(3),2.85(3),3.16(3) Ag - P 3.326(7),3.394(7)

Continued overleaf

TABLE 7.1 continued

MODEL III R = 0.0191 R_W = 0.0264 Extinction parameter 14(2)

Atom	Site	Occn.	x	U_{11}	U_{22}	U_{33}	U_{23}	U_{13}	U_{12}
Ag 1	12h	5.970(17)[a]	0.2375(25)	0.036(3)	0.024(2)	0.0121(9)	-0.003(2)	0	0
Ag 2	6c	0.030(17)	0.25	0.0418[b]	0.0176	0.0176	0	0	0
P	2a	2.0	0.0	0.0100(4)	U_{11}	U_{11}	0	0	0
O	8e	8.0	0.3511(4)	0.0181(8)	U_{11}	U_{11}	-0.0048(8)	U_{23}	U_{23}

a. The sum of the silver occupancies was constrained to equal 6.0

b. Ag(2) was assigned the same temperature factors as derived for Ag(1) in Model I

TABLE 7.2 Final atomic and instrumental parameters derived from the PND data refinements of I-Ag_3PO_4 at 375°C, with estimated standard deviations in parentheses.

Atom	Position	Site symmetry	x	y	z	β_{11} or B	β_{22}	β_{33}	β_{23}
Ag	12h	2	0.291(8)	0.0	0.5	0.017(14)	0.021(6)	0.008(4)	-0.001(4)
P	2a	23	0.0	0.0	0.0	1.2(1)			
O	8e	3	0.3514(5)	x	x	3.8(1)			

a = 6.061(1) Å V = 222.6(2) Å^3

U = 6.3(9)$\times 10^4$ V = -0.8(6)$\times 10^4$ W = 2.6(1.0) $\times 10^3$ (hundredths of degrees 2θ)

R_I = 0.0556 R_P = 0.1070 R_{WP} = 0.0958 R_E = 0.0648

Atomic parameter correlations greater that 80% :-

Ag x - β_{11} 0.98, x - β_{22} 0.86, x - β_{33} 0.86, β_{11} - β_{22} 0.82, β_{11} - β_{33} 0.85, β_{22} - β_{33} 0.95

Distances (Å)

P - O 1.559 Ag - O 2.341, 2.467, 3.168

Ag - Ag 2.533, 3.029, 0.496

Ag - P 3.283

TABLE 7.3

Final derived parameters for II-Na_3PO_4 at 400°C with estimated standard deviations in parentheses

MODEL I $R_I = 0.0218$ AF = 0.0069

Atom	Occn.	x	y	z	B
Na(1)	8.0	0.25	0.25	0.25	7.7(3)
Na(2)	4.0	0.455(3)	x	0.5	"
P	4.0	0.0	0.018	0.020	3.1(2)
O(1)	8.0	0.035(2)	0.105(2)	0.157(2)	4.7(5)
O(2)	8.0	0.0	0.038(2)	-0.217(2)	"

Distances (Å)

P - O(1)'	1.56*	Na(1) - O(1)	2.069,2.501
P - O(1)"	1.55	Na(1) - O(2)	2.475,2.875
P - O(2)'	1.54	Na(2) - O(1)	2.298,2.375,2.448
P - O(2)"	1.53	Na(2) - O(2)	1.789,1.842,1.893 2.153,2.241,2.464

Angles (°)

O(1)' - P -	O(1)"	105.2	
	O(2)'	120.6	
	O(2)"	109.4	
O(1)" - P -	O(2)'	95.3	
	O(2)"	114.4	
O(2)' - P -	O(2)"	111.2	

MODEL II $R_I = 0.0246$ AF = 0.0075

Atom	Occn.	x	y	z	B
Na(1)	8.0	0.25	0.25	0.25	7.8(3)
Na(2)	4.0	0.5	0.5	0.5	15(2)
P	4.0	0.0	0.018	0.020	2.9(3)
O(1)	8.0	0.034(2)	0.104(3)	0.157(2)	5.1(7)
O(2)	8.0	0.0	0.037(3)	-0.218(2)	"

* *Atoms O(1)',O(1)",O(2)' and O(2)" are generated from those given in the table by the symmetry transformations (z,-x,-y),(-z,-y,-x),(z,-y,-z) and (-y,-z,x) respectively.*

TABLE 7.4

Final observed and calculated reflection intensities from the refinements of I-Na_3PO_4 at 400°C

h	k	l	I_{obs}	σI_{obs}	Phase	MODEL I I_{calc}	MODEL II I_{calc}
1	1	1	19329	375	0	19410	19499
2	0	0	8139	243	0	8108	8099
2	2	0	10795	192	0	10783	10732
3	1	1	0	200	π	12	0
2	2	2	3514	172	π	3437	3424
4	0	0	6342	181	0	6337	6369
3	3	1	0	160	π	74	38
2	4	0	0	160	0	78	97
4	2	2	3367	149	0	3351	3357
5	1	1			0		
3	3	3	1988	145	0	2074	2034
4	4	0	2571	141	0	2680	2689
3	5	1	1745	150	0	1657	1637
4	4	2			0		
6	0	0	862	148	0	794	812
2	6	0	1483	154	0	1348	1382
5	3	3	742	117	0	780	767
6	2	2	0	150	π	15	6
4	4	4	962	134	0	942	924
5	5	1			0		
7	1	1	849	220	0	670	656
6	4	0	0	220	0	55	75
6	4	2	531	204	0	727	792

MODEL I R = 0.0218 AF = 0.0069

MODEL II R = 0.0246 AF = 0.0075

TABLE 7.5

Final atomic parameters derived for II-Ag_3PO_4 at 650°C with standard deviations in parentheses.

Atom	Occn.	x	y	z	B
Ag(1)	8.0	0.25	0.25	0.25	15(1)
Ag(2)	4.0	0.5	0.5	0.5	"
P	4.0	0.0	0.025	0.021	3(2)
O(1)	8.0	-0.069(2)	x	-0.145(12)	4(2)
O(2)	8.0	0.0	0.048(16)	0.212(11)	"

$R_I = 0.0746$ AF = 0.0128

Distances (Å)	P - O(1)'	1.50*	Ag(1) - O(1)	2.136,2.946
	P - O(1)"	1.50	Ag(1) - O(2)	2.499
	P - O(2)'	1.58	Ag(2) - O(1)	2.843
	P - O(2)"	1.50	Ag(2) - O(2)	2.255
Angles (°)	O(1)' - P - O(1)"	96.2		
	O(2)'	105.0		
	O(2)"	126.8		
	O(1)" - P - O(2)'	105.0		
	O(2)"	103.3		
	O(2)' - P - O(2)"	116.4		

* *designation of O(1)',O(1)",O(2)' and O(2)" as in Table 7.3*

TABLE 7.6

Final observed and calculated reflection intensities for II-Ag_3PO_4 at 650 °C

h	k	l	I_{obs}	σI_{obs}	Phase	I_{calc}
1	1	1	3956	248	0	3780
2	0	0	1841	189	0	1775
2	2	0	5692	162	0	5787
2	2	2	854	129	π	711
4	0	0	1331	149	0	1401
3	3	1	0	130	π	111
4	2	0	0	130	0	57
4	2	2	773	110	0	603
5	1	1			0	
3	3	3	0	120	π	189

TABLE 7.7(a)

Final derived parameters for $Na_{2.925}Al_{0.025}PO_4$ with estimated standard deviations in parentheses (Na(2) at xx½ (48i))

Atom	Site	Occn.	x	y	z	B
Na(1)	8c	8.0	0.25	0.25	0.25	4.2(4)
Na(2)	48i	3.8	0.458(4)	x	0.5	"
P	96j	4.0	0.0	0.018	0.020	2.4(3)
O(1)	1921	8.0	0.035(3)	0.096(4)	0.166(2)	2.4(5)
O(2)	96j	8.0	0.0	0.045(3)	-0.215(2)	"

a = 7.424(2) Å V = 409.2(3) Å³

R_I = 0.0935 R_P = 0.1616 R_{WP} = 0.1795 R_E = 0.0459

Distances (Å)	P - O(1)'	1.53*	Na(1) - O(1)	2.09,2.50
	P - O(1)"	1.52	Na(1) - O(2)	2.41,2.89
	P - O(2)'	1.52	Na(2) - O(1)	2.24,2.29,2.36
	P - O(2)"	1.52	Na(2) - O(2)	1.81,1.87,1.92,2.12 2.22,2.40

Angles (°)	O(1)' - P - O(1)"	115
	- O(2)'	94
	- O(2)"	108
	O(1)" - P - O(2)'	118
	- O(2)"	115
	O(2)' - P - O(2)"	104

* *The designation of O(1)',O(1)",O(2)'and O(2)" is as in Table 7.3*

TABLE 7.7(b)

Final derived parameters for $Na_{2.925}Al_{0.025}PO_4$ with estimated standard deviations in parentheses (Na(2) at xxx (32f))

Atom	Site	Occn.	x	y	z	B
Na(1)	8c	8.0	0.25	0.25	0.25	4.1(4)
Na(2)	32f	3.8	0.466(3)	x	x	"
P	96j	4.0	0.0	0.018	0.020	2.4(3)
O(1)	1921	8.0	0.035(3)	0.095(4)	0.166(2)	2.4(5)
O(2)	96j	8.0	0.0	0.045(3)	-0.215(2)	"

R_I = 0.0910 R_P = 0.1613 R_{WP} = 0.1794 R_E = 0.0459

TABLE 7.8

7.8(a). Atomic parameters and residuals for models involving three different locations for Na(2) in $Na_{2.4}Al_{0.2}PO_4$

Position	$B_{Na(1)}$	$x_{Na(2)}$	$B_{Na(2)}$	Occn.	B_P	B_O
½ ½ ½ (4b)	2.6(5)	-	7(2)	2.4	1.8(3)	3.3(8)
	$R_P = 0.1936$	$R_{WP} = 0.2013$				
x x ½ (48i)	3.4(4)	0.459(5)	$B_{Na(1)}$	3.1(1)	3.8(5)	1.9(5)
	$R_P = 0.1792$	$R_{WP} = 0.1979$				
x x x (32f)	3.3(3)	0.467(4)	$B_{Na(1)}$	3.1(1)	3.8(5)	1.9(5)
	$R_P = 0.1790$	$R_{WP} = 0.1979$				

7.8(b). Final atomic parameters derived for $Na_{2.4}Al_{0.2}PO_4$ with standard deviations in parentheses

Atom	Site	Occn.	x	y	z	B
Na(1)	8c	8.0	0.25	0.25	0.25	4.5(4)
Na(2)	4b	2.8(1)	0.5	0.5	0.5	"
P	4a	4.0	0.0	0.0	0.0	3.3(5)
O(1)	192ℓ	8.0	0.044(3)	0.109(5)	0.164(3)	2.2(5)
O(2)	96i	8.0	0.0	0.054(2)	-0.203(2)	"

$R_I = 0.1105$ $R_p = 0.1918$ $R_{WP} = 0.2010$ $R_E = 0.0576$

Distances (Å)

P - O(1)	1.50	Na(1) - O(2)	2.38,2.94
P - O(2)	1.56	Na(2) - O(1)	2.64
Na(1) - O(1)	1.96,2.50	Na(2) - O(2)	2.24

Angles (°)

O(1) - P - O(1)'	115*
- O(2)	118
- O(2)'	115
O(1)'- P - O(2)	94
- O(2)'	108
O(2) - P - O(2)'	104

* *In the list of angles, O(1), O(1)', O(2) and O(2)' are derived from the coordinates given in Table 7.8(b) by the transformations (z,-x,-y), (-z,-y,-x), (z,-y,-z) and (-y,-z,x) respectively*

CHAPTER 8

ANHYDROUS SULPHATE SYSTEMS

In common with the orthophosphate systems considered above, the anhydrous sulphates of Group Ia elements and silver are polymorphic. Under ambient conditions, they exist as well-ordered phases but they all have a high-temperature modification in which there is evidence for rotational disorder of the SO_4^{2-} tetrahedra. In this work, we are most interested in the sulphates of lithium, sodium, potassium and silver, all of which support appreciable cation mobility in their high-temperature forms (see Table 8.1).

8.1 Introduction

In an examination of the thermal behaviour of anhydrous sodium sulphate, Kracek[266] reported that there were five distinct phases which he termed I - V. V-Na_2SO_4 is obtained on crystallisation from solution, while I-Na_2SO_4, the highest temperature modification, is stable from ∿240°C until the melting point at 890°C. Of the remaining forms, the II-Na_2SO_4 phase has not been well-characterised. Similarly, although Brodale and Giauque[267] suggested that IV-Na_2SO_4 would be thermodynamically stable in the range 185-241°C, Davies and Sandford[268] found no evidence for its existence in Raman and differential scanning calorimetry (dsc) measurements. III-Na_2SO_4, which is obtained on cooling I-Na_2SO_4, is metastable in the range 0-517K [267], but in the absence of moisture it is kinetically stable at room temperature for an indefinite period[266]. Kracek and Ksanda[269] listed powder X-ray data for the three forms I-, III- and V-Na_2SO_4. The last occurs as the mineral thenardite and a recent single-crystal X-ray study[270] has accurately substantiated the earlier description of its structure[271] in

space-group Fddd. The corresponding silver compound, β-Ag_2SO_4, was reported to be isomorphous[272]. The metastable phase, III-Na_2SO_4, is also orthorhombic, space group Cmcm, and it has the same structure as Na_2CrO_4[273]. The orthorhombic (Pnam) unit cell of β-K_2SO_4 is of similar volume, but with a different atomic distribution[274]; it is isostructural with K_2CrO_4[274]. Lithium sulphate is somewhat anomalous. The monoclinic form found at room temperature[275] undergoes little change until the first-order phase transition[256] at 575°C above which it has face-centred cubic symmetry[276]. An analysis of the structure of the high-temperature form, α-Li_2SO_4, indicates that the SO_4^{2-} groups are freely rotating[256].

The high-temperature forms of the sodium[277], silver[278] and potassium[279] salts are apparently isomorphous, although there has been some controversy over the details of their structures. They form part of a larger group of structurally-similar compounds $(M_A/M_B)_2XO_4$ which ostensibly adopt hexagonal (or trigonal) symmetry[280-282]. A space group $P\bar{3}m1$ (D_{3d}^3) was initially proposed for these isomorphs[283]. This symmetry would allow a completely ordered arrangement of the SO_4^{2-} tetrahedra, but it does not, in itself, give rise to the condition h h $\overline{2h}$,ℓ ℓ = 2n which has been noted for some of these systems[279,284]. Fischmeister[277] proposed the symmetry-group D_{6h} (6/mmm) which, with the above condition, would limit the choice of space-group to $P6_3/mmc$ (D_{6h}^4), and he considered possible models for the structure of I-Na_2SO_4[285]. This symmetry implies rotational disorder of the SO_4^{2-} groups, although stereochemical considerations exclude the possibility of their rotating freely[285]. A disordered scheme is also consistent with the ability of the structure to accommodate large amounts

of CO_3^{2-} [286,281] and with the complete range of solid-solubility for Na_2SO_4/K_2SO_4 at elevated temperatures[276]. Even under ambient conditions, the structures of glaserite ($K_3Na(SO_4)_2$)[283] and aphthitalite ($Na_2K_2(SO_4)_2$)[287] are similar. Calvo and Faggiani[288] refined the structure of $BaNaPO_4$ in $P\bar{3}m1$ and reported that the barium and sodium ions occupied different sites. In $KNaSO_4$, however, thermodynamic data suggests that both cations are evenly distributed over the possible sites[289]. For Ca_2SiO_4, Eysel and Hahn[284] noted the c-glide condition and chose the space-group $P6_3mc$, although van den Berg and Tuinstra[279] found that the structure of α-K_2SO_4 was best described in the non-polar $P6_3/mmc$ (the changes in atomic distribution which are implied by use of the different space-groups are described later in this chapter). It is therefore quite likely that while this group of compounds is isomorphous, that is, its members all have hexagonal (or trigonal) unit cells with $a \sim 6$Å and $c \sim 8$Å, they are not all genuinely isostructural.

In addition to this glaserite-type[280-283] structure, several other discrete phases are found in $(M_A^+/M_B^+)_2SO_4$ systems. Phase diagrams have been reported for Li_2SO_4/Ag_2SO_4[290], Li_2SO_4/Na_2SO_4[291,292], Li_2SO_4/K_2SO_4[292] and Na_2SO_4/K_2SO_4[293, 289]. For $(Na/Li)_2SO_4$ there are at least seven distinct phases, although the structures of most of these compounds are not yet known. $NaLiSO_4$ is trigonal at room temperature, P31c, although the unit cell is larger that those of the glaserite-family with $a = 7.64$Å, $c = 9.76$Å and $Z = 6$[287]. At 556°C it undergoes a first-order transition to a system of body-centred cubic (BCC) symmetry, with $a_o = 6.77$Å, although only three peaks were discernible in the powder X-ray diffraction pattern[294].

The available conductivity data on the high-temperature modifications of the pure salts is summarised in Table 8.1. α-Li_2SO_4 has one of the highest known lithium ion conductivities and a conduction mechanism involving cooperative rotations of the SO_4^{2-} tetrahedra has been proposed[259]. Unfortunately, α-Li_2SO_4 is waxy and so has limited potential in ceramic applications. The physical characteristics may be altered by the incorporation of other cations and $NaLiSO_4$, for example, also supports considerable ionic conductivity[292]. Further measurements have been reported for α-Li_2SO_4 containing varying quantities of Na_2SO_4[295,296], Ag_2SO_4[297,296] and K_2SO_4[295]. The ionic conductivity of I-Na_2SO_4 may be enhanced by doping with di- and trivalent metal ions. Such additions create a concentration of vacancies and the conductivity at 500°C attains a maximum value of $\sigma \sim 1.5 \times 10^{-2}\Omega^{-1}cm^{-1}$ at a 7% population of vacancies[298]. The variation of conductivity with x in $Na_{2(1-x)}M^{2+}_x\square_xSO_4$[298] is, however, quite different from that found in $Na_{3(1-x)}Al_x\square_{2x}PO_4$[239] (Chapter 7).

In this chapter, we describe a single-crystal X-ray study of β-Ag_2SO_4 at room-temperature and powder neutron diffraction (PND) measurements on α-Ag_2SO_4 (490°C) and α-K_2SO_4 (620°C).

TABLE 8.1

Transition temperatures and ionic conductivities of pure anhydrous sulphates

	Li_2SO_4	Na_2SO_4	K_2SO_4	Ag_2SO_4
Transition				
Modification	β→α	III(V)→I	β→α	β→α
Temperature °C	575	242	587	430
High Temperature Structure	FCC	'Glaserite'	'Glaserite'	'Glaserite'
Conductivity				
Temperature °C	600	600	620	602
σ ($\Omega^{-1}cm^{-1}$)	∿1	$\sim 1.3 \times 10^{-1}$	$\sim 10^{-5}$	8.8×10^{-2}
E_a (eV)	0.36	0.84	1.3	1.3
Ref.	241[a]	300[b]	301	297[c]

The conductivity values are those given by a single author.

Other measurements are reported by:-

a Kvist[297]

b Hofer, Eysel and v. Alpen[298]

c Hauffe and Hoeffgen[240], Polischchuk and Shurkhal[303].

8.2 Single crystal X-ray diffraction study of β-Ag_2SO_4

Crystal data: Ag_2SO_4 M = 311.8. Orthorhombic Fddd, a = 5.818(1), b = 12.713(2), c = 10.267(3)Å, U = 759.4Å^3 D_c = 5.46g cm^{-3} for Z = 8 Mo K$\bar{\alpha}$ radiation, λ = 0.71069Å μ = 104.0cm^{-1}.

Ag_2SO_4 (BDH 'Analar') was dissolved in '0.880' ammonia which was allowed to evaporate over several days. Initially, a brown-black scum is formed and crystals then appear on the sides of the container and in the solution. The predominant material obtained by this method of crystallisation is $(Ag(NH_3)_2)_2SO_4$ [304] which grows as large plates or rhombs (we have refined the structure of this compound using X-ray diffraction data, although we do not describe our results here). Fortuitously, the crystal which we first examined, being an irregular rhomb (∿0.3mm square), was of Ag_2SO_4. This, however, occurs only as a minor constituent. In addition to their distinct morphologies, the two materials have different physical properties. Crystals of Ag_2SO_4 are soft and waxy, being easily deformed under mechanical pressure. On exposure to light, in air, they slowly darken, but without any other indications of disintegration. Crystals of $(Ag(NH_3)_2)_2SO_4$, on the other hand, are hard, but they decompose slowly in air to Ag_2SO_4 and ammonia [304]. Both materials are, however, initially colourless.

The selected crystal was mounted on a glass fibre and set-up, in the standard fashion, on the Enraf-Nonius CAD-4F diffractometer. The unit cell and orientation matrix were optimised by least-squares refinement based on the coordinates of 25 reflections of which 21 had 20°< θ < 27°. 3953 reflections were measured in the range θ ⩽ 35°, subject to the condition

that for hkℓ, h+ℓ = 2n. These measurements were made in bisecting geometry using ω-nθ scans (n = 1.67). Lorentz and polarisation corrections were applied and the data merged to yield 318 independent structure amplitudes with $I > 1.5\sigma(I)$, where $\sigma(I)$ was derived from the counting statistics. No absorption correction was made. In addition to the above condition, the apparent systematic absences were consistent with those expected for space-group Fddd.

Initial atomic coordinates were taken from Herrmann and Ilge, and Zachariasen[272] and full-matrix least-squares techniques were used for the refinements. In the final stages, corrections for secondary extinction and anomalous dispersion were included and a three-term truncated Chebyshev polynomial was used as the weighting scheme[4]. Final residuals of $R = 0.046$ and $R_W = 0.053$ were obtained. The derived atomic parameters are given in Table 8.2, with bond lengths and angles in Table 8.3. Observed and calculated structure factors are listed in Appendix V.

The crystal structure of β-Ag_2SO_4 is depicted in Figures 8.1 and 8.2. The atomic parameters which we have derived are in good agreement with those given by Herrmann and Ilge, and Zachariasen[272] and, further, they reveal that β-Ag_2SO_4 is accurately isostructural with thenardite, V-Na_2SO_4[270]. There are, however, some slight differences between these two materials. In β-Ag_2SO_4 all the temperature factors are larger than in V-Na_2SO_4, particularly those of silver, although this may derive from the inclusion of higher-angle data in refinement of the latter[270]. The SO_4^{2-} groups are accurately tetrahedral and the coordination about the metal ions is distorted octahedral. We are not surprised to find that the two shortest Ag-O con-

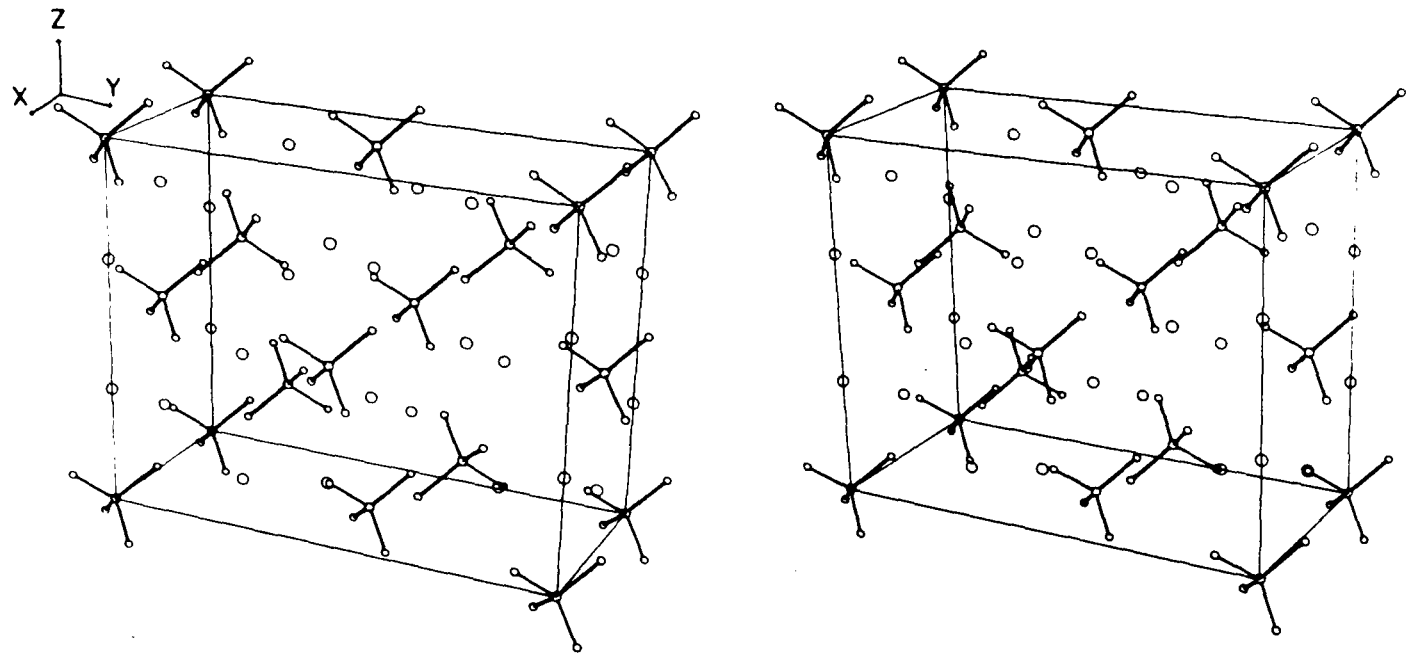
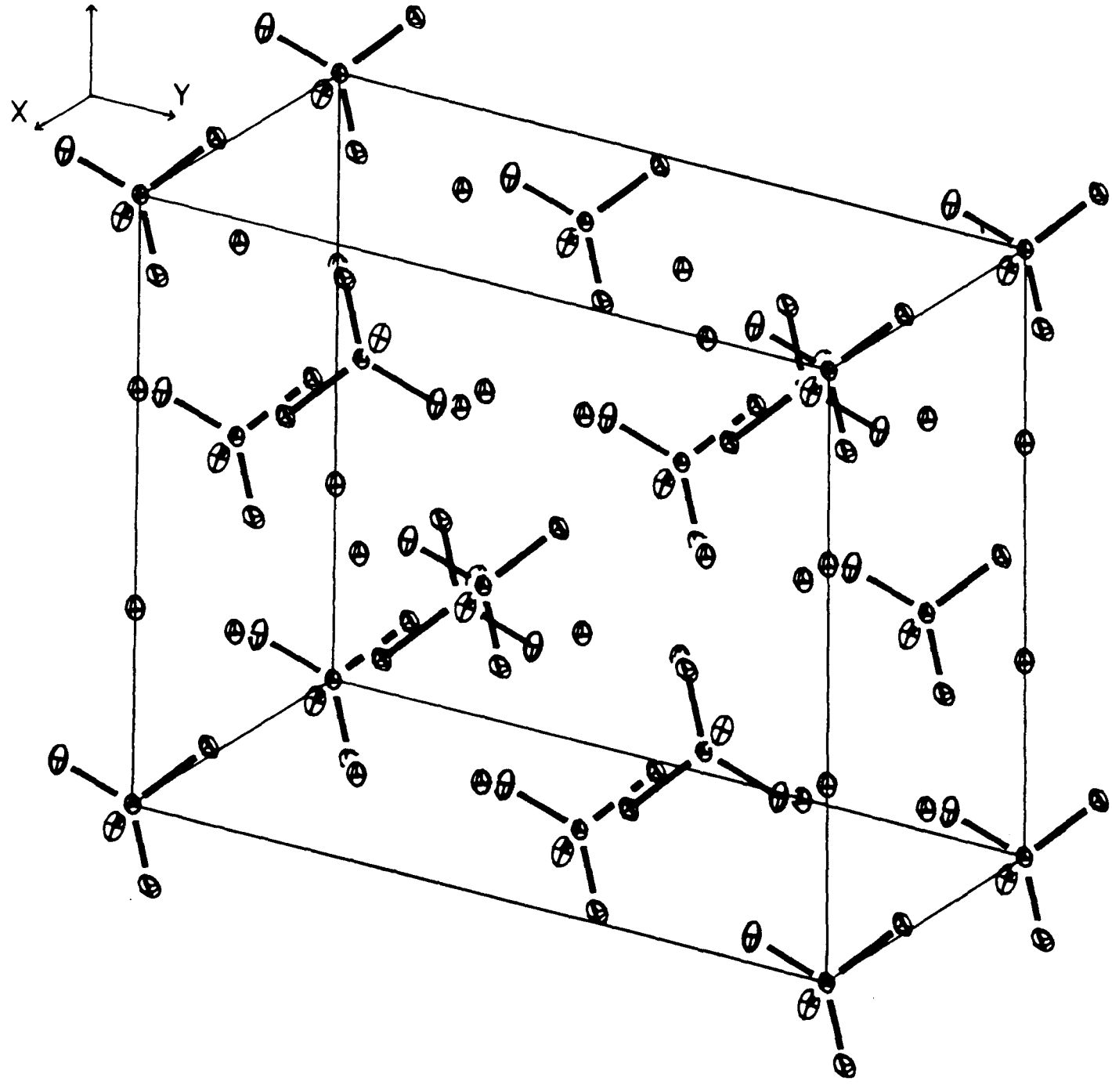


Figure 8.1. A stereoscopic picture of the crystal structure of β-Ag_2SO_4 *as determined by the single crystal X-ray diffraction study.*

Figure 8.2(below). The content of one unit cell of β-Ag_2SO_4, *drawn with thermal ellipsoids.* β-Ag_2SO_4 *is isostructural with thenardite,* V-Na_2SO_4.



tacts (2.407(5)Å) are those to the apical oxygens which are nearly collinear, O-Ag-O. The corresponding distance in V-Na_2SO_4 is 2.334Å. The angle which these contacts make about sodium is 169.3° in the latter case, but in β-Ag_2SO_4 it is 173.2(3)°. This small increase probably reflects the greater preference by Ag^+ to form two short collinear bonds to oxygen, which we have mentioned above. This shortest Ag-O distance compares with that of 2.353(4)Å in I-Ag_3PO_4, a disparity which may be responsible for the different colours of these two salts[250].

8.3 Powder neutron diffraction investigation of α-Ag_2SO_4 at 490°C

Dry Ag_2SO_4 (BDH 'Analar') was loaded, under dry N_2, into a 12mm vanadium can which was sealed with a gold O-ring. The powder neutron diffraction (PND) pattern was recorded on the D2 diffractometer at the ILL, Grenoble at a mean wavelength of 1.2227(16)Å (the experimental configuration was identical to that of I-Ag_3PO_4 at 375°C, section 7.3). The sample was maintained at 490°C in an evacuable furnace with a molybdenum element. The diffraction profile was measured in the range $2° < 2\theta < 85°$ with counts being recorded for ∿25 secs at intervals of 0.1° in 2θ and the data from the three operational counters were collated. In common with the similar measurements on II-Na_3PO_4 at 400°C (section 7.4 and Figure 7.8), the observed background was high and undulating. This diffuse scattering was broadly peaked at $2\theta \sim 35°$ and $2\theta \sim 67°$. No Bragg reflections were discernible above background beyond $2\theta = 50°$.

The observed peaks, apart from that at $2\theta = 31.91°$ from

the Mo furnace-element ($2\theta_{calc}$ = 31.89°), were all indexed on the basis of a trigonal or hexagonal cell with a = 5.51Å and c = 7.49Å. The unit cell volume, U = 196.9Å^3, implies a content of Z = 2 for D_c = 5.26g cm^{-3}. The systematic absences h h $\overline{2h}$ ℓ, ℓ = 2n+1, were apparent. Although the peaks were not all well-resolved, approximate integrated intensities were obtained and employed in the least-squares program of Wiseman[16]. When reasonable structural models had been derived, they were further improved by least-squares profile refinement techniques. Scattering lengths of 0.60, 0.28, 0.583, 0.37 and -0.214 (all x 10^{-14}m) were assumed for Ag, S, O, K and Li in this and the work later described in this chapter.

The observed powder data does not enable a distinction between the trigonal and hexagonal classes to be made and there are therefore 5 possible space groups:- P31c, P$\bar{3}$1c, P6$_3$mc, P$\bar{6}$2c and P6$_3$/mmc. The space group P$\bar{3}$m1 was initially suggested for glaserite and its isomorphs (section 8.1) and, although this symmetry would not, in itself, give rise to the above reflection condition, several models in P$\bar{3}$m1 were examined in least-squares. None of these gave reasonable residuals. For the remaining possibilities, we may use stereochemical requirements to postulate a plausible structure and examine the differences in atomic distributions which are created by the different space-group symmetries. In the manner of Fischmeister[285], the most useful starting point has Ag(1) at 000, Ag(2) at 1/3 2/3 z, and S at 1/3 2/3 z_2, with oxygen distributed tetrahedrally about S. The implications of the possible space-group symmetries for the last three species are displayed in Figure 8.3.

We can distinguish, firstly, between the polar and non-

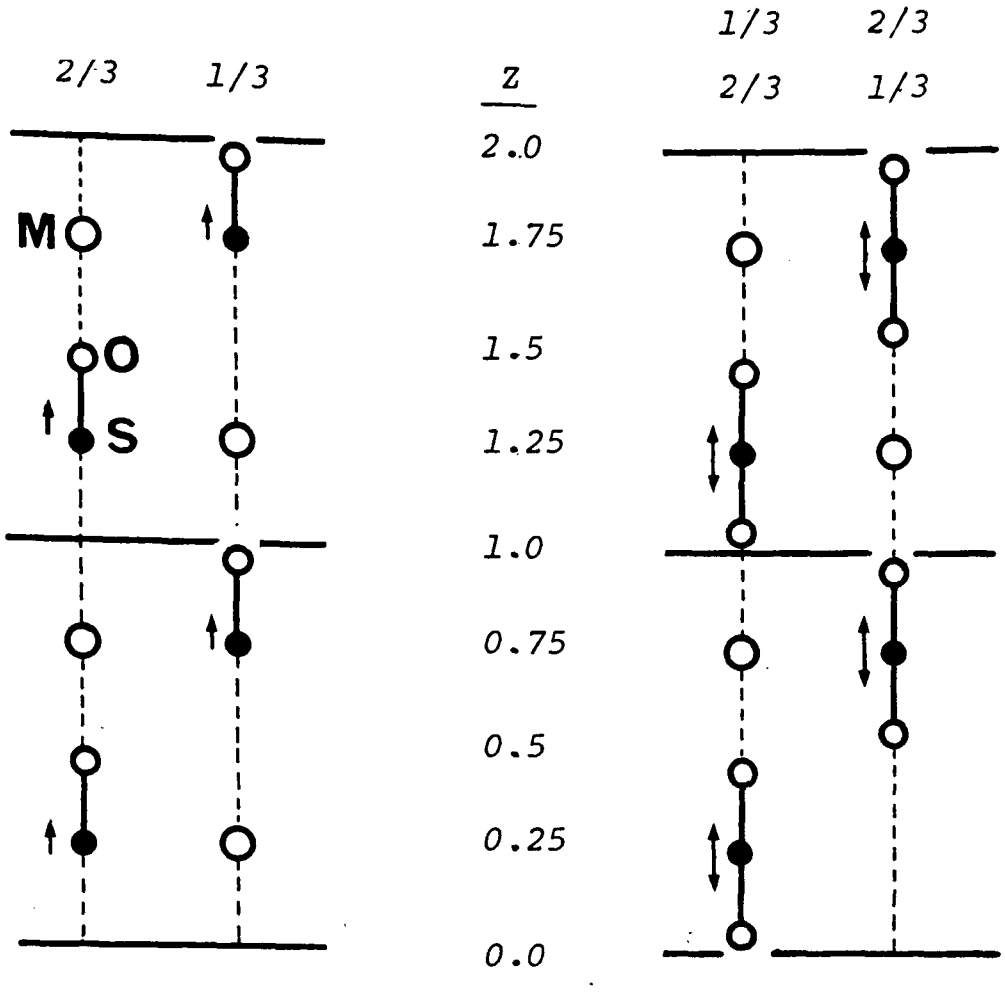


Figure 8.3(a). The atomic distribution along the 1/3 2/3 z and 2/3 1/3 z axes for a non-polar space-group, e.g. P3̄1c, (left) and that for a polar counterpart, e.g. $P6_3/mmc$ (right). Both α-K_2SO_4 and α-Ag_2SO_4 adopt non-polar symmetries in which the 0 0 0 and 1/3 2/3 z sites can be described in identical terms in each of P3̄1c , P6̄2c and $P6_3/mmc$ .The distinction between these groups is determined solely by the atomic species which do not occupy such sites.

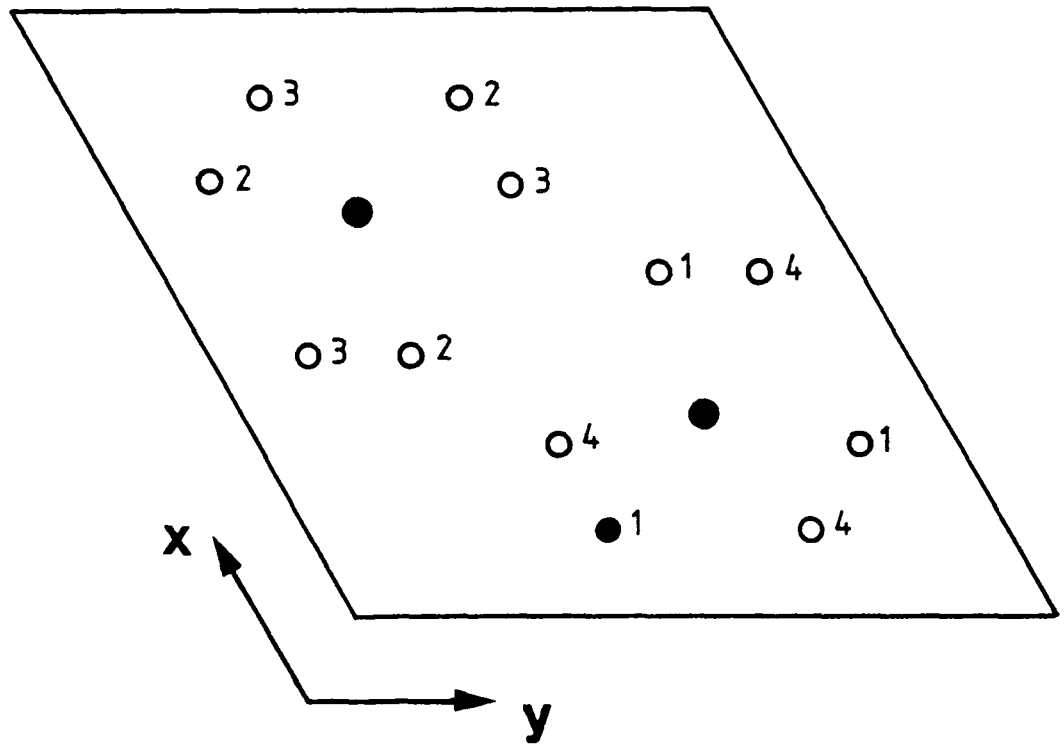


Figure 8.3(b). A plot down <0 0 1> which depicts a general distribution for the remaining oxygens. For an atom at 0.14 0.43 z (shaded) the positions generated by the above three space-groups are :-

P3̄1c	1(z), 2(z̄), 3(1/2+z), 4(1/2 - z)
P6̄2c	1(z and 1/2 - z), 3(1/2 + z and z̄)
$P6_3/mmc$	1(z and 1/2 - z), 2(z̄ and 1/2 + z), 3(1/2 + z and z̄), 4(1/2 - z and z)

polar space groups. For O(1) lying on 1/3 2/3 z, the former give rise to only one configuration whereas the latter generate two orientations with S-O(1) along <0001> and <000$\bar{1}$> respectively. Several models were considered in the polar $P6_3mc$, but these gave only poor agreements between observed and calculated intensities. As much better agreements were obtained in the non-polar space groups, we can restrict the choice of symmetries to $P\bar{3}1c$, $P\bar{6}2c$ and $P6_3/mmc$. Van den Berg and Tuinstra[279] arrived at a similar conclusion in their analysis of α-K_2SO_4.

The distinction between these three remaining possibilities rests on the extent of rotational disorder of the SO_4^{2-} tetrahedra and, in order to probe this distribution, an extensive series of models in both $P\bar{3}1c$ and $P6_3/mmc$ was tested in least-squares. Acceptable residuals were obtained in both space-groups, but the corresponding models in $P6_3/mmc$ had features which were chemically unreasonable. Thus the oxygen coordinates gave rise to S-O distances of $\sim$1.1Å and the sulphur Debye-Waller factor repeatedly converged to excessive values (typically 20Å^2). In Table 8.4, we therefore present the results of our refinements in $P\bar{3}1c$. The derived atomic parameters give rise to both acceptable geometry about sulphur and reasonable Ag-O contacts. Further, the Debye-Waller factors have the relative magnitudes that might be anticipated on the basis of librating SO_4^{2-} functions and mobile Ag^+ ions. The relative neutron scattering lengths are such that the oxygen distribution is defined with greater accuracy than that obtained in the X-ray analysis of α-K_2SO_4[279]. For sulphur, however, the opposite is the case and this, in combination with the difficulty of accurately estimating the background in the observed PND profile, is probably responsible for the low value

of the derived temperature factor. The final residuals were $R_P = 0.2002$, $R_{WP} = 0.1553$ and $R_E = 0.0876$. Final observed and calculated reflection intensities are listed in Appendix V.

In contrast to the case of Ag_3PO_4 (Chapter 7), there is no simple correspondence between the low- and high-temperature modifications of Ag_2SO_4.

8.4 Powder neutron diffraction study of α-K_2SO_4 at 620°C.

K_2SO_4 (HBL Research Reagent) was dried at 400°C for 36 hours before being loaded into a 15mm diameter vanadium can which was sealed with a gold O-ring. The PND profile was measured on the D2 diffractometer at the ILL, Grenoble. A mean wavelength of 1.2213(9)Å was taken from the (311) planes of a Ge monochromator at a take-off angle of ∿42°. This wavelength was calibrated by the profile refinement of 3 peaks recorded from a standard Ni sample, assuming a = 3.5348Å[261]. The sample was maintained at 620°C in an evacuable furnace with a vanadium element for 4½ hours before and then throughout data collection. The diffraction profile in the range $0° < 2\theta < 80°$ was sectioned at intervals of 0.1° in 2θ, with counts being recorded for ∿25 secs at each point. Because of an electrical fault, the apparent background varied discontinuously in one or two steps for each counter. The data were therefore plotted separately and a mean difference between the regions of high and low background calculated for each detector. These differences were added to the low-background regions to bring all the data to the same level. The data from the three counters were then collated[228], although, for each, the sections within which the increases in background occurred were rejected. The results of

this procedure were checked by an examination of the regions to which more than one counter contributed. The variation between the corrected counts for each detector was no larger than that found from the purely statistical fluctuations noted with other D2 data sets.

The course of structure analysis was similar to that outlined above for α-Ag_2SO_4. The systematic absences h h $\overline{2h}$ ℓ, ℓ = 2n+1 were again apparent and the unit cell volume, U = 241.9Å^3, yields a cell content of Z = 2 for D_c = 3.32g cm^{-3}.

Adjustment of the scale factor using the unmodified parameters of van den Berg and Tuinstra[279] afforded residuals R_P = 0.3558 and R_{WP} = 0.3198, with R_E = 0.0516. These were improved to R_P = 0.2990, R_{WP} = 0.2667 when the temperature factors were allowed to vary, but the derived values were 6.0(6), 34(3) and 8.7(6)Å^2 for K, S and O respectively. The oxygen coordinates (4 parameters) were then also included, but the refinements diverged. We then considered a succession of models both in $P\bar{3}1c$ and $P6_3/mmc$. Similar agreements were obtained in both of these space groups and, in Table 8.5, we present the results of the refinements in the latter, $P6_3/mmc$. Although this atomic distribution is chemically reasonable in that the SO_4^{2-} groups are tetrahedral and prohibitively short K-O contacts are avoided, the final residuals of R_P = 0.2301 and R_{WP} = 0.2025 are rather poor. This may indicate that the structure is even more disordered than our model implies, or, more likely, it may reflect some inaccuracy in the observed data deriving from the aforementioned instrumental problems. The final observed and calculated reflection intensities are listed in Appendix V.

This model for α-K_2SO_4 is similar, although not identical, to that given by van den Berg and Tuinstra[279]. In disordered

systems such as these, it is quite likely that different analyses (using different refinement techniques and radiations) will yield slightly different pictures of the structure. The static and dynamic disorder on the one hand limit the number of observed data but, on the other, their description generally requires an increase in the number of variable parameters with respect to a well-ordered situation. For example, at elevated temperatures, the atomic vibrations will probably be distinctly anisotropic so that the use of isotropic components will be only an approximation. Our analyses also indicate that the use of a single Debye-Waller factor for all atomic species may mask irregularities in the structural model.

In broad terms, α-K_2SO_4 is isostructural with α-Ag_2SO_4 although the rotational disorder of the sulphate groups is less pronounced in the latter. This, however, may reflect the different temperatures at which the diffraction data were collected. Our results and those of van den Berg and Tuinstra[279] confirm that the SO_4^{2-} tetrahedra are not rotating freely[285] Each group has a preferred orientation such that one S-O bond is nearly collinear with <0001> and the limited rotational disorder occurs principally about this direction.

8.5 Conclusion

The anhydrous sulphates that we have studied have several structural differences compared with the corresponding orthophosphate systems, although the anion is accurately tetrahedral in both cases. In β-Ag_2SO_4, there is no evidence for distinctly anisotropic behaviour of silver such as that found in I-Ag_3PO_4 (Chapter 7). The silver coordination is octahedral in the former, but tetrahedral in the latter, although both are

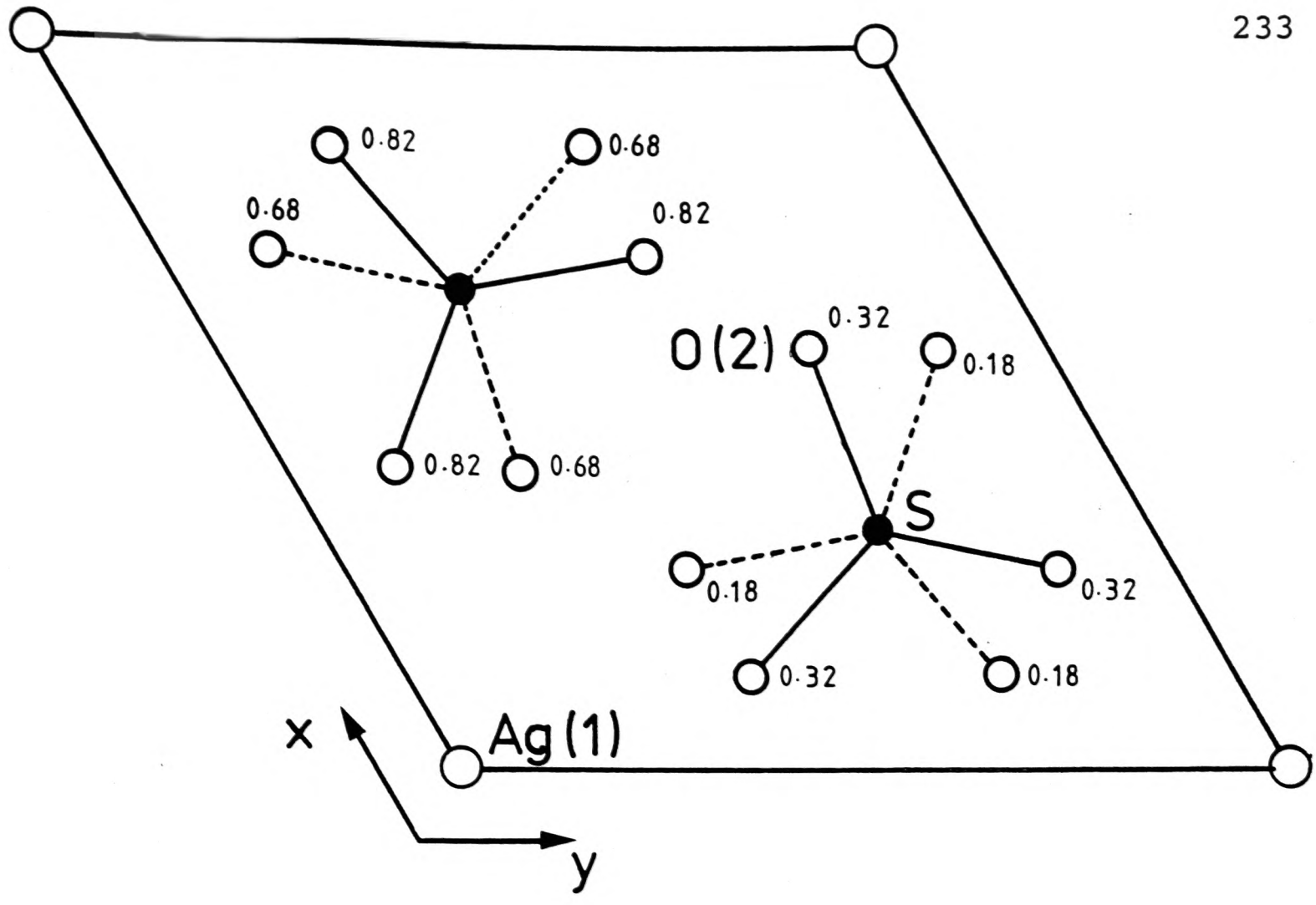


Figure 8.4(a). A projection down <0 0 1> of the structure of α-Ag_2SO_4 *(atoms Ag(2) and O(1) have been omitted for clarity). The* SO_4^{2-} *tetrahedra are 2-fold disordered.*

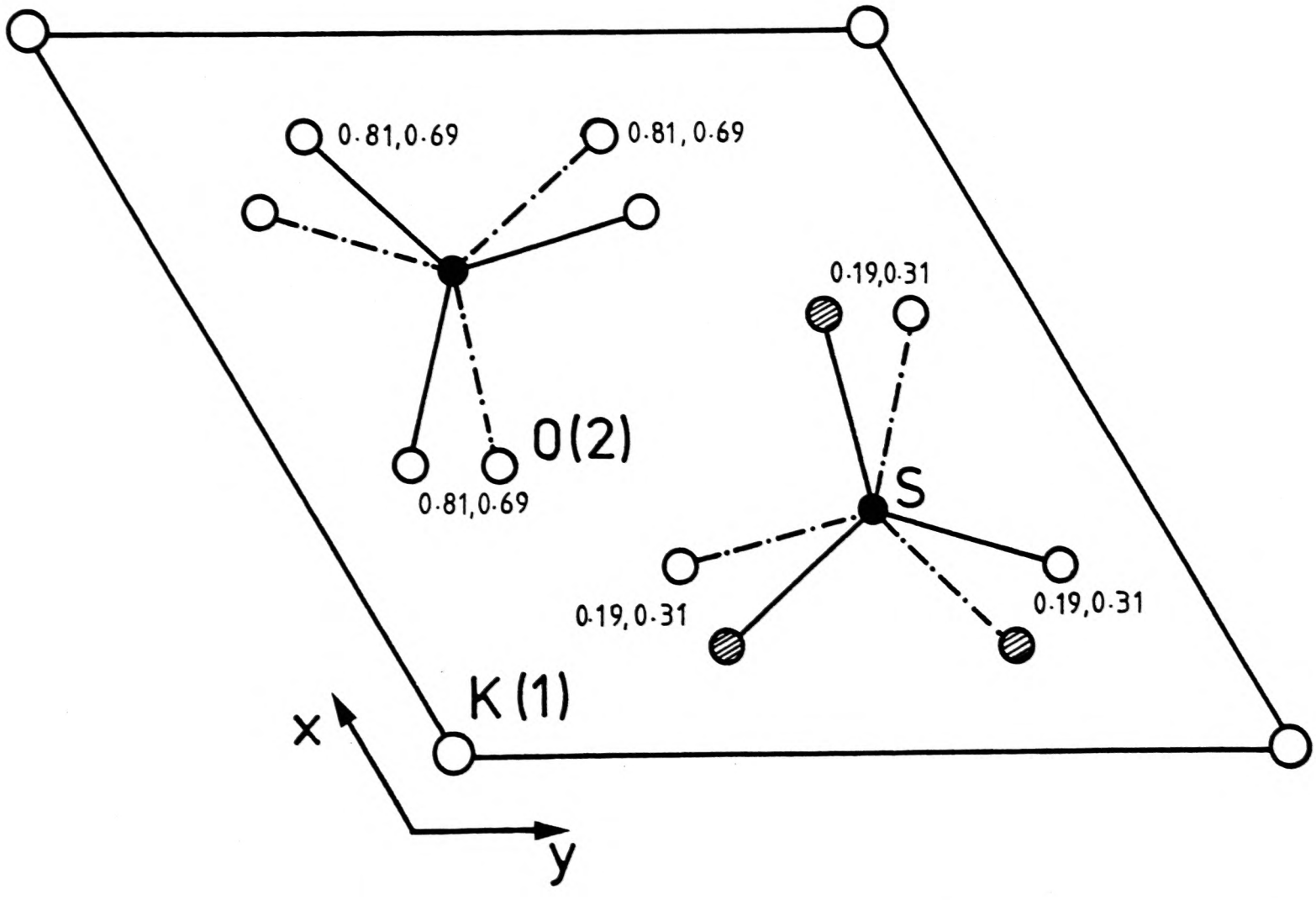


Figure 8.4(b). A projection down <0 0 1> of the structure of α-K_2SO_4 *(atoms K(2) and O(1) have been omitted for clarity). In contrast to the above, the* SO_4^{2-} *tetrahedra are 4-fold disordered. The four orientations are generated from that shaded by a 27° rotation about <0 0 1> and mirror reflections through the z = 1/4 plane.*

slightly distorted. The difference in coordination is probably correlated with the different Ag-O separations found in the two materials.

The β→α transformation in the sulphate occurs at a lower temperature than the corresponding I→II transition in the orthophosphate. The atomic distributions in the high-temperature modifications differ. In α-Ag_2SO_4 the sulphate tetrahedra have only two possible orientations, with one S-O bond lying along <0001> and pointing directly towards an adjacent silver ion. In II-Ag_3PO_4, however, the PO_4^{3-} tetrahedra have a large number of equivalent orientations and, as a reflection of this greater disorder, the symmetry of II-Ag_3PO_4 is higher. The analysis of α-K_2SO_4 suggests that the rotational disorder of the SO_4^{2-} tetrahedra may become more pronounced as the temperature is raised, although, even in this case the disorder is derived mainly from slight rotations about a single axis. In neither material do we find the type of completely random orientation that has been reported in α-Li_2SO_4[256]. This difference may reflect the smaller size of the Li^+ ion. Figure 8.5 displays the PND profiles from a sample of $NaLiSO_4$, as measured at 25°C and 590°C on the D2 diffractometer. In the pattern from the high-temperature modification (Figure 8.5(b)), there is only a single well-defined peak. This is rather unusual for the Bragg diffraction pattern from a solid material, albeit at only 30°C from the melting point. The corresponding pattern for α-Li_2SO_4 is similar[260] so that the atomic distribution in α-$NaLiSO_4$ will probably be considerably more disordered than those found in α-Ag_2SO_4 and α-K_2SO_4. This profile also serves to illustrate the type of problems that are associated with the structural characterisation of this type of material.

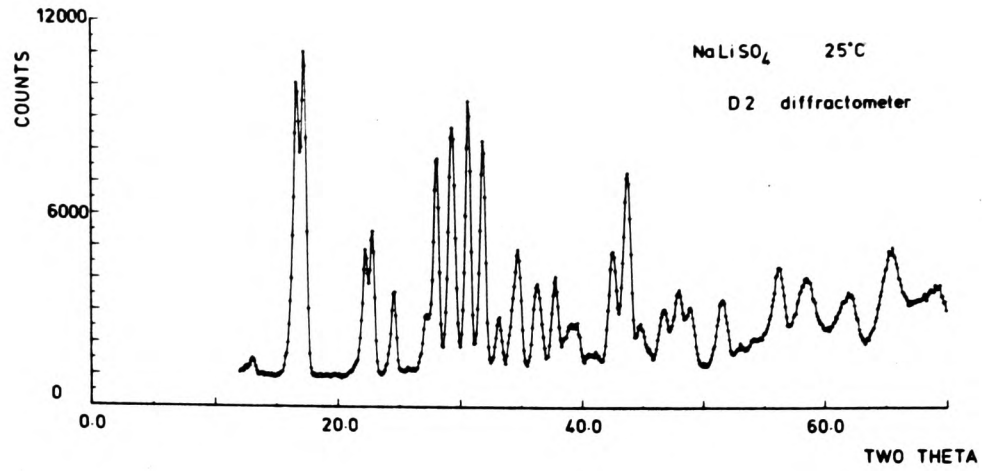


Figure 8.5(a). The observed powder neutron diffraction profile (one counter) for $NaLiSO_4$ at room temperature as measured on the D2 diffractometer (λ = 1.22Å).

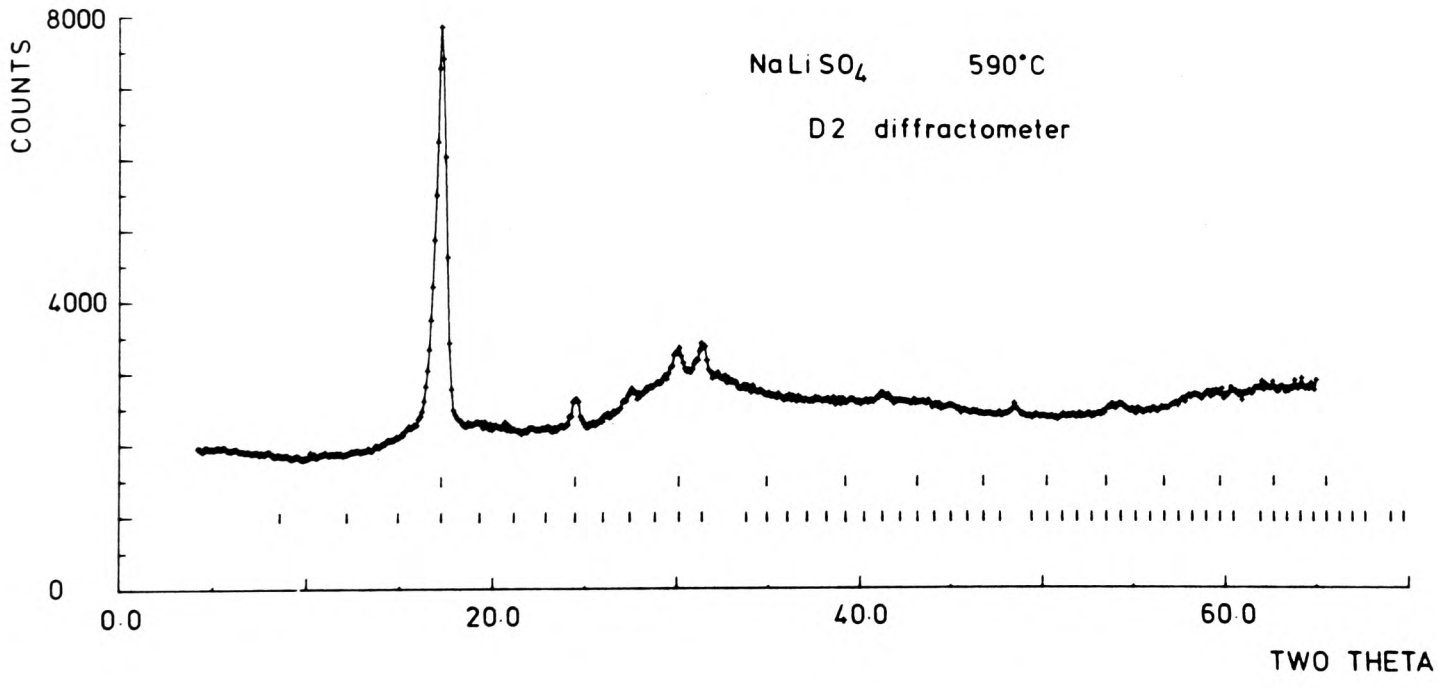


Figure 8.5(b). The observed powder neutron diffraction profile for $NaLiSO_4$ at 590°C as measured on the D2 diffractometer (λ = 1.22Å). The upper reflection bars indicate the positions of allowed reflections based on a body-centred cubic cell, with a = 5.75 Å. The lower bars indicate the positions of reflections calculated on the basis of a tetragonal unit cell, with a = 5.75 Å and c = 8.13 Å.

TABLE 8.2

Final atomic parameters for β-Ag_2SO_4 at 25°C with estimated standard deviations in parentheses.

Atom	Position	Site Symmetry	x	y	z
Ag	16g	2	0.0	0.0	0.3200(1)
S	8a	222	0.0	0.0	0.0
O	32h	1	0.1454(10)	0.0672(4)	-0.0840(6)

Atom	U_{11}	U_{22}	U_{33}	U_{12}	U_{13}	U_{23}
Ag	0.0241(4)	0.0197(3)	0.0360(5)	0.0009(3)	0.0	0.0
S	0.0146(10)	0.0143(110	0.0224(12)	0.0	0.0	0.0
O	0.027(3)	0.021(2)	0.042(3)	-0.004(2)	0.016(2)	-0.001(2)

$R = 0.0459$ $R_W = 0.0534$ Extinction Parameter = 0.5(1)

19 variable parameters, with 318 reflections.

TABLE 8.3

Bond lengths and angles, with estimated standard deviations in parentheses, derived from the final refinements of α-Ag_2SO_4 at 25°C.

Distances (Å)

Ag-Ag	3.245(1)[a]
Ag-S	3.286(1) and 3.446(1)[a]
Ag-O	2.705(6)[b,c], 2.441(5)[d,e], 2.407(5)[f,g]
S-O	1.479(5)

Angles about Ag (°)

O^b-Ag-O^c	52.8(2)	O^f-Ag-O^d	81.5(2)
O^b-Ag-O^f	106.2(2)	O^f-Ag-O^e	95.7(2)
O^b-Ag-O^d	137.4(2)	O^f-Ag-O^g	173.2(3)
O^b-Ag-O^e	89.3(2)	O^d-Ag-O^e	132.4(3)
O^b-Ag-O^g	80.1(1)		

Angles about S (°)

O-S-O^b	110.2(5)
O-S-O^c	109.5(4)
O-S-O^h	108.7(5)

The superscripts refer to the symmetry-related atoms generated by the following transformations:

a. $1/2 + x, \bar{y}, 1/2 - z$

b. $x, \bar{y}, \bar{z}$

c. $\bar{x}, y, \bar{z}$

d. $1/2 + x, y, z - 1/2$

e. $1/2 - x, \bar{y}, 1/2 + z$

f. $1/4 - x, 1/4 - y, 1/4 - z$

g. $x - 1/4, y - 1/4, 1/4 - z$

h. $\bar{x}, \bar{y}, z$

TABLE 8.4

Final atomic parameters derived from the PND data refinements of α-Ag_2SO_4 at 490°C, with estimated standard deviations in parentheses.

Atom	Position	Site Symmetry	x	y	z	B	Occn.
Ag(1)	2b	$\bar{3}$	0.0	0.0	0.0	5.9(5)	2.0
Ag(2)	6h	2	0.734(2)	$\bar{x}$	0.25	"	2.0
S	4f	3	1/3	2/3	0.256(2)	-0.2(1.0)	2.0
O(1)	4f	3	1/3	2/3	0.439(2)	8.5(5)	2.0
O(2)	12i	1	0.133(3)	0.724(3)	0.178(2)	"	6.0

a = 5.511(7)Å c = 7.488(4)Å

U = 1.7 x 10^5 V = -7.7 x 10^4 W = 1.3 x 10^4 (1/100° in 2θ)

R_I = 0.1117 R_P = 0.2000 R_{WP} = 0.1553 R_E = 0.0875

Contact distances (Å)	S-O(1)	1.46
	S-O(2)	1.39
	Ag(1)-O(2)	2.39
	Ag(2)-O(1)	2.41
	Ag(2)-O(2)	2,00, 2.44, 2.74
Bond angles (°)	O(1)-S-O(2)	114.3
	O(2)-S-O(2)	108.2

TABLE 8.5

inal atomic parameters derived from the PND data refinements of
$-K_2SO_4$ at 620°C, with estimated standard deviations in paren-
heses

tom	Posi-tion	Site Symmetry	x	y	z	B	Occn.
(1)	2a	$\bar{3}$m	0.0	0.0	0.0	9.1(5)	2.0
(2)	6h	mm	0.660[a]	$\bar{x}$	1/4	"	2.0
	2c	$\bar{6}$m2	1/3	2/3	0.254[b]	2.9(7)	2.0
(1)	12k	m	0.289(2)	$\bar{x}$	0.430(3)	3.4(4)	2.0
(2)	24ℓ	1	0.147(3)	0.399(2)	0.190(1)	"	6.0

a = 5.890(5)Å c = 8.066(6)Å

J = 1.7×10^5 V = -8.4×10^4 W = 1.3×10^4 (1/100° in 2θ)

R_I = 0.1625 R_P = 0.2301 R_{WP} = 0.2025 R_E = 0.0511

Contact distances (Å)	S-O(1)	1.49
	S-O(2)	1.49
	K(1)-O(1)	3.00
	K(1)-O(2)	2.57
	K(2)-O(1)	2.61, 2.63
	K(2)-O(2)	2.64, 2.71, 2.75
Bond angles (°)	O(1)-S-O(2)	114.4, 121.6, 92.9
	O(2)-S-O(2)	108.7

[a] K(2) coordinates were not allowed to vary in the final cycles

[b] The z-parameter for S(1) was changed from 0.25 to 0.254 so that the S-O bond lengths would be nearly equal. This shift did not affect the residuals, although when the z-parameter was allowed to vary, refinements diverged.

CHAPTER 9

SILVER (I) FLUORIDE

9.1 Introduction

Two binary fluorides of silver are known, AgF and AgF_2. The latter represents the only well-characterised example of Ag^{2+} (d^9) and its crystal structure[305,306] consists of distorted AgF_6 octahedra sharing three vertices. Silver (I) fluoride in common with AgCl and AgBr, allegedly adopts the rock-salt structure with a = 4.92Å[307]. The variation of the lattice constant as a function of anion radius for Ag^+, Li^+, Na^+ and K^+ is depicted in Figure 9.1. When compared with the fluorides of the Group Ia metals, the lattice constant of AgF is somewhat anomalous. This has led to the suggestion that AgF adopts the zinc blende structure (which is found for CuCl, CuBr and CuI); the X-ray powder data[307] would not readily distinguish between these models.

Silver also differs in that it has the possibility of attainable higher valencies which could lead to cation-deficient phases. The reaction:-

$$2AgF \rightarrow Ag_{1+x}F + Ag_{1-x}F$$

has been proposed by Jamieson *et al.*[308]. They investigated the structure of AgF as a function of pressure and noted the formation of both CsCl- and inverse NiAs-type structures. More interestingly, on decompression the X-ray powder pattern of the FCC phase of AgF had doubled lines, corresponding to lattice constants of ∿4.95 and ∿4.84Å respectively. Further, they noted the occurrence of some silver metal which presumably arises from the type of disproportionation proposed in Chapter 7.

Cation-deficient phases with the rocksalt structure are well known. In $Fe_{1-x}O$, for example, the iron vacancies do not occur at isolated cation sites, but, rather, there is a popula-

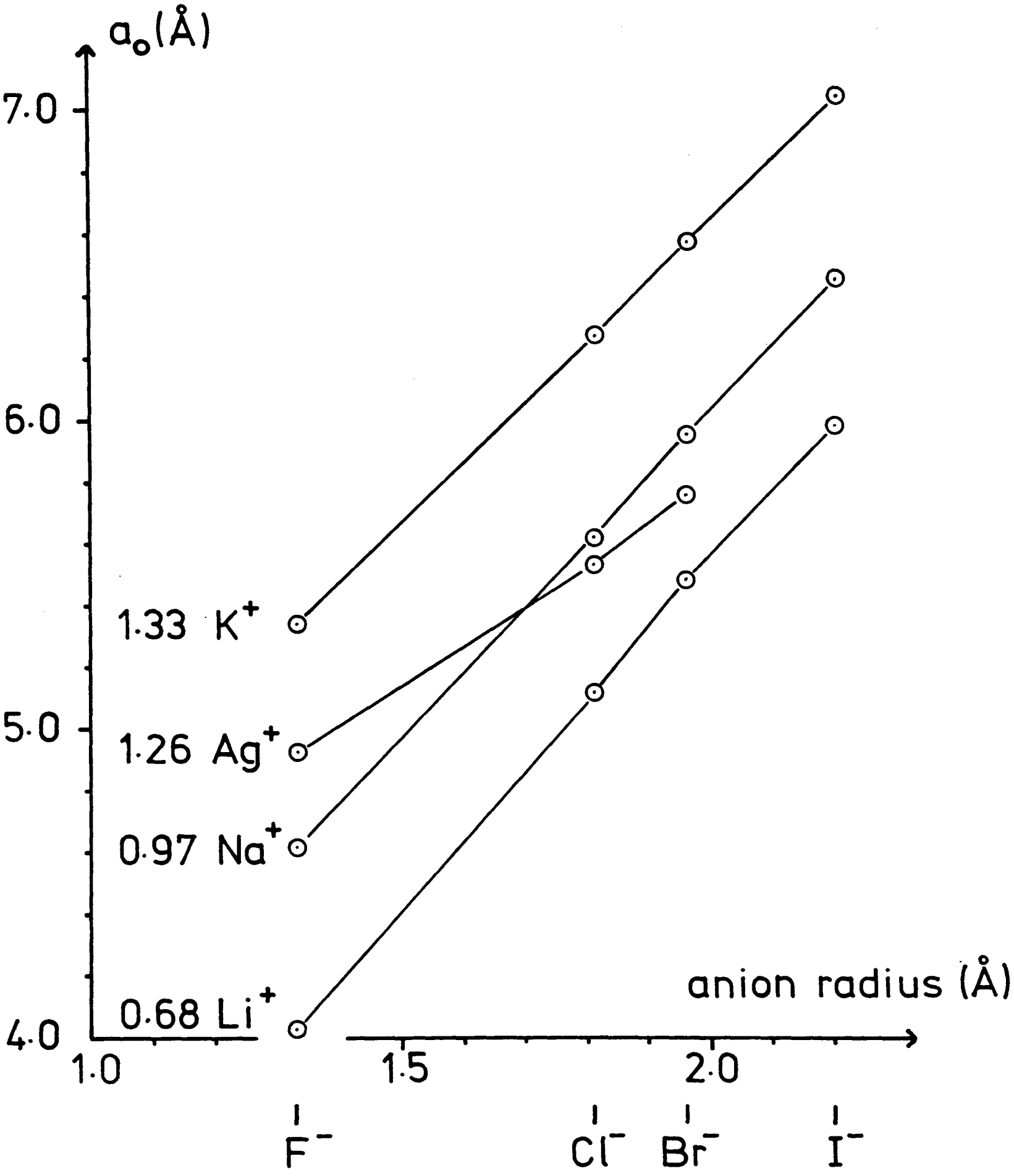


Figure 9.1. The variation of the lattice constant with anion radius for binary halides with the rocksalt structure. Values for the ionic radii were taken from reference 313.

tion of tetrahedral interstitials each of which forms a cluster with surrounding octahedral vacancies[309]. The basic unit comprises one tetrahedral interstitial and four octahedral vacancies as shown in Figure 9.2. These 4:1 clusters may

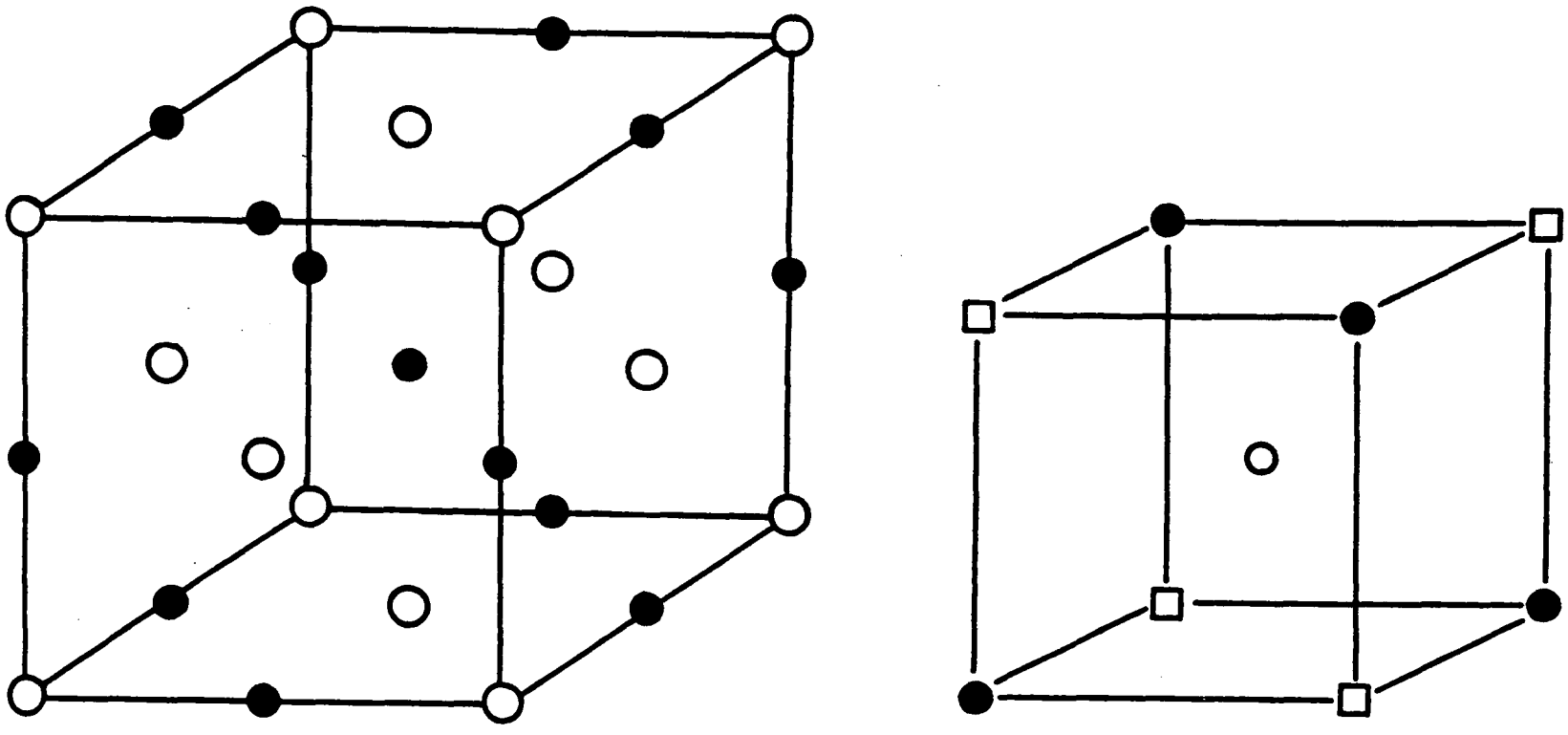


Figure 9.2. The Rocksalt structure. Open and filled circles represent cations and anions respectively. The basic 4:1 cluster found in the cation-deficient $Fe_{1-x}O$ system is also shown (right).

aggregate in a face-sharing fashion to generate clusters with differing vacancy:interstitial ratios[310].

We present here the results of a room temperature PND study of AgF.

9.2 Experimental

A sample (∿10g) of silver (I) fluoride sealed in a cylindrical quartz ampoule was kindly supplied by N. Bartlett of the University of California, Berkeley. The PND profile was measured on the modified triple-axis spectrometer at the Omega West Reactor, Los Alamos Scientific Laboratory*. A mean wave-

* *The data were collected by A.K. Cheetham and J.L. Yarnell.*

length of 1.2796Å was taken from the (220) planes of a Cu monochromator at a take-off angle of ∿60° and calibrated from the diffraction pattern of a NbO standard. The data for AgF were collected over the range $10° < 2\theta < 100°$ in steps of 0.1° in 2θ. The data were analysed using both integrated intensity and full-matrix profile refinement techniques*. The value for the lattice constant obtained from the latter was $a_o = 4.9325(27)$Å. The integrated intensities were calculated as described in section 7.5 and scattering lengths of 0.60 and 0.56 ($\times 10^{-14}$m) were assumed for Ag and F respectively.

9.3 Results

In Fm3m, for silver at 000 (4a) and fluorine at ½½½ (4b), the integrated intensity refinements converged to R_I = 0.0433. The Debye-Waller factors were 2.8(3)Å² (Ag) and 3.6(4)Å² (F). The corresponding observed and calculated reflection intensities are listed in Table 9.1.

Several other models were also tested in least-squares to probe the possible occurrence of defects or defect-clusters. In separate refinements, the silver and fluorine occupancies were allowed to vary, but they converged to 4.0(3) and 4.0(3) respectively, compared with the expected value of 4.0. There was no evidence for occupation of any interstitial sites. The occupancies of a fluorine entered separately at ¼¼¼ (8c), ¼¼0 (24d) and 0.2 0.2 ¼ (96k) converged to values of -0.09(5), -0.04(14) and -0.13(6) respectively. The integrated intensities were converted to structure factor moduli (Equation 11, Chapter 2) which were used as coefficients in Fourier and difference Fourier

* *An interactive Fortran program suite was written by the author for the CDC 7600 at Los Alamos Scientific Laboratory to facilitate the handling of PND data.*

syntheses, but the only significant peaks, other than those of Ag(1) and F(1), were at ½ 0.159 0.159 (48i). The occupancy of this site refined to 0.5(3). The residual was slightly improved R_I = 0.0347, as it had been for all of these refinements. This site is separated by 1.1Å along <110> from F(1); the contact to Ag(1) is 1.86Å. On the basis of the present data set, we cannot unequivocally say that there is no occupation of this site, although this would appear likely.

9.4 Conclusion

We have shown that AgF adopts the rocksalt structure and we find no evidence for the widespread occurrence of defects or defect clusters. The Debye-Waller factors of 2.8Å² (Ag) and 3.6Å² (F) compare with the corresponding values in AgF_2 of 1.4Å² (Ag) and 1.5Å² (F)[305] and in the zinc blende structure of γ-CuBr of 2.8Å² (Cu) and 2.7Å² (Br)[311]. The large values for AgF are probably correlated with the anomalously large value of the lattice constant.

TABLE 9.1

Final observed and calculated reflection intensities from the PND data refinements of AgF at room temperature.

h	k	l	I_{calc}	I_{obs}	$\sigma(I_{obs})$
1	1	1	84	0	80
2	0	0	20955	21459	172
2	2	0	16782	16155	157
3	1	1	123	244	67
2	2	2	5994	5761	121
4	0	0	2721	3135	129
3	3	1	91	0	80
4	2	0	7059	7251	145
4	2	2	4796	4953	131
5	1	1	94	0	80
3	3	3			
4	4	0	1223	1140	117

$R_I = 0.0433$ AF = 0.0248

$B_{ag} = 2.8(3)Å^2$ $B_F = 3.6(4)Å^2$

REFERENCES

To optimise clarity, the most commonly cited journals are abbreviated as follows :-

AC	Acta Crystallographica
ACS	Acta Chemica Scandinavica
CPL	Chemical Physics Letters
FITS,Wisconsin	"Fast Ion Transport in Solids" Eds. P.Vashishta J.N.Mundy, and G.K.Shenoy (Proceedings of the International Conference on Fast Ion Transport in Solids,Electrodes and Electrolytes, Lake Geneva, Wisconsin, U.S.A., May 21-25 (1979)
IC	Inorganic Chemistry
JAC	Journal of Applied Crystallography
JACS	Journal of the American Chemical Society
JACerS	Journal of the American Ceramic Society
JAP	Journal of Applied Physics
JCP	Journal of Chemical Physics
JCS	Journal of the Chemical Society (London)
JES	Journal of the Electrochemical Society
JINC	Journal of Inorganic and Nuclear Chemistry
JMS	Journal of Materials Science
JPC	Journal of Physical Chemistry
JPCS	Journal of the Physics and Chemistry of Solids
JPhys C	Journal of Physics C
JPhys D	Journal of Physics D
JSSC	Journal of Solid State Chemistry
MRB	Materials Research Bulletin
PR	Physical Review

PRL Physical Review Letters

SSC Solid State Communications

"Superionic Conductors" "Superionic Conductors" Ed. by G.D.Mahan and W.L.Roth (Plenum Press, New York, London 1976)

ZK Zeitschrift für Kristallographie

ZN Zeitschrift für Naturforschung

ZPC Zeitschrift für Physikalische Chemie neues folges (Frankfurt)

1. International Tables for X-Ray Crystallography Vols. I - IV
The Kynoch Press,Birmingham (1952,1974)

2. A.L.Patterson ZK A90 517 (1935)

3. M.M.Woolfson "Direct Methods in Crystallography"
Oxford University Press (1961)

4. J.R.Carruthers and D.J.Watkin AC A35 698 (1979)

5. J.Waser AC 16 1091 (1963)

6. J.R.Carruthers CRYSTALS User Manual (1975)
Oxford University Computing Laboratory

7. A.C.Larson in "Crystallographic Computing" p.291
Ed. F.R.Ahmed Munksgaard,Copenhagen (1969)

8. D.T.Cromer and J.B.Mann Los Alamos Scientific Laboratory
Report, LA-3816 (1967)

9. R.Spagna personal communication

10. G.E.Bacon "Neutron Diffraction" 3rd. Edition,Clarendon Press
Oxford (1975)

11. W.Marshall and S.W.Lovesey "Theory of thermal neutron
scattering" Oxford University Press (1971)

12. G.L.Squires "Thermal Neutron Scattering" Cambridge
University Press,Cambridge (1978)

13. G.E.Bacon AC A28 357 (1972)
" AC A30 847 (1974)

14. B.C.Tofield personal communication

15. W.L.Roth,F.Reidinger and S.Laplaca "Superionic Conductors"
pp.223-241 (1976)

16. P.Wiseman D.Phil Thesis Oxford (1974)

17. H.M.Rietveld AC 22 151 (1967)

18. H.M.Rietveld JAC 2 65 (1969)

19. G.Malmros and J.O.Thomas JAC 10 7 (1977)

20. D.Armytage D.Phil Thesis Oxford (1975)

21. S.J.Turner unpublished work

22. G.Caglioti,A.Paoletti and F.P.Ricci Nucl. Instrum. 3 223 (1958)

23. B.T.M.Willis AC 13 763 (1960)

24. M.J.Cooper and J.P.Sayer JAC 8 615 (1975)

25. M.J.Cooper and K.D.Rouse in "Thermal Neutron Diffraction" Ed. B.T.M.Willis Oxford University Press (1970)

26. A.W.Hewat A.E.R.E Report RRL 73/239 Atomic Energy Research Establishment,Harwell,England (1973)

27. T.M.Sabine and P.J.Clarke JAC 10 277 (1977)
P.J.Clarke unpublished (Oxford Rietveld Refinements User Manual (1976))

28. A.R.Rae-Smith,A.K.Cheetham and A.J.Skarnulis JAC 12 485 (1979)

29. "GPCP A general purpose contouring program" User's Manual California Computer Products Inc.(CALCOMP) (1971)

30. A.K.Cheetham and J.C.Taylor JSSC 21 253 (1977)

31. "Neutron beam facilities at the HFR available for users" Institute Laue-Langevin,Grenoble,France (1977)

32. Enraf-Nonius CAD-4F Diffractometer User Handbook,Enraf-Nonius,Delft,Holland (1977)

33. A.H.Baston and D.H.C.Harris Eds. A.E.R.E. Report R9278 (1978)

34. A.W.Hewat Nucl.Inst.Meth. 127 361 (1975)
A.W.Hewat and I.Bailey Nucl.Inst.Meth. 137 463 (1976)

35. G.A.Rankin and H.E.Merwin JACS 38 568 (1916)

36. S.B.Hendricks and L.Pauling ZK 64 303 (1927)

37. W.L.Bragg,C.Gottfried and J.West ZK 77 255 (1931)

38. R.Ridgway,A.Klein and W.O'Leary Trans. Electrochem. Soc. 70 71 (1936)

39. C.A.Beevers and M.A.S.Ross ZK 97 59 (1937)

40. M.O.Lamar,W.M.Hazel and W.J.Leary Ind. Eng. Chem. Anal. Ed. 7 429 (1935)

41. C.A.Beevers and S.Brohult ZK 95 472 (1936)

42. J.Felsche Naturwissenschaften 54 612 (1967)
" ZK 127 94 (1968)

43. C.R.Peters,M.Bettman,J.W.Moore and M.D.Glick AC B27 1826 (1971)

44. F.Reidinger D.Phil Thesis,New York State University,Albany, New York (1979)

45. N.Weber and A.Venero Am. Ceram. Soc. Meeting Paper 4-J1-70 May 1970

46. J.T.Kummer Progr. Solid State Chem. 7 141 (1972)

47. G.Yamaguchi J. Japan Electrochem. Soc. 11 260 (1943)

48. G.Yamaguchi and K.Suzuki Bull. Chem. Soc. Japan 41 93 (1968)

49. M.Bettman and C.R.Peters JPC 73 1774 (1969)

50. O.Greis and D.J.M.Bevan to be published

51. J.O.Bovin AC A35 572 (1979)

52. Ph.Colomban D.Sc Thesis,Université Pierre et Marie Curie, Paris,June 1979

53. W.L.Roth in "Crystal Structure and Chemical Bonding in Inorganic Chemistry" pp.85-102 C.J.Rooymans and A.Rabenau Eds.,North-Holland,The Netherlands (1975)

54. M.Bettman and L.L.Terner IC 10 1442 (1971)

55. A.K.Ray and E.C.Subbarao MRB 10 583 (1975)

56. R.J.Bangham and R.A.Lefever MRB 10 607 (1975)

57. L.R.Rothrock J. Crystal Growth 39 180 (1977)

58. J.B.Bates,G.M.Brown,W.E.Brundage,J.C.Wang and H.Engstrom FITS,Wisconsin pp.261-266 (1979)

59. Y.F.Yao and J.T.Jummer JINC 29 2453 (1967)

60. J.T.Kummer and N.Weber U.S. Patent No.3404036 Oct. 1 (1968) and U.S. Patent No.3413150 Nov. 26 (1968)

61. N.A.Toropov and M.M.Stukalova C.R. Akad. Sci. SSSR 24 459 (1939)
N.A.Toropov and M.M.Stukalova C.R.Akad. Sci. SSSR 27 974 (1940)

62. R.H.Radzilowski and J.T.Kummer IC 8 2531 (1969)

63. R.H.Radzilowski IC 8 994 (1969)

64. M.S.Whittingham,R.W.Helliwell and R.A.Huggins
U.S. Govt. Res. Dev. Report 69 228 (1969)

65. J.A.Little and D.J.Fray FITS,Wisconsin pp.323-327 (1979)

66. H.Saalfeld,H.Mathies and S.K.Datta Ber. Deut. Keram. Ges.
45 212 (1968)

67. T.Nishikawa,T.Nishida,Y.Katsuyama,Y.Kawakita and I.Uei
Nippon Kagaku Kaishi 6 1048 (1974)

68. B.A.Bellamy,A.Hooper,A.E.Hughes,J.M.Newsam,C.F.Sampson and
B.C.Tofield to be published in "Energy and Ceramics"
Elsevier,Amsterdam (1979)

69. P.D.Dernier and J.P.Remeika JSSC 17 245 (1976)

70. T.Kodama and G.Muto JSSC 19 35 (1976)

71. W.L.Roth JSSC 4 60 (1972)

72. T.Kodama and G.Muto JSSC 17 61 (1976)

73. B.C.Tofield,A.J.Jacobson,W.A.England,P.J.Clarke and M.W.Thomas
JSSC 30 1 (1979)

74. K.Kato and H.Saalfeld AC B33 1596 (1977)

75. Ph.Colomban,J.P.Boilot,A.Kahn and G.Lucazeau
Nouv. J. Chim. 2 21 (1978)

76. R.C.T.Slade,T.K.Halstead and P.McGeehin SSC 31 343 (1979)

77. J.H.Kennedy in "Solid Electrolytes" pp.105-141 Ed. S.Geller
Springer-Verlag (1977)

78. A.Imai and M.Harata Japan J. Appl. Phys. 11 180 (1972)

79. A.Hooper JPhys D 10 1487 (1977)

80. M.S.Whittingham and R.A.Huggins JES 118 1 (1971)

81. M.S.Whittingham and R.A.Huggins NBS Special Publication
364 139 (1972)

82. R.H.Radzilowski and J.T.Kummer JES 118 714 (1971)

83. G.C.Farrington,J.L.Briant,M.W.Breiter and W.L.Roth JSSC 24 311 (1978)

84. A.Hooper,B.C.Tofield and C.F.Sampson FITS,Wisconsin pp.409-412 (1979)

85. G.C.Farrington and J.L.Briant to be published

86. G.C.Farrington and W.L.Roth "Superionic Conductors" p.418 (1977)

87. T.Kaneda.J.B.Bates,J.C.Wang and H.Engstrom FITS,Wisconsin pp.371-374 (1979)

88. W.L.Roth and G.C.Farrington Science 196 1332 (1977)

89. G.C.Farrington private communication

90. R.E.Walstedt,R.S.Berg,J.P.Remeika,A.S.Cooper and B.E.Prescott FITS,Wisconsin pp.355-360 (1979)

91. G.C.Farrington and J.L.Briant FITS,Wisconsin pp.395-400 (1979)

92. G.C.Farrington and J.L.Briant MRB 13 763 (1978)

93. J.B.Bates private communication

94. T.J.Whalen,G.J.Tennenhouse and C.Meyer JACerS 57 497 (1974)

95. A.Virkar,G.J.Tennenhouse and R.S.Gordon JACerS 57 508 (1974)

96. J.H.Kennedy and A.F.Sammells JES 119 1609 (1972)

97. I.Wynn Jones and L.J.Miles Proc. Br. Ceram. Soc. 19 161 (1971)

98. A.Imai and M.Harata Japan J. Appl. Phys. 11 180 (1972)

99. J.P.Boilot,A.Kahn,J.Théry,R.Collongues,J.Antoine,D.Vivien, C.Chevrette and D.Gourier Electrochim. Acta 22 741 (1977)

100. J.R.Akridge and J.H.Kennedy JSSC 26 147 (1978)

101. J.R.Akridge,B.Srour,C.Meyer,Y.Gros and J.H.Kennedy JSSC 25 169 (1978)

102. J.R.Akridge and J.H.Kennedy JSSC 29 63 (1979)

103. R.C.Barklie and K.O'Donnell JPhys C 10 4127 (1977)

104. J.Antoine,D.Vivien,J.Livage,J.Théry and R.Collongues
MRB 10 865 (1975)

105. R.C.Barklie , K.O'Donnell and A.Murtagh JPhys C 10
4815 (1977)

106. A.Bergstein and W.B.White JINC 33 1629 (1971)

107. J.M.P.J.Verstegen and J.L.Sommerdijk J. Lumin. 10 31 (1975)

108. J.Antoine,D.Vivien,J.Théry,R.Collongues and J.Livage
JSSC 21 349 (1977)

109. D.Gourier,J.Antoine,D.Vivien,J.Théry ,J.Livage and
R.Collongues Phys. Stat. Solidi (a) 41 423
(1977)

110. R.C.Barklie,K.O'Donnell and B.Henderson JPhys C 11 3881 (1978)

111. R.L.Cohen,J.P.Remeika and K.W.West J. Phys.(Paris) Colloq.
C6-513 (1974)

112. D.B.McWhan,S.J.Allen,J.P.Remeika and P.D.Dernier
PRL 35 953 (1975)

113. D.B.McWhan,P.D.Dernier,C.Vettier,A.S.Cooper and J.P.Remeika
PR B17 4043 (1978)

114. W.L.Roth Trans. Am. Cryst. Assoc. 11 51 (1975)

115. R.R.Dubin,J.S.Kasper,J.B.Bates and T.Kaneda
FITS,Wisconsin pp.361-365 (1979)

116. L.M.Foster FITS,Wisconsin pp.249-254 (1979)

117. L.C.De Jonghe JMS 14 33 (1979)

118. W.N.Unertl,L.C.De Jonghe and Y.Y.Tu JMS 12 739 (1977)

119. G.Collin,J.P.Boilot,A.Kahn,J.Thery and R.Comes
JSSC 21 283 (1977)

120. B.C.Tofield and G.C.Farrington Nature 278 438 (1979)

121. W.A.England,B.C.Tofield and A.J.Jacobson to be published

122. B.C.Tofield and J.M.Newsam FITS,Wisconsin pp.389-393 (1979)

123. Y.Le Cars,R.Comes,L.Deschamps and J.Thery AC A30 305 (1974)

124. J.P.Boilot,J.Thery,R.Collongues,R.Comes and A.Guinier
AC A32 250 (1976)

125. J.P.Boilot,P.Colomban,J.Thery,G.Collin and R.Comes
J. Phys. (Paris) Colloq. C2-204 (1978)

126. J.P.Boilot,A.Kahn,J.Thery,G.Collin and R.Comes
J. Phys. (Paris) Colloq. C7-145 (1977)

127. G.Collin,P.Colomban,J.P.Boilot and R.Comes
FITS,Wisconsin pp.309-314 (1979)

128. W.L.Roth NBS Special Publication 364 129 (1972)

129. D.J.M.Bevan,B.Hudson and P.T.Moseley MRB 9 1073 (1974)

130. H.Sato and Y.Hirotsu MRB 11 1307 (1976)

131. L.C.De Jonghe JMS 10 2173 (1975)

132. L.C.De Jonghe JMS 11 206 (1976)

133. L.C.De Jonghe JACerS 62 289 (1979)

134. R.Stevens JMS 9 801 (1974)

135. R.Stevens and L.J.Miles JMS 11 1911 (1976)

136. R.D.Armstrong,P.M.A.Sherwood and R.A.Wiggins
Spectrochim. Acta .A30 1213 (1974)

137. A.S.Barker,J.A.Ditzenberger and J.P.Remeika PR B14 386 (1976)

138. S.J.Allen and J.P.Remeika PRL 33 1478 (1974)

139. W.M.Risen and W.M.Butler "Superionic Conductors" pp.372-373
(1976)

140. S.J.Allen,L.C.Feldman,D.B.McWhan,J.P.Remeika and R.W.Walstedt
"Superionic Conductors" p.279 (1976)

141. S.J.Allen,A.S.Cooper,F.De Rosa,J.P.Remeika and S.K.Ulasi
PR B17 4031 (1978)

142. U.Strom,P.C.Taylor,S.G.Bishop,T.L.Reinecke and K.L.Ngai
PR B13 3329 (1976)

143. H.R.Chandrasekhar,G.Burns and G.V.Chandrasekhar
SSC 27 829 (1978)

144. R.Frech and J.B.Bates Spectrochim. Acta A35 685 (1979)

145. L.L.Chase,C.H.Hao and G.D.Mahan SSC 18 401 (1976)

146. C.H.Hao,L.L.Chase and G.D.Mahan PR B13 4306 (1976)

147. J.B.Bates and R.Frech CPL 50 89 (1977)

148. A.S.Barker,J.A.Ditzenberger and J.P.Remeika PR B14 4254
(1976)

149. A.C.Anderson FITS,Wisconsin pp.255-259 (1979)

150. J.C.Wang,M.Gaffari and S.Choi JCP 63 772 (1975)

151. D.B.McWhan,S.Shapiro,J.P.Remeika and G.Shirane
JPhys C 8 L487 (1975)

152. S.Shapiro "Superionic Conductors" pp.261-277 (1976)

153. D.B.McWhan,C.M.Varma,F.L.S.Hsu and J.P.Remeika
PR B15 553 (1977)

154. P.J.Anthony and A.C.Anderson PR B16 3827 (1977)

155. P.J.Anthony and A.C.Anderson PR B19 5310 (1979)

156. R.H.Radzilowski,Y.F.Yao and J.T.Kummer JAP 40 4716 (1969)

157. D.Kline,H.S.Story and W.L.Roth JCP 57 5180 (1972)

158. D.Jerome and J.P.Boilot J. Phys. (Paris) Letters 35 L129
(1974)

159. I.Chung,H.S.Story and W.L.Roth Bull. Am. Phys. Soc.
Series II 19 202 (1974)

160. I.Chung,H.S.Story and W.L.Roth JCP 63 4903 (1975)

161. W.Bailey,S.Glowinkowski,H.Story and W.L.Roth
JCP 64 4126 (1976)

162. R.E.Walstedt,R.Dupree,J.P.Remeika and A.Rodriguez
PR B15 3442 (1977)

163. W.L.Roth,I.Chung and H.S.Story JACerS 60 311 (1977)

164. R.R.Dubin,H.S.Story,R.W.Powers and W.C.Bailey
MRB 14 185 (1979)

165. J.L.Bjorkstram and M.Villa FITS,Wisconsin pp.293-296 (1979)

166. D.C.Ailon and C.E.Hayes FITS,Wisconsin pp.301-304 (1979)

167. M.W.Breiter and G.C.Farrington MRB 13 1213 (1978)

168. M.S.Whittingham and R.A.Huggins JCP 54 414 (1971)

169. M.J.Rice and W.L.Roth JSSC 4 294 (1972)

170. W.Van Gool and P.H.Bottelberghs JSSC 7 59 (1973)

171. B.A.Huberman and P.N.Sen PRL 33 1379 (1974)
P.N.Sen and B.A.Huberman PRL 34 1059 (1975)

172. H.Sato and R.Kikuchi JCP 55 677 (1971)
H.Sato and R.Kikuchi FITS,Wisconsin pp.337-340 (1979)

173. G.E.Murch and R.J.Thorn Phil. Mag. 35 493 (1977),
ibid 36 518 (1977), *ibid* 36 529 (1977)

174. D.Wolf FITS,Wisconsin pp.341-344 (1979)

175. S.W.De Leeuw and J.W.Perram FITS,Wisconsin pp.345-348
(1979)

176. L.Glasser Chem. Rev. 75 21 (1975)

177. L.B.Harris and C.J.Vella JAP 37 4294 (1966)

178. J.M.Thomas and T.A.Clarke Trans. Faraday Soc. 65 2718 (1969)

179. A.Potier and D.Rousselet J. Chim. Phys. 70 873 (1973)

180. M.G.Shilton and A.T.Howe MRB 12 701 (1977)

181. W.A.England,A.J.Jacobson and B.C.Tofield
JCS Chem. Comm. 895 (1976)

182. T.Kaneda,J.B.Bates,J.C.Wang and H.Engstrom MRB 14 1053
(1979)

183. J.Jensen and P.McGeehin JMS 13 909 (1978)

184. M.W.Breiter,G.C.Farrington,W.L.Roth and J.L.Duffy
MRB 12 895 (1977)

185. W.L.Roth,M.W.Breiter and G.C.Farrington JSSC 24 321 (1978)

186. P.Colomban,G.Lucazeau,R.Mercier and A.Novak
JCP 67 5244 (1977)

187. G.C.Farrington,J.L.Briant and H.S.Story Extended Abstracts
Second Int. Meeting on Solid Electrolytes,St. Andrews,
Scotland (Sept. 1978)

188. R.C.T.Slade,P.J.Fridd,T.K.Halstead and P.McGeehin
A.E.R.E. Report R9217 (1978)
to be published in JSSC

189. D.Gourier and B.Sapoval JPhys C 12 3587 (1979)

190. J.D.Axe,L.M.Corliss,J.M.Hastings,W.L.Roth and O.Muller
JPCS 39 155 (1978)

191. S.J.Turner personal communication

192. J.B.Bates,T.Kaneda and J.C.Wang SSC 25 629 (1978)

193. W.L.Roth,M.Anne.D.Tranqui and D.Heidelmann
FITS,Wisconsin pp.267-271 (1979)

194. A.R.West MRB 14 441 (1979)

195. R.Collongues MRB 13 1281 (1978)

196. J.P.Boilot,P.Colomban,R.Collongues,G.Collin and R.Comes
PRL 42 785 (1979)

197. L.M.Foster and H.C.Stumpf JACS 73 1591 (1951)

198. J.P.Boilot,J.Thery and R.Collongues MRB 8 1143 (1973)

199. K.Kuwabara and T.Takahashi JSSC 19 147 (1973)

200. L.M.Foster and J.E.Scardefield JES 123 141 (1976)

201. B.M.Foxman,S.J.Laplaca and L.M.Foster "Superionic Conductors"
pp.419-420 (1976)

202. H.C.Brinkhoff JPCS 35 1225 (1974)

203. H.R.Chandrasekhar,G.Burns and G.V.Chandrasekhar
SSC 25 547 (1978)

204. G.Burns,G.V.Chandrasekhar,F.H.Dacol and L.M.Foster
SSC 21 1057 (1977)

205. L.M.Foster and C.V.Arbach "Superionic Conductors" pp.420-421 (1976)

206. R.S.Title and G.V.Chandrasekhar "Superionic Conductors" p.421 (1976)

207. P.Braun Philips Research Reports 12 491 (1957)

208. D.J.Dyson and W.Johnson Trans. Br. Ceram. Soc. 72 49 (1973)

209. W.L.Roth and R.J.Romanczuk JES 116 975 (1969)

210. C.J.M.Rooymans,C.Langerais and J.A.Schulkes SSC 4 85 (1965)

211. G.J.Dudley,B.C.H.Steele and A.T.Howe JSSC 18 141 (1976)

212. G.J.Dudley and B.C.H.Steele JSSC 21 1 (1977)

213. T.Takahashi,K.Kuwabara and Y.Kase Nippon Kagaku Kaishi 1305 (1975)

214. K.Kuwabara and T.Takahashi J. Appl. Electrochem. 7 339 (1977)

215. G.J.Dudley and B.C.H.Steele JMS 13 1267 (1978)

216. J.H.Kennedy and A.F.Sammells JES 121 1 (1974)

217. A.T.Howe and G.J.Dudley JSSC 18 149 (1976)

218. A.T.Howe and G.J.Dudley JSSC 30 157 (1979)

219. K.O.Hever JES 115 826 (1968)

220. J.Dexpert-Ghys,M.Faucher and P.Caro JSSC 19 193 (1976)

221. R.C.Ropp and G.G.Libowitz JACerS 61 473 (1978)

222. G.J.Tennenhouse U.S. Patent 3,446,677 (May 27,1969)

223. M.W.Thomas personal communication

224. J.M.Adams,R.G.Pritchard and A.W.Hewat AC B35 1759 (1979)

225. G.J.May and C.M.B.Henderson JMS 14 1229 (1979)

226. R.E.Newnham and Y.M.De Haan ZK 117 235 (1962)
C.T.Prewitt,R.D.Shannon,D.B.Rogers and A.W.Sleight IC 8 1985 (1969)

227. J.P.Boilot personal communication

228. A.W.Hewat "POWDER retrieval and refinement system" Institute Laue-Langevin Report (1978)

229. J.M.Newsam unpublished work

230. G.Collin,J.P.Boilot,Ph.Colomban and R.Comes JPCS 41 47 (1980)

231. B.C.Tofield and J.M.Newsam unpublished work

232. L.Holden,W.Hayes and B.C.Tofield to be published

233. C.F.Sampson.J.M.Newsam,A.K.Cheetham and B.C.Tofield "Annex to the annual report,1977" Institute Laue-Langevin, Grenoble p.144 (1978)

234. M.S.Lehmann and F.K.Larsen AC A34 580 (1974)

235. A.Lautie,F.Froment and A.Novak Spectroscopy Lett. 9 289 (1976)

236. B.C.Tofield personal communication

237. J.M.Newsam and B.C.Tofield to be submitted to MRB

238. J.M.Newsam and B.C.Tofield to be submitted to Nature

239. A.Hooper,P.McGeehin,K.T.Harrison and B.C.Tofield JSSC 24 265 (1978)

240. K.Hauffe and D.Hoeffgen ZPC 49 94 (1966)

241. A.Kvist and A.Lunden ZN 20A 235 (1965)

242. J.M.Newsam,A.K.Cheetham and B.C.Tofield FITS,Wisconsin pp.435-438 (1979)

243. M.Palazzi and F.Remy Bull. Soc. Chim. France 2795 (1971)

244. R.Masse,I.Tordjman and A.Durif ZK 144 76 (1976)

245. L.Helmholz JPC 4 316 (1936)

246. H.N.Ng,C.Calvo and R.Faggiani AC B34 898 (1978)

247. W.C.Hamilton AC 18 502 (1965)

248. N.N.Greenwood "Ionic Crystals,Lattice Defects and Non-Stoichiometry" Butterworth (1968)

249. "Powder Diffraction File" JCPDS Int. Centre for Diffraction Data,Pennsylvania,U.S.A (1978)

250. A.F.Wells "Structural Inorganic Chemistry" 3rd. Edition pp.267-268 Oxford University Press (1967)

251. B.Wendrow and K.A.Kobe Chem. Rev. 54 891 (1954)

252. B.Wanklyn personal communication

253. K.O.Stromme ACS A28 515 (1975)

254. H.G.Smith and H.A.Levy AC 15 1201 (1962)

255. B.C.Tofield in "Structure and Bonding" Vol. 21 Springer-Verlag,Heidelberg (1975)

256. L.Nilsson,J.O.Thomas and B.C.Tofield to be published

257. A.K.Cheetham,B.E.F.Fender and M.J.Cooper JPhys C 3107 (1971)

258. P.Bendall personal communication

259. A.Kvist and A.Bengtzelius in "Fast Ion Transport in Solids" Ed. W. Van Gool, North-Holland p.193 (1973)

260. R.Aronsson,B.Heed,B.Jansson,A.Lunden,L.Nilsson,K.Schroeder, C.A.Sjoblom,J.O.Thomas and B.C.Tofield FITS,Wisconsin pp.471-474 (1979)

261. H.E.Swanson and E.Tatge NBS Circular 539 Vol. I p.13 (1953)

262. M.Sakata and M.J.Cooper JAC 12 554 (1979)

263. H.S.Kim and G.A.Jeffrey AC B27 1123 (1971)

264. J.Schoonman FITS,Wisconsin pp.631-636 (1979)

265. M.Beniere,M.Chemla and F.Beniere JPCS 40 729 (1979)

266. F.C.Kracek JPC 33 1281 (1929)

267. G.E.Brodale and W.F.Giauque JPC 76 737 (1972)

268. J.E.D.Davies and W.F.Sandford JCS Dalton 1912 (1975)

269. F.C.Kracek and C.J.Ksanda JPC 34 1741 (1930)

270. A.G.Nord ACS 27 814 (1973)

271. W.H.Zachariasen and G.E.Ziegler ZK 81 92 (1932)

272. K.Herrmann and W.Ilge ZK 80 402 (1931)
W.H.Zachariasen ZK 82 161 (1932)

273. H.Fischmeister AC 7 776 (1954)

274. J.A.McGinnety AC B28 2845 (1972)

275. J.G.Albright ZK 84 150 (1932)

276. T.Forland and J.Krogh-Moe ACS 11 565 (1957)

277. H.Fischmeister AC 7 641 (1954)

278. H.Fischmeister ZPC 7 91 (1956)

279. A.J.Van den Berg and F.Tuinstra AC B34 3177 (1978)

280. M.Bredig JACS 63 2533 (1941)

281. M.Bredig JPC 46 747 (1942)

282. M.Bredig JPC 47 587 (1943)

283. B.Gossner Neues Jahrb. Mineral. Geol. B57A 89 (1928)
ZK Strukturbericht 1913-1928 p.278 (1929)

284. W.Eysel and Th.Hahn ZK 131 322 (1970)

285. H.Fischmeister Monatshefte Chemie 93 420 (1962)

286. L.S.Ramsdell Am. Mineral. 24 109 (1939)

287. M.E.Hilmy Am. Mineral. 38 118 (1953)

288. C.Calvo and R.Faggiani Can. J. Chem. 53 1849 (1975)

289. T.Forland and J.Krogh-Moe ACS 13 1051 (1959)

290. H.A.Oeye ACS 18 361 (1964)

291. L-I.Staffansson ACS 26 2150 (1972)

292. B.Heed,A.Lunden and K.Schroeder Electrochim. Acta 22 705 (1977)

293. R.Nacken Neues Jahrb. Mineral. Geol. 24A 1 (1907)

294. T.Forland and J.Krogh-Moe AC 11 224 (1958)

295. A.Kvist ZN 21A 1221 (1966)

296. K.Schroeder and A.Kvist ZN 24A 844 (1969)

297. A.Kvist ZN 22A 208 (1967)

298. H.H.Hofer,W.Eysel and U.v.Alpen ZK 149 88 (1979)

299. S.H.Caulder,K.H.Stern and F.L.Carter JINC 36 234 (1974)

300. K.T.Jacob and D.Bhogeswara Rao JES 126 1842 (1979)

301. M.Natarjan and E.A.Secco Can. J. Chem. 53 1542 (1975)

302. A.L.Geddes and G.L.Bottger IC 8 802 (1969)

303. A.Polischuk and T.M.Shurkhal Ukr. Khim. Zh. 38 833 (1972)
Translated in Soviet Progress in Chemistry 38 92 (1972)

304. R.B.Corey and R.W.G.Wyckoff ZK 87 264 (1934)

305. P.Fischer,D.Schwarzenbach and H.M.Rietveld
JPCS 32 543 (1971)

306. P.Charpin,P.Plurier and P.Meriel Bull. Soc. Fr. Min. Crist
93 2 (1970)

307. H.Ott ZK 63 222 (1926)

308. J.C.Jamieson,P.M.Halleck,R.B.Roof and C.W.F.T.Pistorius
JPCS 36 939 (1975)

309. W.L.Roth AC 13 140 (1960)

310. P.D.Battle and A.K.Cheetham JPhys C 12 337 (1979)

311. N.M.Butt,K.D.Rouse and M.W.Thomas AC A34 759 (1978)

312. N.Bartlett personal communication

313. "Handbook of Chemistry and Physics" Ed. R.C.Weast p.F198
55th. Edition,CRC Press (1974)

APPENDICES

APPENDIX 1

Intensity data for the refinements described in Chapter 4

Deuterium beta alumina at 4.2K A3

Deuterium beta alumina at 298K A6

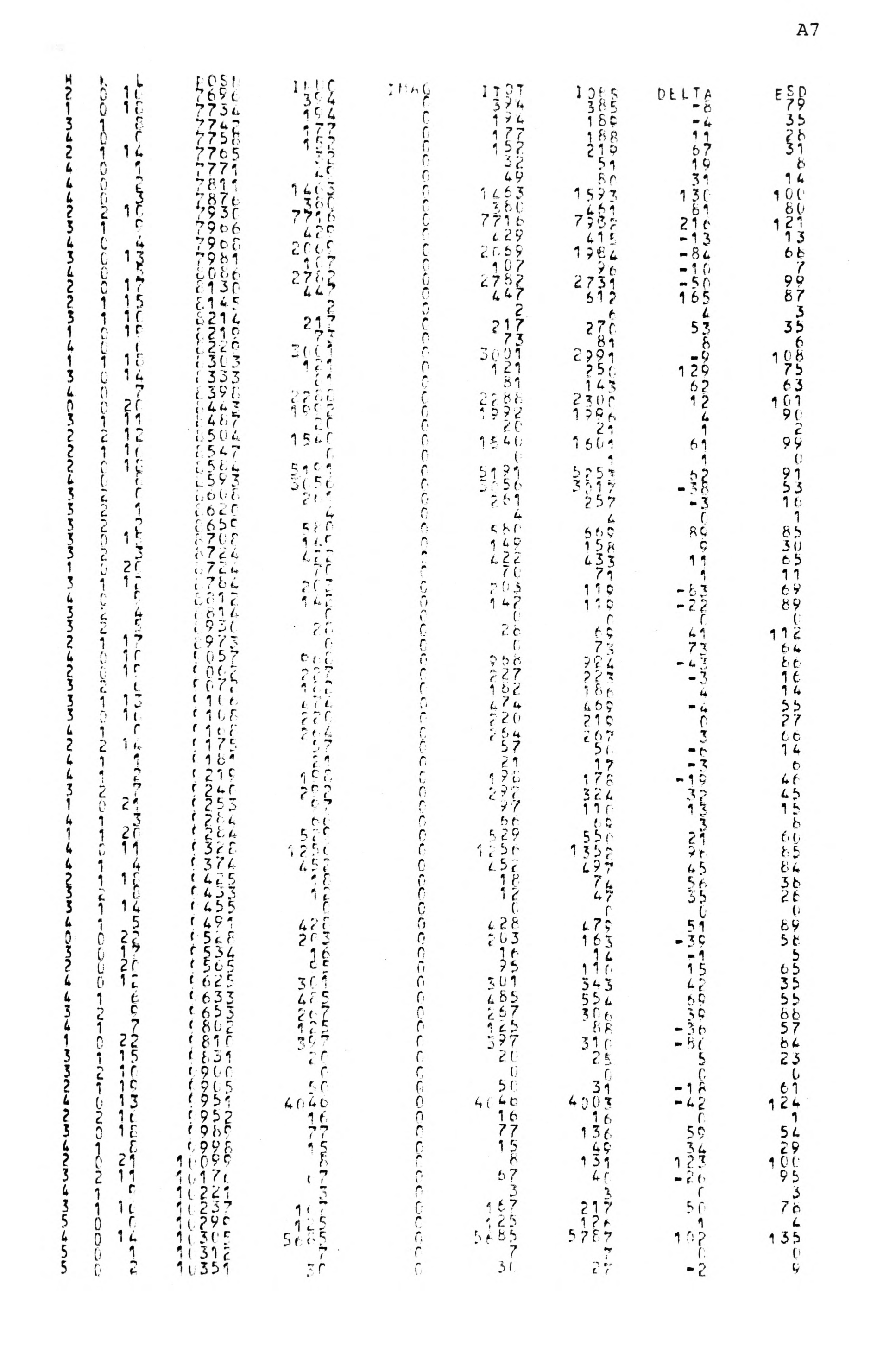
Deuterium beta alumina at 573K A9

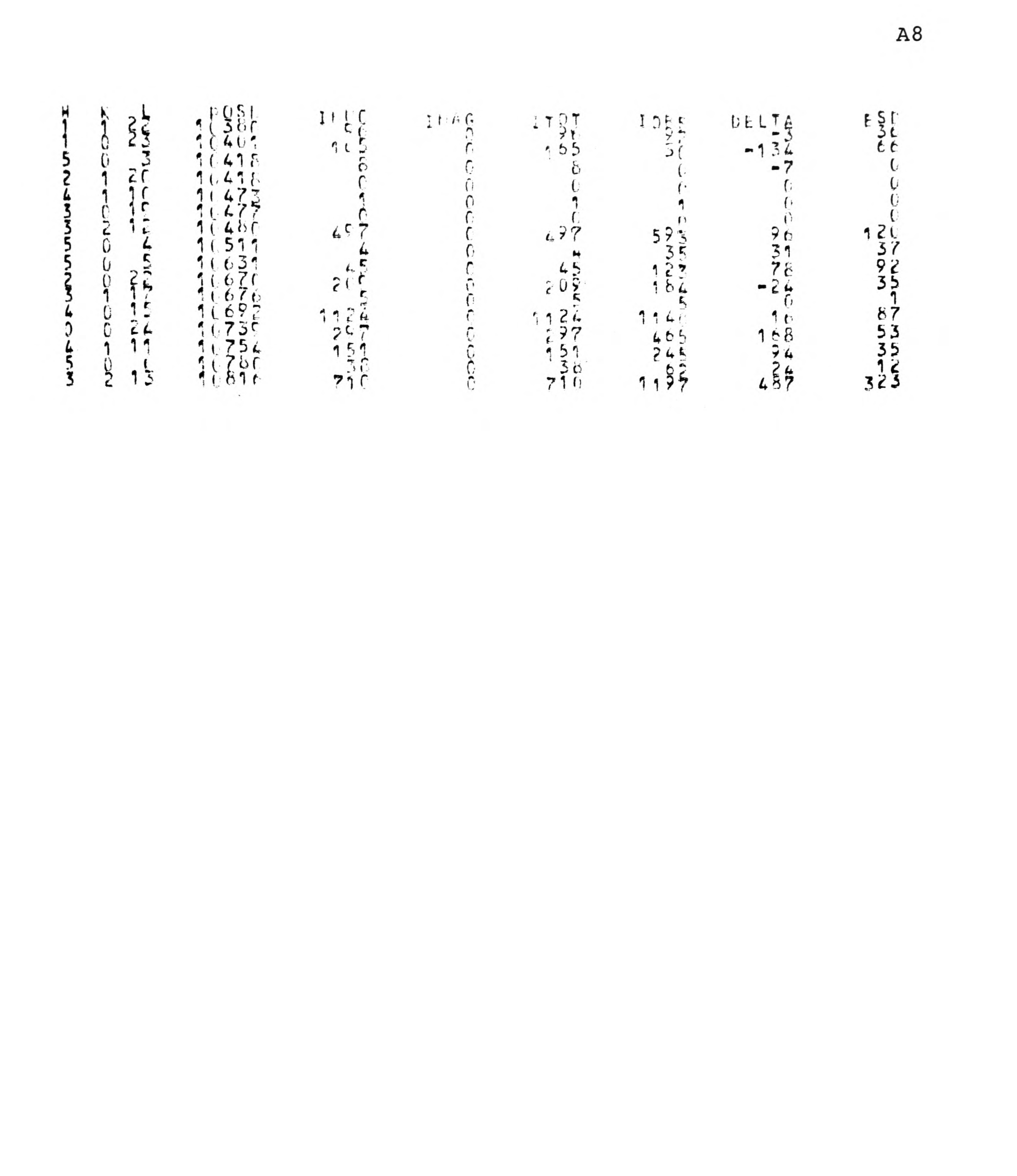
α-Al_2O_3 at 573K deconvoluted from the data on Deuterium beta alumina at that temperature A12

Deuterium beta alumina at 720K A13

'Deuterium beta" alumina' at 4.2K A16

For each reflection,the listing includes the Bragg angle,2θ (POSN),the calculated integrated intensity(INUC and ITOT),the observed integrated intensity(IOBS),the difference between the two(DELTA) and the estimated standard deviation of the observed intensity(ESD).The column headed IMAG is superfluous.





H	K	L	FOSH	IOBS	IMAG	ITST	IOBS	DELTA	ESD
1	0	1	6664	456	0	456	591	135	164
1	0	2	9666	15	0	15	161	146	162
1	1	0	3127	247	0	247	297	50	115
1	1	1	1153	851	0	851	879	28	135
1	1	2	2551	34	0	34	7	-26	109
1	1	3	8889	1237	0	1237	1219	-17	146
1	2	0	5529	1596	0	1596	1575	-20	159
1	2	1	6631	145	0	145	217	72	106
1	2	2	6554	414	0	414	452	18	70
1	2	3	6676	498	0	498	517	19	90
1	3	0	9932	6806	0	6806	7007	201	152
1	3	1	9954	984	0	984	994	10	28
1	3	2	9887	1311	0	1311	1303	-7	22
1	3	3	9888	7968	0	7968	7911	-56	142
2	0	0	4165	9962	0	9962	9672	-289	176
2	0	1	4355	671	0	671	665	-5	13
2	0	2	4375	9672	0	9672	9583	-88	189
2	0	3	4492	1	0	1	0	0	0
2	1	0	4613	8033	0	8033	8144	111	178
2	1	1	4735	1119	0	1119	1129	10	98
2	1	2	4758	497	0	497	212	-284	127
2	1	3	4876	8796	0	8796	8422	-373	162
2	2	0	4884	150	0	150	142	-7	13
2	2	1	4911	124	0	124	68	-55	71
2	2	2	5022	50	0	50	0	-49	0
2	2	3	5046	37	0	37	0	-36	0
2	3	0	5117	152	0	152	74	-77	69
2	3	1	5127	401	0	401	350	-40	78
2	3	2	5151	132	0	132	264	132	51
2	3	3	5262	168	0	168	364	196	73
3	0	0	5467	14	0	14	0	-13	0
3	0	1	5488	2408	0	2408	2499	91	145
3	0	2	5522	22	0	22	25	3	5
3	0	3	5534	934	0	934	859	-64	130
3	1	0	5613	548	0	548	235	-312	254
3	1	1	5633	8	0	8	5	-2	3
3	1	2	5773	18	0	18	0	-17	0
3	1	3	5813	2674	0	2674	2663	-11	126
3	2	0	5912	468	0	468	470	2	45
3	2	1	5945	498	0	498	458	-40	107
3	2	2	5914	756	0	756	868	112	124
3	2	3	5942	52	0	52	53	1	44
3	3	0	5986	359	0	359	457	98	134
3	3	1	6136	552	0	552	585	33	91
3	3	2	6143	495	0	495	522	27	44
3	3	3	6166	745	0	745	788	43	112
4	0	0	6367	9	0	9	294	285	157
4	0	1	6441	1343	0	1343	1502	159	139
4	0	2	6457	8879	0	8879	9210	331	158
4	0	3	6500	0	0	0	0	0	0
4	1	0	6546	8	0	8	0	-8	0
4	1	1	6551	23041	0	23041	23171	130	201
4	1	2	6572	21	0	21	21	0	0
4	1	3	6618	3168	0	3168	3598	430	131
4	2	0	6735	2	0	2	2	0	0
4	2	1	6786	3675	0	3675	3866	191	134
4	2	2	6805	130	0	130	374	244	62
4	2	3	6864	7	0	7	11	4	1
4	3	0	6875	10862	0	10862	11343	481	177
4	3	1	6878	36	0	36	38	2	1
4	3	2	6920	161	0	161	728	567	106
4	3	3	6988	314	0	314	726	412	134
5	0	0	7046	139	0	139	147	8	57
5	0	1	7055	44	0	44	46	2	9
5	0	2	7061	429	0	429	549	120	110
5	0	3	7084	2	0	2	74	72	77
5	1	0	7206	46	0	46	102	56	132
5	1	1	7256	44	0	44	52	8	19
5	1	2	7271	1563	0	1563	1576	13	142
5	1	3	7331	32	0	32	0	-31	0
5	2	0	7355	159	0	159	117	-41	86
5	2	1	7393	384	0	384	402	18	66
5	2	2	7396	292	0	292	308	16	51
5	2	3	7435	84	0	84	34	-50	50
5	3	0	7439	67	0	67	110	43	71
5	3	1	7638	124	0	124	86	-38	105
5	3	2	7685	451	0	451	155	-295	110
5	3	3	7723	76	0	76	54	-21	21
6	0	1	7727	239	0	239	176	-62	60
6	0	2	7741	68	0	68	57	-10	18

H	K	L	IOBS	ICAL	SIGMA	IOBS	ICAL	DELTA	ESD
2	1	14	7752		0	49	59	-9	18
4	1	1	7754		0	88	107	-18	34
4	1	2	7704		0	1256	1542	-285	133
4	1	3	7860		0	333	357	-23	110
2	1	4	7915		0	8801	8602	199	152
3	1	5	7955		0	559	568	-9	21
4	1	6	7952		0	2329	2364	-34	91
3	1	7	7957		0	0	0	0	0
4	1	9	8069		0	2910	3182	-271	140
2	1	10	8117		0	172	227	-54	73
4	1	11	8131		0	115	100	15	68
1	1	12	8207		0	530	290	240	44
4	1	13	8212		0	5	4	1	0
1	1	14	8318		0	3389	3387	2	148
3	1	15	8331		0	33	9	24	71
4	1	16	8432		0	16	17	0	101
2	1	17	8479		0	2516	2619	-102	144
3	1	18	8557		0	1972	1962	10	120
2	1	19	8571		0	24	18	6	2
2	1	20	8575		0	1844	1697	147	130
3	1	21	8611		0	10	81	-70	30
4	1	22	8712		0	6163	6257	-93	120
3	1	23	8807		0	2811	2850	-38	59
3	1	24	8911		0	30	32	-1	3
3	1	25	8923		0	0	0	0	0
3	2	1	8944		0	217	152	65	111
3	2	2	8957		0	49	97	-48	32
1	2	3	8964		0	423	512	-88	106
2	2	4	8971		0	37	36	0	11
3	2	5	8977		0	99	188	-89	102
4	2	6	8991		0	0	72	-71	0
4	2	7	8995		0	0	3	-2	0
2	2	8	9038		0	0	49	-48	0
4	2	9	9047		0	33	0	33	80
2	2	10	9057		0	1201	1081	-79	129
3	2	11	9067		0	307	299	8	28
1	2	12	9073		0	41	38	3	4
3	2	13	9099		0	625	499	126	84
4	2	14	9147		0	201	162	39	30
2	2	15	9157		0	265	301	-35	86
4	2	16	9160		0	70	110	-39	33
4	2	17	9188		0	10	17	-6	6
3	2	18	9219		0	18	162	-143	53
1	2	21	9239		0	228	357	-128	70
4	3	1	9263		0	171	193	-21	37
1	3	2	9270		0	54	63	-8	10
4	3	3	9308		0	475	539	-53	73
4	3	4	9353		0	1658	1580	88	136
2	3	5	9400		0	541	545	-3	349
3	3	6	9412		0	0	0	0	0
3	3	7	9436		0	132	107	75	105
4	3	8	9469		0	0	0	0	0
0	3	9	9514		0	254	305	-40	117
3	3	10	9517		0	248	194	54	68
2	3	11	9550		0	48	37	11	12
4	3	12	9605		0	574	450	124	106
4	3	13	9611		0	188	204	-15	29
3	3	14	9632		0	627	715	-20	91
4	3	15	9779		0	193	196	-12	102
1	3	16	9795		0	0	39	-38	0
3	3	17	9811		0	396	354	32	115
3	3	18	9878		0	45	94	-48	64
2	3	19	9888		0	18	11	7	41
4	3	20	9899		0	16	10	6	19
2	4	16	9932		0	4640	4708	-67	179
3	4	18	9971		0	59	61	-1	2
4	4	8	9974		0	2	2	0	4
2	5	21	10082		0	76	37	39	111
3	5	11	10153		0	468	1	467	134
4	5	9	10197		0	0	45	-44	0
3	5	16	10216		0	0	1	0	0
5	5	0	10273		0	206	306	-99	121
4	5	14	10283		0	55	59	-4	3
5	5	1	10288		0	6257	6435	-157	178
5	5	2	10326		0	23	24	0	1
1	5	22	10363		0	51	68	-6	26
1	5	23	10384		0	12	28	-15	14
5	5	3	10392		0	83	398	-314	122
2	5	20	10399		0	0	3	-2	1
					0	2	20	-17	8

H	K	L	POSN	INTIC	IMAG	ITOT	IOBS	DELTA	FSD
4	1	10	10448	124	0	124	55	-58	40
3	2	12	10456	230	0	260	188	-91	86
5	0	1	10457	6	0	6	4	-1	2
5	0	4	10485	76	0	76	151	75	114
5	0	5	10505	29	0	29	305	276	254

H	K	L	PØSN	INUC	IMAG	ITGT	IØBS	DELTA	ESD
1	0	4	3472	255	0	255	194	-60	188
0	0	6	4111	728	0	728	1496	768	184
1	1	3	4278	4830	0	4830	5493	663	315
2	0	2	4555	52	0	52	380	328	181
1	2	4	5179	812	0	812	292	-519	181
2	1	6	5663	2182	0	2182	2547	465	187
1	2	1	5884	449	0	449	157	-291	181
0	1	2	6020	2	0	2	23	21	72
2	1	8	6033	280	0	280	435	155	169
1	2	5	6546	724	0	724	496	-227	175
2	1	5	6926	343	0	343	935	592	184
1	2	8	7303	1	0	1	0	0	0
2	2	7	7899	283	0	283	80	-202	151
0	3	2	7929	2	0	2	0	-1	0
2	1	6	8172	456	0	456	139	-316	83
0	3	6	8172	456	0	456	139	-316	83
2	3	3	8284	1124	0	1124	742	-381	158
1	3	1	8360	93	0	93	0	-92	0
2	1	2	8477	311	0	311	182	-128	144
1	3	8	8489	42	0	42	0	-41	0
1	0	10	8730	20	0	20	0	-19	0
2	2	0	8893	298	0	298	909	611	156
1	3	4	8945	11	0	11	0	-10	0
1	2	5	9296	82	0	82	0	-81	0
2	4	6	9337	929	0	929	790	-138	180
1	1	2	9641	431	0	431	0	-430	0
2	1	0	9895	111	0	111	0	-110	0
1	4	2	10061	614	0	614	456	-157	161
4	1	4	10114	46	0	46	0	-45	0
1	3	7	10239	76	0	76	0	-75	0

H	K	L	POSN	IOBJC	IMAG	ITOT	IOBS	DELTA	ESD
1	0	5	2601	436	0	436	504	68	164
1	0	6	2963	0	0	0	0	0	0
1	0	8	3124	256	0	256	310	54	112
1	1	2	3150	755	0	755	898	143	127
1	1	7	3247	37	0	37	135	98	117
1	1	4	3287	1085	0	1085	1213	128	148
1	0	8	3525	1630	0	1630	1753	123	167
1	0	1	3628	99	0	99	211	112	97
2	0	0	3650	446	0	446	599	153	76
2	0	1	3672	442	0	442	514	72	80
1	0	10	3930	6944	0	6944	7197	253	150
1	1	9	3950	909	0	909	950	51	24
1	2	4	3984	1715	0	1715	1746	31	30
2	0	5	4162	7869	0	7869	8019	150	138
2	1	10	4352	10308	0	10308	10133	-174	171
1	2	6	4371	456	0	456	460	4	9
2	1	8	4488	9896	0	9896	9937	41	201
2	1	7	4609	5	0	5	132	127	154
1	0	11	4733	8097	0	8097	8151	54	178
1	0	12	4756	68	0	68	104	36	103
2	0	8	4872	557	0	557	643	86	126
2	1	0	4889	8192	0	8192	8125	-66	164
2	1	1	4906	360	0	360	374	14	53
2	1	2	4957	11	0	11	29	18	27
2	1	3	5041	8	0	8	286	278	126
1	1	10	5113	10	0	10	101	91	133
1	0	12	5124	239	0	239	289	50	87
2	0	9	5157	380	0	380	405	25	79
2	1	4	5157	117	0	117	90	-26	57
2	1	5	5304	119	0	119	91	-27	58
2	0	10	5463	103	0	103	154	51	145
2	1	6	5479	2458	0	2458	2682	224	143
1	1	13	5526	26	0	26	33	7	5
3	0	0	5591	893	0	893	997	104	131
3	0	14	5606	348	0	348	325	-22	110
3	0	1	5619	5	0	5	5	0	1
2	1	11	5733	239	0	239	209	-29	60
1	1	12	5808	51	0	51	123	72	104
3	0	4	5839	3034	0	3034	2844	-189	126
3	1	8	5909	526	0	526	533	7	44
2	1	14	5939	521	0	521	594	73	110
3	1	5	5974	723	0	723	867	144	128
2	1	9	6132	31	0	31	5	-25	32
3	1	9	6137	329	0	329	355	26	132
2	1	15	6161	705	0	705	679	-25	102
2	2	0	6364	404	0	404	372	-31	35
2	2	1	6436	723	0	723	548	-74	118
2	0	13	6493	69	0	69	272	203	135
2	2	2	6497	1362	0	1362	1470	108	135
3	2	0	6540	8793	0	8793	8785	-7	155
3	2	1	6555	3	0	3	3	0	0
2	1	16	6568	47	0	47	46	0	1
3	2	2	6611	22502	0	22502	22384	-107	196
2	1	14	6779	125	0	125	124	0	2
3	2	3	6779	3395	0	3395	3719	324	137
2	2	4	6801	182	0	182	202	20	8
1	0	16	6858	3515	0	3515	3906	391	148
3	2	4	6871	9	0	9	33	24	11
2	1	17	6871	1	0	1	1	0	0
3	3	0	6913	10493	0	10493	10892	399	179
3	3	1	6982	89	0	89	92	3	1
3	3	2	7041	146	0	146	633	487	101
3	3	3	7050	231	0	231	701	470	136
3	3	4	7054	103	0	103	184	81	49
3	3	5	7077	12	0	12	16	4	3
3	1	17	7199	543	0	543	689	146	100
3	2	15	7253	50	0	50	122	72	104
3	2	16	7266	57	0	57	0	-56	0
3	1	11	7325	57	0	57	62	5	21
3	3	6	7348	1549	0	1549	1519	-29	143
3	3	7	7367	10	0	10	48	38	30
3	3	8	7392	293	0	293	329	36	106
3	3	9	7432	603	0	603	575	-27	81
3	3	10	7432	262	0	262	242	-19	38
3	2	17	7632	112	0	112	196	84	105
3	3	11	7680	19	0	19	36	17	19
3	3	12	7719	169	0	169	321	151	114
3	3	13	7720	664	0	664	574	-89	119
3	3	14	7720	2	0	2	3	1	1
3	3	15	7720	103	0	103	146	43	53

H	K	L	POSN	INUC	IMAG	ITOT	IOBS	DELTA	ESD
4	0	0	7734	49	0	49	58	19	21
2	1	14	7746	55	0	55	70	15	21
4	1	1	7747	98	0	98	121	23	38
4	1	2	7755	1474	0	1474	1187	-286	133
4	1	3	7855	4207	0	4207	4429	222	112
2	1	0	7908	6583	0	6583	6801	218	150
3	0	0	7943	756	0	756	746	-9	27
4	0	4	7944	2513	0	2513	2477	-35	92
3	1	13	7961	69	0	69	68	0	76
4	0	5	8061	3054	0	3054	3199	145	280
2	1	17	8113	192	0	192	125	-56	83
3	1	15	8126	56	0	56	179	123	55
1	1	19	8191	218	0	218	339	121	35
4	0	6	8203	75	0	75	70	-4	3
1	1	18	8204	3463	0	3463	3172	-290	154
3	1	14	8236	40	0	40	32	-7	92
4	0	7	8312	52	0	52	0	-51	0
3	0	11	8373	2477	0	2477	2500	23	142
2	1	12	8428	1905	0	1905	2049	144	122
4	0	8	8463	1	0	1	1	0	0
2	2	0	8488	1776	0	1776	1792	16	131
4	2	2	8527	50	0	50	47	-2	24
4	2	4	8556	6017	0	6017	5882	-134	123
3	3	1	8567	2381	0	2381	2330	-50	49
3	3	3	8592	9	0	9	0	0	1
3	3	5	8638	28	0	28	29	1	5
3	3	1	8663	347	0	347	303	-43	114
1	3	15	8669	146	0	146	138	-7	46
3	1	2	8697	267	0	267	275	8	64
1	1	12	8760	133	0	133	150	17	50
4	3	3	8763	134	0	134	85	-48	37
4	3	5	8783	40	0	40	18	-21	37
4	3	7	8793	93	0	93	42	-50	86
2	1	16	8901	162	0	162	71	-90	214
4	1	17	8952	92	0	92	52	40	104
2	1	10	9030	10556	0	10556	10448	-7	122
4	1	9	9042	2500	0	2500	2119	0	24
3	1	6	9043	151	0	151	151	0	15
1	1	13	9061	440	0	440	554	114	83
3	1	16	9085	144	0	144	181	37	31
4	1	0	9137	131	0	131	90	-40	52
2	2	14	9150	87	0	87	53	-33	28
4	1	1	9150	129	0	129	78	-50	42
4	1	2	9189	203	0	203	137	-65	58
3	2	7	9210	312	0	312	294	-17	57
1	0	21	9235	433	0	433	402	-30	63
4	1	3	9253	161	0	161	143	-17	23
1	1	20	9265	287	0	287	257	-29	39
4	0	11	9300	1763	0	1763	2055	292	115
4	1	4	9343	948	0	948	956	8	130
2	1	18	9402	5	0	5	3	-1	25
3	2	8	9403	2	0	2	1	0	8
3	1	14	9422	38	0	38	34	-4	64
4	1	5	9459	2588	0	2588	4035	147	114
0	2	22	9509	133	0	133	261	128	69
3	0	17	9510	27	0	27	52	25	14
2	0	20	9544	305	0	305	303	-1	98
4	0	12	9597	275	0	275	254	-10	40
4	1	6	9601	488	0	488	478	-9	63
3	2	9	9622	413	0	413	513	100	128
4	1	7	9689	85	0	85	71	-13	107
1	0	22	9790	436	0	436	343	-92	92
3	1	15	9803	209	0	209	181	-27	72
3	2	10	9869	6	0	6	23	17	12
2	1	19	9881	58	0	58	135	77	53
4	0	13	9921	4585	0	4585	4537	-47	168
2	2	16	9925	98	0	98	96	-1	4
4	0	18	9964	0	0	0	0	0	0
4	1	3	9964	92	0	92	178	86	120
2	0	21	10076	0	0	0	740	740	126
3	2	11	10143	84	0	84	338	254	141
4	1	9	10187	164	0	164	243	79	86
3	1	16	10208	96	0	96	122	26	44
5	0	0	10282	381	0	381	352	-18	18
4	0	14	10274	5708	0	5708	5567	-140	189
5	0	1	10275	2	0	2	0	0	0
5	0	2	10314	98	0	98	94	-3	35
1	1	22	10357	35	0	35	10	-24	13
1	0	23	10379	361	0	361	177	-183	116
5	0	3	10381	21	0	21	11	-9	7

H	K	L	POSN	IOBS	IMAG	ITOT	ICAL	DELTA	ESD
2	1	20	10392	15	0	15	8	-6	6
4	1	10	10437	16	0	16	11	-4	6
3	2	12	10446	266	0	266	183	-82	102
3	0	19	10450	39	0	39	27	-11	16
5	0	4	10473	56	0	56	20	-35	107
5	0	5	10593	15	0	15	105	90	116
2	2	2	10645	468	0	468	572	104	70
3	1	17	10646	45	0	45	55	10	6
4	0	15	10659	1124	0	1124	1461	337	104
0	2	4	10716	665	0	665	925	260	114
4	1	11	10718	3	0	3	4	1	0
5	1	6	10741	0	0	0	0	0	0
3	1	13	10780	734	0	734	634	-99	113
2	1	18	10825	600	0	600	921	321	121
3	3	0	10840	0	0	0	1	1	0
3	3	2	10894	101	0	101	130	29	28
5	0	7	10917	790	0	790	814	24	97
2	1	21	10942	699	0	699	728	29	82
3	0	20	10974	203	0	203	348	145	61
1	0	24	11010	17	0	17	52	35	11
4	1	12	11030	193	0	193	715	522	165
3	1	4	11058	521	0	521	2252	1731	550

H	K	L	PØSN	INUC	IMAG	ITØT	IØBS	DELTA	ESD
0	1	12	3129	314	0	314	409	95	114
1	0	0	3157	330	0	330	489	159	37
1	0	10	3183	301	0	301	720	419	89
1	1	3	3255	2	0	2	118	116	82
1	1	11	3405	279	0	279	167	-111	142
1	1	6	3533	635	0	635	707	72	116
1	2	1	3668	139	0	139	190	51	75
2	0	2	3697	5	0	5	22	17	18
2	0	4	3810	1217	0	1217	1326	109	94
0	1	13	3870	118	0	118	148	30	10
2	0	5	3893	7530	0	7530	7481	-48	100
0	1	15	3935	3621	0	3621	3717	96	87
1	2	9	3958	803	0	803	1108	305	88
1	0	7	4108	683	0	683	920	237	84
0	1	14	4112	384	0	384	683	299	66
2	1	8	4237	373	0	373	678	305	117
1	2	12	4496	141	0	141	456	315	88
0	1	10	4535	12074	0	12074	12370	296	141
1	2	16	4611	242	0	242	574	332	114
0	0	11	4703	163	0	163	59	-103	99
2	0	18	4762	43	0	43	93	50	122
0	1	17	4869	152	0	152	0	-151	0
2	1	1	4907	138	0	138	77	-60	38
1	2	2	4930	87	0	87	56	-30	55
2	1	4	5020	5	0	5	0	-4	0
0	2	13	5068	347	0	347	314	-32	91
1	2	5	5087	12	0	12	16	4	6
2	1	15	5121	113	0	113	201	88	104
1	1	7	5262	123	0	123	18	-104	99
2	1	14	5266	0	0	0	0	0	0
1	2	8	5370	35	0	35	0	-34	0
1	3	19	5398	148	0	148	442	294	117
0	0	0	5606	138	0	138	0	-137	0
0	1	21	5616	6	0	6	3	-2	1
2	1	10	5622	321	0	321	208	-112	54
3	0	3	5668	0	0	0	0	0	0
3	0	3	5668	11	0	11	10	0	2
0	1	20	5670	53	0	53	51	-1	10
0	2	16	5687	1278	0	1278	1443	165	105
1	2	11	5766	637	0	637	926	289	89
1	1	18	5818	133	0	133	227	94	57
3	0	6	5852	88	0	88	112	24	16
3	0	6	5852	267	0	267	339	72	49
2	0	17	5911	242	0	242	44	-197	112
2	1	13	6086	21	0	21	0	-20	0
3	0	9	6150	428	0	428	173	-254	91
3	0	9	6150	4	0	4	2	-1	1
1	0	22	6229	42	0	42	0	-41	0
1	2	14	6262	564	0	564	522	-41	111
0	1	24	6505	1	0	1	28	27	47
0	1	23	6517	165	0	165	533	368	110
3	0	12	6553	70	0	70	67	-2	2
0	3	12	6553	69	0	69	66	-2	2
2	1	0	6569	9448	0	9448	9424	-23	91
1	2	21	6578	1	0	1	1	0	0
2	2	3	6625	968	0	968	1001	33	13
2	0	20	6627	8704	0	8704	9055	351	118
2	1	16	6643	371	0	371	866	495	62
2	2	6	6793	1267	0	1267	1621	354	92
1	3	17	6848	149	0	149	398	249	60
1	3	1	6879	52	0	52	97	45	12
3	1	2	6897	320	0	320	466	146	59
1	3	4	6971	195	0	195	247	52	65
3	1	5	7026	124	0	124	106	-17	47
0	3	15	7054	31	0	31	22	-8	9
3	0	15	7054	90	0	90	64	-25	25
2	2	9	7069	124	0	124	134	10	54
1	0	25	7110	3	0	3	10	7	10
0	2	22	7143	95	0	95	58	-36	70
1	3	7	7171	168	0	168	28	-139	71
3	1	8	7261	35	0	35	90	55	79
2	1	19	7285	2	0	2	41	39	73
1	1	24	7402	0	0	0	0	0	0
2	0	23	7413	511	0	511	509	-1	113
0	1	26	7416	118	0	118	123	5	21
0	2	27	7441	26	0	26	43	17	11
2	1	12	7447	40	0	40	68	28	20
1	3	10	7476	62	0	62	86	24	48
1	2	20	7517	77	0	77	89	12	93
3	1	11	7600	29	0	29	406	377	158

H	K	L	PØSN	INUC	IMAG	ITØT	IØBS	DELTA	ESD
4	0	1	7757	21	0	21	0	-20	0
0	4	2	7774	0	0	0	0	0	0
4	0	4	7844	357	0	357	298	-58	66
1	0	3	7882	81	0	81	74	-6	4
0	2	4	7897	1911	0	1911	1920	9	51
0	2	15	7924	4238	0	4238	4249	11	83
2	1	25	7978	1594	0	1594	1609	15	95
4	3	22	8010	55	0	55	54	0	7
3	1	7	8037	200	0	200	153	-46	25
1	0	14	8039	443	0	443	330	-112	57
0	1	28	8051	15	0	15	10	-4	2
1	4	8	8124	139	0	139	67	-71	101
2	0	23	8271	137	0	137	110	-26	26
1	2	26	8273	744	0	744	567	-176	103
0	1	27	8297	147	0	147	135	-11	9
3	3	21	8327	8	0	8	7	0	0
3	0	21	8327	2	0	2	2	0	0
4	0	10	8332	3990	0	3990	3751	-228	93
0	1	29	8380	50	0	50	44	-5	9
1	3	16	8386	207	0	207	210	3	42
0	0	30	8438	1319	0	1319	1436	117	107
0	4	11	8453	90	0	90	113	23	9
2	3	18	8496	406	0	406	565	159	87
3	1	17	8576	249	0	249	153	-95	76
3	2	1	8605	28	0	28	20	-7	6
2	3	2	8622	231	0	231	131	-99	52
3	2	4	8691	169	0	169	180	11	54
4	0	13	8728	131	0	131	113	-17	61
2	3	5	8743	18	0	18	0	-17	0
2	1	25	8822	3	0	3	31	28	63
3	2	7	8880	71	0	71	33	-37	26
0	4	14	8883	3	0	3	1	-1	1
0	2	28	8894	602	0	602	462	-139	114
2	3	8	8966	15	0	15	26	11	14
1	3	19	8988	168	0	168	123	-44	101
1	0	31	9068	6	0	6	0	-5	0
3	0	24	9101	76	0	76	29	-46	51
0	3	24	9101	20	0	20	8	-11	14
1	2	26	9114	95	0	95	33	-61	41
4	1	0	9159	131	0	131	61	-69	30
2	2	21	9167	36	0	36	18	-17	7
3	2	10	9172	112	0	112	57	-54	22
1	4	3	9210	1	0	1	0	0	0
4	1	3	9210	0	0	0	0	0	0
3	1	20	9212	193	0	193	148	-44	23
2	0	29	9220	16	0	16	13	-2	2
4	0	16	9226	572	0	572	478	-93	71
1	1	30	9278	70	0	70	80	10	55
2	3	11	9292	20	0	20	34	14	22
1	4	6	9365	50	0	50	37	-12	11
4	1	6	9365	272	0	272	203	-68	62
0	4	17	9415	131	0	131	44	-86	55
0	1	32	9429	71	0	71	54	-16	62
0	0	33	9522	9	0	9	0	-8	0
3	2	13	9568	51	0	51	77	26	62
4	1	9	9623	356	0	356	492	136	80
1	4	9	9623	21	0	21	29	8	5
1	3	22	9694	53	0	53	119	66	49
2	3	14	9723	60	0	60	17	-42	70
2	1	28	9734	4	0	4	0	-3	0
4	0	19	9830	78	0	78	0	-77	0
0	2	31	9910	78	0	78	12	-65	81
2	2	24	9943	46	0	46	32	-13	21
3	1	23	9954	57	0	57	39	-17	20
3	0	27	9981	198	0	198	168	-29	39
0	3	27	9981	52	0	52	44	-7	10
4	1	12	9987	91	0	91	84	-6	16
1	4	12	9987	19	0	19	18	0	4
4	0	20	10056	4492	0	4492	4837	345	140
1	2	29	10064	2	0	2	2	0	0
3	2	16	10071	31	0	31	33	2	2
1	0	34	10192	199	0	199	426	227	131
2	3	17	10263	77	0	77	56	-20	23
2	0	32	10277	332	0	332	230	-101	84
0	5	1	10293	67	0	67	63	-3	28
5	0	2	10311	1	0	1	1	0	1
1	1	33	10372	3	0	3	2	0	13
0	5	4	10381	9	0	9	1	-7	44
5	0	5	10434	0	0	0	0	0	0
1	4	15	10462	41	0	41	0	-40	0

H	K	L	PØSN	INUC	IMAG	ITØT	IØBS	DELTA	ESD
4	1	15	10462	70	0	70	0	-69	0
1	3	25	10516	0	0	0	0	0	0
4	0	22	10549	66	0	66	161	95	79
0	5	7	10576	21	0	21	30	9	33
0	1	35	10599	4	0	4	8	4	10
5	0	8	10666	24	0	24	65	41	18
3	2	19	10689	259	0	259	478	219	86
0	1	36	10731	161	0	161	431	270	70
2	1	31	10773	0	0	0	0	0	0
0	4	23	10818	333	0	333	556	223	48
3	1	26	10821	327	0	327	530	203	44
2	2	27	10846	281	0	281	410	129	31
3	3	0	10868	274	0	274	421	147	36
0	5	10	10882	78	0	78	126	48	12
3	3	3	10922	120	0	120	214	94	24
2	3	20	10924	27	0	27	48	21	5

APPENDIX 2

Intensity data for the refinements described in Chapter 5

$Ag_{1+x}Al_{11}O_{17+x/2}$ single crystal neutron study	A20
$AgAl_{11}O_{17}$ at 4.2K PND data	A23
Silver metal at 4.2K (data obtained from the observed profile of $AgAl_{11}O_{17}$ at 4.2K)	A27
$AgAl_{11}O_{17}$ at 298K PND data	A28
$AgAl_{11}O_{17}$ at 573K PND data	A32
$AgAl_{11}O_{17}$ at 773K PND data	A34

For the single crystal data the listing for each reflection includes the observed (/FO/) and calculated (/FC/) structure factors and the phase which,because the structure is centro-symmetric,is restricted to 0 or π.For each reflection derived from powder data,the listing includes the Bragg angle,2θ,(POSN), the calculated integrated intensity(INUC and ITOT),the observed integrated intensity(IOBS),the difference between the two(DELTA) and the estimated standard deviation of the observed intensity (ESD).The column headed IMAG is superfluous.

H	/FØ/	/FC/	PHI
** K= 1	L= 0 **		
0	56	14	0
** K= 2	L= 0 **		
-1	465	452	0
0	168	179	0
** K= 3	L= 0 **		
-1	135	119	180
0	346	319	0
** K= 4	L= 0 **		
-2	2370	2274	0
-1	39	13	0
0	274	263	0
** K= 5	L= 0 **		
-2	208	204	0
-1	290	278	0
0	262	244	180
** K= 6	L= 0 **		
-3	315	312	0
-2	234	214	0
-1	79	64	180
** K= 1	L= 1 **		
0	70	58	0
** K= 2	L= 1 **		
0	209	176	180
** K= 3	L= 1 **		
-1	143	145	0
0	47	35	0
** K= 4	L= 1 **		
-1	75	72	180
0	172	124	0
** K= 5	L= 1 **		
-2	54	30	180
-1	42	31	180
0	173	171	180
** K= 6	L= 1 **		
-2	133	107	180
-1	89	78	0
** K= 0	L= 2 **		
0	450	492	0
** K= 1	L= 2 **		
0	199	186	0
** K= 2	L= 2 **		
0	624	629	180

H	/FØ/	/FC/	PHI
** K= 3	L= 2 **		
-1	45	9	180
0	38	17	0
** K= 4	L= 2 **		
-2	684	647	0
-1	157	141	0
0	642	626	180
** K= 5	L= 2 **		
-2	237	218	0
-1	99	91	0
0	97	102	180
** K= 6	L= 2 **		
-3	106	108	0
-2	490	511	180
** K= 1	L= 3 **		
0	173	170	180
** K= 2	L= 3 **		
0	429	414	0
** K= 3	L= 3 **		
-1	75	65	180
0	146	145	0
** K= 4	L= 3 **		
-1	194	188	0
0	334	295	180
** K= 5	L= 3 **		
-2	229	216	180
-1	139	125	180
0	65	67	180
** K= 6	L= 3 **		
-2	253	221	0
** K= 0	L= 4 **		
0	535	565	180
** K= 2	L= 4 **		
-1	460	452	0
0	880	839	180
** K= 3	L= 4 **		
-1	99	77	180
0	354	336	0
** K= 4	L= 4 **		
-2	764	719	180
-1	68	53	180
0	713	679	180
** K= 5	L= 4 **		

H	/FØ/	/FC/	PHI
-2	65	56	0
-1	268	259	0
0	128	122	180
** K= 6	L= 4 **		
-3	268	251	0
-2	641	635	180
-1	40	43	180
** K= 2	L= 5 **		
0	855	871	0
** K= 3	L= 5 **		
-1	102	106	0
0	245	253	0
** K= 4	L= 5 **		
-1	59	56	180
0	801	784	180
** K= 5	L= 5 **		
-1	217	221	180
0	108	128	180
** K= 6	L= 5 **		
-2	649	667	0
** K= 0	L= 6 **		
0	107	93	0
** K= 2	L= 6 **		
-1	160	146	0
0	1027	1012	0
** K= 3	L= 6 **		
-1	54	49	180
0	249	240	0
** K= 4	L= 6 **		
-2	320	316	0
-1	59	58	180
0	851	838	0
** K= 5	L= 6 **		
-2	140	154	180
-1	267	261	0
** K= 6	L= 6 **		
-3	249	239	0
-2	714	770	0
-1	62	57	180
** K= 2	L= 7 **		
0	827	855	0
** K= 3	L= 7 **		
-1	433	413	0
0	123	129	0

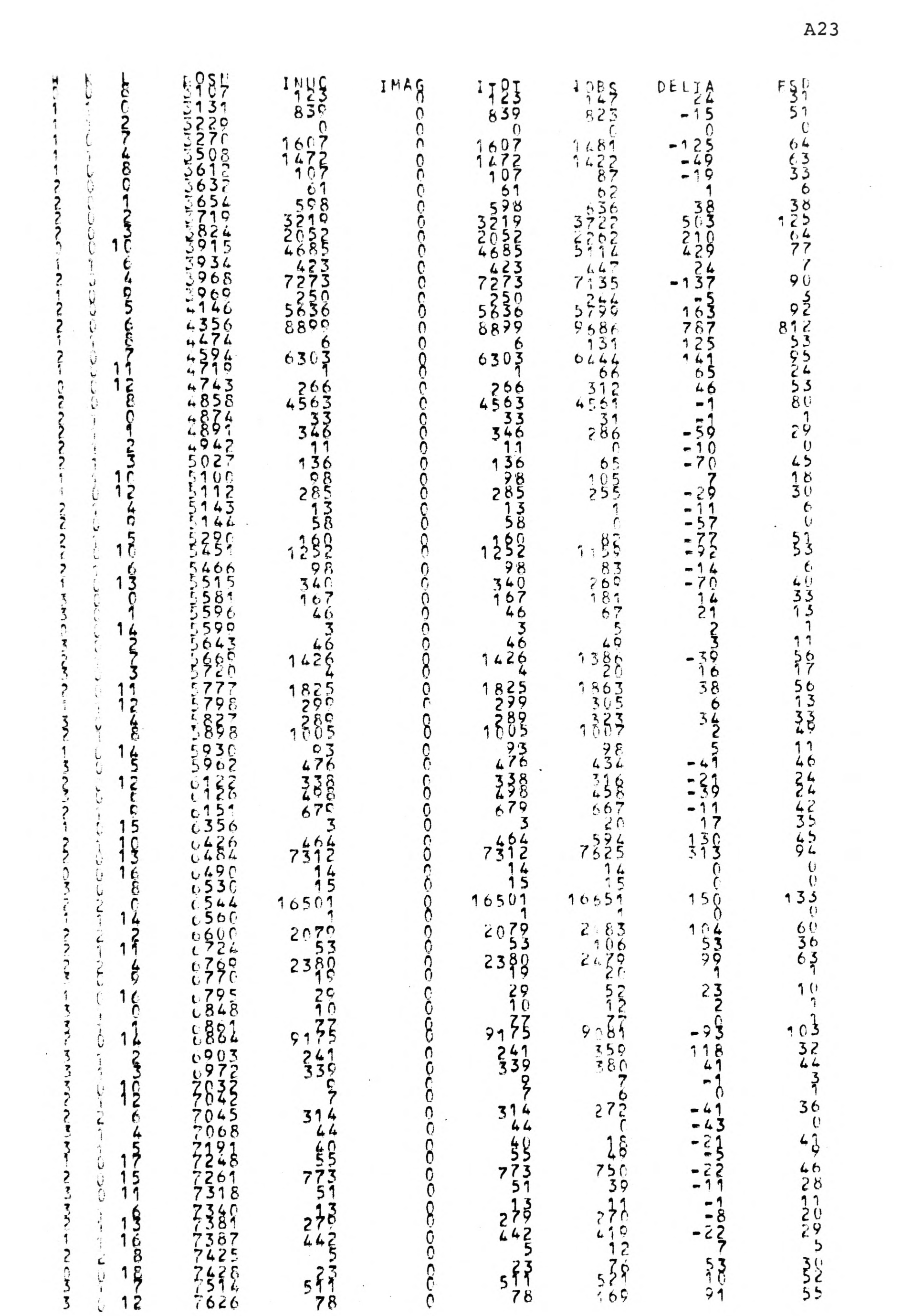
H	/F0/	/FC/	PHI
** K= 4 L= 7 **			
-1	319	291	180
0	715	696	180
** K= 5 L= 7 **			
-2	281	256	0
-1	97	111	180
0	437	439	180
** K= 6 L= 7 **			
-1	298	328	0
** K= 0 L= 8 **			
0	208	220	0
** K= 1 L= 8 **			
0	129	141	0
** K= 2 L= 8 **			
-1	115	104	0
0	850	852	0
** K= 3 L= 8 **			
-1	303	321	0
** K= 4 L= 8 **			
-2	53	33	0
-1	145	147	0
0	803	822	0
** K= 5 L= 8 **			
-2	46	39	0
-1	60	41	180
0	348	361	0
** K= 6 L= 8 **			
-1	306	305	0
** K= 1 L= 9 **			
0	184	166	0
** K= 2 L= 9 **			
0	197	172	0
** K= 3 L= 9 **			
-1	265	243	0
0	36	11	0
** K= 4 L= 9 **			
-1	190	174	180
0	178	174	180
** K= 5 L= 9 **			
0	248	256	180
** K= 6 L= 9 **			
-2	195	149	0
-1	203	173	0
** K= 0 L= 10 **			
0	1489	1575	180
** K= 1 L= 10 **			
0	157	139	0
** K= 2 L= 10 **			
-1	228	208	180
0	542	535	180
** K= 3 L= 10 **			
-1	287	272	0
0	116	87	180
** K= 4 L= 10 **			
-2	1253	1297	180
-1	137	122	0
0	540	565	180
** K= 5 L= 10 **			
-2	78	81	180
-1	75	57	180
0	359	378	0
** K= 6 L= 10 **			
-3	112	93	180
-2	496	481	180
** K= 1 L= 11 **			
0	18	28	0
** K= 2 L= 11 **			
0	650	669	180
** K= 3 L= 11 **			
-1	43	38	180
** K= 4 L= 11 **			
-1	37	22	180
0	646	625	0
** K= 5 L= 11 **			
-2	101	99	0
** K= 6 L= 11 **			
-2	546	558	180
** K= 0 L= 12 **			
0	438	420	180
** K= 1 L= 12 **			
0	178	163	180
** K= 2 L= 12 **			
-1	366	338	0
0	372	373	0
** K= 3 L= 12 **			
-1	34	7	180
0	245	233	0
** K= 4 L= 12 **			
-2	536	533	180
-1	141	140	180
0	362	391	0
** K= 5 L= 12 **			
-2	203	205	180
-1	153	143	0
0	77	82	0
** K= 6 L= 12 **			
-3	127	118	0
-2	363	306	0
** K= 1 L= 13 **			
0	277	288	0
** K= 2 L= 13 **			
0	1159	1193	180
** K= 3 L= 13 **			
-1	174	181	0
0	108	114	180
** K= 4 L= 13 **			
-1	266	296	180
0	931	1017	0
** K= 5 L= 13 **			
-2	289	322	0
-1	86	96	0
** K= 0 L= 14 **			
0	146	122	180
** K= 1 L= 14 **			
0	125	143	0
** K= 2 L= 14 **			
-1	72	48	180
0	1319	1358	0
** K= 3 L= 14 **			
-1	129	135	0
0	59	39	0
** K= 4 L= 14 **			
-2	83	87	0
-1	110	132	0
0	1043	1166	0

H	/FØ/	/FC/	PHI
** K= 5	L= 14	**	
-2	58	53	0
0	142	151	0
** K= 1	L= 15	**	
0	41	22	0
** K= 2	L= 15	**	
0	514	495	180
** K= 3	L= 15	**	
-1	18	31	180
0	218	231	180
** K= 4	L= 15	**	
-1	30	28	180
0	445	452	0
** K= 5	L= 15	**	
-2	86	85	0
** K= 0	L= 16	**	
0	153	163	0
** K= 1	L= 16	**	
0	85	86	0
** K= 2	L= 16	**	
-1	411	430	0
0	535	522	180
** K= 3	L= 16	**	
-1	59	57	0
0	292	315	0
** K= 4	L= 16	**	
-1	75	82	0
0	391	381	180
** K= 5	L= 16	**	
-1	209	238	0
** K= 1	L= 17	**	
0	139	141	0
** K= 2	L= 17	**	
0	365	358	180
** K= 3	L= 17	**	
-1	64	78	0
0	138	139	180
** K= 4	L= 17	**	
-1	142	154	180
0	253	265	0

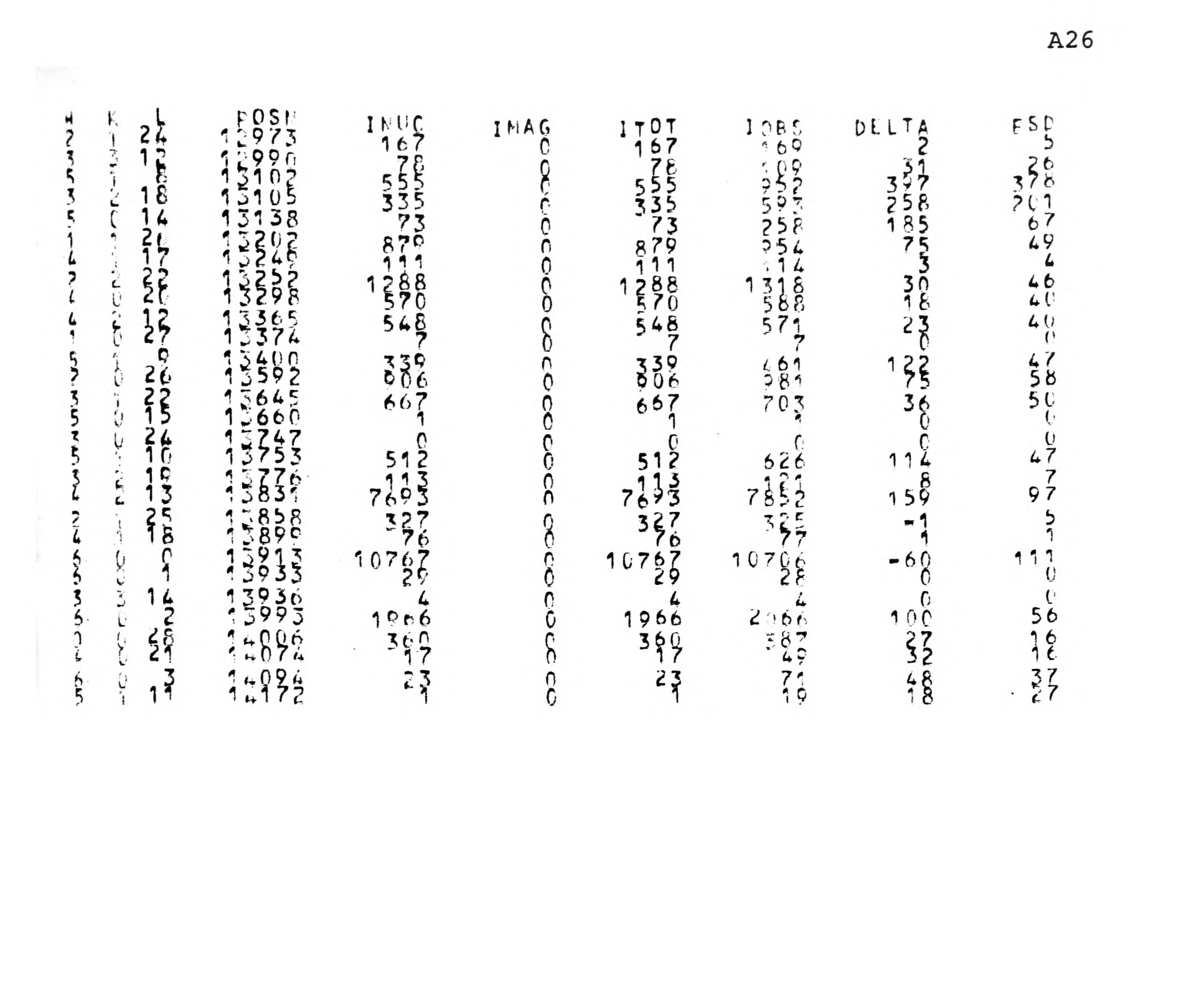
H	/FØ/	/FC/	PHI
** K= 5	L= 17	**	
-2	150	165	0
-1	141	118	0
** K= 0	L= 18	**	
0	301	298	0
** K= 1	L= 18	**	
0	159	141	0
** K= 2	L= 18	**	
-1	291	266	180
0	994	988	180
** K= 3	L= 18	**	
-1	13	18	180
0	205	182	180
** K= 4	L= 18	**	
-2	390	386	0
-1	112	108	0
** K= 5	L= 18	**	
-2	225	186	0
** K= 1	L= 19	**	
0	44	27	180
** K= 2	L= 19	**	
0	231	242	180
** K= 3	L= 19	**	
-1	105	89	180
** K= 4	L= 19	**	
0	225	244	0
** K= 0	L= 20	**	
0	1677	1682	0
** K= 1	L= 20	**	
0	239	229	0
** K= 2	L= 20	**	
-1	232	215	180
0	316	326	0
** K= 3	L= 20	**	
-1	121	107	0
0	294	289	180
** K= 4	L= 20	**	
0	397	372	0
** K= 2	L= 21	**	

H	/FØ/	/FC/	PHI
0	107	107	0
** K= 3	L= 21	**	
-1	250	276	180
0	43	59	0
** K= 4	L= 21	**	
-1	283	309	0
** K= 0	L= 22	**	
0	440	453	0
** K= 1	L= 22	**	
0	304	318	0
** K= 2	L= 22	**	
-1	84	17	0
0	228	193	0
** K= 3	L= 22	**	
-1	150	166	0
** K= 4	L= 22	**	
-2	602	519	0
** K= 1	L= 23	**	
0	170	153	180
** K= 2	L= 23	**	
0	599	574	0
** K= 3	L= 23	**	
-1	69	54	180
0	90	99	0
** K= 0	L= 24	**	
0	792	772	180
** K= 1	L= 24	**	
0	114	105	0
** K= 3	L= 24	**	
-1	98	94	0
** K= 2	L= 25	**	
0	773	786	0
** K= 1	L= 26	**	
0	143	157	0
** K= 2	L= 26	**	
-1	589	534	180
0	571	510	0
** K= 1	L= 27	**	

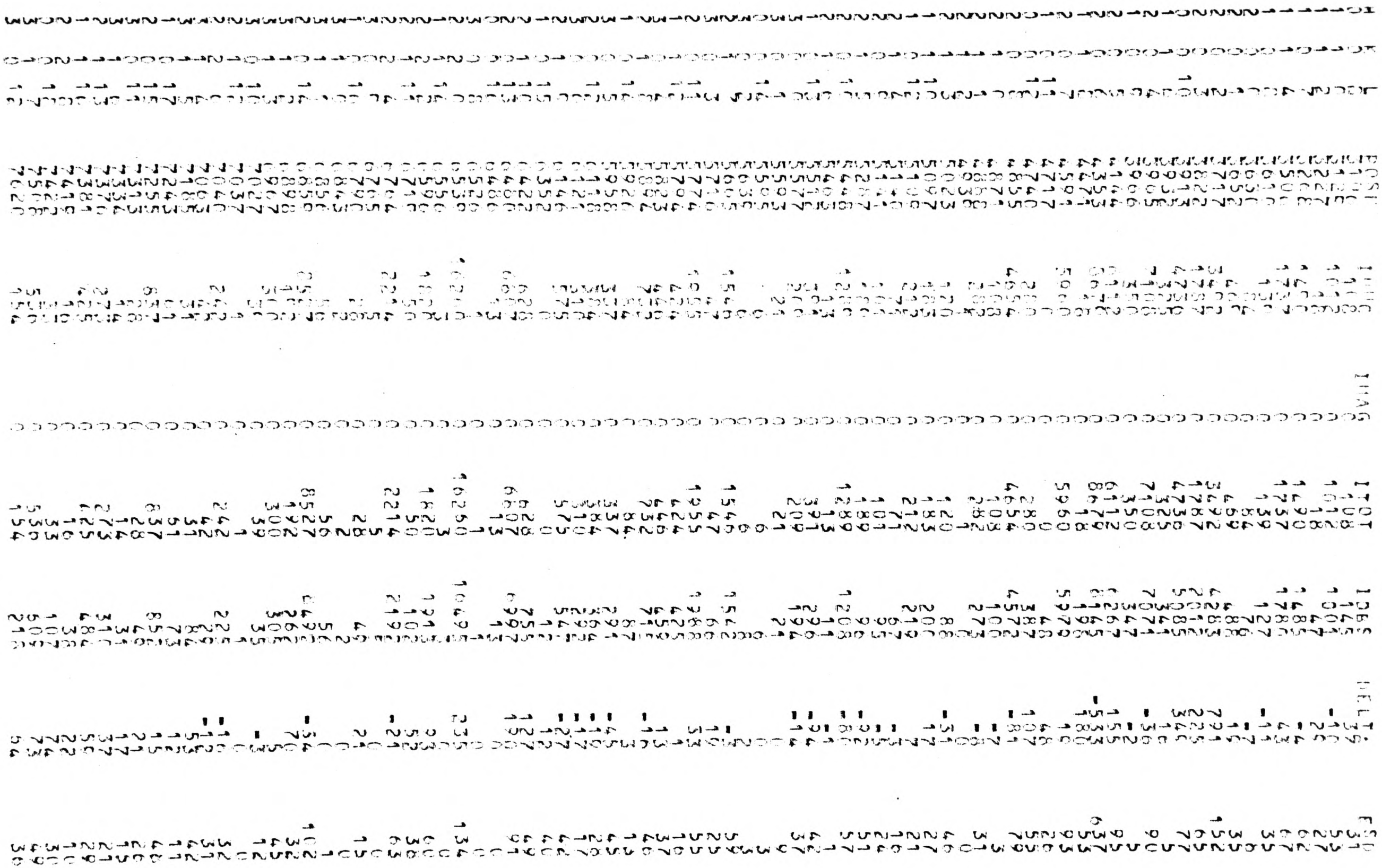
H	/FØ/	/FC/	PHI
0	74	94	180

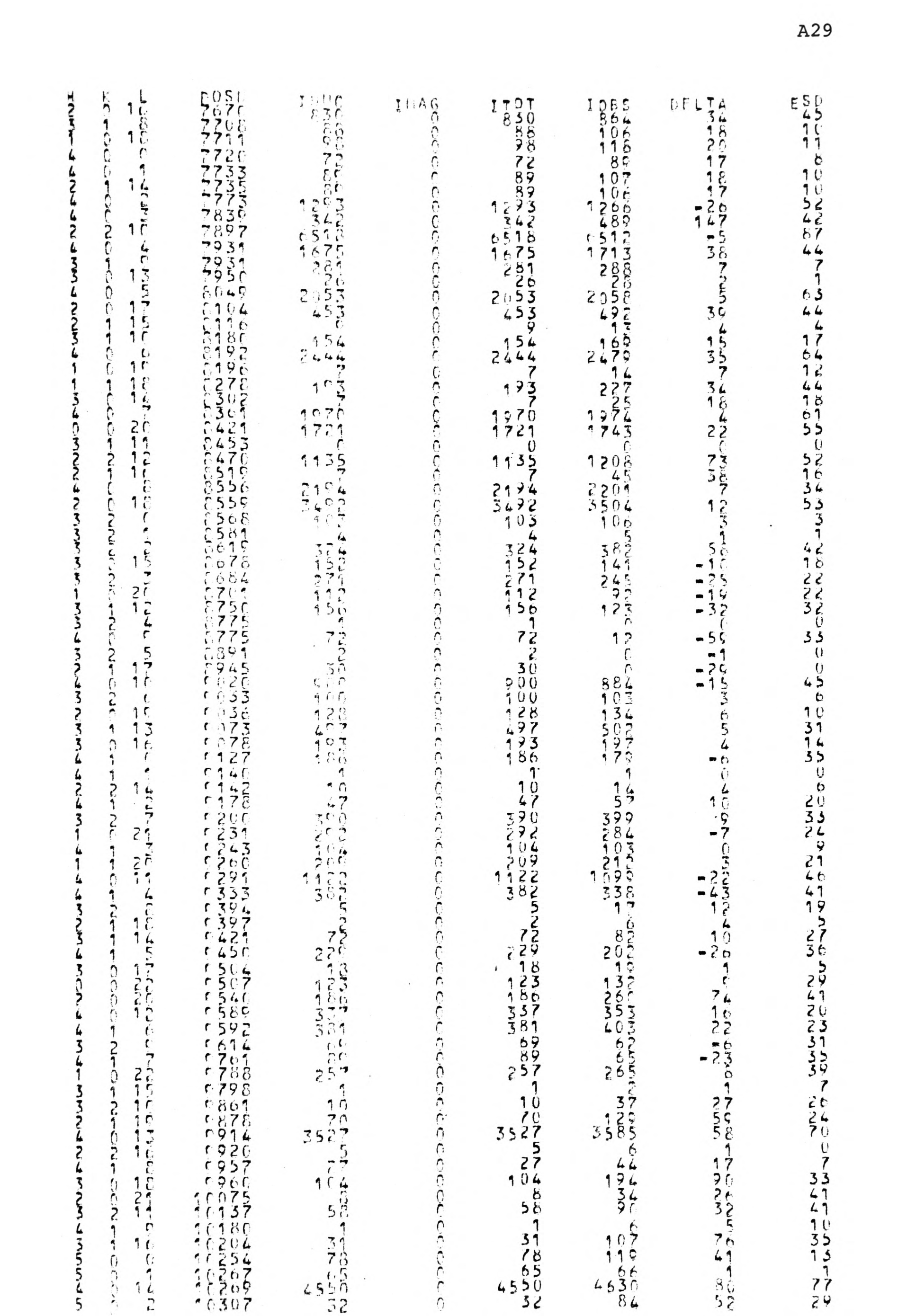


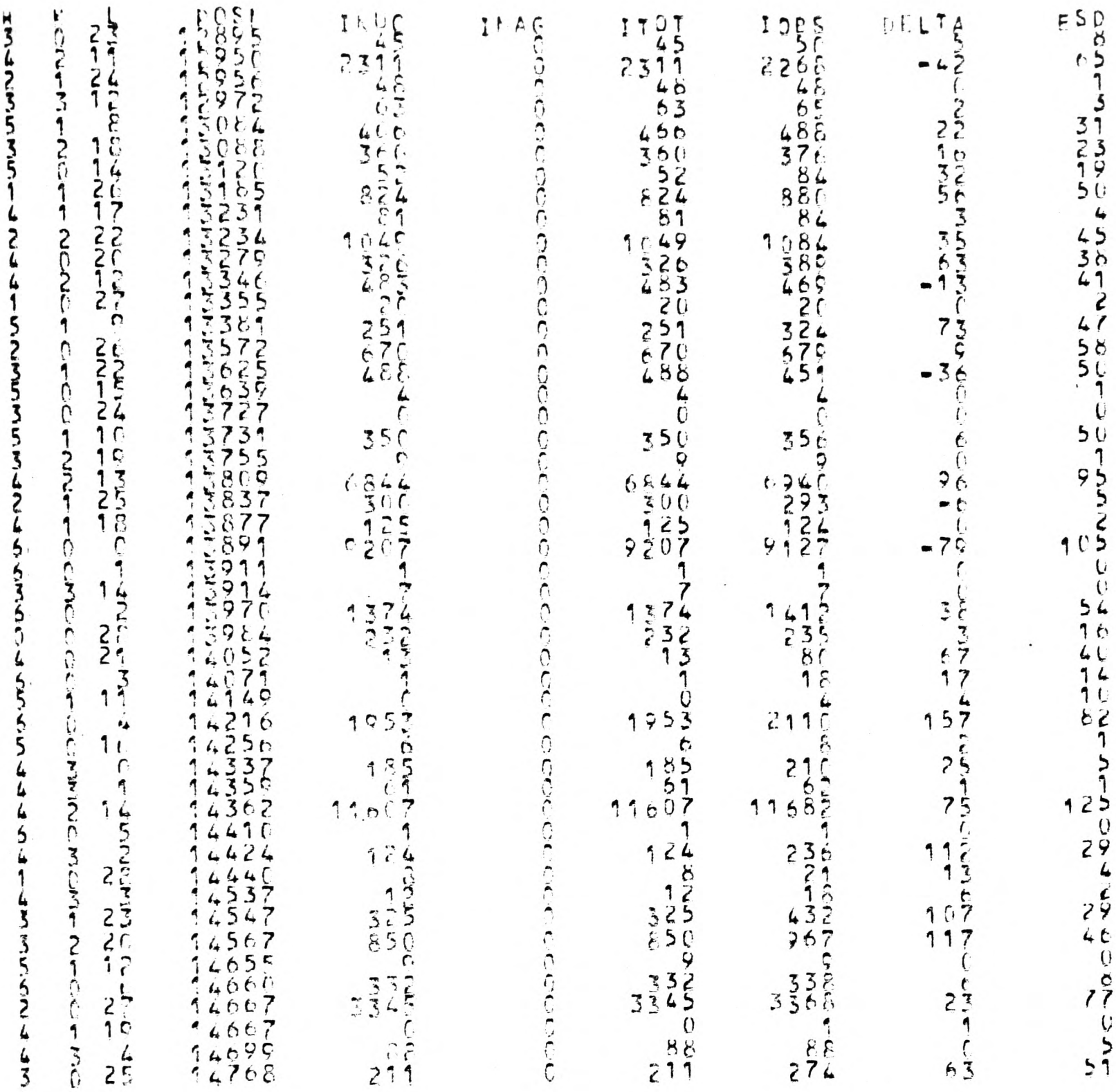
H	K	L	POSN	INUC	IMAG	ITOT	IOBS	DELTA	ESD
2	0	16	7676	937	0	937	925	-11	46
3	1	8	7713	93	0	93	96	3	9
1	0	18	7716	136	0	136	143	7	12
4	0	0	7726	111	0	111	123	12	10
4	0	1	7739	88	0	88	99	11	10
2	1	14	7741	41	0	41	45	4	5
4	0	2	7770	1564	0	1564	1549	-14	54
4	0	3	7845	395	0	395	472	77	40
2	2	10	7903	6640	0	6640	6519	-120	86
4	0	4	7937	1515	0	1515	1586	71	43
3	1	9	7938	274	0	274	288	14	8
3	0	13	7956	0	0	0	0	0	0
4	0	5	8055	2202	0	2202	2234	32	61
2	0	17	8110	530	0	530	698	168	45
2	1	15	8123	4	0	4	8	4	2
3	1	10	8186	259	0	259	282	23	20
4	0	6	8199	2322	0	2322	2291	-30	61
1	0	19	8202	1	0	1	1	0	0
1	1	18	8284	154	0	154	189	35	40
3	0	14	8309	38	0	38	108	70	23
4	0	7	8368	2039	0	2039	2038	0	60
0	0	20	8428	1959	0	1959	1964	5	57
3	1	11	8460	1	0	1	1	0	0
2	2	12	8477	1261	0	1261	1330	69	50
2	1	16	8526	95	0	95	107	12	22
4	0	8	8563	2729	0	2729	2700	-28	38
2	0	18	8565	3719	0	3719	3718	0	51
3	2	0	8575	116	0	116	119	3	3
3	2	1	8588	37	0	37	40	3	4
3	2	2	8627	322	0	322	337	15	39
3	0	15	8685	215	0	215	199	-15	23
3	2	3	8691	205	0	205	196	-8	18
1	0	20	8708	53	0	53	56	3	10
3	1	12	8757	197	0	197	202	5	33
3	2	4	8782	3	0	3	2	0	1
4	0	9	8783	74	0	74	34	-39	31
3	2	5	8898	14	0	14	1	-12	38
2	1	17	8953	75	0	75	93	18	40
4	0	10	9028	1117	0	1117	1208	91	49
3	2	6	9040	73	0	73	82	9	4
2	0	10	9044	86	0	86	97	11	6
3	1	13	9080	596	0	596	588	-7	33
3	0	16	9086	169	0	169	167	-1	11
4	1	0	9135	213	0	213	233	20	31
4	1	1	9148	1	0	1	1	0	0
2	2	14	9150	44	0	44	59	15	12
4	1	2	9186	106	0	106	102	-3	19
3	2	7	9208	633	0	633	611	-21	35
1	0	21	9238	287	0	287	325	38	24
4	1	3	9251	56	0	56	64	8	5
1	1	21	9268	291	0	291	302	11	23
4	0	11	9300	1254	0	1254	1161	-92	45
4	1	4	9341	355	0	355	313	-41	38
3	2	8	9402	36	0	36	95	59	25
2	1	18	9405	7	0	7	19	12	4
3	1	14	9430	80	0	80	116	36	22
4	1	5	9458	299	0	299	241	-57	35
3	0	17	9513	13	0	13	11	-1	3
0	0	22	9515	120	0	120	107	-12	28
2	0	20	9548	223	0	223	212	-10	33
3	2	9	9623	8	0	8	21	13	664
4	1	7	9770	77	0	77	34	-42	31
1	0	22	9796	337	0	337	324	-12	39
3	1	15	9807	0	0	0	0	0	0
3	2	10	9871	5	0	5	10	5	20
2	1	15	9886	111	0	111	162	51	28
4	0	13	9924	3970	0	3970	3855	-114	71
2	2	16	9929	10	0	10	10	0	0
4	1	8	9966	43	0	43	98	55	13
3	0	18	9969	61	0	61	182	121	26
2	0	21	10084	0	0	0	37	37	38
3	2	11	10146	104	0	104	95	-8	41
4	1	9	10190	0	0	0	5	5	4
3	1	16	10214	58	0	58	101	43	36
5	0	0	10264	35	0	35	56	21	7
5	0	1	10277	72	0	72	74	2	1
4	0	14	10279	4760	0	4760	4851	91	78
5	0	2	10317	55	0	55	144	89	32
1	1	22	10366	0	0	0	1	1	0
5	0	3	10383	2	0	2	6	4	2

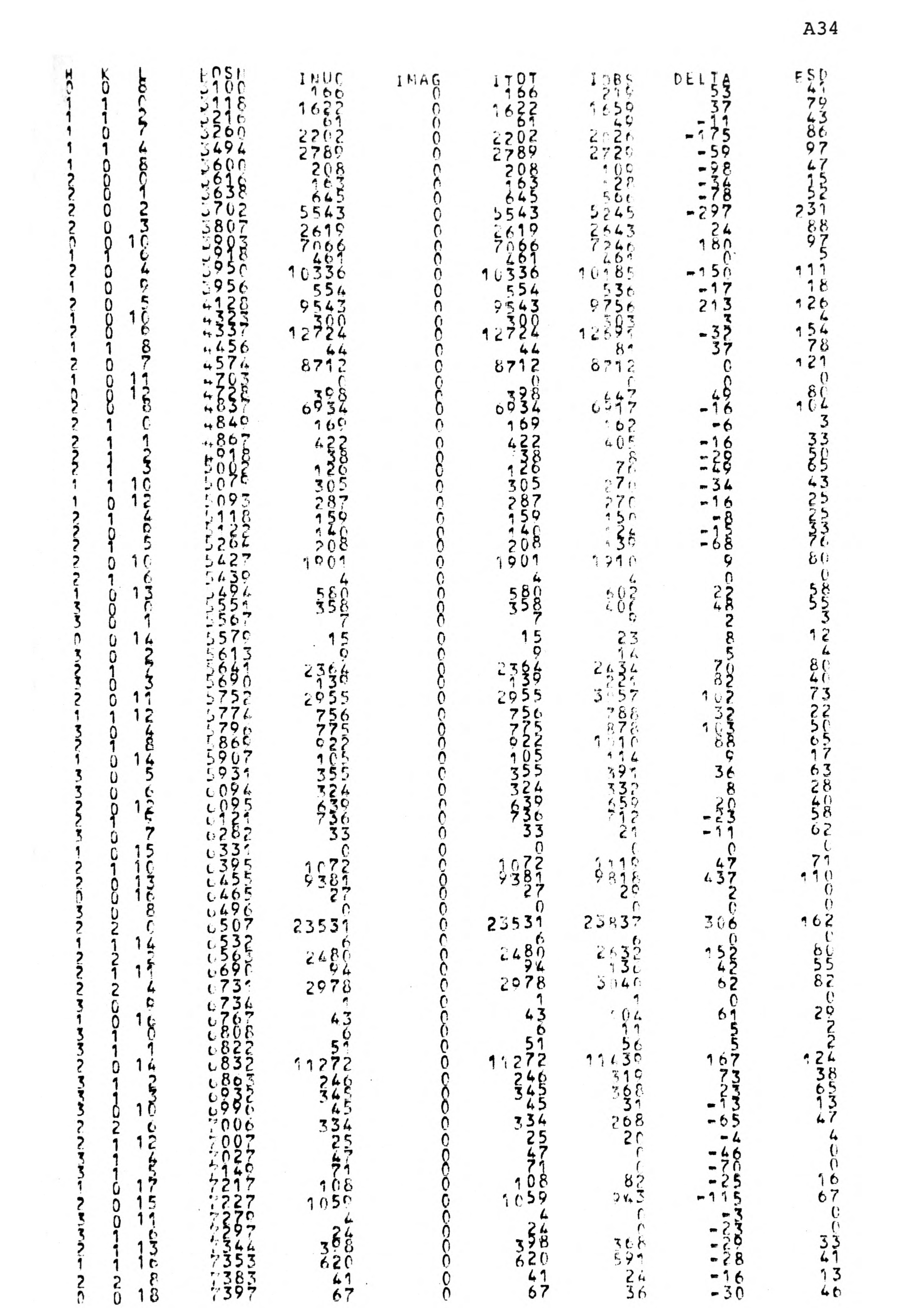


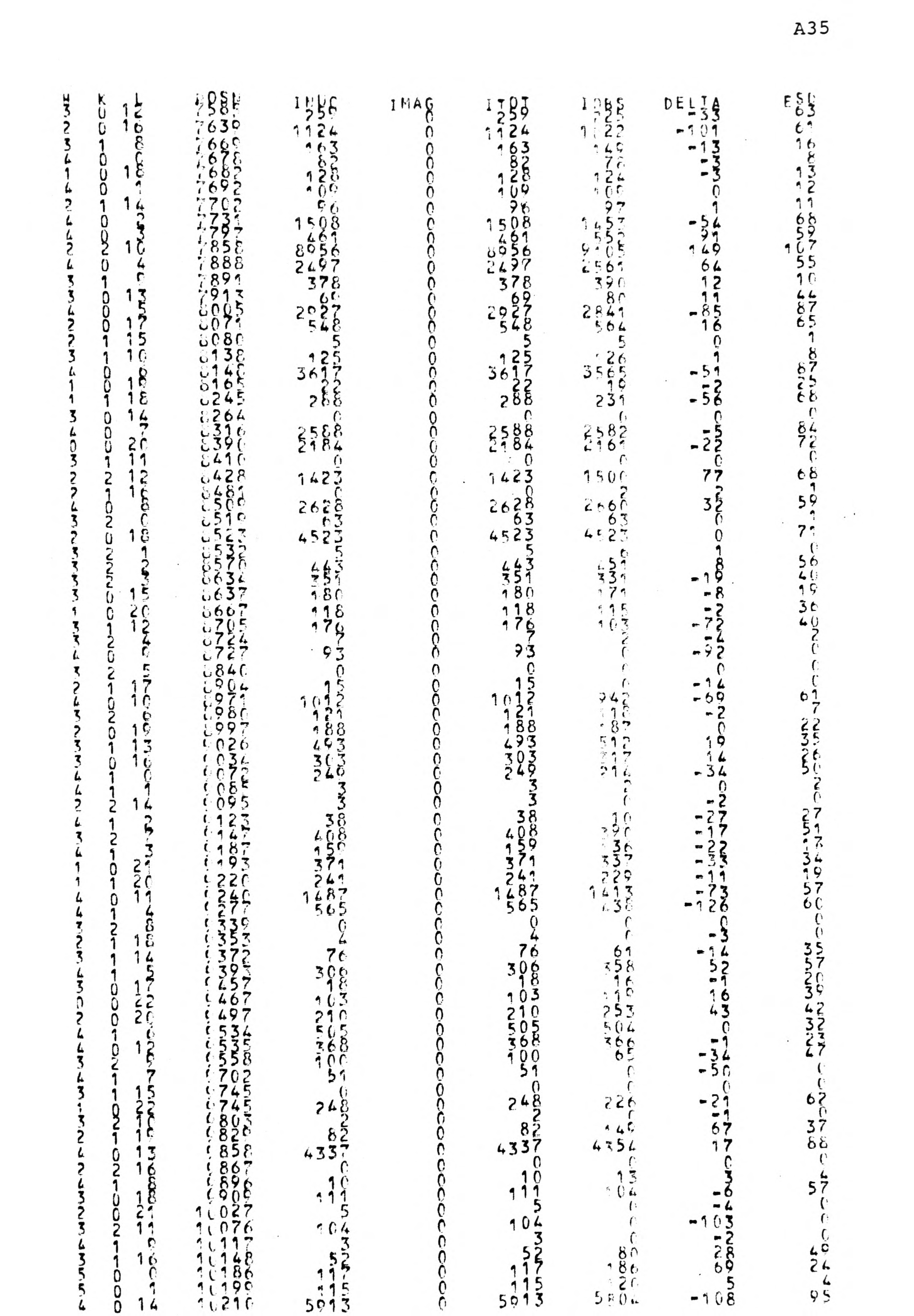
h	k	l	POSN	ITOT	IOBS	DELTA	ESD
1	1	1	3748	1626	1244	-381	154
0	0	2	4357	917	1931	1014	194
2	2	0	6336	935	947	12	164
1	1	3	7605	1396	1418	22	144
2	2	2	8009	432	653	221	232
0	0	4	9599	259	247	-11	140
3	3	1	10817	947	698	-248	129
4	2	0	11239	932	966	34	143
2	2	4	13112	974	1136	162	164











H	K	L	POSL	INUC	IMAG	ITOT	IOBS	DELTA	ESD
5	0	2	10235	24	0	24	42	18	40
5	0	3	10304	6	0	6	0	-5	0
1	1	22	10308	18	0	18	0	-17	0
1	0	23	10332	113	0	113	65	-47	36
2	1	20	10338	37	0	37	25	-11	12
4	1	10	10366	38	0	38	26	-11	9
3	2	12	10377	320	0	320	249	-70	49
3	0	10	10393	0	0	0	0	0	0
5	0	4	10397	17	0	17	0	-16	0
5	0	5	10516	38	0	38	0	-37	0
3	1	17	10583	131	0	131	117	-13	25
4	0	15	10593	701	0	701	626	-74	78
2	0	22	10593	202	0	202	179	-22	23
4	1	11	10645	2	0	2	0	-1	0
5	0	6	10662	0	0	0	0	0	0
0	0	24	10666	314	0	314	253	-60	57
3	2	13	10709	552	0	552	520	-22	57
3	3	0	10758	114	0	114	101	-12	13
2	2	18	10762	458	0	458	394	-63	53
3	3	2	10812	8	0	8	4	-3	16
5	0	7	10836	607	0	607	577	-29	63
2	1	21	10885	255	0	255	279	24	47
3	0	20	10914	302	0	302	270	-31	46
4	1	12	10954	252	0	252	257	5	56
1	0	24	10960	19	0	19	20	1	4
3	3	4	10975	230	0	230	263	33	53
4	0	16	11010	527	0	527	546	19	53
5	0	8	11041	419	0	419	410	-8	33
4	2	0	11051	111	0	111	107	-3	9
3	1	18	11055	139	0	139	133	-5	17
4	2	1	11068	117	0	117	105	-7	15
3	2	14	11075	41	0	41	38	-2	7
4	2	2	11106	1970	0	1970	1833	-136	75
4	2	3	11174	387	0	387	456	67	53
2	0	23	11203	1443	0	1443	1409	-33	63
3	3	6	11246	272	0	272	294	22	27
4	2	4	11271	3139	0	3139	3153	14	74
5	0	9	11275	165	0	165	164	0	4
4	1	13	11298	112	0	112	103	-8	47
4	2	5	11397	3651	0	3651	3598	-52	94
4	0	17	11468	265	0	265	266	1	44
3	2	15	11478	21	0	21	23	2	3
2	1	22	11479	216	0	216	245	29	36
3	0	21	11481	9	0	9	11	2	2
5	0	10	11542	578	0	578	602	24	25
4	2	6	11552	4770	0	4770	4686	-83	87
1	1	24	11559	35	0	35	33	-1	2
3	1	19	11570	42	0	42	35	-6	26
1	0	25	11642	162	0	162	150	-11	62
3	3	8	11644	3	0	3	3	0	1
4	1	14	11680	37	0	37	103	66	45
4	2	7	11738	3267	0	3267	3556	289	94
2	2	20	11821	7624	0	7624	7807	183	11
5	0	11	11843	47	0	47	47	0	2
2	0	24	11870	1109	0	1109	1267	158	64
3	2	16	11924	310	0	310	404	94	41
4	2	8	11957	3825	0	3825	3883	58	64
5	1	0	11968	7	0	7	7	0	0
4	0	18	11972	3327	0	3327	3263	-63	68
5	1	1	11982	39	0	39	60	21	22
5	1	2	12027	0	0	0	0	6	6
0	0	26	12072	176	0	176	120	-55	61
5	1	3	12101	21	0	21	19	-1	3
4	1	15	12104	246	0	246	224	-21	40
3	0	22	12105	0	0	0	0	0	0
2	1	23	12132	57	0	57	50	-6	9
3	1	20	12140	266	0	266	234	-31	43
3	3	10	12171	49	0	49	25	-23	21
5	0	12	12184	28	0	28	13	-14	11
5	1	4	12206	65	0	65	21	-43	16
4	2	9	12210	173	0	173	17	-155	54
5	1	5	12344	53	0	53	0	-52	0
1	0	26	12399	58	0	58	14	-43	34
3	2	17	12421	269	0	269	235	-33	61
4	2	10	12503	1594	0	1594	1713	119	79
5	1	6	12514	1	0	1	1	0	0
4	0	19	12535	225	0	225	226	1	33
5	0	13	12570	45	0	45	51	6	7
4	1	16	12580	357	0	357	395	38	36
2	0	25	12614	2276	0	2276	2397	121	87

H	K	L	POSN	INUC	IMAG	ITOT	IOBS	DELTA	ESD
5	1	7	12721	1169	0	1169	1314	145	83
3	1	21	12778	714	0	714	751	37	59
3	0	23	12805	96	0	96	99	3	8
4	2	1[illegible]	12838	2576	0	2576	2583	7	79
3	3	12	12862	162	0	162	165	3	28
2	1	24	12868	47	0	47	60	13	18
5	1	8	12966	546	0	546	565	19	63
3	2	18	12983	450	0	450	404	-45	39
5	0	14	13008	15	0	15	13	-1	3

APPENDIX 3

Intensity data for the refinements described in Chapter 6

$(NH_4)_{1.25}Al_{11}O_{17.125}$	single crystal X-ray data	A39
$(NH_4)_{1.25}Al_{11}O_{17.125}$	single crystal neutron data	A46
'$H/NH_4Al_{11}O_{17}$'	single crystal neutron data	A50
'$HAl_{11}O_{17}$'	single crystal neutron data	A54

For each reflection,the listing includes the observed (/FO/) and calculated (/FC/) structure factors and the phase which,because the structures are centrosymmetric,is restricted to either 0 or π.In the single crystal neutron diffraction data for ammonium beta alumina (A46-A49),those reflections which are marked with a * have ($\sin\theta/\lambda$) greater than 0.60 and they were not included in the later stages of refinement (see text).

H	/FØ/	/FC/	PHI
** K= 1 L= 0 **			
0	7	6	180
** K= 2 L= 0 **			
-1	127	123	0
0	57	57	180
** K= 3 L= 0 **			
-1	22	22	180
0	94	94	0
** K= 4 L= 0 **			
0	54	55	180
** K= 5 L= 0 **			
-1	68	66	0
0	15	14	180
** K= 6 L= 0 **			
-3	61	59	0
-2	39	39	180
0	221	216	0
** K= 7 L= 0 **			
-2	43	42	0
** K= 8 L= 0 **			
-2	19	20	180
-1	32	32	0
0	16	14	180
** K= 9 L= 0 **			
-3	28	28	0
-2	10	10	180
** K= 10 L= 0 **			
-5	26	26	0
** K= 1 L= 1 **			
0	23	21	0
** K= 2 L= 1 **			
0	116	113	180
** K= 3 L= 1 **			
-1	26	27	0
** K= 4 L= 1 **			
-1	17	17	180
0	88	88	0
** K= 5 L= 1 **			
-2	8	8	0
0	19	19	180
** K= 6 L= 1 **			
-2	69	67	180
-1	11	11	0
** K= 7 L= 1 **			
-3	14	13	0
** K= 8 L= 1 **			
-2	39	40	0
0	32	31	180
** K= 9 L= 1 **			
-2	9	10	180
** K= 10 L= 1 **			
-4	27	26	180
** K= 1 L= 2 **			
0	60	56	0
** K= 2 L= 2 **			
-1	7	6	0
0	85	81	180
** K= 3 L= 2 **			
-1	29	28	0
0	18	19	0
** K= 4 L= 2 **			
-2	103	108	0
-1	30	31	0
0	40	39	180
** K= 5 L= 2 **			
-2	32	32	0
-1	21	20	0
0	10	10	0
** K= 6 L= 2 **			
-3	19	18	0
-2	29	29	180
-1	11	11	0
0	61	61	0
** K= 7 L= 2 **			
-2	15	14	0
-1	19	17	0
0	19	20	0
** K= 8 L= 2 **			
-4	42	48	0
-2	19	20	180
-1	14	14	0
0	15	17	180
** K= 9 L= 2 **			
-4	15	15	0
** K= 1 L= 3 **			
0	49	45	180
** K= 2 L= 3 **			
0	40	45	180
** K= 3 L= 3 **			
-1	23	24	180
0	23	22	0
** K= 4 L= 3 **			
-1	33	33	0
0	60	61	0
** K= 5 L= 3 **			
-2	30	31	180
-1	11	9	180
** K= 6 L= 3 **			
-2	47	47	180
-1	14	15	180
** K= 7 L= 3 **			
-2	14	14	0
-1	18	19	0
0	20	19	160
** K= 8 L= 3 **			
-3	15	15	0
-2	29	28	0
0	23	23	180
** K= 9 L= 3 **			
-4	16	16	180
** K= 10 L= 3 **			
-4	19	18	180
** K= 1 L= 4 **			
0	21	21	180
** K= 2 L= 4 **			
-1	132	130	0
0	78	70	180
** K= 3 L= 4 **			
-1	27	27	180
0	102	105	0
** K= 4 L= 4 **			
-2	106	108	180
-1	14	14	180
0	18	16	180
** K= 5 L= 4 **			
-1	78	75	0
0	19	18	180
** K= 6 L= 4 **			

H	/FØ/	/FC/	PHI
-3	68	67	0
-1	12	12	180
0	64	62	180
** K=	7	L=	4 **
-3	12	12	180
-2	50	50	0
** K=	8	L=	4 **
-4	50	49	180
-1	38	36	0
** K=	9	L=	4 **
-3	31	32	0
-1	9	8	180
** K=	10	L=	4 **
-5	28	28	0
** K=	1	L=	5 **
0	9	8	0
** K=	2	L=	5 **
0	132	129	0
** K=	3	L=	5 **
-1	13	14	0
0	17	17	0
** K=	4	L=	5 **
-1	7	8	180
0	74	74	180
** K=	5	L=	5 **
-1	14	14	180
0	12	12	180
** K=	6	L=	5 **
-2	51	50	0
** K=	7	L=	5 **
-2	16	17	0
** K=	8	L=	5 **
-2	31	31	180
0	29	27	0
** K=	9	L=	5 **
-3	14	13	180
** K=	0	L=	6 **
0	13	13	0
** K=	1	L=	6 **
0	30	29	180
** K=	2	L=	6 **

H	/FØ/	/FC/	PHI
-1	114	114	0
0	148	144	0
** K=	3	L=	6 **
-1	21	21	180
0	108	109	0
** K=	4	L=	6 **
-2	19	19	0
-1	21	20	180
0	90	88	0
** K=	5	L=	6 **
-2	19	19	180
-1	86	84	0
0	15	15	180
** K=	6	L=	6 **
-3	74	72	0
-2	65	63	0
-1	14	13	180
0	13	13	0
** K=	7	L=	6 **
-3	12	13	180
-2	57	56	0
-1	11	10	180
0	11	10	180
** K=	8	L=	6 **
-4	10	10	0
-2	42	42	0
-1	41	41	0
0	38	36	0
** K=	9	L=	6 **
-3	35	36	0
** K=	10	L=	6 **
-5	31	30	0
** K=	1	L=	7 **
0	140	136	0
** K=	2	L=	7 **
0	132	129	0
** K=	3	L=	7 **
-1	128	125	0
0	13	12	0
** K=	4	L=	7 **
-1	103	101	180
0	76	76	180
** K=	5	L=	7 **
-2	87	87	0
0	81	81	180

H	/FØ/	/FC/	PHI
** K=	6	L=	7 **
-2	56	56	0
-1	70	68	0
** K=	7	L=	7 **
-3	64	62	0
-1	52	50	180
0	44	43	0
** K=	8	L=	7 **
-3	45	45	180
-2	36	36	180
0	33	30	0
** K=	9	L=	7 **
-4	35	34	0
-2	38	38	180
-1	34	32	0
** K=	0	L=	8 **
0	99	96	0
** K=	1	L=	8 **
0	52	50	0
** K=	2	L=	8 **
-1	6	3	0
0	111	109	0
** K=	3	L=	8 **
-1	56	56	0
** K=	4	L=	8 **
-2	65	62	0
-1	37	37	0
0	60	61	0
** K=	5	L=	8 **
-2	23	23	0
0	42	41	0
** K=	6	L=	8 **
-2	44	45	0
-1	32	33	0
0	38	36	0
** K=	7	L=	8 **
-3	36	35	0
-1	15	15	0
** K=	8	L=	8 **
-4	34	31	0
-3	20	20	0
-2	31	31	0
0	27	27	0
** K=	9	L=	8 **
-2	24	24	0

H	/FØ/	/FC/	PHI
-1	21	21	0
** K=	1	L= 9	**
0	60	59	0
** K=	2	L= 9	**
0	47	49	0
** K=	3	L= 9	**
-1	53	53	0
** K=	4	L= 9	**
-1	41	42	180
0	34	33	180
** K=	5	L= 9	**
-2	30	31	0
0	35	36	180
** K=	6	L= 9	**
-2	23	23	0
-1	28	29	0
** K=	7	L= 9	**
-3	26	28	0
-1	18	18	180
0	16	16	0
** K=	8	L= 9	**
-3	18	19	180
-2	13	13	180
** K=	9	L= 9	**
-2	19	20	180
-1	16	16	0
** K=	0	L= 10	**
0	123	111	180
** K=	1	L= 10	**
0	62	62	0
** K=	2	L= 10	**
-1	43	43	180
0	80	80	180
** K=	3	L= 10	**
-1	70	71	0
0	28	29	180
** K=	4	L= 10	**
-1	45	45	0
0	54	55	180
** K=	5	L= 10	**
-2	26	26	0
-1	21	21	180

H	/FØ/	/FC/	PHI
0	51	52	0
** K=	6	L= 10	**
-3	21	22	180
-2	44	43	180
-1	38	37	0
** K=	7	L= 10	**
-3	39	39	0
-2	12	11	180
-1	16	16	0
** K=	8	L= 10	**
-3	20	20	0
-2	30	30	180
-1	13	12	180
0	27	25	180
** K=	9	L= 10	**
-3	9	9	180
-2	28	30	0
** K=	1	L= 11	**
0	5	6	180
** K=	2	L= 11	**
0	140	142	180
** K=	4	L= 11	**
0	104	107	0
** K=	6	L= 11	**
-2	79	81	180
** K=	8	L= 11	**
-2	51	52	0
0	45	44	180
** K=	0	L= 12	**
0	32	28	180
** K=	1	L= 12	**
0	15	16	180
** K=	2	L= 12	**
-1	72	72	0
0	23	20	0
** K=	3	L= 12	**
0	56	57	0
** K=	4	L= 12	**
0	15	14	0
** K=	5	L= 12	**
-2	11	11	180
-1	39	38	0

H	/FØ/	/FC/	PHI
** K=	6	L= 12	**
-3	33	32	0
-2	13	12	0
** K=	7	L= 12	**
-2	26	25	0
** K=	8	L= 12	**
-1	14	14	0
** K=	9	L= 12	**
-3	15	14	0
** K=	1	L= 13	**
0	62	63	0
** K=	2	L= 13	**
0	206	217	180
** K=	3	L= 13	**
-1	45	45	0
0	8	8	180
** K=	4	L= 13	**
-1	45	45	180
0	159	162	0
** K=	5	L= 13	**
-2	40	40	0
0	25	25	180
** K=	6	L= 13	**
-2	124	126	180
-1	26	26	0
** K=	7	L= 13	**
-3	20	19	0
-1	24	25	180
0	25	25	0
** K=	8	L= 13	**
-3	22	21	180
-2	81	82	0
0	70	68	180
** K=	9	L= 13	**
-4	20	21	0
** K=	0	L= 14	**
0	150	151	180
** K=	1	L= 14	**
0	39	41	0
** K=	2	L= 14	**
-1	8	9	180

H	/FO/	/FC/	PHI
0	198	206	0
** K=	3	L= 14	**
-1	37	38	0
** K=	4	L= 14	**
-2	109	113	180
-1	31	31	0
0	150	153	0
** K=	5	L= 14	**
-2	24	24	0
0	24	24	0
** K=	6	L= 14	**
-2	117	118	0
-1	20	20	0
0	61	62	180
** K=	7	L= 14	**
-3	16	17	0
-1	16	15	0
** K=	8	L= 14	**
-4	46	48	180
-3	13	14	0
-2	77	80	0
0	69	68	0
** K=	1	L= 15	**
0	18	19	0
** K=	2	L= 15	**
0	15	16	180
** K=	3	L= 15	**
-1	13	13	0
0	12	13	180
** K=	4	L= 15	**
-1	15	15	180
** K=	5	L= 15	**
-2	17	17	0
-1	12	12	0
** K=	6	L= 15	**
-2	11	7	180
-1	10	11	0
** K=	7	L= 15	**
-2	16	15	180
-1	14	14	180
** K=	8	L= 15	**
-3	11	11	180
** K=	9	L= 15	**

H	/FO/	/FC/	PHI
-4	10	11	0
** K=	0	L= 16	**
0	35	36	180
** K=	1	L= 16	**
0	26	26	0
** K=	2	L= 16	**
-1	52	53	0
0	23	25	0
** K=	3	L= 16	**
-1	16	17	0
0	40	41	0
** K=	4	L= 16	**
-2	34	35	180
-1	18	18	0
0	20	21	0
** K=	5	L= 16	**
-2	20	20	0
-1	29	29	0
0	11	10	0
** K=	6	L= 16	**
-3	26	27	0
-2	16	17	0
-1	11	11	0
0	23	23	180
** K=	7	L= 16	**
-2	19	20	0
-1	13	13	0
0	15	15	0
** K=	8	L= 16	**
-4	18	18	180
-1	15	15	0
** K=	9	L= 16	**
-4	13	13	0
-3	14	14	0
** K=	1	L= 17	**
0	46	47	0
** K=	2	L= 17	**
0	42	45	0
** K=	3	L= 17	**
-1	34	34	0
0	14	15	180
** K=	4	L= 17	**
-1	36	37	180
0	37	38	180

H	/FO/	/FC/	PHI
** K=	5	L= 17	**
-2	33	34	0
-1	8	9	0
0	18	18	180
** K=	6	L= 17	**
-2	28	28	0
-1	22	22	0
** K=	7	L= 17	**
-3	13	15	0
-2	15	14	180
-1	22	23	180
0	21	22	0
** K=	8	L= 17	**
-3	19	20	180
-2	18	17	180
** K=	9	L= 17	**
-4	18	19	0
-3	11	10	0
** K=	0	L= 18	**
0	82	83	0
** K=	1	L= 18	**
0	45	47	0
** K=	2	L= 18	**
-1	35	37	180
0	92	92	180
** K=	3	L= 18	**
-1	36	36	0
0	28	29	180
** K=	4	L= 18	**
-2	66	65	0
-1	35	35	0
0	66	66	180
** K=	5	L= 18	**
-2	34	34	0
-1	20	21	180
0	21	21	0
** K=	6	L= 18	**
-3	20	19	180
-2	53	54	180
-1	20	19	0
0	38	38	0
** K=	7	L= 18	**
-3	14	14	0
-2	16	15	180
-1	21	21	0
0	23	23	0

H	/F0/	/FC/	PHI
** K=	8	L= 18	**
-4	30	29	0
-3	14	15	0
-2	39	40	180
** K=	9	L= 18	**
-4	18	19	0
** K=	1	L= 19	**
0	33	35	0
** K=	2	L= 19	**
0	42	44	180
** K=	3	L= 19	**
-1	25	26	0
** K=	4	L= 19	**
-1	25	25	180
0	34	34	0
** K=	5	L= 19	**
-2	25	26	0
0	12	13	180
** K=	6	L= 19	**
-2	24	25	180
-1	14	15	0
** K=	7	L= 19	**
-1	17	16	180
0	18	15	0
** K=	8	L= 19	**
-3	11	12	180
-2	15	16	0
** K=	0	L= 20	**
0	146	150	0
** K=	1	L= 20	**
0	69	68	0
** K=	2	L= 20	**
-1	83	84	180
0	16	16	0
** K=	3	L= 20	**
-1	52	51	0
0	73	75	180
** K=	4	L= 20	**
-2	106	106	0
-1	50	50	0
0	13	13	0
** K=	5	L= 20	**
-2	48	49	0
-1	57	57	180
0	31	30	0
** K=	6	L= 20	**
-3	47	49	180
-2	12	12	0
-1	31	31	0
0	72	69	0
** K=	7	L= 20	**
-3	24	24	0
-2	40	42	180
-1	31	31	0
0	32	32	0
** K=	8	L= 20	**
-4	60	60	0
-3	25	25	0
-1	30	30	180
** K=	1	L= 21	**
0	68	69	180
** K=	2	L= 21	**
0	36	35	180
** K=	3	L= 21	**
-1	56	57	180
** K=	4	L= 21	**
-1	51	51	0
0	26	26	0
** K=	5	L= 21	**
-2	48	48	180
0	35	36	0
** K=	6	L= 21	**
-2	21	21	180
-1	34	35	180
** K=	7	L= 21	**
-3	28	29	180
-1	30	32	0
0	30	28	180
** K=	8	L= 21	**
-3	28	28	0
-2	13	14	0
** K=	0	L= 22	**
0	33	34	0
** K=	1	L= 22	**
0	39	42	0
** K=	2	L= 22	**
0	52	53	0
** K=	3	L= 22	**
-1	29	30	0
** K=	4	L= 22	**
-2	28	28	0
-1	31	32	0
0	42	42	0
** K=	5	L= 22	**
-2	32	35	0
0	15	16	0
** K=	6	L= 22	**
-2	34	33	0
-1	16	18	0
0	21	22	0
** K=	7	L= 22	**
-1	23	24	0
0	26	27	0
** K=	8	L= 22	**
-4	18	19	0
-3	16	17	0
-2	23	24	0
** K=	1	L= 23	**
0	33	33	180
** K=	3	L= 23	**
-1	22	23	180
** K=	4	L= 23	**
-1	27	27	0
** K=	5	L= 23	**
-2	27	26	180
0	12	12	0
** K=	6	L= 23	**
-1	17	16	180
** K=	7	L= 23	**
-1	19	19	0
0	19	20	180
** K=	8	L= 23	**
-3	16	16	0
** K=	0	L= 24	**
0	111	111	180
** K=	1	L= 24	**
0	16	16	0

H	/FO/	/FC/	PHI
** K=	2	L= 24	**
-1	35	36	0
0	16	15	0
** K=	3	L= 24	**
-1	9	8	0
0	28	29	0
** K=	4	L= 24	**
-2	89	91	180
-1	11	11	0
0	10	11	0
** K=	5	L= 24	**
-2	15	16	0
-1	20	22	0
** K=	6	L= 24	**
-3	19	20	0
-2	17	8	0
0	64	64	180
** K=	7	L= 24	**
-2	14	14	0
0	16	15	0
** K=	8	L= 24	**
-4	54	54	180
** K=	1	L= 25	**
0	23	21	0
** K=	2	L= 25	**
0	76	79	0
** K=	3	L= 25	**
-1	21	20	0
** K=	4	L= 25	**
-1	16	16	180
0	63	64	180
** K=	5	L= 25	**
-2	12	12	0
0	16	16	180
** K=	6	L= 25	**
-2	51	52	0
** K=	1	L= 25	**
0	36	36	0
** K=	2	L= 26	**
-1	52	54	180
0	53	53	0
** K=	3	L= 26	**
-1	34	33	0
0	44	46	180
** K=	4	L= 26	**
-2	72	71	180
-1	28	29	0
0	42	41	0
** K=	5	L= 26	**
-2	24	24	0
-1	34	37	180
0	25	23	0
** K=	6	L= 26	**
-3	31	34	180
-2	32	32	0
-1	20	20	0
0	46	46	180
** K=	7	L= 26	**
-3	17	18	0
-2	27	27	180
-1	15	15	0
** K=	1	L= 27	**
0	18	19	180
** K=	2	L= 27	**
0	134	131	0
** K=	3	L= 27	**
-1	14	14	180
** K=	4	L= 27	**
-1	15	15	0
0	104	103	180
** K=	6	L= 27	**
-2	84	85	0
-1	11	9	180
** K=	0	L= 28	**
0	112	112	0
** K=	1	L= 28	**
0	16	15	0
** K=	2	L= 28	**
-1	8	7	0
0	22	22	0
** K=	3	L= 28	**
-1	19	19	0
** K=	4	L= 28	**
-2	85	87	0
-1	12	12	0
0	21	20	0
** K=	5	L= 28	**
0	19	19	0
** K=	6	L= 28	**
-2	21	20	0
-1	15	15	0
0	59	58	0
** K=	7	L= 28	**
-3	18	18	0
** K=	1	L= 29	**
0	13	11	180
** K=	2	L= 29	**
0	15	9	0
** K=	5	L= 29	**
-2	8	10	180
** K=	1	L= 30	**
0	26	28	0
** K=	3	L= 30	**
-1	32	33	0
** K=	4	L= 30	**
-1	22	24	0
** K=	5	L= 30	**
-2	15	15	0
0	28	30	0
** K=	6	L= 30	**
-1	22	23	0
** K=	1	L= 31	**
0	24	22	180
** K=	2	L= 31	**
0	53	55	180
** K=	3	L= 31	**
-1	18	19	180
** K=	4	L= 31	**
-1	19	18	0
0	46	45	0
** K=	5	L= 31	**
-2	16	16	180
0	14	14	0
** K=	6	L= 31	**
-2	36	37	180

H	/F0/	/FC/	PHI
-1	14	13	180
** K=	0	L= 32	**
0	84	84	180
** K=	2	L= 32	**
-1	21	21	0
0	18	16	0
** K=	3	L= 32	**
0	18	18	0
** K=	4	L= 32	**
-2	72	71	180
0	11	12	0
** K=	5	L= 32	**
-1	16	14	0
** K=	1	L= 33	**
0	42	40	180
** K=	3	L= 33	**
-1	36	39	180
** K=	4	L= 33	**
-1	28	31	0
** K=	5	L= 33	**
-2	24	26	180
0	29	31	0
** K=	1	L= 34	**
0	24	22	180
** K=	2	L= 34	**
-1	51	49	0
0	46	45	0
** K=	3	L= 34	**
-1	18	18	180
0	47	45	0
** K=	4	L= 34	**
-1	18	18	180
0	39	38	0
** K=	5	L= 34	**
-2	18	18	180
-1	40	38	0
** K=	1	L= 35	**
0	14	8	0
** K=	2	L= 35	**
0	14	12	0
** K=	0	L= 36	**
0	54	56	0
** K=	2	L= 36	**
-1	37	39	0
** K=	3	L= 36	**
0	32	35	0
** K=	4	L= 36	**
-2	49	47	0
** K=	2	L= 37	**
0	19	17	0
** K=	0	L= 38	**
0	44	47	0
** K=	1	L= 38	**
0	34	20	0
** K=	2	L= 38	**
0	45	43	180
** K=	3	L= 38	**
-1	15	17	0
** K=	1	L= 39	**
0	33	29	180
** K=	3	L= 39	**
-1	28	28	180
** K=	0	L= 40	**
0	86	87	0
** K=	1	L= 40	**
0	18	13	180
** K=	2	L= 40	**
-1	27	28	0
0	46	36	180

H	/F0/	/FC/	PHI

```
   H /FØ/ /FC/ PHI

** K=  1  L=  0 **

   0   58    7   0

** K=  2  L=  0 **

  -1  460  463   0
   0   86   50   0

** K=  3  L=  0 **

  -1  251  248 180
   0  426  416   0

** K=  4  L=  0 **

  -2 2918 3037   0
  -1  207  205 180
   0  133  134   0

** K=  5  L=  0 **

  -2  113  138   0
  -1  429  425   0
   0  332  339 180

** K=  6  L=  0 **

  -3  416  416   0
  -2  170  182   0
  -1  160  159 180
   0 1472 2346   0*

** K=  7  L=  0 **

  -3   93  200 180*
  -2  112  248   0*

** K=  1  L=  1 **

   0  169  161   0

** K=  2  L=  1 **

   0  194  184 180

** K=  3  L=  1 **

  -1   29   13 180
   0   85   80   0

** K=  4  L=  1 **

  -1   53   37 180
   0   93   44 180

** K=  5  L=  1 **

  -2   98   97 180
  -1   39   28 180
   0  109  119 180

** K=  6  L=  1 **

  -2  123  105 180
  -1   55   23 180
   0  171   14   0*

** K=  1  L=  2 **

   0  196  185   0
```

```
   H /FØ/ /FC/ PHI

** K=  2  L=  2 **

  -1  108  116 180
   0  480  496 180

** K=  3  L=  2 **

  -1  152  150   0
   0  108   98 180

** K=  4  L=  2 **

  -2  567  569   0
  -1  365  363   0
   0  493  484 180

** K=  5  L=  2 **

  -2  313  296   0
  -1   83   85 180
   0   61   51   0

** K=  6  L=  2 **

  -3   48   33 180
  -2  473  451 180
  -1   66   71   0*
   0  254  519   0

** K=  1  L=  3 **

   0  230  238 180

** K=  2  L=  3 **

   0  407  403   0

** K=  3  L=  3 **

  -1   87   72   0
   0  118  121   0

** K=  4  L=  3 **

  -1  149  151   0
   0  188  150 180

** K=  5  L=  3 **

  -2  157  130 180
  -1  142  141 180
   0   90   74 180

** K=  6  L=  3 **

  -2  255  255   0
  -1   49   13   0
   0   44   10 180*

** K=  7  L=  3 **

  -2   73  217   0*

** K=  0  L=  4 **

   0  792  855 180

** K=  1  L=  4 **

   0   67   48 180

** K=  2  L=  4 **
```

```
   H /FØ/ /FC/ PHI

  -1  517  524   0
   0 1001 1050 180

** K=  3  L=  4 **

  -1  211  210 180
   0  457  448   0

** K=  4  L=  4 **

  -2  616  620 180
  -1  249  234 180
   0  914  908 180

** K=  5  L=  4 **

  -2   51    7   0
  -1  400  409   0
   0  219  237 180

** K=  6  L=  4 **

  -3  389  377   0
  -2  801  788 180
  -1  148  139 180
   0  248  648 180*

** K=  1  L=  5 **

   0   72   60   0

** K=  2  L=  5 **

   0  955  953   0

** K=  3  L=  5 **

  -1   73   57 180
   0  243  240   0

** K=  4  L=  5 **

  -1   38   15   0
   0  966  991 180

** K=  5  L=  5 **

  -2   98  116 180
  -1  202  196 180
   0   80  111 180

** K=  6  L=  5 **

  -2  755  743   0
  -1   49   50 180*

** K=  0  L=  6 **

   0  149  189   0

** K=  1  L=  6 **

   0   84   78 180

** K=  2  L=  6 **

  -1   57   15   0
   0 1122 1111   0

** K=  3  L=  6 **

  -1   68   58   0
```

H	/F0/	/FC/	PHI	
0	108	93	0	
** K=	4	L=	6	**
-2	124	91	0	
-1	115	104	0	
0	999	976	0	
** K=	5	L=	6	**
-2	73	83	180	
-1	135	107	0	
0	67	79	0	
** K=	6	L=	6	**
-3	125	119	0	
-2	859	839	0	
-1	56	37	0	
** K=	1	L=	7	**
0	399	387	0	
** K=	2	L=	7	**
0	849	844	0	
** K=	3	L=	7	**
-1	586	573	0	
0	130	121	0	
** K=	4	L=	7	**
-1	357	336	180	
0	646	630	180	
** K=	5	L=	7	**
-2	326	319	0	
-1	101	104	180	
0	439	457	180	
** K=	6	L=	7	**
-2	669	669	0	
-1	328	372	0	
** K=	7	L=	7	**
-3	165	391	0*	
** K=	0	L=	8	**
0	272	256	0	
** K=	1	L=	8	**
0	136	130	0	
** K=	2	L=	8	**
-1	320	332	0	
0	899	904	0	
** K=	3	L=	8	**
-1	183	175	0	
0	212	221	0	
** K=	4	L=	8	**

H	/F0/	/FC/	PHI	
-2	333	289	0	
-1	41	2	180	
0	832	845	0	
** K=	5	L=	8	**
-2	56	7	0	
-1	123	132	0	
0	259	283	0	
** K=	6	L=	8	**
-3	74	75	0	
-2	820	827	0	
-1	177	184	0	
0	52	163	0*	
** K=	1	L=	9	**
0	146	143	0	
** K=	2	L=	9	**
0	363	350	0	
** K=	3	L=	9	**
-1	105	85	0	
0	45	29	0	
** K=	4	L=	9	**
-1	166	152	180	
0	378	376	180	
** K=	5	L=	9	**
-2	79	69	0	
-1	74	54	180	
0	230	226	180	
** K=	6	L=	9	**
-2	255	229	0	
-1	180	131	0*	
0	31	29	180*	
** K=	0	L=	10	**
0	1787	1802	180	
** K=	1	L=	10	**
0	182	165	0	
** K=	2	L=	10	**
-1	467	469	180	
0	423	398	180	
** K=	3	L=	10	**
-1	410	400	0	
0	297	297	180	
** K=	4	L=	10	**
-2	1566	1557	180	
-1	280	267	0	
0	400	402	180	
** K=	5	L=	10	**

H	/F0/	/FC/	PHI	
-2	55	22	180	
-1	212	210	180	
0	417	434	0	
** K=	6	L=	10	**
-3	193	203	180	
-2	471	463	180	
-1	312	338	0*	
** K=	7	L=	10	**
-3	440	373	0*	
** K=	1	L=	11	**
0	138	123	0	
** K=	2	L=	11	**
0	718	728	180	
** K=	3	L=	11	**
-1	163	149	0	
0	48	22	180	
** K=	4	L=	11	**
-1	81	50	180	
0	688	680	0	
** K=	5	L=	11	**
-2	111	97	0	
-1	83	71	0	
0	56	16	0	
** K=	6	L=	11	**
-2	527	515	180	
-1	43	39	0*	
** K=	7	L=	11	**
-3	110	19	180*	
** K=	0	L=	12	**
0	428	458	180	
** K=	1	L=	12	**
0	197	205	180	
** K=	2	L=	12	**
-1	590	607	0	
0	99	86	0	
** K=	3	L=	12	**
-1	121	110	180	
0	414	436	0	
** K=	4	L=	12	**
-2	489	489	180	
-1	248	250	180	
0	106	82	0	
** K=	5	L=	12	**

H	/F0/	/FC/	PHI	
-2	300	281	180	
-1	281	284	0	
0	68	76	0	
** K=	6	L= 12	**	
-2	157	151	0	*
** K=	7	L= 12	**	
-3	123	86	0	*
** K=	1	L= 13	**	
0	153	155	0	
** K=	2	L= 13	**	
0	1204	1199	180	
** K=	3	L= 13	**	
-1	60	26	0	
0	128	110	180	
** K=	4	L= 13	**	
-1	221	232	180	
0	1018	1044	0	
** K=	5	L= 13	**	
-2	253	252	0	
-1	54	28	0	
0	52	46	180	
** K=	6	L= 13	**	
-2	866	998	180	*
** K=	7	L= 13	**	
-3	88	56	0	*
** K=	0	L= 14	**	
0	303	304	180	
** K=	1	L= 14	**	
0	119	116	0	
** K=	2	L= 14	**	
-1	319	326	180	
0	1595	1580	0	
** K=	3	L= 14	**	
-1	206	207	0	
0	148	151	180	
** K=	4	L= 14	**	
-2	153	124	180	
-1	173	174	0	
0	1409	1425	0	
** K=	5	L= 14	**	
-2	65	52	0	
-1	76	44	180	
0	164	154	0	
** K=	6	L= 14	**	
-2	647	1202	0	*
** K=	1	L= 15	**	
0	154	154	0	
** K=	2	L= 15	**	
0	707	721	180	
** K=	3	L= 15	**	
-1	127	124	0	
0	170	171	180	
** K=	4	L= 15	**	
-1	86	79	180	
0	618	635	0	
** K=	5	L= 15	**	
-2	124	126	0	
-1	232	230	0	
0	77	55	0	*
** K=	6	L= 15	**	
-2	197	485	180	*
** K=	0	L= 16	**	
0	291	287	0	
** K=	1	L= 16	**	
0	83	56	0	
** K=	2	L= 16	**	
-1	685	676	0	
0	341	335	180	
** K=	3	L= 16	**	
-1	47	46	180	
0	494	504	0	
** K=	4	L= 16	**	
-2	167	142	0	
-1	17	6	180	
0	289	294	180	
** K=	5	L= 16	**	
-2	102	106	0	
-1	379	385	0	
** K=	6	L= 16	**	
-3	434	361	0	
-2	62	173	180	*
** K=	1	L= 17	**	
0	40	51	0	
** K=	2	L= 17	**	
0	287	269	180	
** K=	3	L= 17	**	
-1	77	66	180	
0	190	176	180	
** K=	4	L= 17	**	
-1	113	120	180	
0	195	201	0	
** K=	5	L= 17	**	
-2	135	137	0	
-1	134	83	0	*
** K=	0	L= 18	**	
0	131	100	0	
** K=	1	L= 18	**	
0	183	169	0	
** K=	2	L= 18	**	
-1	398	385	180	
0	1072	1020	180	
** K=	3	L= 18	**	
-1	118	110	0	
0	269	259	180	
** K=	4	L= 18	**	
-2	190	145	0	
-1	200	214	0	
0	901	919	180	
** K=	5	L= 18	**	
-2	258	249	0	
-1	189	158	180	*
** K=	6	L= 18	**	
-3	202	120	180	*
** K=	1	L= 19	**	
0	83	78	0	
** K=	2	L= 19	**	
0	327	339	180	
** K=	3	L= 19	**	
-1	56	78	0	
0	56	42	180	
** K=	4	L= 19	**	
-1	52	47	180	*
0	354	346	0	
** K=	5	L= 19	**	

```
   H /FØ/ /FC/ PHI

  -2  131  123    0 *
** K=  0  L= 20 **
   0 1776 1703    0
** K=  1  L= 20 **
   0  152  156    0
** K=  2  L= 20 **
  -1  168  180 180
   0   67   40 180
** K=  3  L= 20 **
  -1   55   46 180
   0  250  260 180
** K=  4  L= 20 **
  -2 1316 1482    0
  -1   81   35    0
** K=  5  L= 20 **
  -2  108  210    0 *
  -1   87  248 180 *
** K=  6  L= 20 **
  -3  228  210 180*
** K=  1  L= 21 **
   0  356  334 180
** K=  2  L= 21 **
   0   92   81    0
** K=  3  L= 21 **
  -1  366  380 180
   0   51   34    0
** K=  4  L= 21 **
  -1  295  313    0
   0  121  152 180 *
** K=  5  L= 21 **
  -2  145  356 180 *
** K=  0  L= 22 **
   0  882  836    0
** K=  1  L= 22 **
   0  366  351    0
** K=  2  L= 22 **
  -1  213  184 180
   0  449  436    0
** K=  3  L= 22 **
  -1  295  311    0*
```

```
   H /FØ/ /FC/ PHI

   0  142  129 180
** K=  4  L= 22 **
  -1  431  435    0
   0  147  409    0*
** K=  1  L= 23 **
   0  215  228 180
** K=  2  L= 23 **
   0  451  459    0*
** K=  3  L= 23 **
  -1   65   21 180
   0   97  104    0
** K=  4  L= 23 **
  -1  124  177    0*
** K=  5  L= 23 **
  -2  265  169 180*
** K=  0  L= 24 **
   0  750  731 180
** K=  1  L= 24 **
   0  143  115    0
** K=  2  L= 24 **
  -1  181  165    0
   0  628  595 180
** K=  3  L= 24 **
  -1   44   39 180
   0  191  136    0*
** K=  4  L= 24 **
  -2  750  611 180*
  -1   21   42 180*
** K=  5  L= 24 **
  -2  219   94    0*
** K=  1  L= 25 **
   0  137  174    0
** K=  2  L= 25 **
   0  759  797    0
** K=  3  L= 25 **
  -1  131   86    0
** K=  1  L= 26 **
   0  154  183    0
** K=  2  L= 26 **
```

```
   H /FØ/ /FC/ PHI

   0  378  414    0*
** K=  3  L= 26 **
  -1  110  262    0*
   0  215  591 180*
** K=  4  L= 26 **
  -2  900  784 180*
** K=  1  L= 27 **
   0   85   86 180
** K=  2  L= 27 **
   0  567  958    0*
** K=  2  L= 28 **
  -1  114  117    0*
   0  346  561    0*
```

H	/FO/	/FC/	PHI
** K= 1 L= 0 **			
0	53	12	0
** K= 2 L= 0 **			
-1	511	483	0
0	98	65	0
** K= 3 L= 0 **			
-1	227	217	180
0	560	554	0
** K= 4 L= 0 **			
-2	3324	3378	0
-1	163	102	180
0	223	190	0
** K= 5 L= 0 **			
-2	136	171	0
-1	494	501	0
0	365	385	180
** K= 6 L= 0 **			
-3	463	484	0
-2	185	178	0
-1	208	166	180
** K= 7 L= 0 **			
-3	363	330	180
-2	434	451	0
** K= 1 L= 1 **			
0	172	148	0
** K= 2 L= 1 **			
0	183	174	180
** K= 3 L= 1 **			
-1	92	31	0
0	137	132	0
** K= 4 L= 1 **			
-1	63	9	180
0	134	76	0
** K= 5 L= 1 **			
-2	74	71	180
-1	59	13	0
0	156	167	180
** K= 6 L= 1 **			
-2	149	181	180
-1	61	46	0
** K= 7 L= 1 **			
-3	174	155	0
-2	125	82	0
** K= 1 L= 2 **			
0	213	191	0
** K= 2 L= 2 **			
-1	126	113	180
0	555	529	180
** K= 3 L= 2 **			
-1	117	99	0
0	215	163	180
** K= 4 L= 2 **			
-2	648	660	0
-1	320	301	0
0	624	627	180
** K= 5 L= 2 **			
-2	358	351	0
-1	129	31	180
0	101	47	180
** K= 6 L= 2 **			
-3	96	44	0
-2	543	614	180
-1	84	50	0
** K= 7 L= 2 **			
-3	129	99	180
-2	137	65	0
** K= 1 L= 3 **			
0	248	229	180
** K= 2 L= 3 **			
0	412	399	0
** K= 3 L= 3 **			
-1	80	33	0
0	108	62	0
** K= 4 L= 3 **			
-1	151	141	0
0	274	258	180
** K= 5 L= 3 **			
-2	197	208	180
-1	189	197	180
0	99	73	180
** K= 6 L= 3 **			
-2	298	287	0
-1	72	61	180
** K= 7 L= 3 **			
-3	91	47	0
-2	307	292	0
** K= 0 L= 4 **			
0	846	856	180
** K= 1 L= 4 **			
0	90	77	180
** K= 2 L= 4 **			
-1	525	515	0
0	1124	1075	180
** K= 3 L= 4 **			
-1	186	183	180
0	569	562	0
** K= 4 L= 4 **			
-2	728	706	180
-1	208	192	180
0	961	951	180
** K= 5 L= 4 **			
-2	59	35	180
-1	465	473	0
0	224	214	180
** K= 6 L= 4 **			
-3	415	433	0
-2	966	935	180
-1	169	197	180
** K= 7 L= 4 **			
-3	235	209	180
** K= 1 L= 5 **			
0	83	66	0
** K= 2 L= 5 **			
0	1052	1019	0
** K= 3 L= 5 **			
-1	78	8	180
0	312	327	0
** K= 4 L= 5 **			
-1	52	21	0
0	1031	1057	180
** K= 5 L= 5 **			
-2	77	73	180
-1	199	219	180
0	127	143	180
** K= 6 L= 5 **			
-2	958	953	0
-1	48	44	0
** K= 7 L= 5 **			
-3	135	143	0
** K= 0 L= 6 **			
0	206	239	0

H	/FO/	/FC/	PHI
** K= 1 L= 6 **			
0	47	20	180
** K= 2 L= 6 **			
-1	120	61	0
0	1208	1170	0
** K= 3 L= 6 **			
-1	71	68	0
0	131	54	0
** K= 4 L= 6 **			
-2	198	146	0
-1	96	52	0
0	1061	1072	0
** K= 5 L= 6 **			
-2	87	80	180
-1	184	193	0
0	96	74	0
** K= 6 L= 6 **			
-2	1059	1055	0
-1	78	60	0
** K= 7 L= 6 **			
-3	136	77	0
** K= 1 L= 7 **			
0	410	397	0
** K= 2 L= 7 **			
0	918	872	0
** K= 3 L= 7 **			
-1	565	583	0
0	108	89	0
** K= 4 L= 7 **			
-1	418	443	180
0	800	836	180
** K= 5 L= 7 **			
-2	340	358	0
-1	157	171	180
0	553	596	180
** K= 6 L= 7 **			
-2	866	875	0
** K= 7 L= 7 **			
-3	613	595	0
** K= 0 L= 8 **			
0	266	235	0
** K= 1 L= 8 **			
0	81	58	0
** K= 2 L= 8 **			
-1	227	240	0
0	904	885	0
** K= 3 L= 8 **			
-1	210	195	0
0	240	237	0
** K= 4 L= 8 **			
-2	371	330	0
-1	107	67	0
0	936	963	0
** K= 5 L= 8 **			
-2	76	28	180
-1	127	107	0
0	356	420	0
** K= 6 L= 8 **			
-2	977	999	0
** K= 1 L= 9 **			
0	175	147	0
** K= 2 L= 9 **			
0	360	327	0
** K= 3 L= 9 **			
-1	189	156	0
0	82	63	0
** K= 4 L= 9 **			
-1	159	151	180
0	323	309	180
** K= 5 L= 9 **			
-2	107	102	0
-1	63	15	180
** K= 6 L= 9 **			
-2	315	260	0
** K= 0 L= 10 **			
0	1764	1733	180
** K= 1 L= 10 **			
0	257	264	0
** K= 2 L= 10 **			
-1	368	365	180
0	407	393	180
** K= 3 L= 10 **			
-1	426	446	0
0	326	318	180
** K= 4 L= 10 **			
-2	1631	1668	180
-1	279	257	0
0	478	497	180
** K= 5 L= 10 **			
-2	76	43	0
-1	233	229	180
** K= 6 L= 10 **			
-2	583	568	180
** K= 1 L= 11 **			
0	117	104	0
** K= 2 L= 11 **			
0	802	792	180
** K= 3 L= 11 **			
-1	119	86	0
0	60	70	180
** K= 4 L= 11 **			
-1	99	99	180
0	735	775	0
** K= 5 L= 11 **			
-2	99	141	0
-1	68	43	0
0	80	36	0
** K= 6 L= 11 **			
-2	800	769	180
** K= 0 L= 12 **			
0	633	616	180
** K= 1 L= 12 **			
0	289	298	180
** K= 2 L= 12 **			
-1	511	534	0
0	120	96	0
** K= 3 L= 12 **			
-1	149	152	180
0	476	485	0
** K= 4 L= 12 **			
-2	635	641	180
-1	251	251	180
0	174	160	0
** K= 5 L= 12 **			
-2	341	359	180
-1	320	348	0
0	92	100	0

H	/FO/	/FC/	PHI
** K= 6	L= 12	**	
-1	126	76	180
** K= 1	L= 13	**	
0	190	201	0
** K= 2	L= 13	**	
0	1243	1245	180
** K= 3	L= 13	**	
-1	131	89	0
0	111	107	180
** K= 4	L= 13	**	
-1	230	243	180
0	1177	1284	0
** K= 5	L= 13	**	
-2	308	356	0
-1	107	121	0
0	61	69	180
** K= 6	L= 13	**	
-2	1428	1292	180
-1	234	205	0
** K= 0	L= 14	**	
0	172	175	180
** K= 1	L= 14	**	
0	186	183	0
** K= 2	L= 14	**	
-1	228	175	180
0	1717	1732	0
** K= 3	L= 14	**	
-1	228	226	0
0	184	127	180
** K= 4	L= 14	**	
-2	169	134	180
-1	164	155	0
0	1559	1689	0
** K= 5	L= 14	**	
-2	93	97	0
-1	111	19	0
** K= 6	L= 14	**	
-3	109	79	0
-2	1720	1646	0
** K= 1	L= 15	**	
0	130	113	0
** K= 2	L= 15	**	
0	702	629	180
** K= 3	L= 15	**	
-1	100	81	0
0	224	239	180
** K= 4	L= 15	**	
-1	112	126	180
0	604	572	0
** K= 5	L= 15	**	
-2	153	160	0
-1	204	231	0
** K= 0	L= 16	**	
0	256	211	0
** K= 1	L= 16	**	
0	40	9	0
** K= 2	L= 16	**	
-1	582	593	0
0	408	395	180
** K= 3	L= 16	**	
-1	69	41	180
0	528	544	0
** K= 4	L= 16	**	
-2	212	146	0
-1	60	48	0
0	343	320	180
** K= 5	L= 16	**	
-2	116	139	0
-1	407	455	0
** K= 6	L= 16	**	
-3	464	450	0
** K= 1	L= 17	**	
0	77	96	0
** K= 2	L= 17	**	
0	271	279	180
** K= 3	L= 17	**	
-1	46	12	0
0	134	136	180
** K= 4	L= 17	**	
-1	105	124	180
0	259	269	0
** K= 5	L= 17	**	
-2	185	193	0
-1	168	152	0
** K= 0	L= 18	**	
0	220	211	0
** K= 1	L= 18	**	
0	249	254	0
** K= 2	L= 18	**	
-1	358	356	180
0	1139	1155	180
** K= 3	L= 18	**	
-1	129	124	0
0	323	329	180
** K= 4	L= 18	**	
-2	322	221	0
-1	215	223	0
0	1100	1184	180
** K= 5	L= 18	**	
-2	341	349	0
-1	270	251	180
** K= 1	L= 19	**	
0	83	25	180
** K= 2	L= 19	**	
0	368	366	180
** K= 3	L= 19	**	
-1	59	52	180
0	51	38	180
** K= 4	L= 19	**	
-1	14	11	0
0	326	377	0
** K= 5	L= 19	**	
-2	119	61	0
** K= 0	L= 20	**	
0	1692	1759	0
** K= 1	L= 20	**	
0	121	146	0
** K= 2	L= 20	**	
-1	222	219	180
0	108	80	0
** K= 3	L= 20	**	
0	247	242	180
** K= 4	L= 20	**	
-1	157	168	0

H	/FO/	/FC/	PHI
** K= 5	L= 20	**	
-2	341	335	0
-1	320	299	180
** K= 1	L= 21	**	
0	360	339	180
** K= 2	L= 21	**	
0	134	55	180
** K= 3	L= 21	**	
-1	343	347	180
** K= 4	L= 21	**	
-1	426	397	0
** K= 5	L= 21	**	
-2	466	434	180
** K= 0	L= 22	**	
0	779	731	0
** K= 1	L= 22	**	
0	366	363	0
** K= 2	L= 22	**	
-1	180	158	180
0	508	504	0
** K= 3	L= 22	**	
-1	244	268	0
0	188	154	180
** K= 4	L= 22	**	
-1	382	384	0
0	536	496	0
** K= 2	L= 23	**	
0	540	537	0
** K= 3	L= 23	**	
-1	93	88	180
0	91	90	0
** K= 4	L= 23	**	
-1	198	213	0
** K= 0	L= 24	**	
0	812	850	180
** K= 1	L= 24	**	
0	134	118	0
** K= 2	L= 24	**	
0	667	589	180

H	/FO/	/FC/	PHI
** K= 3	L= 24	**	
0	232	230	0
** K= 4	L= 24	**	
-2	915	838	180
-1	129	97	0
** K= 1	L= 25	**	
0	191	247	0
** K= 2	L= 25	**	
0	889	921	0
** K= 3	L= 25	**	
-1	227	233	0
** K= 1	L= 26	**	
0	194	209	0
** K= 3	L= 26	**	
-1	241	266	0
** K= 0	L= 28	**	
0	845	834	0
** K= 2	L= 28	**	
-1	144	103	0
** K= 1	L= 29	**	
0	129	115	0

H	/FO/	/FC/	PHI

H	/F0/	/FC/	PHI
** K= 1 L= 0 **			
0	12	16	0
** K= 2 L= 0 **			
-1	568	401	0
0	147	83	0
** K= 3 L= 0 **			
-1	156	121	180
0	470	290	0
** K= 4 L= 0 **			
-2	3024	2889	0
-1	35	42	0
0	183	145	0
** K= 5 L= 0 **			
-2	182	170	0
-1	353	276	0
0	201	279	180
** K= 6 L= 0 **			
-3	368	295	0
-2	242	143	0
-1	143	89	180
0	2335	2416	0
** K= 7 L= 0 **			
-3	206	233	180
-2	251	151	0
-1	181	145	0
0	257	301	0
** K= 8 L= 0 **			
-4	2009	2231	0
-2	225	169	0
** K= 1 L= 1 **			
0	158	118	0
** K= 2 L= 1 **			
0	260	198	180
** K= 3 L= 1 **			
-1	200	206	0
0	115	35	180
** K= 4 L= 1 **			
-1	99	27	180
0	250	88	0
** K= 5 L= 1 **			
-2	157	89	180
-1	111	31	0
0	199	239	180
** K= 6 L= 1 **			
-2	310	112	180
-1	83	158	0
0	845	111	180
** K= 7 L= 1 **			
-3	140	201	0
-2	149	60	180
-1	133	196	0
0	243	287	180
** K= 8 L= 1 **			
-3	70	58	0
-2	287	59	180
** K= 0 L= 2 **			
0	864	854	0
** K= 1 L= 2 **			
0	256	173	0
** K= 2 L= 2 **			
-1	121	41	180
0	662	568	180
** K= 3 L= 2 **			
-1	144	15	0
0	123	35	0
** K= 4 L= 2 **			
-2	822	828	0
-1	186	111	0
0	609	590	180
** K= 5 L= 2 **			
-2	278	263	0
-1	156	67	0
** K= 6 L= 2 **			
-3	167	96	0
-2	597	557	180
-1	99	58	180
0	667	735	0
** K= 7 L= 2 **			
-3	156	128	180
-2	173	101	0
-1	194	199	0
0	307	313	0
** K= 8 L= 2 **			
-4	583	668	0
-2	488	512	180
** K= 1 L= 3 **			
0	305	235	180
** K= 2 L= 3 **			
0	573	444	0
** K= 3 L= 3 **			
-1	200	137	180
0	206	187	0
** K= 4 L= 3 **			
-1	215	153	0
0	486	335	180
** K= 5 L= 3 **			
-2	214	202	180
-1	211	176	180
0	132	9	0
** K= 6 L= 3 **			
-2	489	355	0
-1	119	128	180
0	472	113	0
** K= 7 L= 3 **			
-3	121	2	180
-2	244	326	0
-1	199	92	0
0	195	111	180
** K= 8 L= 3 **			
-3	128	92	0
-2	444	178	180
** K= 0 L= 4 **			
0	896	888	180
** K= 1 L= 4 **			
0	145	35	180
** K= 2 L= 4 **			
-1	412	394	0
0	1109	990	180
** K= 3 L= 4 **			
-1	164	76	180
0	347	299	0
** K= 4 L= 4 **			
-2	849	851	180
-1	125	16	0
0	925	839	180
** K= 5 L= 4 **			
-2	126	64	0
-1	257	261	0
0	129	139	180
** K= 6 L= 4 **			
-3	232	244	0
-2	821	755	180
-1	126	4	180
0	753	742	180
** K= 7 L= 4 **			
-3	130	78	180

H	/FØ/	/FC/	PHI
-2	296	173	0
-1	127	85	0
0	133	158	0

** K= 8 L= 4 **

-4	683	671	180
-3	85	31	0
-2	761	588	180

** K= 1 L= 5 **

0	125	107	0

** K= 2 L= 5 **

0	1034	916	0

** K= 3 L= 5 **

-1	181	131	0
0	278	200	0

** K= 4 L= 5 **

-1	101	6	0
0	977	941	180

** K= 5 L= 5 **

-2	120	56	180
-1	235	189	180
0	170	124	180

** K= 6 L= 5 **

-2	899	841	0
-1	82	52	0
0	302	106	180

** K= 7 L= 5 **

-3	101	77	0
-2	382	339	0
-1	144	210	0
0	170	223	180

** K= 8 L= 5 **

-2	849	872	180

** K= 0 L= 6 **

0	281	356	0

** K= 1 L= 6 **

0	168	81	180

** K= 2 L= 6 **

-1	215	196	0
0	1241	1123	0

** K= 3 L= 6 **

-1	150	65	180
0	255	266	0

** K= 4 L= 6 **

-2	307	363	0
-1	183	111	180
0	1001	965	0

** K= 5 L= 6 **

-2	205	123	180
-1	281	250	0
0	243	6	180

** K= 6 L= 6 **

-3	276	237	0
-2	902	876	0
-1	218	94	180
0	321	330	0

** K= 7 L= 6 **

-3	256	44	180
-2	320	276	0
-1	197	117	180
0	224	166	180

** K= 8 L= 6 **

-4	292	292	0
-3	194	78	180
-2	825	694	0

** K= 1 L= 7 **

0	394	312	0

** K= 2 L= 7 **

0	1078	949	0

** K= 3 L= 7 **

-1	453	373	0
0	144	169	0

** K= 4 L= 7 **

-1	349	340	180
0	834	789	180

** K= 5 L= 7 **

-2	322	298	0
-1	155	161	180
0	483	441	180

** K= 6 L= 7 **

-2	820	757	0
-1	408	291	0
0	136	109	0

** K= 7 L= 7 **

-3	488	406	0
-2	203	300	0
-1	295	316	180
0	268	317	0

** K= 8 L= 7 **

-2	683	501	180

** K= 0 L= 8 **

0	133	39	0

** K= 1 L= 8 **

0	141	143	0

** K= 2 L= 8 **

-1	66	80	0
0	927	852	0

** K= 3 L= 8 **

-1	289	283	0

** K= 4 L= 8 **

-2	70	21	180
-1	196	179	0
0	787	858	0

** K= 5 L= 8 **

-2	131	30	0
-1	55	41	180
0	427	343	0

** K= 6 L= 8 **

-3	86	67	180
-2	788	812	0
-1	284	308	0
0	126	76	180

** K= 7 L= 8 **

-3	394	373	0
-2	99	97	180
-1	126	50	0
0	131	56	180

** K= 8 L= 8 **

-4	129	74	180
-3	210	162	0
-2	655	741	0

** K= 1 L= 9 **

0	260	265	0

** K= 2 L= 9 **

0	223	182	0

** K= 3 L= 9 **

-1	321	342	0
0	59	33	180

** K= 4 L= 9 **

-1	203	157	180
0	338	251	180

** K= 5 L= 9 **

-2	129	46	0
-1	77	29	0
0	335	361	180

** K= 6 L= 9 **

H	/FØ/	/FC/	PHI
-2	377	199	0
-1	234	257	0
0	497	102	180
** K=	7	L=	9 **
-3	319	308	0
-2	96	55	180
-1	106	88	0
0	124	163	180
** K=	8	L=	9 **
-3	151	27	180
-2	377	302	180
** K=	1	L=	10 **
0	153	136	0
** K=	2	L=	10 **
-1	268	159	180
0	495	446	180
** K=	3	L=	10 **
-1	276	280	0
0	178	70	180
** K=	4	L=	10 **
-2	1185	1377	180
-1	130	97	0
0	487	465	180
** K=	5	L=	10 **
-2	90	43	180
-1	131	62	180
0	305	431	0
** K=	6	L=	10 **
-3	131	72	180
-2	536	430	180
-1	271	216	0
0	1028	1153	180
** K=	7	L=	10 **
-3	353	371	0
-2	117	20	0
-1	94	41	180
0	148	193	180
** K=	8	L=	10 **
-4	911	1076	180
-3	127	100	0
** K=	2	L=	11 **
0	615	591	180
** K=	3	L=	11 **
-1	105	94	180
** K=	4	L=	11 **
-1	78	50	180

H	/FØ/	/FC/	PHI
0	566	624	0
** K=	5	L=	11 **
-2	136	131	0
-1	96	54	180
0	130	119	0
** K=	6	L=	11 **
-2	538	544	180
-1	120	55	180
0	464	97	0
** K=	7	L=	11 **
-3	117	89	180
-2	129	100	0
-1	115	226	180
0	216	285	0
** K=	0	L=	12 **
0	710	703	180
** K=	1	L=	12 **
0	93	195	180
** K=	2	L=	12 **
-1	321	336	0
** K=	3	L=	12 **
-1	106	36	180
0	247	258	0
** K=	4	L=	12 **
-2	546	684	180
-1	171	130	180
0	410	242	0
** K=	5	L=	12 **
-2	250	276	180
-1	181	210	0
0	134	64	0
** K=	6	L=	12 **
-3	126	175	0
-2	553	236	0
-1	127	43	0
0	548	603	180
** K=	7	L=	12 **
-3	127	117	0
-2	178	157	0
-1	194	203	180
0	302	317	180
** K=	8	L=	12 **
-4	489	544	180
-3	133	68	180
** K=	1	L=	13 **
0	242	331	0

H	/FØ/	/FC/	PHI
** K=	3	L=	13 **
-1	188	248	0
0	130	128	180
** K=	4	L=	13 **
-1	244	252	180
0	1147	1092	0
** K=	5	L=	13 **
-2	216	275	0
-1	147	121	0
** K=	6	L=	13 **
-2	1080	1034	180
-1	152	224	0
0	226	97	180
** K=	7	L=	13 **
-3	90	107	0
-2	164	228	180
-1	237	172	180
** K=	0	L=	14 **
0	40	124	0
** K=	2	L=	14 **
-1	44	7	0
0	1180	1516	0
** K=	3	L=	14 **
-1	127	102	0
0	70	82	0
** K=	4	L=	14 **
-2	132	161	0
-1	111	32	0
0	1154	1329	0
** K=	5	L=	14 **
-2	118	15	180
-1	117	80	0
0	91	144	0
** K=	6	L=	14 **
-3	155	66	0
-2	1153	1206	0
-1	143	46	0
0	177	182	0
** K=	7	L=	14 **
-3	118	97	0
-2	220	137	0
-1	136	29	180
** K=	8	L=	14 **
-3	112	24	0
** K=	3	L=	15 **

H	/FØ/	/FC/	PHI
-1	65	53	180
0	197	178	180
** K=	4	L= 15	**
-1	111	54	180
0	586	573	0
** K=	5	L= 15	**
-2	137	95	0
-1	154	170	0
0	77	60	0
** K=	6	L= 15	**
-2	565	505	180
-1	124	11	180
0	74	87	0
** K=	7	L= 15	**
-3	101	33	180
-2	314	303	180
-1	189	199	180
** K=	8	L= 15	**
-3	155	136	180
** K=	0	L= 16	**
0	91	117	180
** K=	1	L= 16	**
0	29	98	0
** K=	2	L= 16	**
-1	276	369	0
0	267	430	180
** K=	3	L= 16	**
-1	62	82	0
0	249	296	0
** K=	4	L= 16	**
-2	124	128	180
-1	127	122	0
0	336	343	180
** K=	5	L= 16	**
-2	134	130	0
-1	213	262	0
0	127	24	0
** K=	6	L= 16	**
-3	227	243	0
-2	311	310	180
-1	62	104	0
0	102	106	180
** K=	7	L= 16	**
-3	77	55	0
-2	240	202	0
-1	182	120	0
** K=	1	L= 17	**
0	58	148	0
** K=	3	L= 17	**
-1	59	61	0
0	131	174	180
** K=	4	L= 17	**
-1	72	77	180
** K=	5	L= 17	**
-2	116	113	0
-1	175	162	0
0	110	58	0
** K=	6	L= 17	**
-2	391	279	180
0	105	85	180
** K=	7	L= 17	**
-3	104	63	180
-2	229	302	180
** K=	0	L= 18	**
0	250	301	0
** K=	1	L= 18	**
0	57	102	0
** K=	2	L= 18	**
-1	157	198	180
0	777	980	180
** K=	3	L= 18	**
-1	57	5	180
0	117	126	180
** K=	4	L= 18	**
-2	239	328	0
-1	56	56	0
0	812	959	180
** K=	5	L= 18	**
-2	180	154	0
-1	109	71	180
0	133	66	180
** K=	6	L= 18	**
-3	79	36	180
-2	1049	898	180
-1	57	61	180
0	299	327	0
** K=	7	L= 18	**
-3	54	107	180
-2	122	12	180
** K=	3	L= 19	**
-1	103	117	180
** K=	4	L= 19	**
-1	105	37	180
** K=	5	L= 19	**
-2	129	129	0
-1	61	4	180
0	134	168	0
** K=	6	L= 19	**
-2	327	255	180
-1	49	75	180
0	360	78	0
** K=	7	L= 19	**
-3	73	139	180
** K=	0	L= 20	**
0	1233	1456	0
** K=	2	L= 20	**
-1	208	305	180
** K=	3	L= 20	**
-1	43	99	0
0	250	360	180
** K=	4	L= 20	**
-2	1083	1306	0
-1	214	214	0
0	206	234	0
** K=	5	L= 20	**
-2	318	306	0
-1	338	328	180
0	52	34	180
** K=	6	L= 20	**
-3	308	295	180
-2	243	221	0
-1	94	102	0
0	1194	1083	0
** K=	7	L= 20	**
-3	55	12	180
** K=	1	L= 21	**
0	43	221	180
** K=	3	L= 21	**
-1	179	168	180
** K=	4	L= 21	**
-1	278	265	0
0	100	69	180
** K=	5	L= 21	**

H	/FØ/	/FC/	PHI
-2	377	331	180
-1	68	35	0
0	191	141	0
** K=	6	L= 21	**
-2	128	59	0
-1	284	163	180
** K=	0	L= 22	**
0	471	674	0
** K=	1	L= 22	**
0	134	323	0
** K=	2	L= 22	**
-1	87	111	180
** K=	3	L= 22	**
-1	113	185	0
0	42	56	180
** K=	4	L= 22	**
-2	668	661	0
-1	262	257	0
0	362	240	0
** K=	5	L= 22	**
-2	370	365	0
-1	61	25	180
0	36	78	0
** K=	6	L= 22	**
-3	41	4	180
-2	323	211	0
-1	157	95	0
** K=	3	L= 23	**
-1	96	111	180
0	72	98	0
** K=	4	L= 23	**
-1	159	124	0
** K=	5	L= 23	**
-2	192	159	180
-1	127	90	180
0	45	13	0
** K=	6	L= 23	**
-2	457	397	0
-1	83	91	180
** K=	0	L= 24	**
0	623	754	180
** K=	2	L= 24	**
-1	60	45	0

H	/FØ/	/FC/	PHI
** K=	3	L= 24	**
-1	96	84	0
0	72	9	180
** K=	4	L= 24	**
-2	822	727	180
-1	152	155	0
** K=	5	L= 24	**
-2	195	206	0
-1	41	17	180
0	82	14	0
** K=	6	L= 24	**
-2	479	460	180
** K=	1	L= 25	**
0	114	226	0
** K=	2	L= 25	**
0	430	609	0
** K=	3	L= 25	**
0	149	130	0
** K=	4	L= 25	**
-1	149	146	180
** K=	5	L= 25	**
-2	86	117	0
-1	160	126	180
0	229	207	180
** K=	0	L= 26	**
0	369	429	180
** K=	2	L= 26	**
-1	499	501	180
0	373	363	0
** K=	3	L= 26	**
-1	163	110	0
** K=	4	L= 26	**
-2	444	370	180
-1	102	93	0
0	346	296	0
** K=	5	L= 26	**
-2	68	93	0
-1	385	384	180
0	100	116	0
** K=	1	L= 27	**
0	62	82	180
** K=	2	L= 27	**

H	/FØ/	/FC/	PHI
0	848	760	0
** K=	3	L= 27	**
0	82	117	0
** K=	4	L= 27	**
-1	17	36	0
** K=	5	L= 27	**
-1	91	108	180
** K=	0	L= 28	**
0	477	413	0
** K=	1	L= 28	**
0	59	76	0
** K=	2	L= 28	**
-1	42	91	0
0	736	643	0
** K=	3	L= 28	**
-1	171	149	0
0	66	44	0
** K=	4	L= 28	**
-2	458	341	0
-1	87	92	0
0	738	634	0
** K=	5	L= 28	**
-2	8	20	0
** K=	1	L= 29	**
0	89	73	0
** K=	2	L= 29	**
0	81	45	0
** K=	3	L= 29	**
-1	160	133	0
0	93	0	180
** K=	4	L= 29	**
0	84	79	180
** K=	0	L= 30	**
0	742	666	180
** K=	1	L= 30	**
0	121	122	0
** K=	2	L= 30	**
-1	176	108	0
0	118	60	0

H	/FØ/	/FC/	PHI
** K= 3 L= 30 **			
-1	221	193	0
0	213	149	0
** K= 4 L= 30 **			
-2	643	583	180
-1	108	91	0
** K= 1 L= 31 **			
0	26	61	180
** K= 2 L= 31 **			
0	384	214	180
** K= 3 L= 31 **			
-1	66	70	180
** K= 0 L= 32 **			
0	1080	855	180
** K= 1 L= 32 **			
0	145	137	180
** K= 2 L= 32 **			
-1	217	104	0
0	160	81	180
** K= 3 L= 32 **			
-1	51	44	180
0	210	71	0
** K= 1 L= 33 **			
0	96	122	180
** K= 2 L= 33 **			
0	314	167	180
** K= 0 L= 34 **			
0	257	241	0
** K= 1 L= 34 **			
0	194	157	180
** K= 2 L= 34 **			
-1	212	192	0

H	/FØ/	/FC/	PHI

H	/FØ/	/FC/	PHI

APPENDIX 4

Intensity data for the refinements described in Chapter 7.

Ag_3PO_4	single crystal X-ray study	A61
Ag_3PO_4	PND study at 375°C(D2 diffractometer)	A63
$Na_{3(1-x)}Al_xPO_4$	x = 0.025 (D2 diffractometer)	A64
$Na_{3(1-x)}Al_xPO_4$	x = 0.2 (D2 diffractometer)	A65

For the single crystal data,the listing for each reflection includes the observed (/FO/) and calculated (/FC/) structure factors and the phase angle.The powder data listings include the Bragg angle,2θ,(POSN),the calculated integrated intensity (INUC and ITOT),the observed integrated intensity (IOBS),the difference between the two (DELTA) and the estimated standard deviation of the observed intensity (ESD). The column headed IMAG is superfluous.

H	/F0/	/FC/	PHI
** K= 1 L= 1 **			
0	371	350	180
** K= 0 L= 2 **			
0	782	773	0
** K= 1 L= 2 **			
0	1145	1143	180
1	790	781	18
** K= 2 L= 2 **			
0	370	364	180
2	1238	1261	170
** K= 1 L= 3 **			
0	593	596	180
** K= 2 L= 3 **			
0	979	980	0
1	670	684	6
** K= 3 L= 3 **			
0	122	123	180
2	490	496	1
** K= 0 L= 4 **			
0	1251	1209	0
** K= 1 L= 4 **			
0	93	90	180
1	305	311	195
** K= 2 L= 4 **			
0	579	577	0
1	729	754	180
2	325	341	196
** K= 3 L= 4 **			
0	90	80	180
1	122	121	195
2	627	637	360
3	272	266	182
** K= 4 L= 4 **			
0	1038	1060	0
2	299	300	6
4	681	668	358
** K= 1 L= 5 **			
0	282	270	180
** K= 2 L= 5 **			
0	710	703	0
1	471	480	346
** K= 3 L= 5 **			
0	210	210	180
2	395	398	354
** K= 4 L= 5 **			
0	57	50	0
1	145	144	159
2	480	484	179
3	116	114	166
** K= 5 L= 5 **			
0	182	187	180
2	312	315	15
4	92	89	205
** K= 0 L= 6 **			
0	665	645	0
** K= 1 L= 6 **			
0	512	508	180
1	349	348	351
** K= 2 L= 6 **			
0	99	92	180
1	101	99	181
2	590	599	185
** K= 3 L= 6 **			
0	440	451	180
1	218	215	357
2	78	78	359
3	283	285	359
** K= 4 L= 6 **			
0	306	315	0
1	340	345	359
2	87	83	152
3	309	309	359
4	310	307	356
** K= 5 L= 6 **			
0	321	337	180
1	218	217	11
2	69	71	360
3	208	201	2
4	243	239	178
5	162	152	345
** K= 6 L= 6 **			
0	60	59	0
2	318	317	176
4	52	39	198
6	158	151	175
** K= 1 L= 7 **			
0	115	112	180
** K= 2 L= 7 **			
0	463	470	0
1	293	293	3
** K= 3 L= 7 **			
0	206	209	180
2	304	308	3
** K= 4 L= 7 **			
1	128	126	181
2	331	331	179
** K= 5 L= 7 **			
0	110	113	180
2	226	222	355
4	69	68	176
** K= 6 L= 7 **			
0	244	251	0
1	175	173	354
3	99	96	353
4	182	177	357
5	107	103	5
** K= 7 L= 7 **			
2	163	158	357
4	64	65	168
** K= 0 L= 8 **			
0	608	596	0
** K= 1 L= 8 **			
0	116	113	180
** K= 2 L= 8 **			
0	153	151	0
1	269	266	180
2	209	206	163
** K= 3 L= 8 **			
0	112	112	180
2	228	227	359
** K= 4 L= 8 **			
0	401	412	0
1	62	61	357
2	118	116	346
4	327	322	360
** K= 5 L= 8 **			
2	196	195	359
5	45	43	87
** K= 6 L= 8 **			
0	163	167	0
1	129	130	180
2	94	99	194
3	119	114	177
4	88	90	9
** K= 7 L= 8 **			
0	59	66	180
2	127	129	358
** K= 1 L= 9 **			

H	/F0/	/FC/	PHI	H	/F0/	/FC/	PHI
0	127	125	180				
** K= 2 L= 9 **							
0	302	300	0				
1	207	205	9				
** K= 3 L= 9 **							
2	187	185	3				
** K= 4 L= 9 **							
0	36	22	0				
2	217	219	179				
** K= 5 L= 9 **							
2	137	137	344				
** K= 6 L= 9 **							
0	155	158	0				
** K= 0 L= 10 **							
0	234	225	0				
** K= 1 L= 10 **							
0	154	155	180				
1	71	70	6				
** K= 2 L= 10 **							
1	83	86	181				
2	202	205	179				
** K= 3 L= 10 **							
0	146	149	180				
1	86	89	359				
2	69	67	357				
** K= 4 L= 10 **							
0	229	232	0				
1	98	107	357				

H	POSN	INUC	I'IAG	ITOT	IOBS	DELTA	FSD
2	2292	3024	0	3024	2062	-961	232
3	2571	38237	0	38237	30182	945	296
2	2825	61500	0	61500	61913	413	335
3	3279	726	0	726	919	193	214
0	3634	20282	0	20282	20814	532	313
4	4054	15276	0	15276	15287	11	277
1	4229	11949	0	11949	12735	786	218
3	4390	30797	0	30797	40079	2282	327
4	4723	367	0	367	446	79	230
3	4879	726	0	726	815	89	210
2	5032	3581	0	3581	3454	-126	86
2	5032	8150	0	8150	7860	-289	195
2	5327	10620	0	10620	13050	2430	258
3	5470	6432	0	6432	6606	174	193
1	5611	1880	0	1880	578	-1301	203
3	5887	3790	0	3790	2866	-923	267
3	6022	278	0	278	228	-49	29
1	6155	10018	0	10018	9795	-222	316
4	6155	4	0	4	4	0	0
3	6544	4326	0	4326	4113	-212	133
3	6544	3096	0	3096	3709	-196	123
2	6671	17113	0	17113	18549	1436	259
2	6922	11117	0	11117	10494	-622	292
3	7169	1545	0	1545	2951	1406	201
4	7169	6	0	6	11	5	1
3	7291	49	0	49	66	17	5
3	7413	797	0	797	649	-147	34
3	7413	4976	0	4976	4054	-921	213
3	7533	888	0	888	801	-87	32
3	7653	5549	0	5549	5293	-255	194
3	7653	2651	0	2651	2529	-121	93
3	7892	258	0	258	285	27	82
3	8010	800	0	800	1064	264	386
3	8010	220	0	220	292	72	106
3	8128	1719	0	1719	2585	866	1046

L	POSN	INUC	I'IAG	ITOT	IOBS	DELTA	FSD
2	2292	3024	0	3024	2062	-961	232
0	2571	38237	0	38237	30182	945	296
2	2825	61500	0	61500	61913	413	335
0	3279	726	0	726	919	193	214
1	3634	20282	0	20282	20814	532	313
4	4054	15276	0	15276	15287	11	277
0	4229	11949	0	11949	12735	786	218
1	4390	30797	0	30797	40079	2282	327
4	4723	367	0	367	446	79	230
0	4879	726	0	726	815	89	210
1	5032	3581	0	3581	3454	-126	86
4	5032	8150	0	8150	7860	-289	195
0	5327	10620	0	10620	13050	2430	258
1	5470	6432	0	6432	6606	174	193
3	5611	1880	0	1880	578	-1301	203
0	5887	3790	0	3790	2866	-923	267
1	6022	278	0	278	228	-49	29
4	6155	10018	0	10018	9795	-222	316
0	6155	4	0	4	4	0	0
1	6544	4326	0	4326	4113	-212	133
4	6544	3096	0	3096	3709	-196	123
0	6671	17113	0	17113	18549	1436	259
1	6922	11117	0	11117	10494	-622	292
4	7169	1545	0	1545	2951	1406	201
0	7169	6	0	6	11	5	1
1	7291	49	0	49	66	17	5
4	7413	797	0	797	649	-147	34
0	7413	4976	0	4976	4054	-921	213
1	7533	888	0	888	801	-87	32
4	7653	5549	0	5549	5293	-255	194
0	7653	2651	0	2651	2529	-121	93
1	7892	258	0	258	285	27	82
4	8010	800	0	800	1064	264	386
0	8010	220	0	220	292	72	106
1	8128	1719	0	1719	2585	866	1046

K	POSN	INUC	I'IAG	ITOT	IOBS	DELTA	FSD
1	2292	3024	0	3024	2062	-961	232
1	2571	38237	0	38237	30182	945	296
2	2825	61500	0	61500	61913	413	335
2	3279	726	0	726	919	193	214
2	3634	20282	0	20282	20814	532	313
2	4054	15276	0	15276	15287	11	277
2	4229	11949	0	11949	12735	786	218
2	4390	30797	0	30797	40079	2282	327
2	4723	367	0	367	446	79	230
2	4879	726	0	726	815	89	210
2	5032	3581	0	3581	3454	-126	86
2	5032	8150	0	8150	7860	-289	195
2	5327	10620	0	10620	13050	2430	258
2	5470	6432	0	6432	6606	174	193
2	5611	1880	0	1880	578	-1301	203
2	5887	3790	0	3790	2866	-923	267
2	6022	278	0	278	228	-49	29
2	6155	10018	0	10018	9795	-222	316
2	6155	4	0	4	4	0	0
2	6544	4326	0	4326	4113	-212	133
2	6544	3096	0	3096	3709	-196	123
2	6671	17113	0	17113	18549	1436	259
2	6922	11117	0	11117	10494	-622	292
2	7169	1545	0	1545	2951	1406	201
2	7169	6	0	6	11	5	1
2	7291	49	0	49	66	17	5
2	7413	797	0	797	649	-147	34
2	7413	4976	0	4976	4054	-921	213
2	7533	888	0	888	801	-87	32
2	7653	5549	0	5549	5293	-255	194
2	7653	2651	0	2651	2529	-121	93
2	7892	258	0	258	285	27	82
2	8010	800	0	800	1064	264	386
2	8010	220	0	220	292	72	106
2	8128	1719	0	1719	2585	866	1046

H	K	L	POSN	INUC	IMAG	ITOT	IOBS	DELTA	ESD
1	0	2	1608	158173	0	158173	176585	18412	612
2	1	2	1864	62633	0	62633	67323	4690	527
0	3	2	2662	97328	0	97328	99475	2147	636
3	2	2	3138	808	0	808	0	-807	0
4	1	2	3283	41599	0	41599	41392	-206	592
0	4	2	3815	73481	0	73481	69510	-3970	684
1	3	2	4176	4273	0	4273	8693	4420	590
2	2	2	4290	130	0	130	0	-129	0
3	1	2	4727	46717	0	46717	41910	-4806	660
4	0	2	5036	28	0	28	0	0	1
0	5	2	5036	25030	0	25030	25646	616	643
1	4	2	5522	34087	0	34087	32416	-1670	673
2	3	2	5800	18958	0	18958	18478	-479	490
3	2	2	5891	2835	0	2835	3353	518	270
4	1	2	5891	894	0	894	1058	164	85
0	6	0	6247	26068	0	26068	24116	-1951	657
3	2	0	6506	9253	0	9253	8385	-867	594
2	4	0	6592	214	0	214	12	-201	82
4	2	0	6927	13082	0	13082	11693	-1388	674
5	1	0	7174	4610	0	4610	4543	-66	543
1	6	0	7174	204	0	204	201	-2	24
6	0	0	7256	18	0	18	45	27	5
2	5	0	7579	20090	0	20090	34614	14524	2447
3	4	0	7818	4103	0	4103	5113	1010	423
1	5	1	7818	138	0	138	172	34	14

Reflection intensities corresponding to the model presented in Table 7.7(a) (page 215) in which Na(2) is at the x x ½ (48i) position.

H	K	L	POSN	INUC	IMAG	ITOT	IOBS	DELTA	ESD
1	0	2	1608	158079	0	158079	176585	18506	612
2	1	2	1864	62684	0	62684	67323	4639	527
0	3	2	2662	97479	0	97479	99475	1996	636
3	2	2	3138	745	0	745	0	-744	0
4	1	2	3283	41672	0	41672	41395	-276	592
0	4	2	3815	73267	0	73267	69510	-3756	684
1	3	2	4176	4364	0	4364	8702	4338	590
2	2	2	4290	106	0	106	0	-105	0
3	1	2	4727	46762	0	46762	41910	-4851	660
4	0	2	5036	18	0	18	18	0	1
0	5	2	5036	25326	0	25326	25656	330	643
1	4	2	5522	34162	0	34162	32416	-1745	673
2	3	2	5800	18954	0	18954	18588	-365	492
3	2	2	5891	2796	0	2796	3372	576	276
4	1	2	5891	772	0	772	931	159	76
0	6	0	6247	25785	0	25785	24111	-1673	657
3	3	0	6506	9216	0	9216	8385	-830	594
2	4	0	6592	222	0	222	14	-207	84
4	2	0	6927	13198	0	13198	11692	-1505	674
5	1	0	7174	4454	0	4454	4453	0	543
1	6	0	7174	266	0	266	266	0	32
6	0	0	7256	23	0	23	58	35	7
2	5	0	7579	20834	0	20834	34704	13870	2453
3	4	0	7818	4022	0	4022	4835	813	409
1	5	1	7818	189	0	189	227	38	19

Reflection intensities corresponding to the model presented in Table 7.7(b) (Na(2) at x x x (32f)).

ESD
56
45
55
44
49
55
55
35
5

DELTA
16
6
27
36
-13
2
-19
1
9
-24
8
5
39
34
-31
-12
-8
32
13
52
-14
-6
-10

OBS
145
29
66
3
18
31
3
9
38
3
18
19
10
2
1
24
7
2
12

IDI
131
28
65
1
16
32
2
4
40
2
13
19
10
3
1
25
4
6
7
1
6
10

IMAG
0
0
0
0
0
0
0
0
0
0
0
0
0
0
0
0
0
0
0
0
0
0
0

INDC
131
28
63
1
16
32
2
4
40
2
13
19
10
3
1
25
4
6
7
1
6
10

POSN
16
18
26
31
32
38
41
42
47
50
50
55
58
59
59
62
65
66
69
71
71
72

KT
0
2
1
2
0
3
2
2
3
1
4
3
4
0
2
3
2
4
5
1
4

LT
2
0
3
2
4
1
0
4
3
5
0
1
2
6
0
5
6
4
1
7
0

HT
0
2
1
2
0
3
4
2
3
1
4
5
4
0
6
3
2
4
5
1
6

APPENDIX 5

Intensity data for the refinements described in Chapter 8.

Ag_2SO_4	single crystal X-ray study	A67
Ag_2SO_4	PND study at 490°C(D2 diffractometer)	A70
K_2SO_4	PND study at 620°C(D2 diffractometer)	A71

For the single crystal data,the listing includes,for each reflection,the observed (/FO/) and calculated (/FC/) structure factors and the phase angle.The powder data listings contain the Bragg angle,2θ,(POSN),the calculated integrated intensity (INUC and ITOT),the observed integrated intensity (IOBS),the difference between the two (DELTA) and the estimated standard deviation of the observed intensity (ESD).The column headed IMAG is superfluous

H	/FO/	/FC/	PHI
** K= 0 L= 0 **			
4	1000	969	0
8	440	451	0
** K= 2 L= 0 **			
2	1578	1473	0
6	762	767	0
** K= 4 L= 0 **			
0	1563	1526	0
4	1174	1093	0
8	380	393	0
** K= 6 L= 0 **			
2	1474	1365	0
6	604	582	0
** K= 8 L= 0 **			
0	1013	1027	0
4	1023	981	0
8	306	319	0
** K= 10 L= 0 **			
2	995	996	0
6	475	473	0
** K= 12 L= 0 **			
0	923	929	0
4	598	597	0
** K= 14 L= 0 **			
2	627	637	0
6	388	395	0
** K= 16 L= 0 **			
0	632	650	0
4	366	380	0
** K= 18 L= 0 **			
2	414	414	0
** K= 1 L= 1 **			
1	214	200	135
3	434	415	225
5	135	127	135
7	45	29	225
** K= 3 L= 1 **			
1	117	121	225
3	362	342	135
5	213	192	225
7	60	52	135
** K= 5 L= 1 **			
1	478	475	135
3	114	105	225
5	80	67	135
7	95	92	225

H	/FO/	/FC/	PHI
** K= 7 L= 1 **			
1	336	348	225
3	58	56	135
5	127	115	225
7	99	95	135
** K= 9 L= 1 **			
1	222	221	135
3	98	96	225
5	101	105	135
7	86	85	225
** K= 11 L= 1 **			
1	211	206	225
3	80	84	135
5	63	63	225
7	56	40	135
** K= 13 L= 1 **			
1	60	54	135
3	154	152	225
5	87	83	135
7	47	29	225
** K= 15 L= 1 **			
1	51	57	225
3	113	119	135
5	72	65	225
** K= 17 L= 1 **			
1	70	68	135
3	77	80	225
5	46	22	135
** K= 19 L= 1 **			
3	52	46	135
** K= 0 L= 2 **			
2	836	788	180
6	221	218	180
** K= 2 L= 2 **			
0	604	628	180
2	297	284	90
4	527	520	180
6	49	53	270
8	129	134	180
** K= 4 L= 2 **			
2	657	645	180
4	73	74	270
6	257	250	180
** K= 6 L= 2 **			
0	777	792	180
2	162	151	90
4	332	326	180
6	41	26	270
8	112	131	180
** K= 8 L= 2 **			
2	433	437	180
4	36	15	90
6	232	236	180
** K= 10 L= 2 **			
0	473	481	180
2	116	124	270
4	256	259	180
8	87	99	180
** K= 12 L= 2 **			
2	310	313	180
4	58	47	90
6	139	144	180
** K= 14 L= 2 **			
0	206	220	180
2	52	24	270
4	210	218	180
** K= 16 L= 2 **			
2	195	208	180
** K= 18 L= 2 **			
2	40	54	90
4	116	124	180
** K= 1 L= 3 **			
1	1128	1221	45
3	928	868	315
5	579	566	45
7	350	354	315
9	188	204	45
** K= 3 L= 3 **			
1	896	906	315
3	961	929	45
5	679	667	315
7	359	352	45
9	167	168	315
** K= 5 L= 3 **			
1	1166	1147	45
3	783	742	315
5	467	452	45
7	326	321	315
** K= 7 L= 3 **			
1	840	846	315
3	743	709	45
5	503	485	315
7	308	310	45
** K= 9 L= 3 **			
1	673	671	45
3	628	633	315
5	463	460	45
7	263	270	315
** K= 11 L= 3 **			
1	684	691	315

H	/F0/	/FC/	PHI
3	482	478	45
5	320	311	315
7	239	237	45
** K= 13	L= 3 **		
1	455	449	45
3	440	435	315
5	343	353	45
7	205	207	315
** K= 15	L= 3 **		
1	391	399	315
3	350	352	45
5	258	264	315
** K= 17	L= 3 **		
1	347	351	45
3	256	262	315
** K= 19	L= 3 **		
1	217	224	315
3	231	234	45
** K= 0	L= 4 **		
0	267	282	180
4	87	85	0
8	41	15	180
** K= 2	L= 4 **		
2	38	26	180
4	75	71	270
** K= 4	L= 4 **		
0	39	22	180
2	240	235	90
4	45	23	180
6	66	54	270
** K= 6	L= 4 **		
2	51	38	180
4	65	55	270
6	47	19	0
** K= 8	L= 4 **		
0	84	86	0
2	48	44	270
4	73	65	180
6	39	4	90
8	45	30	0
** K= 10	L= 4 **		
4	45	31	90
6	37	17	0
** K= 12	L= 4 **		
0	88	30	180
2	94	94	270
** K= 1	L= 5 **		
1	651	725	135

H	/F0/	/FC/	PHI
3	324	320	225
5	241	236	135
7	186	188	225
** K= 3	L= 5 **		
1	449	495	225
3	404	391	135
5	300	298	225
7	170	182	135
** K= 5	L= 5 **		
1	513	501	135
3	404	419	225
5	231	227	135
7	101	108	225
** K= 7	L= 5 **		
1	334	327	225
3	414	415	135
5	224	240	225
7	97	105	135
** K= 9	L= 5 **		
1	278	276	135
3	331	340	225
5	217	225	135
7	81	96	225
** K= 11	L= 5 **		
1	323	321	225
3	239	242	135
5	131	134	225
7	88	94	135
** K= 13	L= 5 **		
1	238	242	135
3	167	163	225
5	149	149	135
** K= 15	L= 5 **		
1	215	216	225
3	123	129	135
5	99	105	225
** K= 17	L= 5 **		
3	102	103	225
** K= 0	L= 6 **		
2	974	1040	0
6	449	423	0
** K= 2	L= 6 **		
0	826	923	0
4	844	795	0
6	48	17	90
8	275	268	0
** K= 4	L= 6 **		
2	877	908	0
6	467	456	0

H	/F0/	/FC/	PHI
** K= 6	L= 6 **		
0	1101	1061	0
4	553	548	0
8	269	274	0
** K= 8	L= 6 **		
2	719	695	0
6	418	426	0
** K= 10	L= 6 **		
0	764	741	0
2	35	9	90
4	474	461	0
** K= 12	L= 6 **		
2	536	534	0
6	291	286	0
** K= 14	L= 6 **		
0	415	402	0
4	403	399	0
** K= 16	L= 6 **		
4	57	1	270
** K= 1	L= 7 **		
1	49	60	45
3	216	225	315
5	105	101	45
7	47	28	315
** K= 3	L= 7 **		
1	163	175	315
3	106	108	45
5	55	62	315
7	60	62	45
** K= 5	L= 7 **		
1	126	125	45
3	114	108	315
5	100	106	45
7	60	67	315
** K= 7	L= 7 **		
1	185	179	315
3	35	32	45
5	66	81	315
7	61	76	45
** K= 9	L= 7 **		
1	166	156	45
5	45	57	45
7	58	80	315
** K= 11	L= 7 **		
1	72	72	315
3	73	92	45
5	82	91	315
** K= 13	L= 7 **		

H	/FO/	/FC/	PHI
1	68	72	45
3	79	86	315
5	40	36	45
** K= 15	L= 7 **		
1	61	48	315
5	59	49	315
** K= 0	L= 8 **		
0	618	671	180
4	354	358	180
8	128	133	180
** K= 2	L= 8 **		
2	470	493	180
6	263	268	180
** K= 4	L= 8 **		
0	513	537	180
2	116	113	270
4	377	363	180
6	55	49	90
8	125	133	180
** K= 6	L= 8 **		
2	463	465	180
6	189	188	180
** K= 8	L= 8 **		
0	398	379	180
2	50	23	90
4	308	315	180
6	49	9	270
** K= 10	L= 8 **		
2	354	345	180
6	155	160	180
** K= 12	L= 8 **		
0	355	317	180
2	54	56	90
4	208	214	180
** K= 14	L= 8 **		
2	232	221	180
** K= 1	L= 9 **		
1	416	451	315
3	324	340	45
5	217	211	315
7	166	163	45
** K= 3	L= 9 **		
1	306	340	45
3	355	360	315
5	294	282	45
7	169	161	315
** K= 5	L= 9 **		
1	411	420	315
3	293	295	45
5	206	200	315
7	150	146	45
** K= 7	L= 9 **		
1	332	323	45
3	276	283	315
5	254	239	45
7	144	136	315
** K= 9	L= 9 **		
1	268	267	315
3	285	267	45
5	210	220	315
** K= 11	L= 9 **		
1	313	295	45
3	201	203	315
5	151	140	45
** K= 13	L= 9 **		
1	206	198	315
5	160	150	315
** K= 0	L= 10 **		
2	242	256	0
6	135	142	0
** K= 2	L= 10 **		
0	299	305	0
2	48	53	270
4	168	170	0
** K= 4	L= 10 **		
2	241	237	0
6	134	134	0
** K= 6	L= 10 **		
0	222	203	0
4	224	207	0
** K= 8	L= 10 **		
2	214	197	0
6	101	112	0
** K= 10	L= 10 **		
0	197	175	0
2	45	36	90
** K= 12	L= 10 **		
2	169	153	0
** K= 1	L= 11 **		
1	210	219	225
3	230	230	135
5	150	145	225
** K= 3	L= 11 **		
1	189	200	135
3	197	198	225
5	159	157	135
** K= 5	L= 11 **		
1	248	246	225
3	164	168	135
5	116	109	225
** K= 7	L= 11 **		
1	228	215	135
3	139	136	225
5	115	112	135
** K= 9	L= 11 **		
1	192	180	225
3	133	126	135
5	105	109	225
** K= 11	L= 11 **		
1	184	164	135
** K= 0	L= 12 **		
0	306	332	0
4	153	164	0
** K= 2	L= 12 **		
2	230	240	0
4	47	14	90
6	153	158	0
** K= 4	L= 12 **		
0	245	252	0
2	52	6	90
4	194	197	0
6	49	14	270
** K= 6	L= 12 **		
2	231	233	0
** K= 8	L= 12 **		
0	176	175	0
** K= 1	L= 13 **		
1	174	162	315
3	124	117	45
** K= 3	L= 13 **		
1	179	164	45
3	102	110	315
** K= 5	L= 13 **		
1	139	127	315
** K= 7	L= 13 **		
1	144	120	45
** K= 2	L= 14 **		
0	162	157	180

H	K	L	POS	INUC	IMAG	ITOT	IOBS	DIF	ESD
1	1	1							
0	1	0	1421	2192	0	2192	3165	973	130
0	1	1	1696	8337	0	8337	8388	51	86
0	1	-1	1696	8337	0	8337	8388	51	86
0	0	2	1828	5722	0	5722	6027	305	138
0	1	2	2344	8890	0	8890	9088	198	102
0	1	-2	2344	8890	0	8890	9088	198	102
1	1	0	2513	17355	0	17355	16255	-1100	211
1	1	1	2684	0	0	0	38	38	132
0	0	3	2784	0	0	0	109	109	109
0	2	0	2918	872	0	872	1175	303	196
0	2	-2	3486	3650	0	3650	3985	335	127
0	2	2	3486	3650	0	3650	3985	335	127
0	0	4	3760	1536	0	1536	0	-1536	0
1	1	3	3808	0	0	0	0	0	0
1	2	0	3910	2859	0	2859	2489	-370	179
1	2	-1	4029	1489	0	1489	2479	990	136
1	2	1	4029	51	0	51	85	34	5
0	1	4	4055	53	0	53	110	57	6

H	K	L	POS	INUC	IMAG	ITOT	IOBS	DIF	ESD
1	1	1							
0	1	-4	4055	53	0	53	110	57	6
0	2	3	4100	174	0	174	449	275	76
0	2	-3	4100	174	0	174	449	275	76
1	2	-2	4368	622	0	622	643	21	169
1	2	2	4368	37	0	37	38	1	10
0	3	0	4468	2990	0	2990	2290	-700	156
0	3	-1	4575	81	0	81	91	10	5
0	3	1	4575	81	0	81	91	10	5
1	1	4	4598	2134	0	2134	2678	544	182
0	0	5	4766	0	0	0	0	0	0
0	2	-4	4852	29	0	29	58	29	7
0	2	4	4852	29	0	29	58	29	7
0	3	2	4884	190	0	190	238	48	18
0	3	-2	4884	190	0	190	238	48	18
1	2	3	4891	1037	0	1037	1265	228	91
1	2	-3	4891	1022	0	1022	1247	225	90
0	1	-5	5013	7	0	7	24	17	4
0	1	5	5013	7	0	7	24	17	4

H	K	L	POS	INUC	IMAG	ITOT	IOBS	DIF	ESD
1	1	1							
0	0	5	4416	0	0	0	0	0	0
0	2	4	4509	19	0	19	38	19	118
1	2	3	4555	1633	0	1633	750	-883	293
0	3	2	4555	129	0	129	59	-70	23
0	1	5	4646	753	0	753	869	116	252
2	2	0	4867	8648	0	8648	9664	1016	374
2	2	1	4954	0	0	0	0	0	0
0	3	3	4997	893	0	893	1340	447	142
1	1	5	5081	0	0	0	0	0	0
1	3	0	5082	1945	0	1945	1596	-349	185
1	2	4	5165	3	0	3	3	0	0
1	3	1	5166	2332	0	2332	2132	-200	134
2	2	2	5207	2345	0	2345	2143	-202	117
0	2	5	5289	4334	0	4334	2956	-1378	219
0	0	6	5370	120	0	120	208	88	8
1	3	2	5412	3376	0	3376	7064	3688	258
0	1	6	5571	2014	0	2014	3176	1162	161
0	3	4	5571	2150	0	2150	3391	1241	172
2	2	3	5611	0	0	0	0	0	0
0	4	0	5690	321	0	321	1156	835	82

H	K	L	POS	INUC	IMAG	ITOT	IOBS	DIF	ESD
1	1	1							
1	1	6	5958	5161	0	5161	7870	2709	242
0	4	2	5997	2971	0	2971	4039	1068	148

H	K	L	POS	INUC	IMAG	ITOT	IOBS	DIF	ESD
1	1	1							
0	1	0	1342	15700	0	15700	20459	4759	345
0	1	1	1596	109424	0	109424	117847	8423	435
0	0	2	1709	34513	0	34513	30354	-4159	303
0	1	2	2193	25580	0	25580	24352	-1228	329
1	1	0	2361	31326	0	31326	32272	946	340
1	1	1	2518	0	0	0	1222	1222	246
0	0	3	2593	0	0	0	1243	1243	210
0	2	0	2738	16166	0	16166	14108	-2058	330
0	2	1	2876	35328	0	35328	38535	3207	343
0	2	2	3259	22226	0	22226	28826	6600	391
0	0	4	3493	3138	0	3138	3614	476	349
1	1	3	3549	0	0	0	0	0	0
1	2	0	3660	10468	0	10468	10909	441	346
0	1	4	3768	7	0	7	17	10	2
1	2	1	3768	68	0	68	167	99	14
0	2	3	3821	12593	0	12593	14235	1642	367
1	2	2	4078	915	0	915	1321	406	315
0	3	0	4177	3620	0	3620	1771	-1849	220
1	1	4	4274	6290	0	6290	4137	-2153	115
0	3	1	4274	12900	0	12900	8476	-4424	239

H	K	L	POS	INUC	IMAG	ITOT	IOBS	DIF	ESD
1	1	1							
0	4	1	5767	401	0	401	1945	1544	93
1	3	3	5806	471	0	471	2050	1579	81
1	2	5	5882	1895	0	1895	4778	2883	144